Functional Analysis of the ALS/FTD Associated gene *FUS* using a Novel *in vitro* Genomic DNA Expression System

Thesis submitted for the degree of Doctor of Philosophy

Matthew Thomas

Department of Physiology, Anatomy and Genetics

Keble College

University of Oxford

November 2013

Abstract

Aggregations of fused in sarcoma (FUS), a multifunctional RNA processing protein, define a pathological subtype of both frontotemporal dementia (FTD) and amyotrophic lateral sclerosis (ALS), whilst mutations in the *FUS* gene are causative for ALS. To model the impact of *FUS* mutations, expression vectors containing the entire genomic sequence of *FUS*, up and downstream regions, and native promoter sequences have been generated. The constructs have been tagged with an mCherry fluorescent tag, and three separate pathological mutations (R244C, R521C, and P525L) have been separately inserted. Transgenic mice have been generated using the WT and P525L *FUS* vectors to provide a highly physiological model of *FUS* in disease.

Within transfected HEK293 cells, insertion of the P525L and R521C *FUS* mutations leads to relocalisation of FUS from the nucleus to the cytoplasm. R521C and P525L mutant FUS incorporates into cytoplasmic aggregations of untranslated mRNA and RNA binding proteins known as stress granules. The strong relocalisation seen with P525L-FUS is associated with a gain of cytotoxicity. Reversal of this cytoplasmic relocalisation by demethylation of FUS rescues this cytotoxicity, suggesting a toxic gain of cytoplasmic function in the majority of *FUS* mutations. By contrast, insertion of the R244C mutation leads to neither relocalisation, stress granule association, nor cytotoxicity. Notably the R244C mutation, located away from the nuclear localization domain in which the majority of *FUS* mutations are found, leads to the presence of smaller FUS fragments in western blot analyses. These fragments appear not to be due to splicing defects in FUS but rather are due to post-translational modifications or aberrant protein cleavage. These data suggest an alternative pathway for *FUS* toxicity based upon a nuclear loss of function.

Acknowledgements

This thesis would not have been possible without the funding of Alzheimer's Research UK, and the support of my supervisors Richard Wade-Martins and Javier Alegre-Abarrategui, whose generous time and assistance was appreciated throughout. I must also acknowledge all the members of the Richard Wade-Martins group who helped me along the way. Drs Michele Lufino, Tara Caffrey, Liz Hartfield and Brent Ryan were ever available to share their excellent scientific suggestions and time. All those within my own office, especially Max, Heike, Paul and Milena, deserve great thanks for general discussions, help and amusement, my apologies for the amount of mess I created. Special thanks must also go to Hugo Riberio Fernandes, whose selfless policy of ensuring he lost every game of Pro Evolution Soccer played during his four years in Oxford ensured his colleagues remained happy and motivated.

I also wish to thank my parents, brother and Eleanor Boulden for their support throughout my DPhil.

I acknowledge the use, directly or via modification, of text and figures from the article "RNA dysfunction and aggrephagy at the centre of an amyotrophic lateral sclerosis/frontotemporal dementia disease continuum" (Brain, May 2013, 136(5), pp1345-1360) (Thomas et al., 2013). Elements of this article are reproduced with the kind permission of Oxford University Press as part of a non-commercial DPhil thesis.

Contents

Abbreviations

- AdOx - Adenosine-2',3'-dialdehyde
- ALS – amyotrophic lateral sclerosis
- AMI-1 - 7,7'Carbonylbis (azanediyl)bis(4-hydroxynaphthalene-2-sulfonic acid)
- ANOVA – analysis of variance
- BAC – bacterial artificial chromosome
- BCA – bicinchoninic acid assay
- BIBD – basophilic inclusion body disease
- bp – base pair
- cDNA – complementary DNA
- CMV - cytomegalovirus
- DAPI - 4',6-diamidino-2-
- phenylindole
- dNTP(s) – deoxynucleoside triphosphate
- DMSO – dimethyl sulfoxide
- DSBR – double strand break repair
- DTT – dithiothreitol
- DMEM – Dulbecco's modified Eagle medium
- EC (cells) – electrocompetent
- EDTA - Ethylenediamine tetraacetic acid
- EtBr – ethidium bromide
- fALS – familial amyotrophic lateral sclerosis
- FBS – fetal bovine serum
- FTD – frontotemporal dementia
- FTLD – frontotemporal lobar degeneration
- GFP – green fluorescent protein
- HEK(293) – human embryonic kidney
- hrs – hours
- HRP – horseradish peroxidase
- hnRNP – heterogenous nuclear ribonucleoprotein
- ICC – immunocytochemistry
- IP – immunoprecipitation
- kb – kilobase
- kDa – kilodalton
- LB (broth) – Luria Bertani
- LMN – lower motor neuron
- MALDI-TOF – matrix-assisted laser desorption/ionisation – time of flight
- MND – motor neuron disease
- MQW – milliQ water
- NIFID – neuronal intermediate filament disease
- NLS – nuclear localisation sequence
- O/N - overnight
- PAC – phage artificial chromosome
- PAGE – polyacrylamide gel electrophoresis
- PBS – phosphate buffered sulphate
- PCR – polymerase chain reaction
- PFA - paraformaldehyde
- PFGE – pulse field gel electrophoresis
- RAN – repeat associated non-AU(T)G translation
- RCF – relative centrifugal speed
- RPM – revolutions per minute
- RRM – RNA recognition motif
- RT-PCR – reverse transcribed polymerase chain reaction
- SAP – shrimp alkaline phosphatase
- S / AS – sense / antisense
- SDS – sodium dodecyl sulphate
- siRNA – small interfering RNA
- STEP – sequential insertion of target with overlapping primers
- tau – microtubule associated protein tau
- TBS – tris-buffered saline
- UPS – ubiquitin proteasome system
- UMN – upper motor neuron
- V - volts
- WT – wild type
- ZFN – zinc finger (domain)

1. Chapter One - Introduction

1.1. FUS: An RNA processing protein with important disease links

Originally named for its presence in an oncogenic fusion protein fused in sarcoma (FUS) (also known as translocated in liposarcoma) is a multifunctional RNA binding protein encoded by the *FUS* gene (Crozat et al., 1993; Rabbitts et al., 1993). Encoded across 15 exons at the chromosome 16p11.2 locus, FUS is a 526 amino acid protein containing both RNA and DNA binding domains and, along with EWS and TAF15, comprises the FET family of proteins (FUS, EWS, TAF15) (see Figure 1) (Tan and Manley, 2009).

The FET family of proteins are predominantly located in the nucleus of the cell, although they shuttle back and forth to the cytoplasm, and are expressed in all human fetal and adult tissues so far examined (Andersson et al., 2008; Morohoshi et al., 1998; Tan and Manley, 2009; Zinszner et al., 1997). All three of the FET proteins contain a RNA binding domain (RRM), RGG repeat rich regions likely to bind mRNA, N terminal regions rich in glutamine, glycine, serine and threonine residues, and a zinc finger domain likely to interact with DNA (see Figure 1) (Lagier-Tourenne et al., 2010).

Thirteen alternative FUS transcripts have been reported so far, of these 3 are thought to form coding mRNAs. Two of these transcripts result in proteins predicted to differ in length by a single amino acid by comparison to most frequent FUS transcript (525 and 527 amino acids respectively, compared to 526 for the most commonly described 'usual' FUS transcript). A further coding transcript is predicted to undergo nonsense mediated decay (data from Ensemble and NCBI genomes).

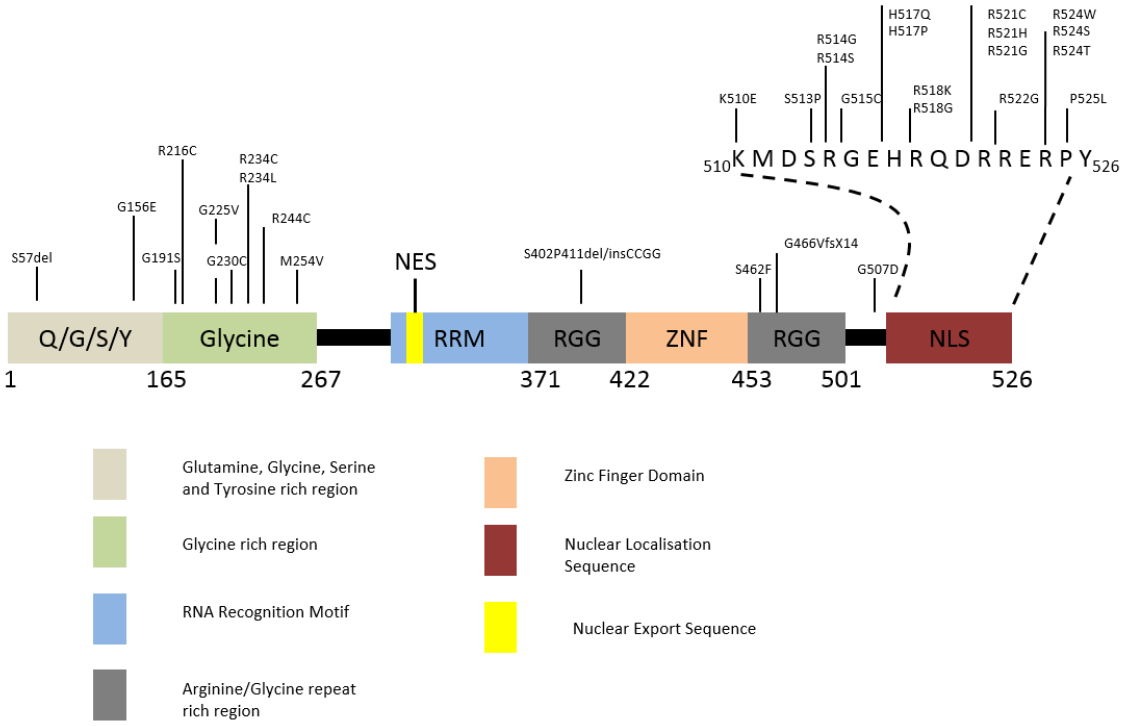

1.1.1. Figure 1 – FUS protein domains and ALS associated mutations

FUS contains several conserved protein domains/motifs, many of which have a role in RNA/DNA binding. The majority of ALS associated mutations in *FUS* cluster within the C-terminal nuclear localisation sequence, although a number are also found in the glycine-rich region, possibly important for protein-protein interactions (Lagier-Tourenne et al., 2010).

So far no functional data describing the impact, or frequency, of these alternative transcripts is available.

Alongside the functional domains described above, FUS also contains a non-classical C-terminal R/HKx$_{2-5}$PY nuclear localisation sequence (PY-NLS) which is responsible for active import of FUS from the cytoplasm to the nucleus through binding to the nuclear import protein transportin/ karyopherin beta 2 (Figures 1 and 2) (Dormann et al., 2010; Lee et al., 2006).

Loss or mutation of this NLS results in an accumulation of cytoplasmic FUS (Dormann et al., 2010). Notably, the PY-NLS is not the only determinant of FUS nuclear import; arginine methylation at the RGG repeat rich region located next to the NLS (see Figure 1) also affects binding to transportin (Dormann et al., 2012). Under normal circumstances asymmetric arginine dimethylation by protein arginine methytransferase 1 and 8 (PRMT 1/8) affects the binding of FUS to transportin in a manner that makes the exact sequence of the NLS critical (see Figure 2) (Dormann et al., 2012; Scaramuzzino et al., 2013). However artificially removing these methyl residues causes the demethylated RGG region to strongly interact with transportin and compensate for the loss of binding affinity at the NLS (See Figure 2) (Dormann et al., 2012). Whether arginine methylation at the RGG motif is utilised to affect the cytoplasmic to nuclear FUS ratio naturally is unclear.

Unsurprisingly, given its domain architecture, FUS has been shown to bind both RNA and DNA (single and double stranded), consistent with a role in RNA processing and transcription (Lagier-Tourenne et al., 2010). Indeed, the manner in which FUS was initially, and then later independently, discovered gives some immediate clues as to its normal role within the cell. In the oncogenic fusion proteins FUS was originally described in, it is the promoter and N terminal region of FUS that fuses with the C terminal domains of DNA binding proteins. This fusion confers a transcriptional activation domain from FUS onto a DNA binding domain of the fusion partner leading to aberrant transcriptional activation – and hence demonstrates a role for FUS in transcription (Prasad et al., 1994). FUS has also been shown to associate with components of the

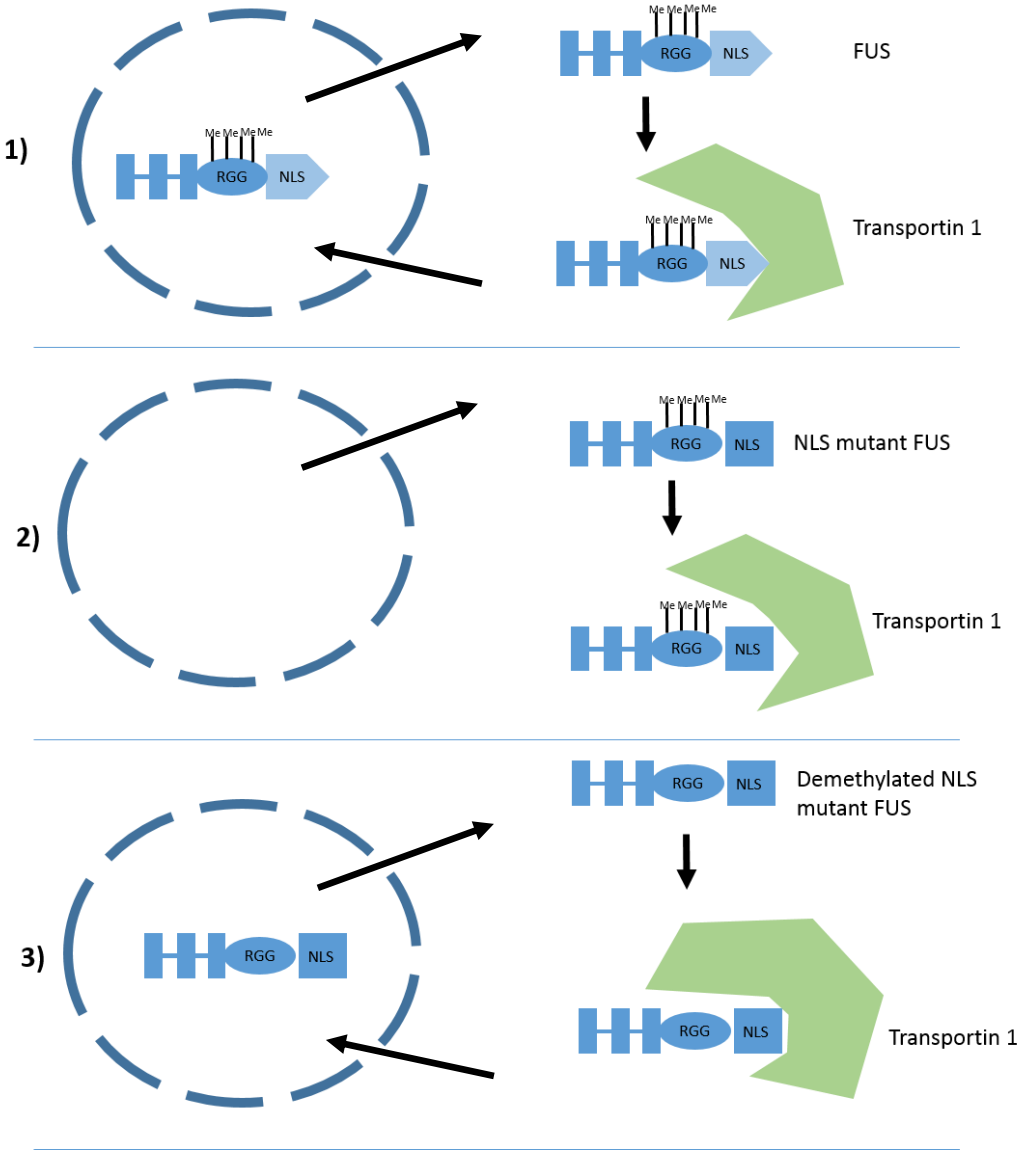

1.1.2. Figure 2 – Import of FUS by Transportin 1 is modified by RGG domain demethylation

1. Under normal conditions the PY-NLS of FUS binds to transportin which actively imports FUS back to the nucleus

2. NLS mutations in FUS prevent binding to transportin 1 causing a loss of FUS in the nucleus (and increased cytoplasmic localisation)

3. Demethylation of arginine residues in the RGG domain of FUS allows transportin 1 to bind FUS even in the presence of NLS mutations

core TFIID transcription complex that forms part of the RNA polymerase II pre-initiation complex as well as with RNA polymerase II itself (Bertolotti et al., 1999; Yang et al., 2000). As well as associating with these core transcription factors FUS also appears to have specific roles in regulating the transcription of certain genes. FUS, for example, acts as a co-activator of NF-κB, playing an important role in regulating NF- κB mediated transcription (Uranishi et al., 2001).Interestingly, FUS also regulates the transcription of the important cell cycle associated gene *cyclin D1* through an unusual mechanism. Binding of non-coding RNAs (ncRNAs), induced by DNA damage, modifies the structure of FUS. The newly modified FUS then inhibits histone acetyl-transferases acting at the *cyclin D1* promoter leading to concomitant transcriptional repression (Wang et al., 2008). As such FUS appears to have both specific, regulatory, and general roles in transcription (Figure 3) (Fiesel and Kahle, 2011).

Furthermore, FUS was independently found as a constituent part of the heterologous nuclear ribonucleoprotein (hnRNP) complex (P2 subunit) suggesting a role in the processing of pre-RNA (Calvio et al., 1995). FUS is also a component of the pre-spliceosomal A complex and shows an enrichment for binding RNA at splice acceptor sites (although with no clear sequence specificity) (Hoell et al., 2011). Knock down of FUS affects spliceosomal gene expression suggesting both an active and passive role for FUS in general pre-mRNA maturation (Fiesel and Kahle, 2011; van Blitterswijk et al., 2013). Notably, FUS appears to also have a role in specific alternative splicing events. Using the well-characterised adenovirus gene E1A as a readout, it has been demonstrated that overexpression of *FUS* promotes the use of a distal 5’ splice site within exon 1 of EA1. Stimulating this alternative splicing event requires both the RRM and RGG repeat regions of FUS, suggesting alternative splicing may be an important role in the normal activity of FUS (Lerga et al., 2001). Notably mutations within the C terminus of *FUS* have been shown to differentially affect the ability of FUS to alternatively splice EA1, whilst RNA-Seq performed on various FUS mutants expressed in HEK293 cells demonstrated changes in target mRNA exon skipping

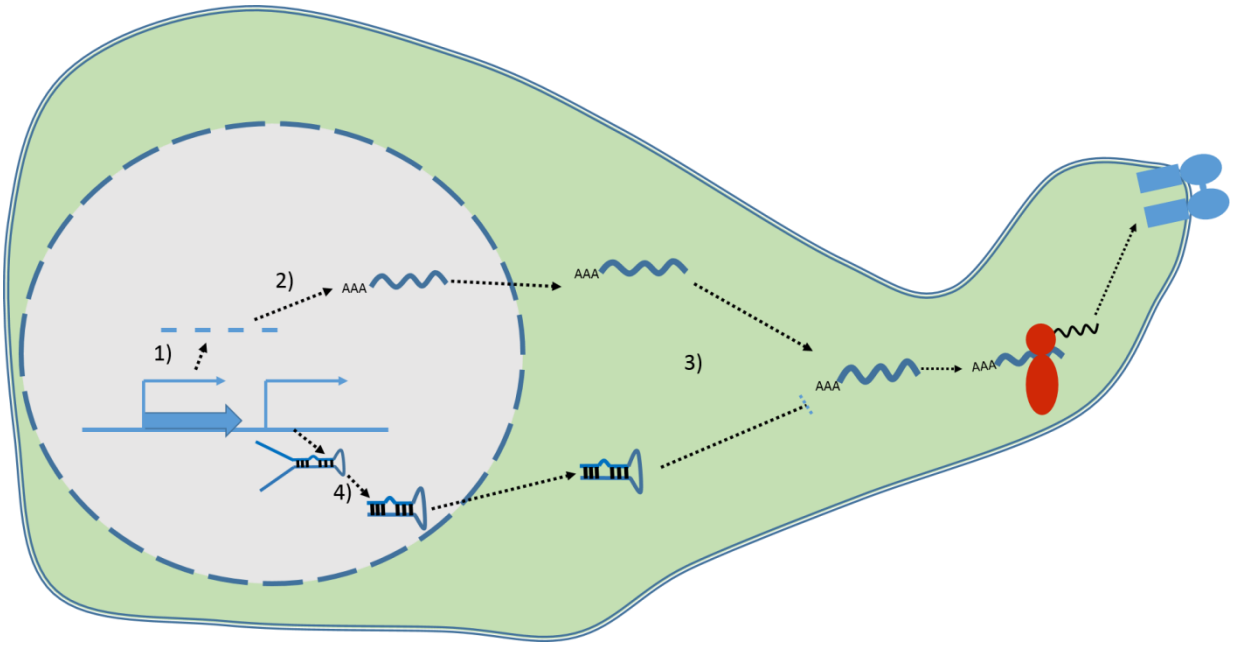

1.1.3. Figure 3 - FUS is an RNA processing protein with multiple nuclear and cytoplasmic roles

1) FUS has both general and specific roles in controlling transcription of genes into pre-mRNA.
2) FUS has a general role in the splicing of pre-mRNA into mature mRNA as well as a role in regulating specific alternative splicing events.
3) FUS appears to have a role in the transport of mRNA to dendritic spines or axonal terminals to allow spatially restricted protein translation and hence correct protein localisation patterns.
4) FUS interacts with Drosha to regulate the production of miRNA from pri-miRNAs, and hence control mRNA stability and translation.

(Kino et al., 2011; van Blitterswijk et al., 2013). It is clear, therefore, that FUS appears to have both a general role in splicing introns from pre-mRNA and in the specific regulation of alternative splicing. FUS appears to also have yet further RNA related roles in the cell: both transport of mRNA to dendritic spines and regulation of miRNA production have recently been added to the list of cellular roles undertaken by FUS (Figure 3). Transport of mRNA prior to translation allows the subcellular localisation of nascent polypeptides to be predetermined and may be of great importance in neurons, where proteins must be trafficked from the cell body to synapses located at the furthest projections. Initiating protein synthesis at the postsynapse of hippocampal neurons through glutamate receptor activation leads to an actin-dependent translocation of FUS to dendritic spines. FUS-mRNA complexes are then seen at these spines, consistent with an active role in nascent mRNA transport (Fujii et al., 2005; Fujii and Takumi, 2005). Recent findings have also demonstrated a general interaction between FUS and the Drosha complex, which is required for microRNA (miRNA) processing (Gregory et al., 2004). Furthermore, FUS appears to contribute toward the production of a specific subset of miRNAs by recruiting Drosha to certain pri-miRNA sites (Morlando et al., 2012). As such, FUS again seems to have both a general and a more specific regulatory role in a key RNA related pathway. In summary, FUS clearly has multiple roles at all levels of RNA processing and appears to have both core and highly specific regulatory functions.

FUS is linked, genetically or pathologically, to two related neurodegenerative diseases, amyotrophic lateral sclerosis (ALS) and frontotemporal dementia (FTD), where it appears to sit at the centre of a pathogenic pathway linking both diseases. Given the central position of FUS in both ALS and FTD many of the key questions in FUS research are currently focussed on the contribution of FUS to a central, unifying, pathogenesis pathway. In order to explore what these key questions might be, a review of ALS and FTD, focussing on the overlapping clinical, pathological and genetic features of these two neurodegenerative diseases is presented below.

In this introduction I will explore:

1. Clinical features/presentations of ALS and FTD
2. Pathological features of, and overlaps between, ALS and FTD
3. Genetic contributions to ALS and FTD
4. Possible molecular mechanisms of pathogenesis in ALS and FTD

I will then go on to explore the role of FUS in the molecular pathogenesis of ALS and FTD in more detail and suggest important questions within this topic that this thesis may help address.

1.2. Amyotrophic lateral sclerosis and frontotemporal dementia

Amyotrophic lateral sclerosis (ALS) is a subtype of motor neuron disease (MND) that affects upper and lower motor neurons causing muscular paralysis and eventual death through respiratory failure in 3 to 5 years (Cleveland and Rothstein, 2001). A prevalence of 2-3 per 100,000 is generally described for ALS, with incidence increasing substantially above the age of 60 – reflected in a median age of onset of 67 – 68 years (Yoshida et al., 1986). ALS is more common in men than women, with a ratio of 1.5:1 reported, and has a clear genetic component; approximately 5–10% of patients have a familial history of ALS (fALS) (Cleveland and Rothstein, 2001; Yoshida et al., 1986). ALS is classically associated with upper and lower limb paralysis due to a loss of motor neurons at all levels of the motor system. Physical manifestations of ALS hence encompass both upper (UMN) and lower motor neuron (LMN) loss and the disease course is characterised by a gradual, insidious, onset and progressive spread of symptoms (Mitchell and Borasio, 2007).

By contrast, frontotemporal dementia (FTD) is the second most common cause of presenile dementia, and includes four clinical subgroups: semantic dementia, progressive nonfluent aphasia,

behavioural variant FTD, and FTD with MND/ALS (Josephs et al., 2011; Snowden et al., 2007). The prevalence of FTD is not entirely clear but has been estimated at 3.6 per 100,000 between the ages of 50 – 59, rising to 9.4 per 100,000 between 60 and 69 before falling to 3.8 per 100,000 at 70 – 79 (Rosso et al., 2003). The overall median age of onset for FTD is approximately 58, with a reported range at onset of 21 to 85 years (Neary et al., 2005). No clear differences between male and female prevalence are seen (Neary et al., 2005; Rosso et al., 2003). Neuropathologically FTD, together with the atypical Parkinsonian disorders progressive supranuclear palsy and corticobasal degeneration, are defined under the bracket of frontotemporal lobar degeneration (FTLD) which is characterised by atrophy of the frontal and temporal brain lobes. For clarity, during this thesis I will refer both the pathological and clinical syndrome as FTD.

1.2.1. Clinical features of ALS and FTD

Patients with FTD present with a range of clinical changes that can be grouped into two main patterns; progressive and gradual changes in either behavioural features or language use (McKhann et al., 2001). Within the possible behavioural changes seen, the most common is a lack of social awareness: many patients show extremely impulsive and socially inappropriate behaviours (McKhann et al., 2001). The behavioural changes seen do not usually fulfil the criteria for a true amnesic syndrome; most patients keep track of day-to-day events and show a relative preservation of memory (McKhann et al., 2001). The early manifestation of behavioural changes is one of the key clinical features that separates FTD from Alzheimer's disease and can lead to FTD being mistaken for disorders such as schizophrenia. The prominence of behavioural changes in this subgroup leads to the term behavioural variant FTD (bvFTD) being used to classify the disorder. An overview of the clinical characteristics used to diagnose FTD is shown in Box 1.

The alternative FTD presentation is that of language dysfunction with a relative preservation of memory (McKhann et al., 2001). Patients displaying language dysfunction can be further split into two clear groups based on the exact linguistic difficulties encountered. Patients who present with

Box 1 – Clinical diagnosis of FTD

Central Diagnostic Criteria

- Progressive onset and gradual disease progression
- Early loss of insight and emotion blunting
- Early decline in modulating behaviour to appropriate social settings
- Early decline in regulating personal conduct

Supportive Diagnostic Criteria

- Behavioural disorders
  - Decline in personal hygiene
  - Lack of mental flexibility and increasingly stereotyped behaviour
  - Lack of persistence at tasks and lack of concentration
  - Hyperorality and changes in diet
  - Cravings for sweet foods
- Speech and Language Disorders
  - Stereotypy of speech
  - Altered speech patterns including aspontaneity and economy of speech.
  - Repetition of the speech output of others
  - Unprovoked repetition of a set response in the absence of a suitable stimulus
  - Mutism
- Physical Signs of FTD
  - Akinesia, rigidity and tremor
  - Primitive reflexes
  - Incontinence
  - Low blood pressure

Investigative Diagnosis Criteria

- Predominant frontal or anterior temporal abnormality in structural or functional imaging
- Normal on conventional electroencephalograms (EEGs)
- Significant impairment in neuropsychiatric tests of frontal lope function

Modified from Neary et al., 2005 (McKhann et al., 2001; Neary et al., 2005)

problems expressing language – word definition is understood, but word selection is compromised – are diagnosed with primary progressive aphasia (PPA). By contrast patients diagnosed with semantic dementia (SD) show compromised understanding of word meaning (McKhann et al., 2001). Notably patients with FTD-FUS tend, despite the sporadic nature of most disease cases, to have a particularly recognisable set of symptoms, which include relatively early ages of onset and very prominent behavioural abnormalities including highly repetitive, stereotyped, ritualistic and even psychotic behaviours. Language defects appear to be less prominent in FTD cases with FUS pathology, perhaps reflecting a predominantly frontal (and caudate) atrophy with a relative sparing of temporal neurons (Mackenzie et al., 2008; Neumann et al., 2009; Snowden et al., 2011; Urwin et al., 2010)(Rohrer and Warren, 2011).

Within ALS, the area of disease onset varies and tends to determine the early symptoms of disease. Bulbar onset leads to slurring of speech and/or difficulty swallowing due to weakness in the tongue and pharyngeal muscles. Cervical onset begins with predominant upper limb symptoms, often first realised in difficulty with shoulder abduction (proximal weakness) or in pincer movement at the hand (distal weakness). By contrast, lumbar onset shows predominant lower motor neuron symptoms often highlighted by tripping or difficulty climbing stairs (Mitchell and Borasio, 2007). A key tenet in the diagnosis of ALS is that symptoms should spread with definite ALS described as showing “lower motor neuron and upper motor neuron signs in three regions” (World Federation of Neurology Research Group on Motor Neuron Diseases. Revised El Escortial criteria). Key clinical features required for a diagnosis of ALS are shown in Box 2, together with frequently described disease symptoms. The highly related syndromes of progressive muscular atrophy and primary lateral sclerosis differ from ALS in having only upper (primary lateral sclerosis) or lower (progressive muscular atrophy) motor neuron involvement (Mitchell and Borasio, 2007). Clinical diagnosis criteria and frequently observed symptoms are summarised in Box 2.

1.2.2. Treatment and care in ALS and FTD

Box 2 – Clinical diagnosis of ALS – El Escorial criteria

Required features for a diagnoisis of ALS;

1. Signs of lower motor neuron degeneration
2. Signs of upper motor neuron degeneration
3. Progressive spread of signs within or between regions

Features absent in order for a diagnosis of ALS to be made;

1. A lack of electrophysiological evidence of other disease that might explain the upper and/or lower motor neuron degeneration
2. A lack of neuroimaging evidence of other disease that might explain the upper and/or lower motor neuron degeneration

Possible Symptoms seen;

1. Weakness and muscular wasting (atrophy)
2. Fasisculations and muscle cramps
3. Spasticity
4. Shortness of breath (dyspnoea)
5. Difficulty swallowing (dysphagia)
6. Difficulty in speech production (dysarthria)
7. Emotional lability
8. Sleep disturbances
9. Constipation
10. Drooling and thick mucous secretions

Modified from Brooks et al, 1994 (Brooks, 1994; Kiernan et al., 2011; Mitchell and Borasio, 2007)

So far no truly effective treatments have been developed for either ALS or FTD (Seltman and Matthews, 2012). Within ALS, Riluzule – an inhibitor of glutamate release – has been used as a pharmacological modifier of disease progress, but only causes limited symptomatic benefits and an average increase in life expectancy of 3 to 6 months (Kiernan et al., 2011). Whilst Riluzole demonstrated that pharmacological interventions may be possible, further drugs tested have proved negative or ambiguous in their benefit to ALS patients and have been reviewed in more detail elsewhere (Gordon et al., 2013). Drug design in FTD has so far focussed on neurotransmitter replacement (glutamate NMDA receptor agonists, serotonin uptake inhibitors and acetylcholinesterase inhibitors have all be used), or are symptomatic treatments utilising already available drugs (Seltman and Matthews, 2012).

As is the case in ALS, pharmacological interventions have been unsuccessful; no FDA approved treatments or disease modifying therapies exist for FTD, despite multiple trials of putative drugs (Seltman and Matthews, 2012). Given the increasing burden, and terrible symptoms, of these conditions in an increasingly aged population the drive to create new drugs is one of great importance.

In the absence of pharmacological treatments in both FTD and ALS, disease care has focussed on the management of symptoms and on social and psychiatric care (Neary et al., 2005). Given the insidious, progressive, and terminal nature of both diseases, social and psychiatric care is often required throughout the disease course, from diagnosis until death. The current lack of biomarkers or clear and quick diagnostic tests for either disease means diagnosis is often slow and uncertain, increasing the need for support networks for patients and carers (Kiernan et al., 2011). Symptomatic management will vary between patients and disease type, but might, as an example, include respiratory support in ALS and the use of antipsychotic drug support in FTD (Boxer and Boeve, 2007; Gordon et al., 2013).

1.2.3. An ALS and FTD disease continuum – clinical overlaps

Whilst at first glance perhaps appearing to be quite different diseases, clinical data have demonstrated for some time that ALS and FTD are highly related conditions, occupying two poles of a disease continuum (Lomen-Hoerth et al., 2002). Up to 50% of ALS sufferers display some degree of cognitive impairment, whilst up to 16% of patients diagnosed with FTD display a motor neuron disease phenotype, usually first recognised by the presence of fasciculations or difficulty swallowing (Hodges et al., 2004; Kertesz et al., 2007; Lomen-Hoerth et al., 2002; Ringholz et al., 2005). Patients presenting with both FTD and ALS symptoms are frequently diagnosed as having a mixed FTD-ALS syndrome (McKhann et al., 2001).

The multiple overlaps between ALS and FTD highlight the possibility that at least one central pathogenesis pathway leading to the onset and progression of these two diseases may be shared. Given the role of FUS in both ALS and FTD it is possible that FUS may act within this shared pathway. Therefore, the pathological and genetic links between the two diseases will now be explored.

1.3. Molecular pathology of ALS and FTD

ALS and FTD share both a loss of neurons and the presence of aggregations of misfolded proteins within affected cells, example images of FTD/ALS patholohgy are shown in figure 4. In FTD it is largely the neurons of the prefrontal and anterior temporal neocortex that are lost (Neary et al., 2005). By contrast, loss of motor neurons and supporting astrocytes is the defining feature of ALS, with aggregations forming in the LMNs of the spinal cord and brainstem and in the UMNs of the corticospinal tract (Barbeito et al., 2004; Matsumoto et al., 1993; Sasaki and Maruyama, 1994). The aggregations in these motor neurons were originally classified by their microscopic appearance,

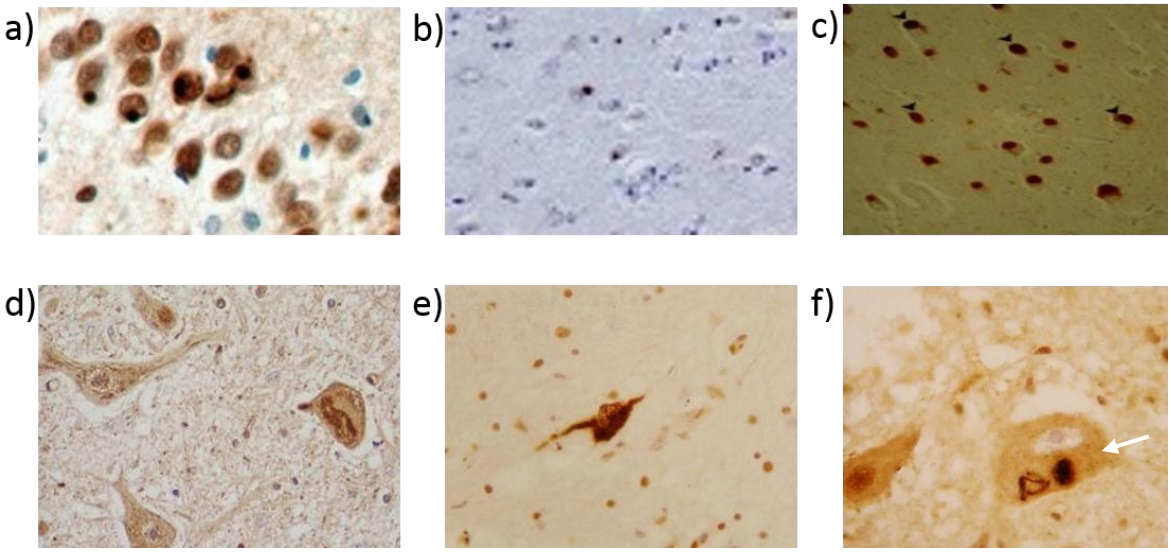

Figure 4 – Molecular pathology in FTD and ALS

a) Immunocytochemistry demonstrates intracytoplasmic FUS inclusions within granular cells of the dentate gyrus in an FTLD case (Seelaar et al., 2010). b) Intracytoplasmic TDP-43 inclusions in an FTLD case (Dopper et al., 2011). c) Rounded Pick bodies containing aggregated Tau within a patient diagnosed with bvFTD (Sieben et al., 2012). d) Ubiquitin immunohistochemistry demonstrates skein like inclusions in the motor neurons of an ALS-SOD1 case. e) Intracytoplasmic FUS is seen in a post-mortem ALS-FUS case. f) Immunohistochemistry to TDP-43 in and ALS-TDP case. A TDP-43 inclusion and concomitant cytoplasmic relocalisation is highlighted by the arrow (Ince et al., 2011) (d,e and f).

.

with the most commonly described types being Lewy body-like inclusions (LBIs), skein-like inclusions and (less specific to ALS) Bunina bodies (He and Hays, 2004; Kawashima et al., 1998; Sasaki and Maruyama, 1994). Within FTD, rounded ubiquitin-positive intraneuronal inclusions and dystrophic neurites, Pick's bodies (tau positive rounded intraneuronal inclusions), neurofibrillary tangles, and cases without any clear histopathological features, were described (Neary et al., 2005). The identity of the constituent proteins found in these inclusions emerged slowly with time and by 2006 neuropathological studies had defined FTD by the presence of two major inclusion types: those immunopositive for tau, and those positive for ubiquitin (FTD-U/FTLD-u) (Forman et al., 2006; McKhann et al., 2001). Likewise, ALS was split into two pathological groups: ALS with aggregations of superoxide dismutase 1 (SOD1, an enzyme that removes superoxide radicals in the cell) and ALS with ubiquitin positive inclusions (Johnston et al., 2000; Mather et al., 1993). Since 2006, key discoveries have shown that aggregations of ubiquitinated 43 Kb TAR DNA binding protein (TDP-43) or fused in sarcoma (FUS), two highly related RNA processing proteins, account for the vast majority of ubiquitin-positive inclusions in both FTD and ALS (Arai et al., 2006; Neumann et al., 2009; Neumann et al., 2006). TDP-43 positive inclusions are present in 90% of cases of FTD-U and non-SOD1 ALS cases (Mackenzie and Rademakers, 2008; Neumann et al., 2006; Seelaar et al., 2010). FUS-positive inclusions account for the majority of remaining ubiquitin-positive TDP-43-negative inclusions in both ALS and FTD (Kwiatkowski et al., 2009b; Neumann et al., 2009). Notably, within FTD, FUS pathology is highly heterogenous, with three related, overlapping but distinct patterns of pathology, aFTLD-u (atypical FTD with ubiquitin positive inclusions), BIBD (basophilic inclusion body disease) and NIFID (neuronal filament inclusion body disease) described depending on the morphology, distribution and staining tendencies of the FUS inclusions present. Briefly, BIBD cases are characterised by the presence of basophilic neuronal cytoplasmic inclusions found predominantly within subcortical regions (Mackenzie et al., 2011b). NIFID is somewhat rarer and is characterised by intracytoplasmic inclusions which stain, alongside FUS, positive for class IV neuronal filament proteins (Mackenzie et al., 2011b). aFTLD-u, the most

Pathological disease divisions	Causative genes	Protein species found in inclusions
ALS-SOD1	*SOD1,* sporadic	**SOD1**, p62, ubiquitin, ubiquilin 2 (Wicks *et al.*, 2009; Deng *et al.*, 2011a; Deng *et al.*, 2011b; Hortobágyi *et al.*, 2011)
ALS-TDP	*TARDBP*, *C9ORF72* *OPTN/* *UBQLN2* Sporadic	**TDP-43**, p62, ubiquitin, ubiquilin 2, optineurin (Mackenzie *et al.*, 2007; Deng *et al.*, 2011b; King *et al.*, 2011)
ALS-FUS	*FUS* *UBQLN2* Sporadic	**FUS**, p62, ubiquitin, ubiquilin 2 optineurin (Bäumer *et al.*, 2010; Deng *et al.*, 2010; Ito *et al.*, 2011; Williams *et al.*, 2012)
FTD-FUS	Unknown, sporadic	**FUS**, p62, ubiquitin, optineurin (Neumann *et al.*, 2009; Seelaar *et al.*, 2010; Ito *et al.*, 2011)
FTD-TDP	*GRN/VCP/* *TDP-43/* *C9ORF72* Sporadic	**TDP-43**, p62, ubiquitin, ubiquilin, ubiquilin 2, optineurin (Neumann *et al.*, 2007; Deng *et al.*, 2011b; King *et al.*, 2011; Brettschneider *et al.*, 2012)
FTD-*MAPT*	*MAPT* Sporadic	**Tau**, p62, ubiquitin (Dickson *et al.*, 2011; Kovacs *et al.*, 2012)

1.3.1. Table 1 – Major pathological disease subtypes in ALS and FTD

Major pathological disease subtypes along the ALS-FTD spectrum are shown from ALS-SOD1 (dark blue), through shared TDP-43 or FUS pathology (light blue/red) to FTD-tau (dark red) at the opposite pole. Associated causative mutations and characteristic inclusion constituents are shown for each pathological subtype. FUS and TDP-43 define large subtypes of both ALS and FTD whilst SOD1 and Tau pathology define distinct pathological subtypes at each end of the continuum (shown in darker blue/red). Notably, the presence of p62 and ubiquitin is shared between all inclusion types.

frequently found subgroup is largely characterised by rounded intracytoplasmic ubiquitin (and FUS) positive inclusions, as well as occasional irregularly shaped intranuclear inclusions (Snowden et al., 2011). All three groups have now been brought under the umbrella of FTLD-FUS, but do appear to be distinct, if closely related subgroups (Mackenzie et al., 2009). Following these seminal discoveries, cases of FTLD-U/ALS-U were renamed to reflect the underlying pathology, for example FTLD-TDP or ALS-FUS (see Table 1) (Mackenzie et al., 2009).

More recently, inclusions containing p62, ubiquilin 2 or optineurin have been found in ALS/FTD cases associated with mutations in the genes encoding their respective proteins as well as in other familial and sporadic cases (Brettschneider et al., 2012; Deng et al., 2011b; Maruyama et al., 2010; Mizuno et al., 2006). Inclusions positive for p62 and ubiquilin 2 appear to be a more general marker of ALS/FTD pathology found in both TDP-43 and SOD1 positive sporadic cases, while optineurin pathology appears to be specific to non-SOD1 forms of disease (see Table 1). (Deng et al., 2011a; Hortobágyi et al., 2011; King et al., 2011; Maruyama et al., 2010)

Considering the wide range of inclusion types additionally immunopositive for p62 and ubiquilin 2, it is tempting to view the pathways involved as shared between the different ALS/FTD subtypes, in a manner similar to ubiquitination. Ubiquitin, p62 and ubiquilin 2 all have a role in clearing proteins from the cell and so it is possible that their presence in inclusions represents failed attempts to remove aggregated proteins rather than a primary cause of protein aggregation (Bence et al., 2001; Ciechanover and Brundin, 2003; Ko et al., 2004; Moscat and Diaz-Meco, 2009). However, as discussed later, the presence of mutations in the genes encoding p62 (*SQSTM1)* and ubiquilin 2 (*UBQLN2)* suggest that both may have a more direct role in disease pathogenesis (Deng et al., 2011b; Fecto et al., 2011). Similarly, although less widespread, the importance of optineurin pathology is also supported by the presence of disease associated mutations in the optineurin gene, *OPTN* (Maruyama et al., 2010).

1.4. Genetics of ALS and FTD

1.4.1. Loci Linked to both ALS and FTD

Genetic links between ALS and FTD were first noted by the presence of several cases of familial ALS-FTD with, in some cases, even a change of phenotype from FTD to ALS between generations (Gunnarsson et al., 1991; Hudson, 1981). Multiple specific genetic links between ALS and FTD have now been described - the genes underlying these links, together with central genes involved in ALS or FTD alone, are listed together with their functions, clinical phenotypes and frequencies, inheritance patterns and associated neuropathology in Table 2.

Mutations in *TARDBP*, which encodes TDP-43, are responsible for 4-6% of non-SOD1 familial ALS cases and around 1% of apparently sporadic ALS (Andersen and Al-Chalabi, 2011). Furthermore, rare mutations in *TARDBP* are also causative for FTD (Borroni et al., 2009; Kovacs et al., 2009; Lagier-Tourenne et al., 2010). It should, however be noted that very few *TARDBP* mutations have been described in FTD, and that studies demonstrating *TARDBP* mutations in pure FTD cases have not provided sufficient evidence (either a lack of segregation analysis or suitably large control numbers) for the causative nature of these mutations (Borroni et al., 2009; Synofzik et al., 2013). A rare report of a *TARDBP* 3' UTR variant in multiple affected families, provides some evidence for a pathogenic nature, however a lack of control numbers, segregation analysis, and the fact that the variant is within a non-coding area all argue against accepting causality as a given (Gitcho et al., 2009a). Care should therefore be given before stating that *TARDBP* mutations are definitively causative for FTD, although increasing numbers of *TARDBP* variants in FTD do suggest a likely disease-association (Benajiba et al., 2009; Borroni et al., 2010; Borroni et al., 2009; Kovacs et al., 2009). Mutations in *FUS*, a pathological protein involved in both diseases, are causative of approximately 1% and 4% of apparent sporadic and familial ALS, respectively, but are yet to be shown definitively to be causal for FTD; only a single case of FTD with *FUS* mutations has been

putatively assigned (Chio et al., 2011; Kwiatkowski et al., 2009b; Lai et al., 2011; Van Langenhove et al., 2010; Vance et al., 2009). In a significant recent discovery expanded GGGGCC hexanucleotide repeats in the first intron of the *C9ORF72* gene have been shown to segregate in FTD, ALS and FTD-ALS cases (Dejesus-Hernandez et al., 2011b; Renton et al., 2011).

C9ORF72 encodes a protein of relatively unknown function; however, the prevalence of repeat expansions within both ALS and FTD make *C9ORF72* expansions one of the most exciting recent discoveries in the ALS and FTD field. More than 30 GGGGCC repeats within *C9ORF72* are classified as pathological, however this estimate may stem more from technical difficulties using repeat primed RT-PCR than from the actual length of expansion seen in disease cases (Carrasquillo et al., 2010; Renton et al., 2011). Southern blots have generally found disease-associated expansions to be of between 700 and 1600 repeats (Dejesus-Hernandez et al., 2011b). Recent reports have suggested, through bioinformatics, that C9ORF72 may be related to the DENN (differentially expressed in normal and neoplastic cells) family of proteins and may function as a GDP/GTP exchange factor to activate Rab GTPases and regulate membrane trafficking (Levine et al., 2013). However the role of the C9ORF72 protein, suggested to now be referred to as DENNL72, has yet to be proved *in vivo* or *in vitro*.

Estimates for the prevalence of expanded *C9ORF72* repeats in ALS and FTD have consistently shown that the locus represents, in at least some populations, the single greatest genetic cause of ALS, FTD and ALS-FTD (Dickson et al., 2011; Kim et al., 2012). Studies in European, Northern American and Australian populations have suggested an overall average frequency of around 35% in familial ALS and 8% in sporadic ALS, with prevalence rising as high as 83% and 73% in Belgian and Swedish cohorts respectively (Cook et al., 2012b; Dejesus-Hernandez et al., 2011b; Dickson et al., 2011; Dormann et al., 2012; Gijselinck et al., 2012; Kim et al., 2012; Majounie et al., 2012; Renton et al., 2011).

Mutated Gene	Function	Clinical phenotype	Mode of Inheritance	Neuropathology in mutation cases
C9ORF72	DENN protein (Levine et al., 2013)	ALS (+++), FTD (+++), FTD-ALS (+++) (Dejesus-Hernandez *et al.,* 2011; Renton *et al.,* 2011; Majounie *et al.,* 2012)	Dominant	ALS/FTLD-TDP (Simón-Sánchez *et al.,* 2012)
TARDBP	RNA processing protein (Lagier-Tourenne et al., 2010)	ALS (++), FTD (+), FTD-ALS (+) (Kabashi *et al.,* 2008; Sreedharan *et al.,* 2008; Benajiba *et al.,* 2009; Borroni *et al.,* 2009)	Dominant, recessive	ALS-TDP (Van Deerlin et al., 2008)
VCP	Protein turnover via UPS and autophagy (Dai and Li 2001)	ALS (++/+), FTD (+*), FTD-ALS (+) (Guyant-Marechal *et al.,* 2006; Gitcho *et al.,* 2009; Johnson *et al.,* 2010)	Dominant	ALS/FTLD-TDP (Gitcho et al., 2009)
FUS	RNA processing protein (Lagier-Tourenne et al., 2010)	ALS (++), rare FTD (Kwiatkowski et al., 2009; Vance et al., 2009; Blair *et al.,* 2010; Van Langenhove *et al.,* 2010)	Dominant, recessive	ALS-FUS (Mackenzie et al., 2011)
UBQLN2	Protein turnover via UPS and autophagy (Ko et al., 2004)	ALS (+), FTD-ALS (+) (Deng et al., 2011b)	Dominant (X-linked) in ALS	ALS-TDP/ALS-FUS (Deng et al., 2011b)
SQSTM1	Autophagy, inflammation and apoptosis (Moscat and Diaz-Meco 2009)	ALS (+), FTD (+) (Fecto *et al.,* 2011; Rubino *et al.,* 2012)	Unclear, segregation yet to be shown	Unclear

1.4.2. Table 2 – Shared Genetic Contributions to ALS and FTD

The normal cellular function, associated clinical phenotype, frequency in disease, mode of inheritance and associated neuropathology are shown for genes linked to both ALS and FTD. Notably segregation analysis has yet to be performed for *SQSTM1* associated cases meaning these mutations may act as risk factors rather than causative mutations.

+ Mutations are usually a rare cause of the disorder (>2% of familial cases)

++ Mutations in the gene are generally causative for familial forms at a reasonable frequency (2-8 % of familial cases)

+++ Mutations are often a common cause of familial disease (>8%)

* VCP mutations are more often described as part of the mixed disorder inclusion body myopathy associated with Paget's disease of the bone and frontotemporal dementia (IBMPFD).

By comparison the frequency of expanded *C9ORF72* repeats in Japanese and Chinese ALS populations appears to be much lower (<5%), consistent with recent suggestions of an initial founding effect due to the repeat expansion arising once within northern Europe (Cook et al., 2012b; Dormann et al., 2012; Kim et al., 2012; Lagier-Tourenne et al., 2012). Fewer studies of the prevalence of expanded *C9ORF72* repeats in FTD cohorts have been published but prevalence again seems to be very high with an average of around 20% and 8% suggested for familial and sporadic European populations, respectively (Dejesus-Hernandez et al., 2011b; Dickson et al., 2011; Gijselinck et al., 2012; Majounie et al., 2012; Renton et al., 2011; Snowden et al., 2012; van der Zee et al., 2013).

At lower frequencies, mutations in the valosin containing protein (V*CP*) gene lead to both ALS and FTD (Johnson et al., 2010; Mackenzie et al., 2010). Evidence for the causative nature of *VCP* mutations in pure FTD cases remains relatively weak, although *VCP* mutations do appear to cause the mixed IBMPFD disorder that presents with symptoms of FTD and *in vivo* and *in vitro* data supports a causative link in ALS cases (Bartolome et al., 2013; Nalbandian et al., 2013). Similarly mutations in *SQSTM1*, encoding the p62 protein, have been described in both ALS and FTD cases, although segregation analysis has yet to be performed in either ALS or FTD families. As such, *SQSTM1* mutations may function as risk factors rather than being directly pathogenic (Fecto et al., 2011; Rubino et al., 2012). Furthermore *UBQLN2,* encoding ubiquilin 2, has recently been linked to ALS, ALS-FTD and FTD at relatively low frequencies (see Table 2). Whilst rare in many populations, segregation of *UBQLN2* mutations in ALS pedigrees has been demonstrated, providing good evidence of causality (Deng et al., 2011b; Gellera et al., 2013; Williams et al., 2012b). Whilst *UBQLN2* mutations have been described in FTD, they appear to be extremely rare and are yet to be shown to definitively lead to disease (Lattante et al., 2013; McLaughlin et al., 2014; Synofzik et al., 2012).

1.4.3. Loci linked primarily to FTD

Mutations in the gene progranulin (*GRN*) cause a substantial number of FTD cases; upwards of 20% of familial FTD and around 5% of sporadic cases (Table 3) (Baker et al., 2006; Cruts et al., 2006; Pickering-Brown et al., 2006; Snowden et al., 2006). Pathologically, FTD with *GRN* mutations is characterised by TDP-43 positive inclusions, but overlaps with ALS are generally rare (Beck et al., 2008; Chen-Plotkin et al., 2011; Schymick et al., 2007). Given that mutations in *GRN* lead to TDP-43 pathology, which underlies much of ALS and FTD, the paucity of *GRN* mutations in ALS compared to FTD is somewhat surprising and may reveal key differences between the susceptibility of different neuronal populations (motor vs. cortical/hippocampal) to specific cellular insults.

Mutations in the gene microtubule associated protein tau (*MAPT*) lead to FTD-tau and FTDP-17 (frontotemporal dementia with Parkinsonism linked to chromosome 17). Notably, *MAPT* genetic variants are also associated with Parkinson's disease, whilst the tau protein is pathologically linked to Alzheimer's disease through tau tangle formation (Table 3) (Michel, 1993; Wider et al., 2010; Wszolek et al., 2006). Finally, mutations in CHMP2B (encoding charged multivesicular body protein 2 b) lead to cases of FTD without TDP-43, FUS or tau positive inclusions, but have so far only been identified in a single Danish family (Isaacs et al., 2011). The full genetic basis of FTD, including selected associated genes with unclear pathogenicity, but interesting links to other neurodegenerative disorders or pathogenesis pathways, is summarised in table 3 (AD and FTD mutation database; Baker et al., 2006; Gass et al., 2006; Gitcho et al., 2009b; Guyant-Marechal et al., 2006; Hu et al.; Isaacs et al., 2011; Neary et al., 2005; Rohrer and Warren, 2011; Seelaar et al., 2011; Stanford et al., 2004).

Gene	Protein	Inheritance Pattern	Locus	Comment
MAPT	Microtuble associated protein tau	AD	17q21.32	Associated with FTDP-17. Frequent
GRN	Progranulin	AD	17q21.1	Frequent
TARDBP	TAR DNA binding protein (TDP-43)	AD/AR	1q36	Infrequent, few mutations described.
C9ORF72	Chromosme 9 open reading frame 72/DENNL72	AD	9p13.2-21.3	Very frequent
CHMP2B	Charged multivesicular body protein 2B	AD	3q11.2	Found only in a single Danish family, associated with an unusual molecular pathogenesis
PSEN1	Presenilin 1	AD, incomplete penetrance	14q24.3	Mainly associated with AD. Few mutations described, unclear role in FTD
VCP	Valosin containing protein	AD	9p13.3	Associated with IBMPFD
FUS	Fused in sarcoma	-	16p11.2	Only one mutation of unproven pathogenicity described
SQSTM1	p62	-	5q35.3	Unclear pathogenicity, perhaps risk factor

1.4.4. Table 3 – The Genetic Basis of FTD

Genes associated with FTD are shown together with their encoded proteins, inheritance pattern and genetic locus (Cruts et al., 2006; DeJesus-Hernandez et al., 2011a; Guyant-Marechal et al., 2006; Isaacs et al., 2011; Pickering-Brown et al., 2006; Renton Alan et al., 2011; Rohrer and Warren, 2011; Seelaar et al., 2011; Snowden et al., 2006; Weihl et al., 2009).

1.4.5. Loci linked primarily to ALS

As with FTD, mutations in several genes cause ALS almost exclusively. The most common of these exclusively ALS-linked genes is *SOD1* (superoxide dismutase 1) (Battistini et al., 2005; Pasinelli and Brown, 2006; Rosen et al., 1993). Similar to *MAPT* mutations in FTD, SOD1-linked ALS has a pathology separate to that of other ALS cases; inclusions positive for SOD1 and negative for TDP-43 or FUS are seen (Cleveland and Rothstein, 2001). Mutations in the *OPTN* (optineurin), *SQSTM1* (p62) and *UBQLN2* (ubiquilin 2) genes have all been described in ALS, while deposition of the proteins encoded by their respective genes have been found in cases with and without mutations. It should, however, be noted that the frequency of *UBQLN* and *OPTN* (especially in European populations) mutations in ALS cases is low, whilst segregation analysis is yet to be performed for *SQSTM1* mutations (Renton et al., 2014). The associated functions, pathology and inheritance patterns for these genes are shown in Table 1 and 2 whilst their genetic contributions to disease are shown in Tables 2 and 4. Mutations in various other genes have been linked to ALS including *Alsin* (*ALS2*), *senataxin* (*SETX*), *vesicle-associated membrane protein- (VAMP)-associated-protein protein B/C* (*VAPB)*, *angiogenin* (*ANG*) and *ataxin-2* (*ATXN2*) (Andersen and Al-Chalabi, 2011). Notably, the evidence of causality in some of these cases, such as *ANG*, *SETX* and *VAPB* is questionable with few families described, a lack of segregation analysis or too low control numbers (Renton et al., 2014). Many genes in which variants are discovered in ALS (and FTD) patients appear to be ascribed disease causing status before sufficient evidence is available, attention is drawn to a review of the current state of evidence for ALS genes (Renton et al., 2014). Most notable of these genes, within the scope of this thesis, is *ATXN2* which encodes a polyglutamine (polyQ) protein also associated with spinocerebellar ataxia type2 (SCA2). The presence of greater than 34 polyQ repeats in *ATXN2* leads to SCA2 while intermediate repeat numbers (23-34) are strongly associated with ALS (Elden et al., 2010). A full list of genes causative for ALS is shown in Table 4.

Gene	Protein	Inheritance Pattern	Locus	Name of Disease/ Comment
SOD1	Cu/Zn superoxide dismutase	AD/AR	21q22	ALS1, frequent
ALSin	ALSin	AR	2q33	ALS2, not true ALS
SETX	Senataxin	AD	9q34	ALS4, weak evidence
SPG11	Spatacsin	AR	15q15-21	ALS5
FUS	Fused in sarcoma	AD/AR	16p11.2	ALS6, frequent
VAPB	VAMP-associated protein B/C	AD	20q13	ALS8, not replicated
ANG	Angiogenin	AD	14q11	ALS9, unclear evidence
TARDBP	TAR-DNA binding protein	AD	1q36	ALS10, frequent
FIG4	PI(3,5)P(2)5-phosphatase	AD	6q21	ALS11, not replicated
OPTN	Optineurin	AD/AR	10p13	ALS12, rare in Europe
ATXN2	Ataxin 2	AD	12q24	ALS13
VCP	Valosin containing protein	AD	9p13-p12	ALS14
C9ORF72	Chromosome 9 open reading frame 72/DENNL72	AD	9p13.2-21.3	ALS-FTD2, very frequent
MAPT	Microtubule associated protein tau (tau)	AD	17q21.1	ALS-FTDP, not pure ALS
UBQLN2	Ubiquilin 2	Dominant	Xp11.21	ALS-X, X-linked, rare

1.1.1. Table 4 – The genetic basis of ALS

Selected genes linked to ALS are shown alongside their encoded proteins, inheritance pattern, genetic locus and disease name.

(Andersen and Al-Chalabi, 2011; Belzil et al., 2009; Dejesus-Hernandez et al., 2011b; Del Bo et al., 2011; Deng et al., 2011a; Deng et al., 2011b; Elden et al., 2010; Fecto et al., 2011; Hirano et al., 2011; Johnson et al., 2010; Kabashi et al., 2008; Kiernan et al., 2011; Kwiatkowski et al., 2009b; Renton et al., 2011; Rosen et al., 1993; Rubino et al., 2012; Schymick et al., 2007; Tümer et al., 2012; Van Langenhove et al.; Vance et al., 2009; Williams et al., 2012a; Wu et al., 2012; Wu et al., 2007).

It should be noted that many further genes have been associated with ALS but have unproved pathogenicity, such as *SQSTM1*, and are listed elsewhere (Andersen and Al-Chalabi, 2011). Notably, as discussed in more detail below, these ALS- and FTD-linked genes segregate into two major functional groups; those associated with RNA processing and those involved in protein degradation pathways. The convergence of ALS and FTD genes into these pathways highlights RNA processing and cargo specific autophagy as central to the pathogenesis within the ALS/FTD continuum.

1.5. Pathogenesis Pathways – RNA processing at the centre of an ALS-FTD disease continuum

Genetic and pathological analysis has therefore demonstrated that *TARDBP*, *FUS* and *C9ORF72* are at the centre of the ALS-FTD spectrum. Notably all three genes may share a common link to cellular RNA dynamics.

1.5.1. FUS and TDP-43 link RNA processing to ALS and FTD

The evidence for the involvement of TDP-43 and FUS in RNA-related pathways is strong; both are RNA processing proteins with roles in multiple steps of RNA regulation including RNA transcription, splicing, transport, translation and microRNA production (Figure 2) (Lagier-Tourenne et al., 2010).

Indeed, dual knockdown experiments in zebrafish suggest that TDP-43 and FUS operate within the same disease-associated pathway, with FUS acting downstream of TDP-43 (Kabashi et al., 2011).

The role of FUS and TDP-43 in RNA processing is mediated through direct interaction with RNA. Both FUS and TDP-43 bind RNA via two RNA recognition motif (RRM) protein domains (Hoell et al., 2011; Tollervey et al., 2011). TDP-43 binding sites are found in the RNA encoding TDP-43*,* FUS, and other RNA processing proteins such as poly(A)-binding protein cytoplasmic 1 (PABPC1), suggesting TDP-43 and FUS may participate in a large co-regulatory network (Sephton et al., 2011). Down-regulation of TDP-43 in the mouse brain has been shown to reduce levels of FUS by 60% suggesting feedback and crosstalk mechanisms are required to maintain precise expression levels across this network (Polymenidou et al., 2011; Sephton et al., 2011; Tollervey et al., 2011). Notably, TDP-43 RNA targets include genes important for synaptic function, neurotransmitter release and the neurodegeneration related genes progranulin (*GRN),* α-synuclein (*SNCA),* tau *(MAPT)* and ataxin 1 and 2 (*ATXN1/2)* (Polymenidou et al., 2011; Sephton et al., 2011). Dysfunction in this complex network of RNA binding proteins is, therefore, likely to have severe downstream consequences. It is, however, important to note that FUS and TDP-43 have many thousands of targets within the genome; TDP-43, for example, has binding sites in approximately 30% of transcribed mouse genes (Polymenidou et al., 2011). Individual studies have highlighted different sets of genes targeted by these RNA binding proteins making the physiological importance of single reported interactions difficult to understand without further molecular insights (Polymenidou et al., 2011; Sephton et al., 2011; Tollervey et al., 2011). A recent study has, however, cast some light on transcripts regulated by both FUS and TDP-43, and hence likely central to understanding the downstream effects of FUS/TDP-43 dysfunction that leads to ALS/FTD. Whilst FUS and TDP-43 have largely distinct binding patterns - only 86 shared gene regulation events were highlighted in the study – genes that are regulated by both FUS and TDP-43 are highly enriched for the presence of very long introns (Lagier-Tourenne et al., 2012). Notably the co-regulated genes in this study also were enriched for neuronal functionality, suggesting a conserved role for FUS and TDP-43 in maintaining levels of neuronal proteins whose pre-RNA feature

elongated introns (Lagier-Tourenne et al., 2012). Aside from affecting mRNA translation, FUS and TDP-43 also have clear roles in alternative splicing with, for example, knockdown of TDP-43 in SH-SY5Y cells leading to 228 splicing changes amongst genes containing alternative isoforms (Tollervey et al., 2011). Interestingly, TDP-43 activity is required for inclusion of exon 18 of *sortilin 1. Sortilin 1* encodes a receptor for progranulin, although not the receptor mediating the effects of progranulin on neurite outgrowth, and regulates progranulin levels, providing a possible link between TDP-43 RNA processing dysfunction and disease (Gass et al., 2012; Polymenidou et al., 2011; Rubino et al., 2012; Xi et al., 2012). It is clear, therefore, that a loss, or aberrant gain, of RNA processing function due to defects in FUS or TDP-43 action may have a serious impact on cellular health – especially within neuronal tissue.

1.5.2. *C9ORF72* RNA foci may lead to dysfunctional RNA processing

Further to the clear role of TDP43 and FUS in RNA pathways, the recent discovery of the *C9ORF72* hexanucleotide expansion in ALS and FTD has provided additional evidence that impairment of RNA processing could be a general mechanism of disease in ALS and FTD. Abnormal intranuclear RNA foci containing the expanded *C9ORF72* RNA transcript have been described in cases of FTD with *C9ORF72* mutations (DeJesus-Hernandez et al., 2011a; Lee et al., 2013; Zamiri et al., 2013). The formation of RNA foci has previously been suggested to sequester RNA binding proteins impairing their function (Miller et al., 2000; Simón-Sánchez et al., 2012). Indeed, the hexanucleotide motif of *C9ORF72* has been predicted *in silico* to interact with the A2/B1 regions of the hnRNP complex which contains FUS and directly interacts with TDP-43 (Buratti et al., 2005; Dejesus-Hernandez et al., 2011b; Iko et al., 2004). Recent data has repeatedly demonstrated the formation of repeat length dependent intranuclear C9ORF72 RNA foci which appear to be able to bind RNA binding proteins such as ASF/SF2, hnRNPA1 and hnRNP-H (Lee et al., 2013; Zamiri et al., 2013). Furthermore, *in vitro* studies have demonstrated that these foci may be neurotoxic (Lee et al., 2013). It is, however, not yet clear how the sequestering of RNA-binding proteins in the nucleus could lead to the more widespread

cytoplasmic aggregates of TDP-43 found in cases with the *C9ORF72* mutation (Dejesus-Hernandez et al., 2011b; Hsiung et al., 2012). Expanded RNA repeats have, however, been described as sequestering RNA binding proteins in various other neurological disorders. In myotonic dystrophy, the most common adult onset muscular dystrophy, expression of RNA containing either expanded CUG or CCUG repeats leads to the presence of nuclear RNA foci and the sequestering of RNA binding proteins such as the splicing regulator Musclebind-like-1 (MBNL1) (Jiang et al., 2004; McKhann Gm, 2001; Miller et al., 2000; Rosso et al., 2003; Yoshida et al., 1986). As a direct result of MBNL1 sequestration downstream genes such as *BIN1* have been shown to be mis-spliced, with these alterations in *BIN1* splicing shown to lead to muscle weakness and T tubule alterations in mouse models (Nakashima-Yasuda et al., 2007). The possible parallels between this example and *C9ORF72*, FUS, and TDP-43 are clear.

A further possibility for the mechanism of toxicity in C9ORF72-associated FTD and ALS was recently highlighted by the discovery of aggregated dipetides, resulting from translation of the GGGGCC repeats through a repeat associated non-AUG translation mechanism known as RAN translation, in post-mortem tissue. These dipetides, resulting from either sense or antisense translation of the RNA repeat expansion, are found in the p62/ubiquitin positive, TDP-43 negative inclusions which characterise C9ORF72-asscoiated ALS/FTD (Mann et al., 2013). Further molecular details of this mechanism are review elsewhere (Gendron et al., 2014)

Additional links between RNA processing and neurodegeneration were recently provided by the discovery of mutations in the *EXOSC3* gene, which encodes a component of the RNA exosome complex, in pontocerebellar hypoplasia and spinal motor neuron degeneration (Wan et al., 2012). Given the current rate of discovery of mutations in RNA processing protein genes in neurodegenerative disease, dysfunction of RNA processing is clearly evolving into a central theme within neurodegeneration. This association appears to be especially common in conditions affecting motor neurons, with *TARDBP, FUS*, *C9ORF72* and *EXOSC3* adding to information previously gained

from *SMN* (survival of motor neuron) within the motor neuron condition spinal muscular atrophy (Lefebvre et al., 1995; Wan et al., 2012). Within the ALS-FTD continuum overall, dysregulation of RNA processing, either through repeat expansions at the *C9ORF72* locus or mutations in the *FUS* and *TARDBP* genes, appears to be of great importance.

1.6. Clustering of ALS and FTD linked genes into protein degradation pathways highlights a further possible pathogenesis pathway

The protein degradation machinery of the cell has long been demonstrated to be of critical importance in dealing with the misfolded and aggregated proteins that define many neurodegenerative disorders (Rubinsztein, 2006). Two major pathways for protein recycling are seen in the cell; the ubiquitin-proteasome system (UPS), where proteins are specifically targeted for destruction within the proteasome by the addition of poly-ubiquitin residues, and macroautophagy, where long-lived proteins and organelles are sequestered within autophagosomes which then fuse with lysosomes leading to the degradation of vesicle cargo. Knockout of the key autophagy gene *Atg7* in a mouse model led to severe neurodegeneration and the accumulation of poly-ubiquitinated aggregates, demonstrating both the importance of autophagy within long-living non-dividing neuronal cells, and its relevance to neurodegenerative disease (Komatsu et al., 2006). Furthermore, several neurodegeneration-linked genes, for example *GBA* and *LRRK2* in Parkinson's disease and *OPTN* and *SQSTM1* in ALS/FTD have been linked to autophagy (Alegre-Abarrategui et al., 2009; Bjørkøy et al., 2006b; Velayati et al., 2010; Wild et al., 2011). The possible involvement of the UPS in neurodegeneration is highlighted by the ubiquitination of aggregates in multiple disorders, and through, as discussed later, the presence of mutations in *UBQLN2* and *VCP* in ALS and FTD. Although

clear evidence of a causal role of UPS defects in neurodegeneration has been elusive, various pieces of evidence have linked protein aggregate toxicity to UPS defects and have been reviewed in detail elsewhere (Dennissen et al., 2012). Importantly, TDP-43 aggregations appear to be degraded through both autophagy and the UPS, meaning both pathways could be of relevance to ALS/FTD pathogenesis (Brady et al., 2011).

1.6.1. Ubiquilin 2, p62, Optineurin and VCP highlight aggrephagy as a central ALS/FTD pathway

Four genes, *UBQLN2*, *SQSTM1*, *OPTN* and *VCP,* linked to ALS and/or FTD have strong links to protein degradation pathways, highlighting this important pathway as central to pathogenesis within the ALS-FTD continuum.

1.6.1.1. Ubiquilin 2/ *UBQLN2*

Ubiquilin 2 is a member of the four-strong ubiquilin family of proteins which regulate the destruction of ubiquitinated proteins via the UPS or autophagy. Ubiquilin family proteins all contain both a ubiquitin-like and ubiquitin-associated domain (UBL/UBA) (Ko et al., 2004). The ubiquitin-like domain is responsible for binding proteasome subunits, whilst the ubiquitin-associated domain functions in binding poly-ubiquitin chains, suggesting ubiquilin proteins function in the recognition and transport of ubiquitinated proteins to the proteasome for destruction (Ko et al., 2004). Furthermore, ubiquilin also appears to function in autophagy through binding the autophagosomal protein LC3, to transport certain ubiquitinated cargoes or aggregates to the autophagosome for degradation (Rothenberg et al., 2010). Rare mutations in *UBQLN2* have been linked to ALS and ALS-FTD and have been suggested to lead to an impairment of protein degradation by the UPS, perhaps reducing clearance of aggregated proteins (Deng et al., 2011b). Pathologically, ubiquilin 2 co-localises with TDP-43 and FUS, suggesting ubiquilin 2 acts within the pathway required for degradation of TDP-43 and FUS aggregations and remains trapped in aggregates that are not degraded (Deng et al., 2011b; Williams

et al., 2012b). As such, ubiquilin 2 loss of function could impact upon the clearance of spontaneously forming ALS/FTD aggregates. Notably, *UBQLN1,* encoding a further member of the ubiquilin family, has strong links to neurodegenerative conditions (Mah et al., 2000). Ubiquilin pathology has recently been suggested to be present, and act as a marker, in ALS and FTD-TDP cases with *C9ORF72* expansions (Brettschneider et al., 2012).

1.6.1.2. p62/ *SQSTM1*

Notably, p62, another protein linked to ALS and FTD and involved in protein degradation pathways, has also been shown to bind poly-ubiquitin chains. Unlike ubiquilin 2, p62 appears to function in autophagy only, acting as a cargo receptor recruiting large poly-ubiquitinated aggregates to autophagosomes (Bjørkøy et al., 2005, 2006). *In vivo,* p62 coats TDP-43 inclusions, and p62 overexpression has been reported to reduce the formation of TDP-43 aggregates (Brady et al., 2011). As such, depletion of p62 might be expected to lead to the formation of intracellular aggregates. However, in an apparent contrast p62 also appears to have a role in aggregate formation. Autophagy-mediated degradation of p62 is required to prevent the build-up of ubiquitinated p62-containing aggregates (Komatsu et al., 2007). Furthermore, p62/*SQSTM1* knockdown in autophagy deficient mice suppresses the formation of ubiquitinated protein aggregates within neurons (Komatsu et al., 2007). As such, maintaining 'homeostatic levels of p62' may be important in both the formation, marking for autophagic destruction, and subsequent fusion of aggregates with autophagosomes (Komatsu et al., 2007).

1.6.1.3. Optineurin/ *OPTN*

Remarkably, in a manner similar to p62 and ubiquilin 2, optineurin seems to act as an "autophagy receptor", binding ubiquitinated aggregations to direct them to autophagosomes (Wagner et al., 2008; Wild et al., 2011). Optineurin, like p62, contains a LC3 interacting motif allowing direct binding of LC3 at autophagosomal membranes (Wild et al., 2011). ALS-associated mutations in *OPTN* appear

to affect ubiquitin binding motifs, suggesting that loss of ubiquitin binding activity is the pathogenic feature of *OPTN* mutations in ALS (Maruyama et al., 2010). It would therefore appear that ubiquilin 2, p62 and optineurin all function in a selective type of autophagy referred to as aggrephagy due to its role in the specific elimination of ubiquitinated protein aggregates through the lysosome (Yamamoto and Simonsen, 2011). Dysfunction in any of these three proteins would be expected to lead to an inability of ubiquitinated aggregates to be removed, consistent with the neuropathology of ALS and FTD.

1.6.1.4. VCP

VCP (also known as p97), a member of the diverse AAA-ATPase protein super family, has a role in protein turnover by the UPS (Dai and Li, 2001). VCP complexes bind ubiquitinated target proteins and structurally remodel them through an ATP-dependent unfolding process to allow targeting to the proteasome (Meyer et al., 2012). Expression of dominant-negative mutant VCP leads to accumulation of ubiquitinated proteins, suggesting defects in VCP may impair recruitment of proteins to the proteasome (Dalal et al., 2004). In the context of ALS and FTD-associated inclusions it is tempting to speculate that the unfolding activity of VCP may be required to separate individual aggregated proteins from within large inclusions for destruction by the proteasome. Furthermore, in a notable convergence VCP, like ubiquilin 2, p62 and optineurin, appears to also have a role in autophagy. VCP mutations cause inclusion body myopathy associated with Paget's disease of the bone and frontotemporal dementia (IBMPFD), which is characterised by the accumulation of non-functional autophagosomes together with p62 and LC3 due to defects in vacuole maturation (Ju et al., 2009). Specifically, VCP seems to have a role in the selective maturation of ubiquitin containing autophagosomes to autolysosomes, suggesting that defects in this pathway may have a role in both FTD and IBMPFD (Tresse et al., 2010). As such, like ubiquilin 2, OPTN and p62, VCP may well also function at the interface of the UPS and autophagy, selectively coupling target protein ubiquitination

to autophagy. Whilst acting at a different stage of the pathway, VCP provides further evidence that 'aggrephagy' may well be at the heart of the ALS-FTD disease spectrum.

1.6.2. Aggrephagy and the ALS/FTD continuum

VCP, ubiquilin 2, optineurin, and ubiquilin 2 all act in coupling ubiquitinated target proteins to autophagy, or more specifically, aggrephagy. The clustering of ALS/FTD associated proteins within the aggrephagy pathway suggests it is primarily defects within cargo specific autophagy (as opposed to common aspects of autophagy), rather than the system classically associated with the clearance of ubiquitinated proteins – the UPS – that is impaired within certain ALS and FTD cases. Further genes encoding proteins acting within the aggrephagy pathway, especially those coupling ubiquitin to LC3, such as NBR1, would make excellent candidate genes for ALS and FTD. Given the suggested involvement of the UPS in ALS and FTD it is also noteworthy that cargo-specific autophagy can take over in situations where the UPS is not working to full capacity, indeed it appears that the two systems are interconnected and impairment of one is likely to affect the other (Korolchuk et al., 2010). It is possible, therefore, that aggrephagy is largely used when the UPS is overwhelmed by the production of protein aggregates a possible outcome in TDP-43 and FUSopathies. Therefore defects in the UPS are still of interest within the ALS/FTD continuum and should be investigated further.

1.7. Autophagy and RNA processing pathways may interact within the pathogenesis of ALS and FTD

1.7.1. Defects in autophagy pathways may affect RNA processing protein function

Alterations in protein degradation and RNA processing pathways therefore seem important in ALS and FTD, but could these pathways be interrelated? One possibility is that the impairment of protein degradation pathways in neurons affected in ALS and FTD results in the abnormal function of RNA-binding proteins such as FUS or TDP-43 (Figure 4). In support of this hypothesis, the pathology in cases harbouring mutations in the *VCP*, *OPTN* and *UBQLN2* genes is dominated by abnormal cytoplasmic levels and aggregations of TDP-43 (Deng et al., 2011a, b; Gitcho et al., 2009b; Maruyama et al., 2010; Neumann et al., 2007; Ritson et al., 2010). Cases with *SQSTM1* mutations await pathological characterisation, but it would be no surprise to find TDP-43 pathology. In the case of FUS, despite some reports of FUS accumulation in *UBQLN2* mutation cases, *in vitro* mislocalisation of FUS in response to autophagy/UPS defects has not been shown in the same manner as TDP-43. As such, the link between protein degradation and RNA dysfunction may go through TDP-43 solely, with relocalisation of FUS occurring through a more primary defect. It is notable that in ALS and FTD cases with mutations in protein degradation genes, pathology is specific to TDP-43 (and perhaps FUS), suggesting a direct link between impaired protein degradation and accumulation of RNA processing proteins as opposed to general accumulation of aggregation prone proteins such as SOD1 or tau. Additional support for this hypothesis comes from studies in primary hippocampal cortical neurons and motor neuron lines, in which the direct manipulation of protein degradation pathways by either proteasome or autophagic inhibition, or expression of mutant VCP, resulted in TDP-43 relocalisation (Ritson et al., 2010; van Eersel et al., 2011). Once cytoplasmically localised, TDP-43 and VCP appear to interact and enhance neurotoxicity and aggregation (Ritson et al., 2010). Within the cytoplasm, it is possible that accumulation of FUS and TDP-43 over a threshold level leads them to aggregate. Alternatively, small aggregates could spontaneously form even under normal conditions, but are usually degraded by cellular recycling pathways (Figure 5). In any case, both FUS and TDP-43 have been shown to be intrinsically aggregation-prone, with an initial seeding reaction important for wild-type and mutant TDP-43 aggregation (Furukawa et al., 2011; Johnson et al., 2009; Sun et al., 2011). Therefore, rapid recognition and destruction of small aggregates could be of crucial importance,

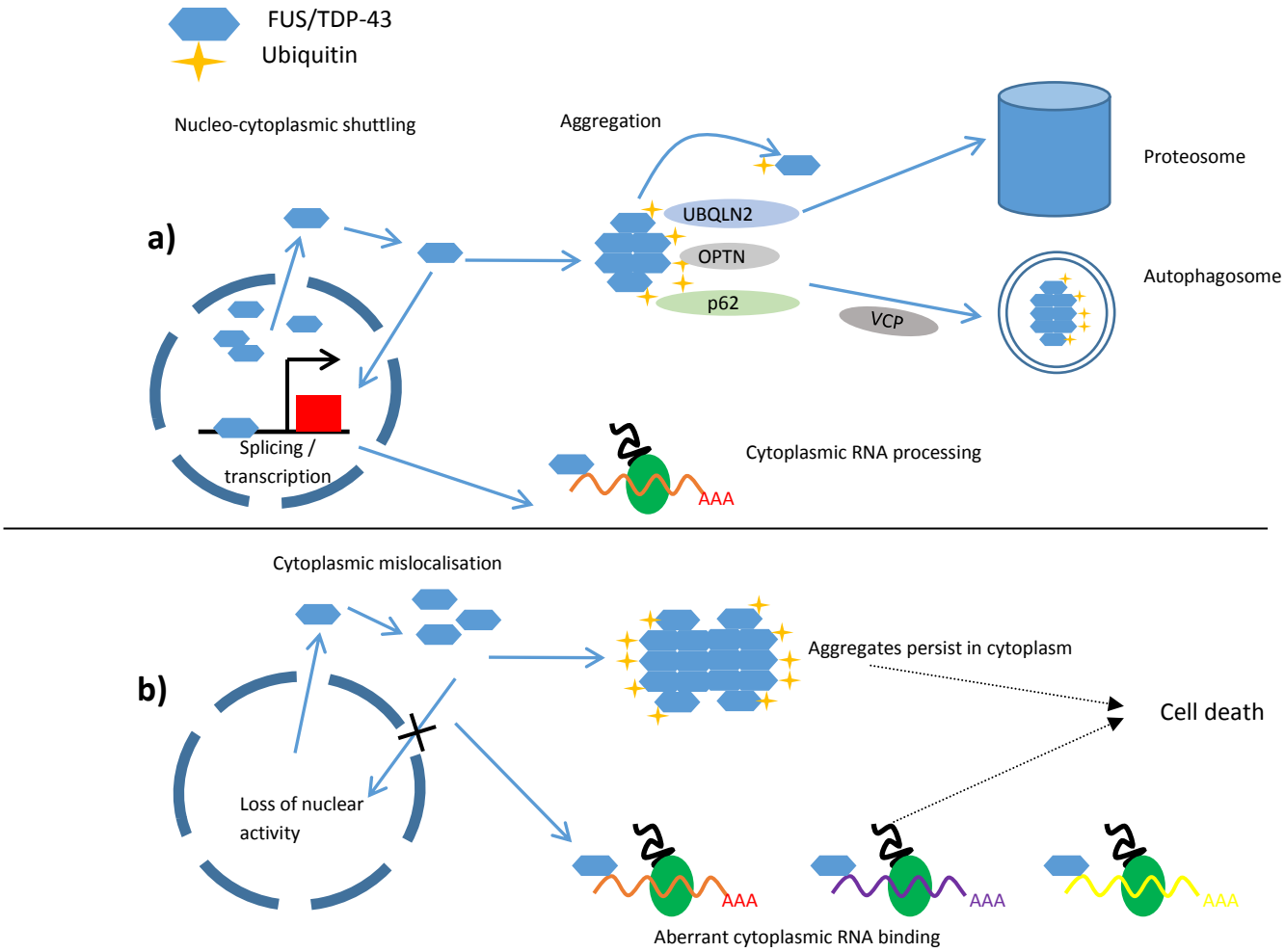
FUS/TDP-43
Ubiquitin
Nucleo-cytoplasmic shuttling
Aggregation
Proteosome
UBQLN2
OPTN
p62
VCP
Autophagosome
a)
Splicing /
transcription
Cytoplasmic RNA processing
AAA
Cytoplasmic mislocalisation
b)
Aggregates persist in cytoplasm
Cell death
Loss of nuclear
activity
AAA
AAA
AAA
Aberrant cytoplasmic RNA binding
Cellular stress or genetic factors lead to
RNA foci which sequester RNA binding
proteins such as TDP-43
Impaired
protein
degradation
Cytoplasmic mislocalisation
c)
Proteosome
UBQLN2
OPTN
p62
VCP
Cell
death
Loss of nuclear
activity
AAA
AAA
AAA
Aberrant cytoplasmic RNA binding, leading to
miss-processing of aggrephagy related genes.

1.7.2. Figure 5 – Pathogenesis pathways in sporadic and familial disease

Possible disease-associated pathways are shown for FUS and TDP-43. Some of the molecular details have so far only been demonstrated for TDP-43, but similar events are also highly likely within the pathobiology of FUS.

a) Normal cellular functions of FUS/TDP-43. FUS and TDP-43 shuttle between the nucleus, where they regulates splicing and transcription, and the cytoplasm, where further RNA targets are bound. Any stochastically forming aggregates are degraded by the UPS or autophagy.

b) Defects in protein degradation lead to a loss of nuclear FUS/TDP-43, either by directly affecting nuclear import/export or by failed aggregate destruction. Relocalisation of FUS/TDP-43 causes a loss of nuclear, and concomitant gain of cytoplasmic, RNA processing.

c) Loss of FUS or TDP-43 from the nucleus, due to mutations, or sequestration in either stress granules or RNA repeat expansions, causes dysfunctional RNA processing. Loss of normal TDP-43 action may lead to defects in aggregate clearance.

before a threshold of aggregated, cytosolic, TDP-43 is reached. In support of this idea, it is notable that three of the four autophagy/UPS proteins linked to ALS-TDP function in coupling ubiquitinated protein material to the proteasome or autophagosome rather than at later degradation steps.

In a notable aside, protein degradation pathways, in this case protein cleavage rather than autophagy or the UPS, are strongly linked to the pathobiology of TDP-43. Biochemical analysis of aggregated TDP-43 demonstrates not only ubiquitination and phosphorylation, but also the presence of 25 and 35 kDa C terminal fragments (Neumann et al., 2006). C terminal TDP-43 fragments, generated through either caspase- or calpain-dependent cleavage, replicate many features of TDP-43 proteinopathies when exogenously expressed, and appear to enhance cellular toxicity and aggregation (Yamashita et al., 2012; Zhang et al., 2009; Zhang et al., 2007). Loss of the N terminal region of TDP-43, which contains a NLS, may also cause the cytoplasmic relocalisation of TDP-43 seen in post-mortem neurons. Notably, one study has suggested that siRNA-mediated knock down of progranulin, replicating the effect of progranulin mutations, increases the susceptibility of TDP-43 to caspase mediated cleavage. Although not replicated in a further study, this result does suggest a mechanism through which altered protein cleavage could link progranulin mutations to TDP-43 pathology (Zhang et al., 2007). Whilst similar cleavage has not been reported in the case of FUS, it is likely that if it were to occur it would lead to relocalisation and disease.

1.7.3. Defects in RNA processing proteins may lead to dysregulation of protein degradation pathways

On the other hand, it is possible that in some cases, such as those with mutations in FUS or TDP-43, a primary alteration in RNA processing leads to a secondary impairment in protein degradation (Figure 5).

1.7.3.1. TDP-43 regulates protein degradation pathway genes

In support of this hypothesis, depletion of TDP-43 has been shown to reduce the level of expression of the important autophagy-related protein Atg7, leading to an inhibition of autophagy (Bose et al., 2011). Similarly siRNA knockdown of TDP-43 in primary cortical neurons causes an increased vulnerability of cells to proteasome inhibition (van Eersel et al., 2011). TDP-43 also appears to bind and regulate the stress response gene Nrf2, which is linked to the formation of ubiquitinated aggregates and is regulated by the autophagy-related protein p62 (Colombrita et al., 2012). Furthermore, knockdown of TDP-43 has been shown to produce down regulation of histone deacetylase 6 (HDAC6), a protein with diverse links to neurodegenerative diseases (Cook et al., 2012a; Fiesel et al., 2010; Pandey et al., 2007). In a remarkable convergence, HDAC6, a ubiquitin binding protein, appears to function within the aggrephagy pathway with a suggested function very similar to that of VCP – maturation of ubiquitin specific autophagosomes to lysosomes (Lee et al., 2010). Loss of TDP-43 function can, therefore, be linked to the ubiquitin-specific autophagy pathways that have been so strongly highlighted by mutations in *SQSTM1 VCP, OPTN* and *UBQLN2.*

1.7.3.2. FUS and protein degradation pathways

Meanwhile, analysis of RNA binding targets of FUS using RIP-chip (RNA binding protein immunoprecipitation and microarray analysis) in NSC-34 cells highlighted ubiquitin-dependent proteolysis as a functional gene category enriched for FUS binding (Colombrita et al., 2012). FUS binding was mapped to five separate members of the Cullin family of proteins, which form part of the cullin-RING E3 ubiquitin ligases, placing FUS as an important regulator of protein ubiquitination genes (Colombrita et al., 2012). Furthermore wild type and mutant FUS binding has been mapped to the transcripts of *UBQLN1*, *UBQLN2*, *SQSTM1* and *VCP* (Hoell et al., 2011). Notably in the experiments of Hoell *et al*, transcripts that are uniquely bound by mutant FUS show an overrepresentation of ubiquitin associated proteolysis functions, providing a clear link between defective RNA processing proteins and protein degradation (Hoell et al., 2011). Notably FUS binding

has also been mapped to *OPTN* mRNA, although this result was not found in a second UV-CLIP experiment by the same authors (Colombrita et al., 2012). Furthermore, FUS also appears to bind the mRNA of components of the eukaryotic translation initiation factor 2 required, as discussed earlier, for induction of starvation dependent autophagy (Colombrita et al., 2012; Hoell et al., 2011).

1.7.3.3. RNA processing proteins and dysfunctional protein degradation

Data from various studies have highlighted the fact that FUS and TDP-43 can bind to, and likely regulate, the mRNA of many autophagy/UPS associated genes. As such, impaired function of FUS and TDP-43 due to pathogenic mutations could drive defects in either ubiquitin specific or general protein clearance pathways in the cell through dysregulation of RNA processing. It is again, however, necessary to note that many thousands of FUS and TDP-43 binding sites have been mapped within the transcriptome meaning the biological relevance of these interactions needs further investigation before individual interactions can be ascribed important disease associated functions.

Another possible mechanism by which RNA binding proteins could lead to defects in autophagy or the UPS is through simple overloading of these pathways through their aberrant accumulation. The fact that ubiquilin 1 and 2, OPTN and p62 have are all found in FUS and/or TDP-43 aggregates in postmortem disease lends support to this idea. Furthermore, it is also notable that in *C9ORF72*-associated ALS and FTD cases the presence of ubiquilin and p62 positive, TDP-43 negative aggregates containing dipeptides resulting from RAN translation of the C9ORF72 repeat have been noted (Brettschneider et al., 2012; Mann et al., 2013; Troakes et al., 2012). A gene with a putative RNA-mediated mechanism of toxicity may, therefore, lead to the aggregation, and hence impairment of, proteins required for normal cellular protein degradation pathways.

As such, defects in RNA processing proteins could well have downstream effects on protein degradation pathways, either through improper regulation of key UPS or autophagy related genes or

through their tendency to form large disease associated aggregates overwhelming cellular clearance mechanisms (Figure 3).

1.8. The molecular pathogenesis of FUS in ALS and FTD

The key role of FUS at different stages of RNA processing is clear, but how do mutations in *FUS* cause disease? In the neurons of all ALS and FTD patients with FUS pathology, FUS relocates from the nucleus to the cytoplasm and forms aggregates (Arai et al., 2006; Deng et al., 2010; Neumann et al., 2009). Three possible causes of cytotoxicity in mutant and/or cytoplasmically localised FUS can be proposed: loss of normal nuclear function leading to dysregulation of nuclear DNA and RNA binding, gain of extraneous cytoplasmic RNA binding activity, or aggregation-related toxicity independent of FUS function.

1.8.1. Evidence for a loss of function mechanism for *FUS* mutations

The finding that the majority of FUS mutations cluster within a nuclear localisation sequence (NLS) and directly lead to a loss of normal nuclear localisation makes a loss of nuclear function an attractive idea for FUS toxicity (see Figure 1) (Dormann et al., 2010). Many of the roles assigned to FUS, such as transcriptional regulation and pre-mRNA splicing, take place in the nucleus and loss of FUS in mouse models leads to severe developmental problems suggesting a vital nuclear role for FUS (Hicks et al., 2000; Kuroda et al., 2000). Furthermore, FUS toxicity in yeast has been shown to be suppressed by over-expression of RNA processing proteins such as the human or yeast RNA helicases *UPF1/ECM32* which function in RNA quality control and appear to compensate for loss of FUS activity (Ju et al., 2011). A loss-of-function mechanism is also supported by an apparent correlation between the degree of mutation-induced relocalisation and phenotypic severity of associated disease (Dormann et al., 2010; Mackenzie et al., 2011a). These findings do not, however, necessarily

show FUS mutations act solely through a loss of function mechanism – a toxic role in the cytoplasm could give similar data.

1.8.2. Evidence for a gain of function mechanism for *FUS* mutations

With regard to a cytoplasmic toxic gain-of-function, experiments expressing *FUS* heterologously on a background containing WT, endogenous, FUS are instructive as loss of function events should be masked. Human wild type and mutant FUS is equally toxic when expressed in yeast due to the lack of NLS conservation across species (Ju et al., 2011). Addition of a yeast NLS abrogates toxicity, suggesting that toxicity is directly due to cytoplasmic accumulation (Ju et al., 2011). Similarly, overexpression of wild type *FUS* in several mouse models leads to toxicity, as does the expression of mutant *FUS* even in the presence of endogenous mouse wild type (and hence nuclear) FUS (Huang et al., 2011). Even if somewhat artificial, these experiments suggest a gain of toxicity event is possible for FUS.

Analysis of RNA binding by wild-type or mutant FUS shows an altered, rather than simply reduced, set of binding targets in cytoplasmically-localised mutant FUS (Hoell et al., 2011). Furthermore, use of serially deleted *FUS* expression constructs in a yeast model demonstrated that both N and C terminal regions, including RNA binding domains, are required for toxicity - suggestive of aberrant functionality in miss-localised FUS (Ju et al., 2011; Sun et al., 2011). These results suggest cytoplasmic localisation of FUS may result in aberrant RNA regulation and possible toxicity. A further argument for a gain-of-function effect is seen in the weak clearance of FUS from the nuclei of many affected neurons, arguing against complete loss of nuclear action (Neumann et al., 2009).

1.8.3. Aggregation and FUS toxicity

The evidence for direct toxicity of FUS aggregates remains unclear; one study using expression of a series of deletion constructs of FUS in yeast demonstrated aggregation was only weakly correlated with toxicity (certain constructs that formed aggregations did not show toxicity) whilst a further

contradictory yeast study has demonstrated that FUS aggregation is correlated with toxicity and highly dependent on expression level (Ju et al., 2011; Sun et al., 2011). A rat model of FUS dysfunction demonstrated FUS associated toxicity in the absence of aggregates, suggesting their formation may not be required for toxicity, at least at early disease stages (Huang et al., 2011).

In summary, the mechanism by which FUS mutations lead to disease seem to be intrinsically linked to loss of nuclear localisation, but whether this leads to a loss of nuclear function, a gain of cytoplasmic function, or a combination of the two, is still very much unclear. Given the importance of FUS in the ALS-FTD continuum, answering the question of how FUS mediates toxicity in affected neurons is clearly of great importance.

1.8.4. Relocalisation of FUS in sporadic disease

Whilst the cause of cytoplasmic relocalisation of FUS in familial ALS with *FUS* mutations is clear (NLS mutations, see Figure 1), how the relocalisation seen in sporadic ALS and FTD occurs is currently unclear.

1.8.4.1. Localisation patterns of the FET family proteins EWS and TAF15 provide clues to the relocalisation mechanism of sporadic FUSopathies

A recent clue as to how FUS might relocalise in FTD was provided by the presence of the other FET family proteins, TAF15 and EWS, in cytoplasmic FUS positive inclusions (Neumann et al., 2011). In a series of studied sporadic FTD-FUS cases, TAF15 was found in the FUS-positive inclusions in all cases investigated. EWS staining was more variable but a degree of co-localisation with FUS aggregates was seen in all cases (Neumann et al., 2011). Crucially, whilst TAF15 and EWS pathology was seen in all FTD cases, in a series of 6 ALS-FUS cases (with *FUS* mutations) no TAF15/EWS pathology was seen (Neumann et al., 2011). Given the presence of FUS mutations in ALS-FUS cases, and the lack of FUS

mutations in FTD, these findings suggest that the relocalisation pathway of FUS in sporadic FTD may be quite different from that in fALS cases.

1.8.4.2. FET protein relocalisation may be linked to defects in transportin 1 function

One similarity shared between the three FET family proteins (FUS, TAF15 and EWS) is their active nuclear import by transportin 1 (Figure 2). As such, defects in transportin could lead to a relocalisation of all three FET proteins. In a cellular model in which transportin-mediated nuclear import is inhibited relocalisation of all three FET proteins into cytoplasmic puncta (stress granules) was seen. By contrast, expression of mutant FUS alone did not lead to relocalisation of TAF15 and EWS (Neumann et al., 2011). Strikingly, a further report demonstrated that the FUS/TAF15/EWS inclusions in FTD were also frequently immunoreactive to transportin 1, but not for non-FET family transportin targets (Neumann et al., 2012). ALS-FUS inclusions did not show transportin immunoreactivity (Neumann et al., 2012). Somewhat elegantly, in a recent report of a single case of ALS-FUS without *FUS* mutations transportin 1, EWS and TAF15 were found colocalised with FUS positive inclusions (Takeuchi et al., 2013). This finding suggests that the presence of transportin in aggregates may not reflect basic differences between ALS and FTD, but rather between genetic (with *FUS* mutations) and sporadic (without *FUS* mutations) FUSopathies (Takeuchi et al., 2013). Further sporadic ALS-FUS cases will need to be assessed to determine whether this does prove to be the case.

As such, it appears that the cytoplasmic relocalisation of FUS in FTD and sALS is likely due to a more general dysfunction in the import of FET family proteins by transportin 1. The manner through which this disruption of import occurs is unclear, a lack of relocalisation in other transportin 1 targets argues against a general loss of function, but screening FTD-FUS cases for transportin mutations appears to be an important task (Neumann et al., 2012).

1.8.4.3. Arginine methylation status of FET proteins may lead to changes in Transportin 1 mediated import patterns

One possibility for the mechanism through which FET protein relocalisation may occur is through changes in the arginine methylation status of FUS, TAF15 and EWS. A further shared feature of the three FET proteins, alongside PY-NLS architecture, is that arginine methylation affects their cytoplasmic/nuclear localisation ratio by modulating biding affinity to transportin 1 (Figure 2) (Araya et al., 2005; Dormann et al., 2012). Notably, a further difference between ALS and FTD-FUS is seen in the methylation status of aggregated FUS. In the aggregations of mutant FUS in ALS no arginine methylation is seen – consistent with cytoplasmic localisation (see Figure 2 and earlier discussion) (Dormann et al., 2012; Scaramuzzino et al., 2013). By contrast, unmethylated FUS is found in FTD-FUS inclusions (Dormann et al., 2012). The finding is somewhat difficult to reconcile with current cell model based data in which hypomethylation of FUS is associated with increased nuclear, not cytoplasmic, localisation (Dormann et al., 2012; Scaramuzzino et al., 2013; Tradewell et al., 2012). The results of demthylation studies with FUS have, however, been mixed; increased cytoplasmic localisation of FUS at certain treatment times, and exacerbated FUS associated toxicity in a *Drosophila PRMT1* homologue (*dart1)* (a key FUS arginine methylating enzyme) knock out model have been reported (Scaramuzzino et al., 2013; Tradewell et al., 2012). Given hypomethylation increases the binding affinity of FUS for transportin it is possible that chronically hypomethylated FUS could effectively sequester transportin 1, leading to FUS-transportin aggregates and leaving further un-bound FUS free to accumulate in the cytoplasm. As such, it is possible that changes in the arginine methylation status of FET family proteins, perhaps due to aberrant PRMT protein function/levels, could lead to changes in nuclear-cytoplasmic FET protein ratios in the absence of mutations. Investigating the effect of arginine (de)methylation on FUS localisation, aggregation, and cytotoxicity will be important in understanding the role of methylation status in sporadic disease.

Generation of *PRMT* null transgenic animals will be required to study the long term impact of FUS hypomethylation.

Of note, mutations in another nuclear import factor, transportin 3, were recently shown to lead to lead to limb-girdle muscular dystrophy type F giving precedent for the possibility of disrupted nuclear import leading to a specific degenerative human disease (Melià et al., 2013).

1.8.4.4. Stress Granules and FUS

A further possible explanation for the propensity of FUS to deposit in the cytoplasm lies in the association of FUS with stress granules. Stress granules are aggregations of RNA and RNA-binding proteins thought to function in a protective manner during periods of cellular stress by protecting untranslated mRNA from destruction or modification in the cytoplasm. Mutant FUS, in a notable parallel with the highly related ALS/FTD-associated RNA binding protein TDP-43, localises to stress granules under conditions of cytoplasmic stress, such as heat shock or induction of reactive oxidative species through arsenite exposure (Bosco et al., 2010a; Colombrita et al., 2009). Experiments in yeast that demonstrated a correlation between FUS aggregation and toxicity (as discussed earlier) were also notable for the finding that these aggregates appear to be highly related to stress granules. (Sun et al., 2011). This finding infers that FUS must localise to stress granules to mediate toxicity and is somewhat surprising - stress granule sequestration of FUS is likely to ameliorate any aberrant RNA binding functionality in the cytoplasm - unless stress granules, or their possible ubiquitinated derivatives, are either actively or passively (through sequestering FUS/TDP-43) toxic. Furthermore, screens in yeast for suppressors of FUS toxicity highlighted various stress granule components including the yeast homolog of PABP-1, a protein involved in stress granule assembly, inferring that stress granules may be key to FUS mediated toxicity (Ju et al., 2011). It is also notable that the requirement of RNA binding activity for toxicity may reflect binding to stress granules rather than aberrant cytoplasmic processing targets.

It is, therefore, possible that periods of extended cellular stress, even in the absence of disease-associated mutations, may lead to a cytoplasmic relocalisation and sequestration of key RNA binding proteins within stress granules (Figure 5). In support of this idea, in mouse models of neural injury (axotomy) cytoplasmic TDP-43 levels have been shown to increase in the post-injury period, with TDP-43 interacting with components of RNA granules (Moisse et al., 2009). Furthermore, in SH-SY5Y cells exposed to oxidative stress FUS mRNA levels have been shown to be decreased by 40%, consistent with either direct *FUS* mRNA sequestration in stress granules or downstream sequestration of *FUS* regulating proteins such as TDP-43 (Blechingberg et al., 2012). As such, cellular stress could provide a mechanism for sporadic disease in which stress granule mediated sequestration, rather than specific mutations, leads to dysfunction of key RNA binding proteins such as FUS and TDP-43.

1.8.4.5. Stress granules and postmortem FUS immunoreactive aggregates

Recent evidence has also suggested that stress granules may transition, over time, into the larger ubiquitinated aggregates seen in postmortem disease tissue: both FUS and TDP-43 positive aggregates in postmortem tissue colocalise with key stress granule proteins such as TIA-1, PABP-1 and eIF3 (Dormann et al., 2010; Liu-Yesucevitz et al., 2010). Furthermore, TDP-43-containing stress granules have been shown to survive as cytoplasmic aggregates once cellular stress is removed, a finding not replicated for non-TDP-43 stress granules, and to be less likely to disassemble in the presence of chemical inhibitors (Parker et al., 2012). Whether this finding also holds for FUS-containing stress granules is unclear and warrants further investigation. These data suggest that FUS- and TDP-43-containing stress granules may transition to disease-associated aggregates, perhaps through the formation of overly stable stress granules. As such, stress granules may provide a mechanism through which cellular stress leads to the sequestration of RNA processing proteins with a concomitant loss of function in these proteins. Alternatively, cellular stress may promote the

formation of toxic aggregations of TDP-43 or FUS via an intermediate stress granule state. The importance of stress granules in disease is further highlighted by their association with other neurodegeneration-associated proteins, including survival of motor neuron (SMN), huntingtin and ataxin-2 (Elden et al., 2010; Hua and Zhou, 2004; Ratovitski et al., 2012).

1.9. Current Models of Disease in ALS and FTD

1.9.1. Early rodent models of ALS and FTD – *SOD1*, *MAPT*, and *GRN*

Mouse models of ALS have been used to investigate the impact of mutations, deletions or overexpression of genetically linked loci for some time. The most commonly modelled gene is SOD1, with upwards of 12 rodent models generated (Van Den Bosch, 2011). The first SOD1 mouse was published in 1994 and contained multiple copies of human genomic SOD1 containing the G93A mutation. These mice, alongside most of the more recent SOD1 models, recapitulate certain basic features of human ALS relatively well; progressive hind limb weakness, paralysis, and death are all observed (Gurney et al., 1994; Van Den Bosch, 2011). Crossing these mice to strains deficient in genes within putative SOD1 pathways has allowed important inferences to be made. SOD1 toxicity has frequently been suggested to be caused by defects in the normal function of SOD1 - converting superoxide radicals to hydrogen peroxide. However, crossing a SOD1 mutant mouse to a mouse deficient in the catalysis of superoxide had no effect on the lifespan or phenotype of the mouse, suggesting this pathway is not responsible for SOD1 mutant toxicity (Subramaniam et al., 2002). Whilst rodent models of SOD1 mutations have clearly answered some specific questions, they have largely failed to answer important general questions within the ALS field. The mechanisms by which mutant SOD1 confers toxicity remains unclear and the ability of these rodent models to accurately recapitulate human disease is still questionable. Furthermore, models of SOD1 mediated toxicity are

likely applicable only to ALS-SOD1 – a seemingly distinct disease entity with little overlap with the larger ALS-FTD disease continuum. Further, more relevant, models of disease are therefore likely to be required to explore mechanisms of pathogenesis throughout the ALS-FTD spectrum, an idea supported by the lack of therapeutic interventions developed for ALS since the first SOD1 mouse almost 20 years ago.

In a manner similar to SOD1 transgenics in ALS, multiple rodent models have been generated to model genetic changes at the two largest and earliest discovered FTD loci – *GRN* and *MAPT*. Multiple *MAPT* mouse models have been generated, largely expressing Tau from heterologous promoters (Roberson, 2012). Similarly to SOD1 models in ALS, these transgenics have generated interesting data as to the molecular pathogenesis of Tau mutations, but have largely failed to answer wider questions about the onset and progression of frontotemporal dementia (Roberson, 2012). Furthermore, these mouse models, like those for SOD1, do not recapitulate the FUS and TDP-43 pathology seen at the centre of the ALS–FTD spectrum.

GRN knockout rodent models have been heavily used to study the role of progranulin in FTD due to the loss-of-function usually caused by *GRN* mutations. Early and late behavioural abnormalities are seen in the absence of motor phenotypes, a notable result given the lack of *GRN* mutations in ALS (Roberson, 2012). In one model ubiquitinated and phosphorylated TDP-43 was found in the cortex and thalamus of aged $GRN^{-/-}$ mice, recapitulating a core feature of FTD with *GRN* mutations (Yin et al., 2010). However, further models have failed to reproduce the TDP-43 immunoreactive aggregates seen in FTD with *GRN* mutations and questions have been raised as to the suitability of modelling a supposed haploinsufficiency within a homozygous knockout model (Ghoshal et al., 2012; Roberson, 2012).

As such, rodent models of the most common ALS/FTD loci have failed to recapitulate many of the key features of human disease, and none has consistently demonstrated the TDP-43/FUS pathology

central to the core ALS-FTD continuum. In order to address this issue rodent models of TDP-43 and FUS have been developed over the last five years.

1.9.2. *TARDBP* transgenic rodent models

Multiple TDP-43 models have now been published. Early models of TDP-43 overexpression using heterologous promoters and cDNA transgenes demonstrated very high toxicity for both mutant and wild type TDP-43 and developed symptoms quite different from those normally found in ALS/FTD, suggesting both gene expression levels and timing are critical (Xu et al., 2010; Xu et al., 2011). More recent models have expressed TDP-43 in a post-natal manner only, in the hope of overcoming early toxicity. A rat model of TDP-43 using this approach demonstrated a gain of toxicity for the *TARDBP* M337V mutation compared to WT *TARDBP*. Whilst paralysis, death and motor neuron degeneration was seen, degeneration was not specific to motor neurons (Zhou et al., 2010). Models of TDP-43 dysfunction expressing the full genomic *TARDBP* locus and native promoter have also been published and demonstrate many of the features of both ALS and FTD including astrocytosis, memory and motor deficits, and the formation of ubiquitinated TDP-43 inclusions (Swarup et al., 2011). This genomic DNA model of TDP-43 highlights the way forward for transgenic models of ALS and FTD; minimising toxicity due to chronic overexpression and allowing the more subtle impact of individual mutations can be properly dissected.

1.9.3. Mouse models of FUS dysfunction in ALS and FTD

Rodent modelling of *FUS* began with the production of *FUS* knockout mice before moving onto the expression of mutant and WT cDNA constructs from heterologous promoters. Of the two knockout models of *FUS* that have been published, one led to early post-natal death, whilst outbreeding in the second model led to mice displaying lowered fertility and defects in chromosome axis pairing (Hicks et al., 2000; Kuroda et al., 2000). Four mouse models expressing WT or mutant *FUS* have currently

been published, all based on cDNA expression constructs. A rat model expressing *FUS* under the control of a tetracycline inducible promoter - allowing expression to be restricted to post-natal time points only – was published in 2011 and recapitulates certain features of FUSopathies (Huang et al., 2011). Overexpression of *FUS* containing the R521C mutation (Figure 1), but not WT *FUS*, led to progressive paralysis. Little motor neuron degeneration, but considerable loss of frontal cortex and dentate gyrus neurons, was seen. FUS positive inclusions were not, however, reported and high levels of WT *FUS* overexpression also lead to neuronal loss suggesting chronic overexpression may have led to as much toxicity as the inserted mutation itself (Huang et al., 2011).

Similarly, in a recent homozygous WT *FUS* cDNA overexpression model very severe toxicity was observed; aggressive early-onset tremors, progressive hind-limb paralysis and death after approximately 12 weeks were all reported. Whilst FUS-positive inclusions were seen, these were not additionally immunoreactive for ubiquitin (a key finding in FTD/ALS-FUS). Notably, mice hemizygous for the overexpression construct did not display a phenotype, suggesting that FUS toxicity in this model is due to chronic overexpression and may have little relevance to fALS with *FUS* mutations or sporadic FTD-FUS (Mitchell et al., 2013).

A mouse model generated by Verbeek et al utilised somatic brain transgenesis (using recombinant adeno-associated virus) to express a cDNA construct containing a highly toxic form of mutant FUS missing the C terminal NLS (FUS Δ14) (Verbeeck et al., 2012). Expression was therefore present only upon injection of the *FUS* construct, allowing expression to be restricted to post-embryonic development. Mice were assessed after 3 months and displayed no phenotype or neurodegeneration at this early time point. A portion of neurons in mice expressing the *FUS* Δ14 construct did however develop FUS neuronal cytoplasmic inclusions (NCIs) positive for FUS, ubiquitin and p62 after 3 months, showing a good resemblance to human FUS pathology in ALS/FTD. Expression of R521C *FUS* or WT *FUS* did not result in NCIs (Verbeeck et al., 2012). Whilst this model displays some features of human FUS pathology, the lack of phenotype and neurodegeneration

across the short time tested limit its suitability for investigating FUSopathies or for modelling possible therapeutic strategies. The presence of FUS aggregates in the absence of neurodegeneration, whilst not being ideal in a model of FTD/ALS, does however allow some interesting inferences to be made. The presence of aggregates without concomitant neuronal death suggests aggregate formation may be an early feature of disease, and may not be immediately or chronically toxic. An even more severe FUS truncation (amino acids 1 – 359 only (of 526)) was overexpressed in the model of Shelkovnikova et al (Shelkovnikova et al., 2013). The overexpression of such a severe deletion unsurprisingly resulted in high levels of toxicity, with mice showing very early and rapidly progressing neurodegeneration with death occurring inside 5 months (Shelkovnikova et al., 2013). Whilst a limited number of inclusions were seen in the neurons of affected mice these were not positive for ubiquitin (Shelkovnikova et al., 2013). A clear phenotype was seen in this model, but the sheer level of toxicity and lack of neuropathological features limit its use. Any chance of screening compounds that might ameliorate disease is reduced by the rapid and severe phenotype that seems unlikely to be modifiable. Current *FUS* rodent models are summarised in Table 5. Overall, it can be seen that, although many FUS mouse models have been generated, all suffer from fairly serious experimental problems such as a lack of key neuropathological features seen in human disease, expression of unrealistically severe mutations (truncations) or overly high transgene expression levels, leading to an almost-certainly unmodifiable disease course. An ideal FUS model would express FUS containing a pathological mutation at a level equal to, or not vastly higher than, physiological mouse or rat levels, show a time dependent gradual and progressive phenotype (perhaps only after 2 years) and recapitulate key pathological findings in human disease (neuronal loss, FUS NCIs containing ubiquitin and p62). Currently no FUS rodent model achieves all these aims. Clearly, when modelling a human disease that can take 70 plus years to present it may be necessary to increase the impact of transgene toxicity through moderately raised expression levels or selection of the most deleterious mutations. However, the extremely rapid neuronal loss and death seen in chronic overexpression models is not likely to allow detailed mechanistic analysis

Model	Mutations	Insert	Promoter	Expression	Key Findings
Mitchell et al., 2013. cDNA overexpression	WT only	cDNA	Heterologous, constitutive (mouse prion protein promoter)	Constitutive, overexpressed	Mice homozygous for WT FUS overexpression constructs developed aggressive early tremors, progressive hind limb paralysis and eventual death in 12 weeks. Motor but not cortical neurons lost. FUS positive inclusions seen but not ubiquitin immunoreactive. Mice hemizygous for the overexpression construct displayed no phenotype.
Shelkovnikova, TA et al., 2013. cDNA overexpression.	WT, Severe C terminal truncation (amino acids 1-359 expressed)	cDNA	Hetrologous, constitutive, neuronal expression (Thy 1)	Constitutive. Overexpressed	Extremely rapid degeneration seen with FUS_{1-359}. Early and rapidly progressing phenotype with lifespan of lower than 5 months. Some FUS positive inclusions in LMNs though most not positive for ubiquitin.
Verbeek et al., 2012. Somatic brain transgenesis using AAV1	WT, R521C, Δ14 (C terminal truncation)	cDNA	Heterologous, constitutive, expressed only post-nataly	Post embryonic intracerebroventricular injection. Overexpressed	Expression of Δ14 truncation lead to the presence of FUS NCIs positive for ubiquitin and p62. Not seen in WT or R521C. 3 month time point.
Huang et al., 2011 Post-natal cDNA overexpression	WT, R521C	cDNA	Heterologous. Tertacyline inducible (Tre-miniCMV)	Post embryonic. Overexpressed	Mutant (R521C) FUS, but not WT, causes progressive paralysis. Little loss of motor neurones but significant neuronal loss in frontal cortex and dentate gyrus. No FUS inclusions seen. High overexpression of WT FUS shows moderate neurodegeneration.
Hicks et al., 2000	Knockout	-	-	Knockout	Homozygous knockout mice die within 16hrs of birth. Defective B lymphocyte development. Neurological phenotypes not assessed.
Kuroda et al., 2000	Knockout	-	-	Knockout	Outbred homozygous knockouts display male sterility and reduced female fertility. Increased number of unpaired or mispaired chromosomal axes in pre-meiotic spermatocytes.

1.9.4. Table 5 – *FUS* Rodent Models Currently Published

Current published rodent models of *FUS* dysfunction are listed alongside key methodological details and a brief summary of any key findings (Hicks et al., 2000; Huang et al., 2011; Kuroda et al., 2000; Lanson and Pandey, 2012; Mitchell et al., 2013; Shelkovnikova et al., 2013; Verbeeck et al., 2012)

and the testing of possible disease modifying treatments. A detailed methodological discussion on the advantages and disadvantages of transgene expression methods in transgenic models can be found in the introduction to Chapter One.

1.10. Conclusions: FUS is a Central Player within the ALS-FTD continuum but the molecular mechanisms by which FUS dysfunction leads to neuronal death remain unclear

As we have seen, FUS is strongly linked to both ALS and FTD by genetics and/or neuropathology. FUS appears to be central to a shared RNA processing pathway that, alongside defects in aggrephagy, defines the overlap between ALS and FTD. However, the majority of disease models in ALS and FTD focus on genetic causes of ALS and FTD that operate by distinct and non-overlapping pathogenic mechanisms. Furthermore, the models of FUS dysfunction currently available suffer from serious methodological flaws and have failed to answer important questions about the role of FUS in ALS and FTD.

In this thesis I aim to generate a more physiologically-relevant model of FUS dysfunction that can be used both *in vivo* and *in vitro* to generate an accurate model of FTD/ALS-FUS. Important questions to answer using this model will include;

- Can a more physiological and regulated model of *FUS* dysfunction, and hence ALS/FTD-FUS be generated?
- Do mutations in *FUS* lead to toxicity through a gain of toxicity, a loss of function, or a combination of the two?
- Is the toxicity of mutant *FUS* directly due to cytoplasmic relocalisation?
- Can relocalisation of FUS be inhibited by arginine demethylases?
- Does inhibition of relocalisation reverse any toxicity seen?
- What is the role of stress granules in the formation of cytoplasmic FUS aggregations?

2. Chapter 2 - Methods

Here I describe specific details of methodologies referred to in the results chapters. I begin with the techniques required for the cloning, manipulation and purification of bacterial DNA (Chapter Three) and progress onto those required for the *in vitro* analysis of these DNA constructs within a cell culture model (Chapter Four and Five). A list of chemicals, compounds, kits and buffer components, can be found in the appendix. The rationale for, and the analysis of, individual methods are discussed in the relevant results sections.

2.1. Cloning and DNA manipulation methodologies

2.1.3. Generation of targeting vectors for recombination

2.1.1.1. Long range PCR

Templates over 1 kb were amplified using the Roche Long Expand Kit (see Appendix). Primers of between 80 and 100 bp (Invitrogen/ EurofinsMWG) were utilised to maximise homology arm length (see Chapter 3).

Primer sequences:

BAC to PCYPAC2 transfer:

1. Sense:

   AGGCTGGGTGGCCTCTGAAGCATAGCTGAGCTCTGCACATGCCAGCAGGCTAGAAGCAGGAAAACACACAAGTTGATTGACCCGGAACCCT TAATATAA

2. Antisense:

   GACAGGGAAGTGGGAAGATAGGGTCGGGGGTTGGAGAGCAGGAAGTGGGGCTGGGCGGTGCAGGCCTGGAAGTCAAAAATCATTTAATT GGTGGTGCTGC

FUS to pBACe3.6 transfer:

1. Sense:

   GAACGGACAGGGAAGTGGGAAGATAGGGTCGGGGGTTGGAGAGCAGGAAGTGGGGCTGGGCGGTGCAGGCCTGGAAGTCAGACGATGA
   GCGCATTGTTAG

2. Antisense:

   GCTGGAGGCTGGGTGGCCTCTGAAGCATAGCTGAGCTCTGCACATGCCAGCAGGCTAGAAGCAGGAAAACACACAAGTTGTCAACCCAGTC
   AGCTCCTTC

Insertion of exon 6 and 15 RpsL-neo cassettes:

1. Exon 6 Sense:

   CGGCGGCGGCGGTGGTGGTTACAACCGCAGCAGTGGTGGCTATGAACCCAGAGGTG GCCTGGTGATGATGGCGGGATC

2. Exon 6 Antisense:

   CCTGGCTCATGAGACACCTACCCCATGCCACCTCTGCCTCCACGGCCACCTCCACTCAGAAGAACTCGTCAAGAAGG

3. Exon 15 sense:

   ATAATGGATACTTAATTTTTTTTTTTTTTTTTGCAGGGGTGAGCACAGACAGGATGGC CTGGTGATGATGGCGGGATC

4. Exon 15 antisense:

   CTGGGTACAGGACAAAAAGCTGTTCCAGAACCTGGGGAGCCAGGCTAA TTAATACTCAGAAGAACTCGTCAAGAAGG

Reaction conditions for Long range PCR reactions are shown in the table below;

Reaction Components	**Volume (µl) per reaction**
Roche Long Expand Buffer 3	1.25
dNTPs (8mM)	2.5
Forward Primer (1µM)	1.25
Reverse Primer (1µM)	1.25
Roche Long Expand Taq mix	0.19
Template DNA	0.2 - 4 µg
MilliQ Water	To 12.5µl

Reaction conditions:

95°C – 10 minutes

95°C – 30 seconds

54-62°C – 30 seconds (optimised to specific primer)

68°C – 2-9 minutes (optimised to template length)

} X 34 cycles

68°C – 10 minutes

2.1.1.2. Long range PCR product purification

Successful PCR amplification was confirmed by gel electrophoresis and ethidium bromide staining. The PCR product was then run through a PCR purification column (see appendix) before being digested with Dpn1 to destroy unmethylated, template, DNA (37°C, 3 hrs). The digested DNA was then run through the purification column again, eluting a volume of 25 µl for electroporation.

2.1.1.3. Dpn1 digest

Reaction Components	**Volume (µl) per reaction**
Purified PCR product	85
NEB buffer 4	10
MilliQ Water	5
Dpn1 enzyme (NEB)	5

2.1.1.4. Colony PCR

Colony PCR was used to screen large numbers of bacterial colonies for correct recombination events, utilising primers to the newly formed donor/recipient vector junctions (2.1.1.5). Bacterial colonies were picked from agar plates into 12.5 µl of milli-Q water (MQW), of which 2.5 µl was used as template DNA, with the remainder available to seed further cultures.

Reaction Components	**Volume (µl) per reaction**
Amplitaq Gold PCR buffer 10x	1.5
$MgCl_2$ (25mM)	1.5
dNTPs (8mM)	1.5
Forward Primer (1µM)	0.75
Reverse Primer (1µM)	0.75
AmpliTaq Gold Taq	0.083
Bacterial Pick	2.5
MilliQ Water	7.54

PCR reaction conditions;

95°C – 10 minutes

95°C – 20 seconds
50°C – 20 seconds
72°C – 1 minute
} X 34 cycles

72°C – 5 minutes

2.1.1.5. Exon / Junction PCR

After each round of recombination the presence of newly formed vector junctions was screened by PCR. Additionally, the presence of the full length FUS gene was checked using primers spanning each of the 15 FUS exons together with up and downstream regions (see list of primers, 2.1.1.6).

Reaction Components	**Volume (µl) per reaction**
Amplitaq Gold PCR buffer 10x	1.2
dNTPs (8mM)	1.5
Forward Primer (1µM)	1.5
Reverse Primer (1µM)	1.5
$MgCl_2$ (25mM)	1.2
AmpliTaq Gold Taq	0.1
Template DNA	400 ng
MilliQ Water	To 12.5 µl

PCR reaction conditions;

95°C – 10 minutes

95°C – 20 seconds
58°C – 20 seconds
72°C – 1 minute
} X 34 cycles

72°C – 5 minutes

2.1.1.6. List of primers used for Exon/Junction PCR

Primer Location/Name	Primer Sequence
Exon 1 Sense	tgttggaacttcgttgcttg
Exon 1 Antisense	tactcttctccgcggcttc
Exon 2 Sense	cgccagtttgttcctcttct
Exon 2 Antisense	ctcacctttgggttgcttgt
Exon 3 Sense	ccacggacacttcaggctat
Exon 3 Antisense	tgagctgagacagcaccact
Exon 4 Sense	gtttagagggtggtgctgga
Exon 4 Antisense	cccctaccccaattacacct
Exon 5 Sense	cagcagcaaagctatggaca
Exon 5 Antisense	cagcctcagcaacagagaca
Exon 6 Sense	gtggctatggacagcaggac
Exon 6 Antisense	aggagtgggatcatcggttt
Exon 7 Sense	ccgtggtggcttcaataaat
Exon 7 Antisense	ctgctccaggttagcacaca
Exon 8 Sense	ctcgggaccaaggatcac
Exon 8 Antisense	ttgaaggtccccgaattaaa
Exon 9 Sense	aggcctgggtgagaatgtta
Exon 9 Antisense	agctggcaacaaccactaaga
Exon 10 Sense	tggaggtttacatgtgaggtagg
Exon 10 Antisense	tgcaagacacattaatccgaaa

Exon 11 Sense	tccggaaatcctatcaaggtc
Exon 11 Antisense	ggtctgctccctctccaagt
Exon 12 Sense	caaacttggagagggagcag
Exon 12 Antisense	atggggaataggcaagacct
Exon 13 Sense	ttctccttagcacctgtgaga
Exon 13 Antisense	ttcccattcccctatgttcc
Exon 14 Sense	gaaaggcagacctggtgcta
Exon 14 Antisense	taccagcctctccaagccta
Exon 15 Sense	ccaattcctgatcacccaag
Exon 15 Antisense	ctgggcagggtaatctgaac
Upstream 25 kb Sense	ctgaggcgagagcatcactt
Upstream 25 kb Antisense	ccttatggcaccctcatttc
Upstream 20 kb Sense	gagacgtcctcctgcttctg
Upstream 20 kb Antisense	tattggccagtctggtttca
Upstream 15 kb Sense	tttgtgggccagaagagttc
Upstream 15 kb Antisense	acttcacagccagcacgtaa
Upstream10 kb Sense	ctgcccagcatttactttcc

Upstream 10 kb Antisense	gaggcaaaagcatgtggatt
Upstream 5 kb Sense	ctgaggcagagaactgcaaa
Upstream 5 kb Antisense	cactgcacccagctcagata
Downstream 15 kb Sense	ggagagcaatggcatgatta
Downstream 15 kb Antisense	gaggttgcagtaaggggaca
Downstream 10 kb Sense	ggttagacccttagggagca
Downstream 10 kb Antisense	ctctgtacgggaaggtcctg
Downstream 5 kb Sense	gatgtgctgtccctgtgaga
Downstream 5 kb Antisense	aatcggtgtgattgtgcaac
PYCARD Sense	agaccagagtgggaggaagg
PYCARD antisense	gcagctttcagcttgaacttct
TRIM72 Sense	ctgaccagtccgtccagctaag
TRIM72 Antisense	gggtggaggaggagtaggagt
PRSS36 Sense	gctcttccccttgaggagt
PRSS36 Antisense	gccctaggaacctcacctct
RP11-388M20_FUSpCYPAC2 Junction A Sense	tccccctgcaaatttctcta
RP11-388M20_FUSpCYPAC2 Junction A Antisense	cggaccctatcttcccactt
RP11-388M20_FUSpCYPAC2 Junction B Sense	tgtggaaggtaggggagcta
RP11-388M20_FUSpCYPAC2 Junction B Antisense	ggtaaggtagccggatgc
FUSpCYPAC2_FUSpBACe.36 Junction A Sense	cgaggagagaggggttcttc
FUSpCYPAC2_FUSpBACe.36 Junction A Antisense	acatgaactgaggggacagg

FUSpCYPAC2_FUSpBACe.36 Junction B Sense	cgcctacaaggtacacatca
FUSpCYPAC2_FUSpBACe.36 Junction B Antisense	Acaccagcctcctccagtta

2.1.1.7. 4 primer STEP PCR

4 long, overlapping, primers are used to amplify RpsL-neo and mCherry during tagging to maximise the length of homology arms (see results).

Primers used were:

1. Rpsl-neo cassette insertion:

a) RpsL-neo_SS:

CCAGGCGTCGGTACTCAGCGGTGTTGGAACTTCGTTGCTTGCTTGCCTGTGCGCGCGTGCGCGGACATGGCCATAACTTCGTATAATG

b) RpsL-neo_SA:

GATCCCGCCATCATCACCAGGCCCGCCCTTGCTCACCATGGATAACTTCGTATAGCATACATTATACGAAGTTATGGCCATGTCCGCG

c) RpsL-neo_AA:

TCCCACTGAAAACGAAAAGCCCAGCTGGGAGGCCTCGGCCGGGTGCGCCGCCGCCGTCGCCTCGCGCCCTTACCTACCGTTTGAGGCCATT

d) RpsL-neo_AS:

GGGCGGGGCGTAAGCTAGCAGCCTCCACCGGCGGCATGGACGAGCTGTACAAGGGAGCTGGAGCTGGAATGGCCTCAAACGGTAGGTAAG
G

2. mCherry/LoxP Insertion

a) mCherry_SS:

TAGGCGGCGGAGCGTACTTAAGCTTCGACGCAGGAGGCGGGGCTGCTCAGTCCTCCAGGCGTCGGTACTCAGCGGTGTTGGAACTTCGTTG
CTTGCTTGC

b) mCherry_SA:

GTTATCCTCCTCGCCCTTGCTCACCATGGATAACTTCGTATAGTATACATTATACGAAGTTATGGCCATGTCCGCGCACGCGCGCACAGGCAA

GCAAGCAACGAAGTTCCAACACC

c) mCherry_AA:

ATCCCACACGGGATCGCCGCCCCGGTCCCACTGAAAACGAAAAGCCCAGCTGGGAGGCCTCGGCCGGGTGCGCCGCCGCCGTCGCCTCGCG

CCCTTACCTACCGTTTGAGGCCATTCCAG

d) mcherry_AS: GCATGGACGAGCTGTACAAGGGAGCTGGAGCTGGAATGGCCTCAAACGGTAGGTAAGG

PCR reaction conditions;

Reaction Components	**Volume (µl) per reaction**
Roche Long Expand Buffer 2	2.5
dNTPs (8mM)	4.33
Forward Sense (SS) Primer (1µM)	1.6
Forward Antisense (SA) Primer (10nM)	1.6
Reverse Antisense (AA) Primer (1µM)	1.6
Reverse Sense (AS) Primer (10nM)	1.6
Roche Long Expand Enzyme	0.35
Template DNA	2.4 µg
MilliQ Water	To 25 µl

PCR programme;

95°C – 10 minutes

95°C – 20 seconds

56°C – 20 seconds } X 37 cycles

68°C – 2 minutes

68°C – 5 minutes

2.1.2. Electroporation of BAC and PAC DNA

2.1.2.1. Generation of electrocompetent *E. coli*

1.5 ml of bacterial culture was grown within Luria Bertani (LB) medium, with relevant antibiotics, for 12 hours at 37°C in a shaking incubator. This culture was then tipped into 100 ml of LB medium (plus antibiotics) and grown in the same manner to an optical density (OD_{600}) of between 0.35 and 0.40. The bacterial culture was transferred to a 250 ml centrifuge flask and chilled on ice for 40 minutes. Bacteria were subsequently spun at 5000 rpm at 4°C for 15 minutes (Avanti J-E centrifuge, rotor 10.5). The supernatant was removed and bacteria were washed three times in 100 ml of pre-chilled 10% glycerol, with spins of 6000, 7000 and 7500 rpm (15 minutes, 4^{o}C, rotor 10.5) between each wash. Excess glycerol was removed, and 50 µl aliquots of electrocompetent bacteria were snap frozen on dry ice.

2.1.2.2. Induction of Red/ET expression

Bacteria containing the Red/ET plasmid were made electrocompetent in the same manner as above with the addition of the following modifications to induce expression of Red/ET;

1. Bacteria were initially grown at 30°C until an optical density of between 0.1 and 0.13.

2. 1.5 ml of 10% L-Arabinose was added to each culture to induce expression from the pBAD/RedET plasmid. Cultures were then incubated at 37°C until an optical density of 0.35 – 0.40

2.1.2.3. Electroporation of plasmid DNA

Electroporation of DNA into bacterial cells was carried out using a Bio-Rad Gene Pulser Xcell system using the following parameters;

- Voltage – 1800 V
- Capacitance – 25 µF
- Resistance – 200 Ω

In general, electrocompentent *E. coli* (EC cells), together with the DNA to be inserted, were added to a chilled 1 mm BioRad cuvette. The electroporation was performed according to the parameters above. Media was then added to the cuvette, mixed, and added to a 2 ml culture tube and incubated, before plating on LB agar.

Three electroporation protocols were used depending on the DNA to be electroporated, the specifics of which were;

1 - Electroporation of long PCR products for homologous recombination

i - 50 µl of electrocompetent *E. coli* were added to the cuvette with 8 µl of purified PCR product

ii - Electroporation

iii - 550 µL of LB broth added

iv - Electroporated bacteria were incubated for 1 hour 15 minutes at 37^{o}C before plating

2 - Electroporation of Red/ET

i - 25 µl of NEB electromax DH10B cells were added to the cuvette together with 1 µl of 1 ng/µl RedET.

ii - Electroporation

iii - 450 µl SOC media added

iv - Electroporated bacteria were incubated for 1 hour at 30^{o}C before plating

3 - Electroporation of whole PAC/BAC vectors

i - 25 µl of NEB electromax DH10B cells were added to the cuvette together with 1 µl of relevant maxiprep / dialysed miniprep DNA

ii – Electroporation

iii - 450 µl SOC media added

iv - Electroporated bacteria were incubated for 1 hour at 37^{o}C before plating

Transformation efficiency of electroporations into 'home made' EC cells was assessed by electroporating 1 µl of a 10 pg/µl pUC19 plasmid DNA stock (Invitrogen) in the same manner as above. 50 µl of electroporated bacteria were grown overnight on ampicillin containing media at 37°C and the number of colonies formed was counted. The number of colony forming units (CFU) per µg of DNA added was then calculated using the following formula;

$$\frac{\text{CFU in control plate}}{\text{Pg pUC19 used}} = \frac{\text{Total volume of culture}}{\text{Volume plating media}} \times \frac{1\text{x}10^{6}\ \text{pg}}{\mu\text{g}}$$

EC cells with an efficiency of above $1\text{x}10^{8}$ were considered acceptable for insertion of long PCR products, with those used ranging between $4\text{x}10^{8}$ and $5\text{x}10^{9}$.

2.1.3. Plasmid DNA isolation

2.1.3.1. Bacterial plasmid minipreps

1.5 ml bacterial cultures were grown for 16 hrs, transferred to an Eppendorf tube, and pelleted at 5000 rpm in a benchtop centrifuge. The bacterial pellet was resuspended in 70 µl STET buffer (see appendix) and 200 µl of lysis buffer added (see appendix). After 5 minutes the solution was neutralised by addition of 150 µl ammonium acetate (7.5 M), placed on ice for 5 minutes, and spun at 13000 rpm (20 minutes, 4°C) to pellet cell debris. The supernatant was removed to a clean tube and 250 µl of isopropanol was added, before spinning at 10,000 rpm (8 minutes, room temperature) to pellet DNA. After aspiration of the supernatant the pellet was washed with 70% ethanol and re-spun. Pellets were air dried and then resuspended in 50 µl TE containing 5 µg/ml RNase A (see appendix).

2.1.3.2. Bacterial plasmid maxipreps

Maxipreps were performed to prepare large quantities of purified BAC DNA from *E. coli* cells, using a Plasmid Maxiprep Kit according to the manufacturer's instructions (Qiagen, see Appendix). Briefly, 250 ml of LB media plus antibiotics was seeded with a 1.5 ml starter culture (as miniprep procedure) and grown for 12 - 16 hours. The culture was pelleted at 5000 rpm (Avanti JE centrifuge, rotor 10.5) and resuspended in a buffer containing RNase. Bacteria were then lysed, neutralised, and spun to remove debris before being added to purification columns. After washing DNA was eluted using

warm (55°C) elution buffer into Oakridge tubes. 10.5 ml of isopropanol was added to precipitate DNA and tubes were spun at 14,000 rpm (Avanti JE centrifuge, Rotor JA-17, 4°C, 30 minutes). Pelleted DNA was washed with 10 ml 70% ethanol and the previous spin was repeated. After allowing the pellet to air dry, DNA was resuspended in 250 µl TE (see appendix) overnight at 4°C. DNA concentration was checked using a Nanodrop spectrophotometer.

2.1.3. Restriction digests

2.1.3.1. Miniprep DNA digests

Restriction digests of miniprep DNA were carried out according to the basic protocol below, with buffer types and reaction temperature matched to the enzyme used.

Reaction Components	**Volume (µl) per reaction**
NEB Restriction Digest Buffer (1-4, matched to enzyme)	2
BSA (if required)	0.2
Restriction Enzyme	0.5
Miniprep DNA	8
MilliQ Water	9.3

Mixes were incubated for 3 hours at 30 or 37°C depending on the enzyme used.

2.1.3.2. Maxiprep digests

Maxiprep digests were performed according to the same protocol as those for minipreps but using defined amounts of DNA, ranging from 400 – 800 ng depending on the number of expected bands.

2.1.4. Separation of DNA fragments

2.1.4.1. Gel electrophoresis

DNA fragments of up to 10 kb were separated using 1% agrarose gel electrophoresis. Bands were visualised through ethidium bromide staining and band size was estimated by comparison to a suitable ladder.

2.1.4.2. Pulse field gel electrophoresis (PFGE)

For separation of large DNA fragments (5 – 200 kb) PFGE was used. Briefly, samples were loaded into a 0.5% agarose gel and run using a BioRad PFGE system for 16 hours. Gels were stained with ethidium bromide for 1 hour to visualise bands.

2.1.5. Engineering mutations

2.1.5.1. TA cloning

Exons 6 and 15 of FUS were amplified by PCR (Roche Expand High Fidelity, see below and appendix) and cloned into a pGEMT vector using TA cloning. Purified PCR products were ligated into a pGEMT vector according to the manufacturer's protocol (16°C overnight incubation) (Promega PGEMT Easy Vector System). 1 µl of the ligation reaction was then electroporated into ElectroMax DH10B cells (Invitrogen) as per 2.1.2.3. After plating on amplicillin, colonies were screened by colony PCR using junction specific primers.

Roche Expand High Fidelity PCR System Reaction Conditions;

Reaction Components	Volume (µl) per reaction
Roche HiFi Buffer 2	2.5
dNTPs (8 mM)	4.33
Forward Primer (1 µM)	3.2
Reverse Primer (1 µM)	3.2
High Fidelity Taq Polymerase	0.35
Template DNA	400 ng
MilliQ Water	To 25 µl

PCR programme;

95°C – 10 minutes

95°C – 20 seconds
58°C – 20 seconds
72°C – 1 minute
} X 34 cycles

72°C – 5 minutes

Primer sequences used were;

Primer Name/Location	Primer Sequence
FUS Exon 6 Amplification Sense	caaacctttagtgctactttacaatc
FUS Exon 6 Amplification Antisense	tctctattcagtggtaggatgg
FUS Exon 15 Amplification Sense	agggttttgttgagaaagtgg
FUS Exon 15 Amplification Antisense	ggcagggtaatctgaacagg

FUS Exon 6 – pGEMT Junction Check Sense	taatacgactcactataggg
FUS Exon 6 – pGEMT Junction Check Antisense	tttttggaaacaagtatcattactcaa
FUS Exon 15 – pGEMT Junction Check Sense	taatacgactcactataggg
FUS Exon 15 – pGEMT Junction Check Antisense	Ccttctccccgaacactgta

2.1.5.2. Sequencing

Sanger sequencing was utilised to identify DNA sequences of amplified and mutated sequences. Sequences were analysed using ContigExpress (Vector NTI, Invitrogen) and changes noted through comparisons to both previous vector sequences (pre-manipulation) and consensus DNA sequences.

2.1.5.3. Pre-Sequencing amplification

The region of interest was amplified by PCR using a high fidelity Taq polymerase (as in 2.1.5.1) and checked by gel electrophoresis. To remove excess primers and dNTPs, which could contaminate the sequencing reaction an ExoSAP reaction was carried out according to the parameters below.

Reaction Components	**Volume (µl) per reaction**
PCR product	20
10 x SAP buffer	1
Shrimp Alkaline Phosphatase (500 U/µl)	1
Exonuclease 1 (20 U/µl)	0.1
MilliQ Water	0.9

The reaction was incubated at 37°C for 1 hour before being terminated by heating to 80°C for 20 minutes.

2.1.5.4. Sanger Sequencing

Purified DNA template was then subjected to the BigDye Terminator v3.1 sequencing protocol.

Reaction Components	**Volume (µl) per reaction**
PCR product/DNA template	5
5 x Sequencing Buffer	1.75
Primer (10 µM)	1
BigDye Mix	0.5
MilliQ Water	1.75 µl

Reaction conditions;

96°C – 1 minute

96°C – 10 seconds

50°C – 5 seconds } X 30 cycles

60°C – 4 minutes

After running the sequencing protocol, samples were purified before analysis. 4 µl of a 125 mM EDTA/3 M sodium acetate mix was added to each well followed by 50 µl of ethanol. The sequencing plate was then spun at 3000 RCF (4°C, 30 minutes), inverted, and spun at 185 RCF to remove the supernatant. Sample pellets were washed with 70% ethanol (re-spun at 1650 RCF, inverted, and spun at 185 RCF to removed ethanol), left to dry and taken to the sequencing facility for analysis (Department of Zoology, Oxford).

2.1.5.5. Site Directed Mutagenesis

Site directed mutagenesis (SDM) was achieved using 20-25 bp primer pairs directed to opposite sense and antisense DNA strands and containing a central base pair mis-match corresponding to the mutation to be inserted (see Chapter 3 for details). Primer pairs were as follows;

Primer Name/Location	**Primer Sequence**
R244C Sense	tgaacccagaggttgtggaggtggccg
R244C Antisense	cggccacctccacaacctctgggttca
R521C Sense	tgagcacagacaggattgcagggagaggc
R521C Antisense	gcctctccctgcaatcctgtctgtgctca
P525L Sense	gatcgcagggagaggctgtattaattagcctggc
P525L Antisense	gccaggctaattaatacagcctctccctgcgatc

SDM was run using the PfuUltra II Fusion Hot Start DNA polymerase kit (see Appendix).

Reaction Components	**Volume (µl) per reaction**
10x PfuUltra II reaction buffer	5
Forward Primer (125 ng/µl)	1
Reverse Primer (125 ng/µl)	1
dNTPs (10 mM)	1
DNA (10 ng/µl)	1
Pfu II Fusion Hot Start Taq	1
MilliQ Water	38.5

PCR programme;

95°C – 1 minute

95°C – 30 seconds
55°C – 1 minute } X 30 cycles

68°C – 10 minutes

After the SDM reaction, 1 µl Dpn1 was added (37°C, 1 hour) to remove the original template DNA. 3 µl of the reaction product was checked by gel electrophoresis to assess reaction success.

2.1.5.6. FUS-pDEST site directed mutagenesis

Whilst the same protocol was used to engineer the R244C mutation into the pDEST-FUS cDNA vectors (as was used for the BAC vectors) a few changes were required for mutagenesis to run correctly. The same R244C S/AS primers that were used for BAC mutagenesis were used for cDNA mutagenesis.

The reaction components were as in 2.1.5.5, whilst the PCR programme was changed to;

95°C – 1 minute

95°C – 30 seconds
60.4°C – 1 minute } X 35 cycles

68°C – 10 minutes

Temperature gradient PCR demonstrated that the annealing temperature of 60.4 ^{o}C was critical for reaction success.

2.1.6. Production of purified supercoiled BAC DNA – dual caesium chloride banding

Starter cultures of 1.5 ml LB broth, relevant antibiotics (chloramphenicol) and a bacterial 'pick' containing the BAC plasmid were grown at 37^{o}C in a shaking incubator. After 8 hrs the starter culture was transferred to a 1 L culture (LB broth plus chloramphenicol), and grown for a further 16 hrs. The bacterial culture was pelleted and resuspended in GTE buffer (see appendix). Bacteria were lysed (see appendix) for five minutes before cold ammonium acetate (7.5 M) was added. Bacterial debris was removed by centrifugation (Beckman Coulter Avanti J-E, Rotor 10.5, 9000 rpm, 30 minutes, 4^{o}) and the supernatant filtered before 0.7 volumes of isopropanol were added to precipitate the DNA. DNA was then pelleted (Beckman Coulter Avanti J-E, rotor 17, 14000 rpm, 30 minutes, 4^{o}C) and the supernatant removed. The pelleted DNA was resuspended in 7.5 ml TE, and caesium chloride (CsCl) was added to make a 48.6% CsCl solution. 200 µl of 10 mg/ml ethidium bromide (EtBr) was added and the solution was filtered. The DNA/CsCl/EtBr solution was then spun for 20 hours in a Beckman Coulter L-90-K Ultracentrifuge (Rotor 70.1 Ti, 50,000 rpm, 25^{o}C) before the lower (supercoiled) DNA/EtBr band was removed using a 16G needle and syringe. 11 ml of 48.6% CsCl and 200 µl of EtBr were added to the recovered solution and the ultracentrifugation step was repeated. The lower DNA/EtBr band was again removed and recovered into a total volume of 1 ml TE. Ethidium bromide was extracted by sequential partitioning using salt saturated butanol. DNA was then precipitated in 70% ethanol over ice, and pelleted (Beckman Coulter Avanti J-E, rotor 17, 14000 rpm, 30 minutes, 4^{o}C). The supernatent was removed, and the DNA resuspended in 0.5 ml TE before being sodium acetate/ethanol precipitated, re-pelleted, dried and resuspended in 100 µl TE. The purified DNA/TE solution was then dialysed to remove excess salts, and the DNA concentration was established using a Nanodrop spectrophotometer.

2.2. Expression analysis in mammalian cells (HEK293)

2.2.1. Cell culture

2.2.1.1. HEK293 cell culture

HEK293 cells were grown in vented T75 tissue culture flasks (see Appendix) at 37^{o}C and 5% carbon dioxide. Cell growth media used was Dulbecco's modified eagle medium (DMEM, High Glucose) supplemented with;

- 10% Fetal Bovine Serum
- Penicillin-Streptomycin (1x)
- L-Glutamine (2 mM)

Flasks of cells were split on reaching 90% confluencey using Trypsin-EDTA to dissociate cells and re-seeded at the required density with fresh media.

Cells for analysis were seeded either in 6 cm dishes (5 x 10^5 cells seeded) or in 12 well tissue culture plates containing sterilised, poly-L-lysine coated, 19 mm coverslips (1 x 10^5 cells seeded).

2.2.2. HEK293 cell Transfection

2.2.2.1. BAC DNA Transfection

Lipofectamine was used to transfect BAC maxiprep into HEK293 cells according to a modified version of the manufacturers protocol (Invitrogen). 6 cm dishes were seeded with 1x10^6 cells in DMEM media (10% FBS, 1% Penicillin/Streptomycin, 1% L-Glutamine added) and grown for 24 hours at 37°C. Transfection reagents were assembled in two tubes; A and B, containing:

a) 250 µl OptiMEM, 4 µg BAC maxiprep DNA, 10 µl Plus reagent

b) 250 µl OptiMEM, 16 µl lipofectamine

Tube B was added to tube A, dropwise, and left for 20 minutes to allow complex formation. Cells to be transfected were washed 3 times with OptiMEM, 1 ml of OptiMEM was added, and complexes were gently dropped onto the cells and left for 4 hours. OptiMEM/complexes were then removed with 3 washes and DMEM growth media added to the cells.

2.2.2.2. cDNA Vector transfections

DNA from high copy number plasmids was transfected in the same manner as DNA from low copy (BAC) plasmids. The greatly reduced volume of maxiprep required for 4 µg of DNA was accounted for in the final volume by reducing the amount of Optimem added.

2.2.2.3. siRNA transfections

siRNA were transfected into cells using Lipofectamine 2000. The following basic protocol describes the transfection of an siRNA into a 6 cm dish at a 50 nm concentration. The protocol was scaled to allow higher siRNA concentrations by varying the amount of siRNA added to the siRNA-OptiMEM mix.

All steps were carried out using RNAase free pipettes and pipette tips, with RNAse Zap (Invitrogen) sprayed on all surfaces to reduce the amount of RNA degradation seen. Nuclease free water was used to resuspend siRNA to 50 µM working stocks.

The following two mixes were generated first:

Reaction Components	Volume (µl) per reaction
OptiMEM	296.4
siRNA (50 µM stock)	3.6

Reaction Components	Volume (µl) per reaction
OptiMEM	294
Lipofectamine 2000	6

Lipofectamine and OptiMEM were mixed for five minutes before 300 µl of the lipofectamine/OptiMEM mix was added, dropwise, to the siRNA mix. The siRNA/Lipofectamine/OptiMEM mix was incubated at room temperature for 20 minutes to allow complex formation.

Cells to be transfected were washed three times in OptiMEM to remove the seeding media (containing antibiotics and serum). 3 ml of OptiMEM was left after the final wash and the siRNA/Lipofectamine/OptiMEM mix was added dropwise. Cells were incubated for 4 hours before being washed 3 times in PBS and having the relevant growth media added.

2.3. *In vitro* transgene analysis

2.3.1. Reverse Transcriptase PCR (RT-PCR)

RNA was harvested from cells 2 or 4 days post transfection using Trizol/Chloroform extraction according to the manufacturer's instructions (Invitrogen).

cDNA synthesis was performed according to the following protocol;

Mix 1:

Reaction Components	**Volume (µl) per reaction**
Random Primers (150 ng/µl)	1
RNA extract	2 µg
dNTPs (10 mM)	1
MilliQ water	To 13 µl

Mix 1 was heated to 65°C for 5 minutes before being transferred to ice for 2 minutes. The following components were then added to mix 1;

Reaction Components	**Volume (µl) per reaction**
5 X First Strand Buffer	4
0.1 M DTT	1
RNaseOUT	1
Superscript III Reverse Transcriptase	1

The combined mix was incubated at 25°C for 5 minutes and then moved to 50°C for 1 hour. The reaction was then inactivated by heating at 70°C for 15 minutes. Residual RNA was removed by adding 1 µl RNase H and incubating at 37°C for 20 minutes.

PCR was then performed on the cDNA mix as in 2.1.5.1, using 1 µl of cDNA per reaction.

2.3.1.1. Long Range RT-PCR

Long range RT-PCR was performed using cDNA isolated as in 2.3.1, but required a specific PCR programme to generate the longer PCR products required to assess full length wild type and mutant FUS splice forms. PCR reaction conditions are shown below;

Reaction Components	**Volume (µl) per reaction**
Kapa HiFi HotStart Readymix (2X)	12.5
Forward Primer (10 µM)	0.75
Reverse Primer (10 µM)	0.75
cDNA	0.83
MilliQ water	10.7

The Following PCR cycling programme was used;

PCR conditions

95°C – 3 minutes

98°C – 20 seconds

60°C – 20 seconds

72°C – 2 minutes 45 seconds

X 34 cycles

72°C – 5 minutes

Primers used to assess full length FUS mRNA production were as follows;

mCherry Sense – tccccgactacttgaagctg

Exon 13 Antisense – cctgggccatctggtttag

Exon 15 Antisense – ctctccctgcgatcctgtc

2.3.2. Western Blotting

HEK293 cells were lysed on ice using RIPA buffer (with protease inhibitors, see Appendix) and sonication. Lysate was centrifuged at 3500 RCF (4^{o}C) and the supernatant was retained. Protein concentration was quantified using a BCA assay. Briefly, 1 mg/ml bovine serum albumin (BSA) was used to generate a range of standards. 12 µl of serially diluted BSA, from 1000 µg/ml to 15.6 µg/ml, was loaded in triplicate into a 96 well plate. Cell lysates were diluted approximately 10 fold (depending on the approximate number of cells harvested) and a 12.5 sample added to the 96 well plate in triplicate. 100 µl of a 50:1 copper sulphate: bicinchoninic acid solution was then added to each sample and the plate incubated at 37˚C for 30 minutes. Protein concentration was then estimated using a Biorad xMark platereader, measuring absorbance at 550 nm. A standard curve was generated from the BSA standard and unknown protein concentrations were then extrapolated.

Unless otherwise stated, 25µg of protein was heated to 95°C in Laemmli buffer (see Appendix) and loaded into a 10% SDS-polyacrylamide gel which was run at 140 V. Blotting onto polyvinyidene diflouide (PVDF) membrane was achieved using either a BioRad mini-PROTEAN tetra cell running at 100 V for 70 minutes, or a BioRad TurboBlot system. After transfer, membranes were blocked in 3% milk / TBS 0.1% TWEEN at 4°C overnight. Membranes were then incubated in 3% milk / TBS 0.1% TWEEN containing the relevant primary antibody for 1 hour. Three washes were performed with TBS 0.1% TWEEN before incubation with a HRP conjugated secondary antibody for 1 hour (BioRad, 1 in 5000). After washing, membranes were developed using Amersham ECL western blotting reagents and visualised using a BioRad Gel Doc system.

2.3.2.1. List of Antibodies used

Antibody	**Supplier**	**Western Blot Conditions** (1hr, 20°C unless otherwise stated)	**Immunofluoresence conditions** (1hr, 20°C unless otherwise stated)
Mouse anti-FUS	Proteintech (11570-1-AP)	1-5000	1-500
Rabbit anti-mCherry	Abcam (ab125096)	1-2000	-
Mouse anti-mCherry	Clontech (632543)	1-5000	1-2500
Rat anti-HA	Roche (11867423001)	1-3000	1-500
Rabbit anti-HA	Abcam (ab9110)	-	1-250
Rabbit anti-TIA-1	Sigma Aldrich (AV40981)	-	1-100
Goat anti-TIA-1	Santa Cruz (sc-1751)	-	1-100
Rabbit anti-cleaved caspase 3	Cell Signalling (9664s)	-	1-100, 4°C, 16hrs
Rabbit anti-sortilin 1	Abcam (ab16640)	1-1000	1-100
Rabbit anti-ubiquitin	Dako (20458)		1-100, 4°C, 16 hrs
Rabbit anti-ubiquitin	Santa Cruz (sc-9133)		1-100, 4°C, 16 hrs
Rabbit anti-p62	Abcam (ab109612)		1-100, 4°C, 16 hrs
Rabbit anti-HSP-70	Cell Signalling (4872)		1-100, 4°C, 16 hrs

2.3.3. Immunofluorescence / Immunocytochemistry

1 x10^5 cells were seeded on poly-L-lysine coated coverslips and transfected (if required) 24 hours later. After 3 days, cells were fixed by addition of 4% paraformaldehyde (PFA) directly to the cell media (one fourth of the total volume). After 5 minutes, cells were washed 3 times with PBS and then fixed for a further 5 minutes with 4% PFA. Fixed cells were then washed 3 times with PBS.

Cells were then permeabilised and blocked using serum matching the species the secondary antibody was raised in (blocking buffer, see appendix). Incubation with the required primary antibody, diluted in blocking buffer, was performed for either 3 hours or overnight at 4^{o}C (depending on the specific antibody used, see antibody table for specific conditions). Incubated cover slips were then washed in a wash buffer (see appendix) and stained with a fluorescently conjugated secondary antibody (Alex Fluor, Invitrogen, 1-500 diluted in blocking buffer) for 40 minutes in the dark. Cells were then washed three times with wash buffer and, if required, stained with DAPI (added to the wash buffer at a 1-1000 dilution). Finally, stained cells were then mounted onto slides using FluorSave to maintain fluorescence and then viewed using fluorescence microscopy.

2.3.4. Immunoprecipitation

2.3.4.1. Immunoprecipitation of FUS-mCherry

Semi-confluent (70%) 10 cm dishes of HEK293 cells were transfected with a scaled version of the normal transfection protocol (see 2.2.2.1) and cells were harvested after 4 days. After lysis with RIPA buffer and sonication (see appendix) cell debris was removed by centrifugation at 3500 g. The cell lysate was then precleared by addition of 25 µl of Dynabeads Protein G (Invitrogen) and subsequent rotation at 4 °C for one hour. 50 µl of Dynabeads Protein G were washed in 0.1 M pH5 sodium citrate before conjugation to a mix of 6 mg of Abcam anti-mCherry and 1.5 mg Clontech anti-mCherry antibodies (see antibody list for details) over one hour of rotation at 4°C. Antibody-Dynabead conjugates were washed three times in sodium citrate buffer before Dynabeads were removed from the precleared lysate by magnetic separation. Antibody conjugated Dynabeads were added to the precleared lysate and rotated for 16 hours at 4°C. After rotation, the Dynabeads were washed eight times in PBS with 3% NP-40. Immunoprecipitated mCherry-FUS was then eluted from

the Dynabeads by addition of Laemmli buffer (see Appendix) and heating to 95^{o}C for five minutes. The elution was fully cleared of remaining Dynabeads and run on an 8% acrylamide gel before being stained with Brilliant Blue R Staining Solution overnight. Briefly, gels were submerged in Brilliant Blue R staining solution for one hour at room temperature. Stained gels were then washed and incubated in a 10% acetic acid, 20% methanol destaining solution, with paper tissues to absorb the removed staining solution, until bands were clearly visible and background staining disappeared.

2.3.4.2. Immunoprecipitation of pDEST-FUS cDNA vectors

Immunprecipitation proceeded as in 2.2.5.1 except for the use of 8 mg Roche High Affinity Rat anti-HA and 4 mg Abcam Rabbit anti-HA instead of the antibodies specified in 2.2.5.1 (see antibody list for details). Proteins were separated on a 10% polyacrylamide gel.

2.3.5. Drug treatments

2.3.5.1. Sodium arsenite induction of stress granules

Sodium Arsenite (Sodium (meta) arsenite, Sigma Aldrich) was added directly to the growth media of cells to a final concentration of 0.5 mM (from a 50 mM stock reconstituted in water). Cells were incubated with sodium arsenite for one hour before being immediately fixed. Milli-Q water was used as a treatment control.

2.3.5.2. Mg132 Treatment

Mg132 (Z-Leu-Leu-Leu-al, Sigma Aldrich) was added, from 20 mM stock reconstituted in water, directly to the growth media of cells to generate the required final concentration. Cells were incubated with Mg132 for 2 hours unless otherwise stated. Cells were then immediately fixed. Milli-Q water was used as a treatment control.

2.3.5.3. Bafilomycin Treatment

Bafilomycin (Bafilomycin A1, Sigma) was reconstituted to 10 µM using DMSO before being added directly to cells in their culture medium to a final concentration of 50 nM. Cells were incubated with bafilomycin for 16 hrs before being immediately fixed. DMSO was used as a treatment control.

2.3.5.4. Hydrogen peroxide treatment

30% w/v hydrogen peroxide was diluted in chelex resin treated MilliQ water to 10mM. This 10mM solution was then added directly to the growth media of cells to the required final concentration (50-200nM, see results for specific concentrations used). After 16 hours cells were harvested or fixed for the relevant experiment. Chelex treated water was used as a treatment control.

2.3.5.5. Periodate-oxidised adenosine (AdOx) treatment

Adox (Adenosine, periodate oxidised) was reconstituted in water to a concentration of 1mM. This 1 mM solution was then added directly to cells containing growth media to a final concentration of 20 µM. Cells were pretreated with AdOx for 4 hours before transfection, AdOx was added to the transfection media (OptiMEM) and was re-added to clean growth media every 24 hrs until fixation. Milli-Q water was used as a treatment control.

2.3.5.6. AMI-1 treatment

AMI-1 (AMI-1, sodium salt hydrate) was reconstituted in DMSO to a concentration of 1mM and protected from light. AMI-1 was added to cell growth media to give a treatment concentration of 200 µM. Cells were pretreated for 4 hours before transfection, AMI-1 was added to the transfection media (OptiMEM) and was re-added every 24 hours to fresh cell media. DMSO was used as a treatment control.

2.3.6. siRNA treatments

2.3.6.1. siRNA transfections

siRNAs were transfected 24 hours after cells were seeded according to the protocol in 2.2.1.3

2.3.6.2. PRMT1 siRNA treatments

PRMT1 siRNA treatments took place 24 hours after cells were seeded, with an siRNA concentration of 100 nM. After 48 hours both the *PRMT1* siRNA and the BAC FUS-mCherry constructs to be assessed were transfected using the protocol for BAC transfections (2.2.2.1). Cells were fixed and stained a further 72 hours later.

2.3.6.3. Scrambled siRNA transfections

Scrambled siRNAs (Invitrogen) were transfected at the same concentration and time points as the siRNA of interest in the relevant experiment.

2.3.7. Cell counting

Cell counting was achieved by counting cells in 10 separate, random, microscope fields (60x objective, between 60 and 120 cells depending on cell density) per coverslip. Three coverslips were counted per experiment, to give a total number of cells counted of approximately 180-360 per genotype, per experiment. Treatments and genotypes were masked before counting, so as to ensure counting was performed blind.

2.3.8. Statistical analysis

Statistical tests were performed using GraphPad Prism. Tests used are highlighted with the relevant experimental result. n=3 data points were used unless otherwise stated. One-way ANOVA was used for data with multiple comparisons, alongside a suitable post-hoc to correct for these multiple comparisons (Bonferroni correction for comparing pairs of experimentally pre-defined means, Tukey test for comparing all means, Dunnet test for conditions where all means are compared to a pre-selected control mean) (see individual results for exact methodology). Student's T-tests were used for data with only a single comparison.

2.4. Appendix

2.4.1. List of Chemicals and Compounds Used

Chemical/Compound/Kit	**Manufacturer**	**Catalogue Number**	**Comments**
Acrylamide/Bis Solution (30%)	BioRad	161-0154	
AdOx (Adenosine, periodate oxidised)	Sigma-Aldrich	A5304	Reconstituted in MilliQ water
Agarose	Sigma-Aldrich	A5304	
AMI-1	Sigma-Aldrich	A9232	Reconstituted in DMSO
Ammonium Persulfate	Sigma-Aldrich	A3678	
Amplitaq Gold PCR System	Invitrogen	N8080245	
Bacterial Artificial Chromosome RP11-388M20	CHORI BACPAC Resources	RP11-388M20	
Bafilomycin	Sigma-Aldrich	B 1793	Reconstituted in DMSO
BigDye / Sequencing Buffer	Invitrogen	Internal Source	

Brilliant Blue R Staining Solution	Sigma-Aldrich	B6529	
Caesium Chloride	Sigma-Aldrich	C4036	
Chloramphenicol	Sigma-Aldrich	CO378	Diluted in 70% EtOH
DAPI	Invitrogen	D1306	
DMSO (Hybi-Max)	Sigma-Aldrich	D2650	
Dulbecco's modified eagle media (High Glucose)	PAA	Exx-009	
dNTPs	Invitrogen	10297-018	
Dynabeads Protein G	Invitrogen	10003D	
Ethidium Bromide (10mg/ml)	Sigma-Aldrich	E1510	
ElectroMax DH10b electrocompetent *E. coli*	Invitrogen	18290-015	
Expand Long TemplatePCR System	Roche	11681834001	
Fetal Bovine Serum	Invitrogen/Gibco	10437-028	
Fluorsave	Calbiochem/Merck Millipore	345789	
GeneClean Gel Extraction Kit	MP Biomedicals	111001200	
Hydrogen Peroxide (30% w/w)	Sigma-Aldrich	H1009	Diluted in Chelex Water
Kanamycin (sulphate)	Sigma-Aldrich	K0879	Diluted in MilliQ water
Kapa HiFi Ready Mix Hot Start DNA Polymerase	Kapa Biosytems	KR0370	
L-Arabinose	Sigma-Aldrich	A3256	
LB Agar Granules	Merk Millipore	71752	
LB Broth Granules	Merk Millipore	71753	

L-Glutamine	Sigma-Aldrich	G7514	
Lipofectamine	Invitrogen	18324012	
Lipofectamine 2000	Invitrogen	11668019	
MG132 (Z-Leu-Leu-Leu-Al)	Sigma-Aldrich	C2211	Reconstituted in MilliQ water.
OptiMEM	Invitrogen	31985-088	
Plasmid Maxiprep Kit	Qiagen	12162	
PCR Purification Kit (QIAquick)	Qiagen	28104	
pDEST-FUS Plasmid	Addgene	26374	
Penicillin/Streptomycin	Sigma-Aldrich	P4333	
Pfu Ultra Hot Start DNA Polymerase II	Agilent	600670	
pGEMT Easy Vector System	Promega	A1360	
poly-L-lysine	Sigma-Aldrich	P4707	
Protease Inhibitors, Complete, Mini	Roche	11 836 170 001	
Random Primers (cDNA production)	Invitrogen	48190-011	
Restriction Enzymes (Various)	NEB	Various	
RNAseH	Invitrogen	18021-014	
RNase Zap	Sigma-Aldrich	R202	
Expand High Fidelity PCR System	Roche	11 732 641 001	
Scrambled siRNA	Invitrogen	12935-100	
Shrimp Alkaline Phosphatase (FastAP)	Thermo Scientific	EF0654	
Silencer Select siRNA	Invitrogen	4392420	Reconstituted in

			RNase free water
Sodium (meta)arsenite	Sigma-Aldrich	S7400	
Superscript Reverse Transcriptase III	Invitrogen	18080-044	
TBE, 10x	Sigma-Aldrich	T4415	
TEMED	Sigma-Aldrich	T9281	
Tetracycline	Sigma-Aldrich	T8032	Diluted in 70% EtOH
Trypsin EDTA	Invitrogen/Gibco	15400-054	
Trizma Base	Sigma-Aldrich	T1503	
Trizma HCL	Sigma-Aldrich	T5941	
Trizol	Invitrogen	15596-026	
Vented Tissue Culture Flasks	Corning	Various	
12 Well Tissue Culture Plate	Corning / Sigma-Aldrich	CLS3513	

2.4.2. Buffers Used

Buffer	**Components**
GTE Buffer	50 mM Glucose 25 mM Tris, pH8 10 mM EDTA, ph8
Immunofluoresence Wash Buffer	TBS 0.1% (v/v) Triton X-100
Immunofluoresence Blocking Buffer	TBS 0.1% (v/v) Triton X-100 10% Serum (to match secondary antibody)
Laemmli Buffer	60 mM Tris pH 6.8

	2% (w/v) SDS 10% (v/v) Glycerol 5 % (w/v) β-mercaptoethanol 0.01% (w/v) Bromophenol Blue
Lysis Buffer (bacterial)	1% (w/v) SDS 0.2 M NaOH
RIPA	50 mM Tris HCl pH 7.4 1% (v/v) NP-40 0.5% (w/v) Na-deoxycholate 150 mM NaCl 0.1% (w/v) SDS
STET	5% (v/v) Triton X-100 50 mM EDTA 50 mM Tris, pH8
TE	10 mM Tris, pH 8 1 mM EDTA
Western Blot Running Buffer	250 mM Trizma Base 2.5 M Glycine 1% (w/v) SDS
Western Blot Transfer Buffer	250 mM Trizma Base 2.5 M Glycine

2.4.3. Bacterial Strains Used

All bacteria used were DH10B *E. coli*, with the following genotype: F⁻*mcr*A Δ(*mrr-hsd*RMS-*mcr*BC) Φ80*lac*ZΔM15 Δ*lac*X74 *rec*A1 *end*A1 *ara*D139Δ(*ara*,*leu*)7697 *gal*U *gal*K λ⁻*rps*L *nup*G

2.4.4. Plasmids Used

Plasmid	**Source**	**Comment**
Human BAC RP11-388M20	CHORI BACPAC resources	Contained FUS locus
pBACe3.6 (9.5 kb core of backbone used)	Internal	Used as donor sequence in recombination, provided plasmid replication elements.
pCYPAC2 (6.8 kb core of backbone used)	Internal	Used as mid-stage recombination plasmid
pSC101-BAD-gbaA (pBad/pRedET)	Genebridges	Expressed recombination proteins
pGEM-T	Promega	Used to manipulate exons for sequences
pDest-FUS-HA	Addgene plasmid number 26374	cDNA FUS ORF fused to CMV promter and HA tag.

3. Chapter 3 - Generation of BAC-based Genomic Expression System for the ALS and FTD Associated Gene *FUS*

3.1. Genomic expression systems – a highly regulated method for physiological transgene expression

3.1.1. Current cDNA based vectors suffer from confounding experimental effects

Transgene expression systems have classically utilised cDNA constructs that express coding DNA sequences from a strong, heterologous, and constitutive promoter, leading to non-physiological expression patterns within many, or all, tissues of a model organism. The use of cDNA transgene expression systems can cause several experimental problems. Expression levels of a gene driven by a strong heterologous promoter are likely to be considerably above physiological levels, leading to greatly increased cellular concentrations of the encoded protein. This may, in turn, lead to a tendency for the encoded protein to aggregate, either due to a simple increase in the cellular concentration of folding intermediates, or through the overwhelming of the molecular chaperones usually required to guide the folding of nascent polypeptides into proteins with correct tertiary structure. The interaction properties of proteins are also likely to depend on cellular concentration. As such, expression of a protein at high levels can cause spurious results as to the aggregation tendency and interaction profile of heterologously expressed proteins (Zhang et al., 2004). The high energetic cost to a cell of constitutive high expression of a transgene may also lead to further confounding experimental effects; high transgene expression can induce cytotoxicity independent of the specific effect of the transgene expressed. Furthermore, using a heterologous promoter means that expression is seen either throughout the transgenic organism, or is restricted (using a tissue specific promoter) to an area where expression is assumed to be normally found. In both these cases it is unlikely that endogenous expression patterns are accurately recapitulated, especially through

development, and is likely to lead to either aberrant expression of the transgene in areas not normally seen, or a failure to express a transgene at all times and regions required.

Experimental issues with cDNA expression systems have led to a drive to generate more physiological models of transgene expression. Systems giving more control over the level, timing and localisation of transgene expression have therefore been developed. These systems allow accurate modelling of transgenes expressed in either normal or disease (mutated) states. These requirements become of even greater relevance within the field of neurodegeneration where many of the relevant genes have specific expression patterns; expressing a gene normally found only within the CNS throughout an organism would generate a poor model of a neurodegenerative disease (Heintz, 2001).

3.1.2. Features and advantages of BAC-based genomic expression vectors

In order to replicate the correct expression pattern of a gene at a time when bioinformatics does not allow exact expression patterns to be determined from sequence alone, it is necessary to utilise as much of a gene and its regulatory regions as possible. The main obstacle to this approach is one of size; manipulating not only the exons of a gene, but also (possibly very large) introns, native promoter sequences and up and downstream regulatory regions, mean the size of vector inserts can increase from approximately 5 -10 kb in cDNA vectors, to anywhere from 50 to 250 kb within genomic expression vectors. To allow expression of such large sections of genomic DNA, bacterial artificial chromosomes (BACs), based on the *E. coli* F plasmid, were developed to allow inserts of up to 300 kb to be maintained and manipulated within *E. coli* (Shizuya et al., 1992). BAC vectors allow entire genomic loci to be modified within *E. coli*, and then expressed within either cell culture or animal models. To this end, when high-capacity, stable, vectors were required for the herculean task of assembling complete libraries of genomic DNA for the human genome project, BAC vectors

proved the tool of choice (Lander et al., 2001). The large capacity of BAC vectors meant that approximately 20,000 individual vectors could give complete coverage of the 3.2 billion base pairs of the human genome (NIH National Human Genome Research Centre). These vectors stably maintained this coverage once inserted in a bacterial host, and large quantities of their encoded DNA could also be extracted for sequencing purposes (Lander et al., 2001; Venter et al., 2001)

The ability to encode whole genomic loci, including native promoters and regulatory regions, within BAC vectors allows a huge improvement in the specificity and accuracy of transgene expression. The GENSAT project (Gene Expression Nervous System ATlas) to map expression levels and locations of important CNS genes through development utilised BAC vectors containing promoter sequences of interest fused to a reporter gene. The precision of these promoter and regulatory regions is such that expression patterns can be defined to a single cell level, fully recapitulating the expression of the endogenous gene (Gong et al., 2003). The ability to direct expression of a transgene to a specific region is of great use when modelling the effect of mutations or genetic variation that do not effect disease through a simple loss of function but through more complex mechanisms including dominant-negative or gain of function mutations, or even changes in gene expression levels.

A further benefit of genomic DNA expression methods for genetic loci with complex contributions to disease can be clearly seen at the *microtubule asscociated protein tau (MAPT)* locus, where certain *MAPT* haplotypes are associated with progressive supranulcear palsy (PSP), corticobasal degeneration (CBD) and Parkinson's disease (Caffrey et al., 2006; Fidani et al., 2006; Wade-Martins, 2012). Expression of different *MAPT* haplotypes results in changes in the inclusion of *MAPT* exon 10 through altered alterative splicing. These differences in exon 10 inclusion affect the number of microtubule binding domains found in the mature protein and may be responsible for increased PSP and CBD disease susceptibility (Caffrey et al., 2006). This complex genetic contribution could not be modelled in a cDNA vector as the vast majority of haplotype specific differences (outside the coding DNA sequence) would be missing. Furthermore, alternative splicing of exons could not be

investigated due to the lack of introns in cDNA vectors. As such, many genetic contributions to disease can only be modelled through vectors expressing large genomic inserts.

Further examples of the use of BAC vectors in the defining the importance of genetic changes in neurodegenerative diseases have been seen in attempts to generate transgenic models of α-synuclein (*SNCA*) dysfunction. Dominant mutations in *SNCA*, together with *SNCA* duplications and triplications, lead to Parkinson's disease (PD), and many rodent models of *SNCA* dysfunction have been generated (Chesselet and Richter, 2011). Traditional, cDNA based models, of *SNCA*-linked often feature aberrant phenotypes not seen in human disease (Chesselet and Richter, 2011). A BAC-based model of PD, expressing the full genomic *SNCA* locus recently demonstrated an association between overexpression of *SNCA* at 'disease relevant' levels and early defects in dopamine release in the dorsal striatum (Janezic et al., 2013). This deficit in dopamine release preceded both age dependent loss of dopaminergic neurons and characteristic motor impairments. Furthermore, these effects were seen in the absence of α-synuclein aggregation (a cardinal feature of PD) and suggest that early disease processes may, contrary to many suggestions, not depend on the formation of protein aggregates (Janezic et al., 2013).

Remaining in Parkinson's disease, a further example of a successful BAC-based transgenic model was seen in the expression of whole genomic copies of WT and mutant *LRRK2* (Li et al., 2009). Expression of mutant *LRRK2*, shown to be causative for PD, lead to progressive motor deficits which, importantly, could be reversed using Levodopa (a dopamine replacement used to treat human PD). Furthermore, hyperphosphorylated tau and tau positive dystrophic neurites, both seen in LRRK2-associated PD, were observed (Li et al., 2009). This BAC-based genomic expression model provided the first model of genetic PD that recapitulated multiple important features of human disease and, together with the α-synuclein model discussed earlier, highlights the advances in transgenic models made possible by BAC technology.

The ability of genomic reporter constructs to generate better, more physiological, models of genetic dysfunction in disease should help herald a new era of transgenic models in which more subtle phenotypes, and an absence of chronic toxicity, allow the dissection of the molecular events that link mutations to end-stage disease.

Finally, it is worth briefly discussing novel techniques that have arisen since this project began that might be utilised in the future. Genome engineering, or the specific and direct alteration of DNA sequences within living cells or organisms, may now herald an age where physiologically expressing expression vectors, both *in vitro* and *in vivo*, may be surplus to requirement. Recent developments, such as TALEN nucleases and the cas-CRISPR system, now mean specific DNA base changes can be made anywhere within the genome of a cell through the directed insertion of double strand DNA breaks (DSBs). Repair of these DSBs through either error-prone non-homologous end joining (NHEJ), leading to somewhat random DNA deletions or insertions, or, more specifically, by homology directed repair (HDR) (a separately transfected template with homology arms is provided) allows sequence directed mutagenesis or the insertion of small genetic loci (Christian et al., 2010; Cong et al., 2013; Li et al., 2011). Therefore, in order to examine the impact of a given pathological mutation one can now directly insert the mutation within the matching endogenous gene of the cell/organism without recourse to expression vectors. Furthermore, it is now possible to not only make single base pair deletion/insertion/substitutions, but also to specifically insert larger sequences such as small epitope tags at essentially any desired location (Yang et al., 2013). Several advantages of this system, compared to either transiently transfected or stably integrated genomic expression vectors can be seen. Firstly, genome engineering technologies may allow much more rapid and low cost insertion of mutations or tags. Secondly, whilst BAC-based vectors greatly minimise the likelihood of non-physiological expression patterns, direct genome engineering should ensure that gene expression patterns are identical to that seen in ‘wild type’ cells. Thirdly, by only changing the genotype of the modified cell/organism at a single point (compared to the addition of a large expression plasmid or DNA sequence), comparisons between unmodified cells/organisms should be easier and more

widely possible. However, some issues do still exist with genome engineering techniques, such as the possibility of off-target effects, requirements for certain sequence motifs to be close to the targeted nucleotide(s) and low efficiencies of modification (Cho et al., 2014). One further benefit of transgene expression systems that may be very notable is the ability to roughly choose the expression levels of the encoded protein, either through addition of an exogenous promoter or, due to the random insertion number of vectors (within concatemers) during pronuclear injection, by selecting between rodent lines of varying expression levels. Given many disease-associated mutations require overexpression for a phenotype to be seen within an experimentally acceptable timescale, this feature of expression vectors may continue to be useful for some time.

3.1.3. Manipulation of BAC-based genomic expression vectors require specialised techniques

Size differences between BAC vectors and cDNA vectors mean the methodologies for manipulating the two systems differ considerably. cDNA vectors allow the insertion and manipulation of transgenes through the general paradigm of molecular biology - complementary restriction enzyme digests of the insert and target sequences and subsequent ligation of the two into a complete circular vector (which can be transformed into bacterial cells). The high efficiency of ligation reactions means no selective pressure is required to gain the desired product at a reasonable efficiency. By contrast this 'cut and paste' mechanism is rarely successful in large BAC vectors due to the low frequency of unique restriction sites and relative difficulty of manipulating such large linear DNA fragments (Copeland et al., 2001). To meet the challenges of engineering BAC vectors, systems have been developed to allow the insertion of a locus of interest through homologous recombination (Box 1). Initially, systems based on *E. coli* recombination pathways were utilised (with modifications to prevent linear dsDNA degradation by RecBCD exonucleases) to allow transfer of loci containing homology into a target sequence (Copeland et al., 2001). These systems, however, led to

constitutive homologous recombination activity and host genome instability (Copeland et al., 2001). A more recently designed system, RedET recombination, provides exogenous phage lamda recombination enzymes that are induced only at the time recombination is desired (Muyrers et al., 1999). The mechanism of action is shown in Box 1. In this system a locus to be inserted is PCR amplified using primers containing arms homologous to a complementary target molecule (Box 1).

The homology arms drive exchange of the donor and target regions, allowing insertion of any sequence into a target in a site-specific manner (Box 1). The low efficiencies of homologous recombination mean DNA sequences to be inserted must carry a selectable marker. Initially, selective markers that would be inserted alongside the donor sequence, leaving an artefact of modification. This issue has been successfully solved by utilising a two-step approach and a dual selection marker whereby a positively selected marker is inserted first at the target site and then replaced by the donor sequence in the second round via a negative selection step. In this manner recombineering can now allow seamless and highly accurate transfer of extremely large donor sequences into a target of essentially unlimited size.

3.1.1. Cre-Lox recombination technology

A further notable use of recombination based technology, Cre-Lox site specific recombination, has allowed additional refinements in transgene expression. First developed in 1988, Cre-Lox systems utilise a site-specific Phage P1 recombinase known as Cre, which mediates recombination only between specific 34 bp DNA sequences known as LoxP sites (Sauer and Henderson, 1988). This sequence specificity allows recombination between two distant sites (inserted into a transgene) to be driven at very high efficiencies, without leading to off target events elsewhere in the host genome. Depending on the relative orientation of the two inserted LoxP sites, addition of Cre recombinase can lead to inversion, translocation, or deletion of the sequences flanked by the LoxP sites (Nagy, 2000) (Figure 1).

3.1.2. Box 1: Vector manipulation by RedET recombination – 'recombineering'

Homologous recombination allows the seamless and accurate transfer, or manipulation, of large genomic loci through the insertion of the site specific regions of homology. These regions of homology are inserted using 'homology arms' of up to 150 bp attached to the ends of standard PCR primers. These regions of homology drive strand exchange and homologous recombination allowing a donor sequence to be inserted with absolute precision into a target.

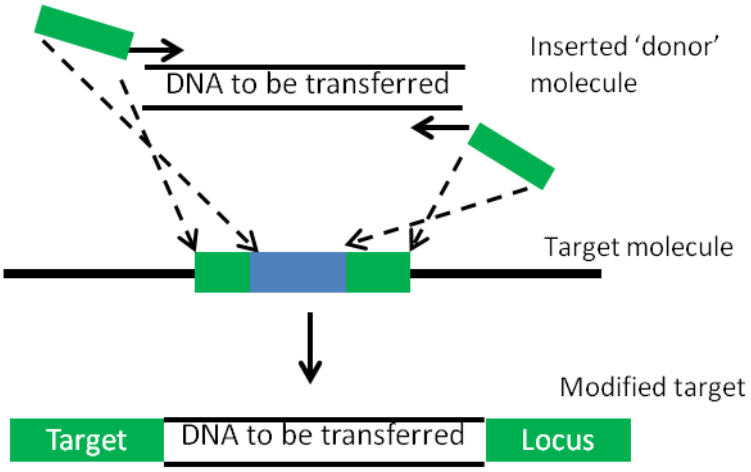

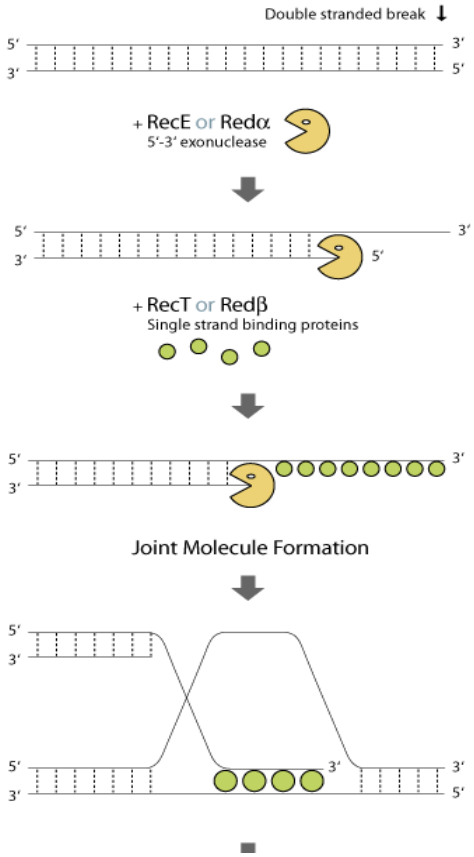

Modified from www.Genebridges.com
DNA Replication

Recombination in the Red/ET system is driven by a pair of phage λ derived proteins, Redα and Redβ. Redα acts as a 5'→ 3' exonuclease resecting the free 5' DNA ends at a double strand break. Recβ is a single strand binding protein (SSBP) required to bind to the single strand produced by Recα to produce the nucleoprotein strand required for strand invasion, D loop formation, and DNA polymerisation.

Recα/β are expressed from the pSC101-BAD-gbaA (pRedET) plasmid as part of a Recγβα operon expressed under the arabinose inducible pBAD promoter.

As such the following steps are taken to induce insertion of a target DNA locus into a recipient molecule:

1. Addition, and induction, of the pSC101-BAD-gbaA (pRedET) plasmid to electrocompetent *E.coli* containing the target molecule.
2. PCR amplification of the 'donor' molecule with primers containing homology arms to the target locus.
3. Insertion of this PCR product to the electrocompetent induced pSC101-BAD-gbaA *E.coli*
4. Plating of bacteria onto media with antibiotics added/removed depending on the sensitivity/resistance encoded by the 'donor' molecule.

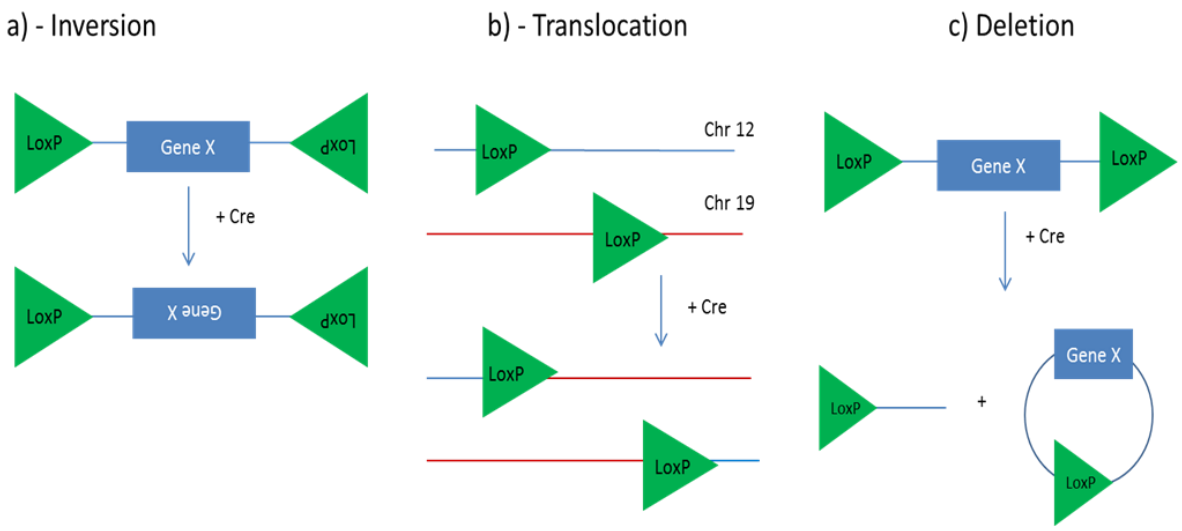

Figure 1: Cre-LoxP recombination: inversions, translocations and deletions

The requirement for homologous sequences to pair-up before strand invasion means the relative orientation of LoxP sites determines the direction in which recombination between two LoxP sites occurs. Placing the two LoxP sites in opposite directions causes an inversion of the central sequence (a), whilst placing two LoxP sites in the same orientation within a single DNA sequence leads to a deletion between the two sites whilst (c). Placing two LoxP sites on different DNA strands (i.e. separate chromosomes) leads to a translocation of DNA from one strand/chromosome to the other (b).

3.1.3. A novel genomic BAC-based expression system for *FUS*

In this chapter we describe the generation of a BAC-based genomic expression vector for the ALS and FTD associated gene *FUS*. The full genomic *FUS* locus together with up- and down-stream regions were cloned into a BAC vector, tagged with the mCherry fluorescent protein and modified with a LoxP site between the promoter and exon 1 of *FUS*. Three pathological mutations, R244C, R521C and P525L, were separately engineered to generate a total of four *FUS* expression vectors (three mutants and a wild type). An overview of the cloning process is shown in Figure 2.

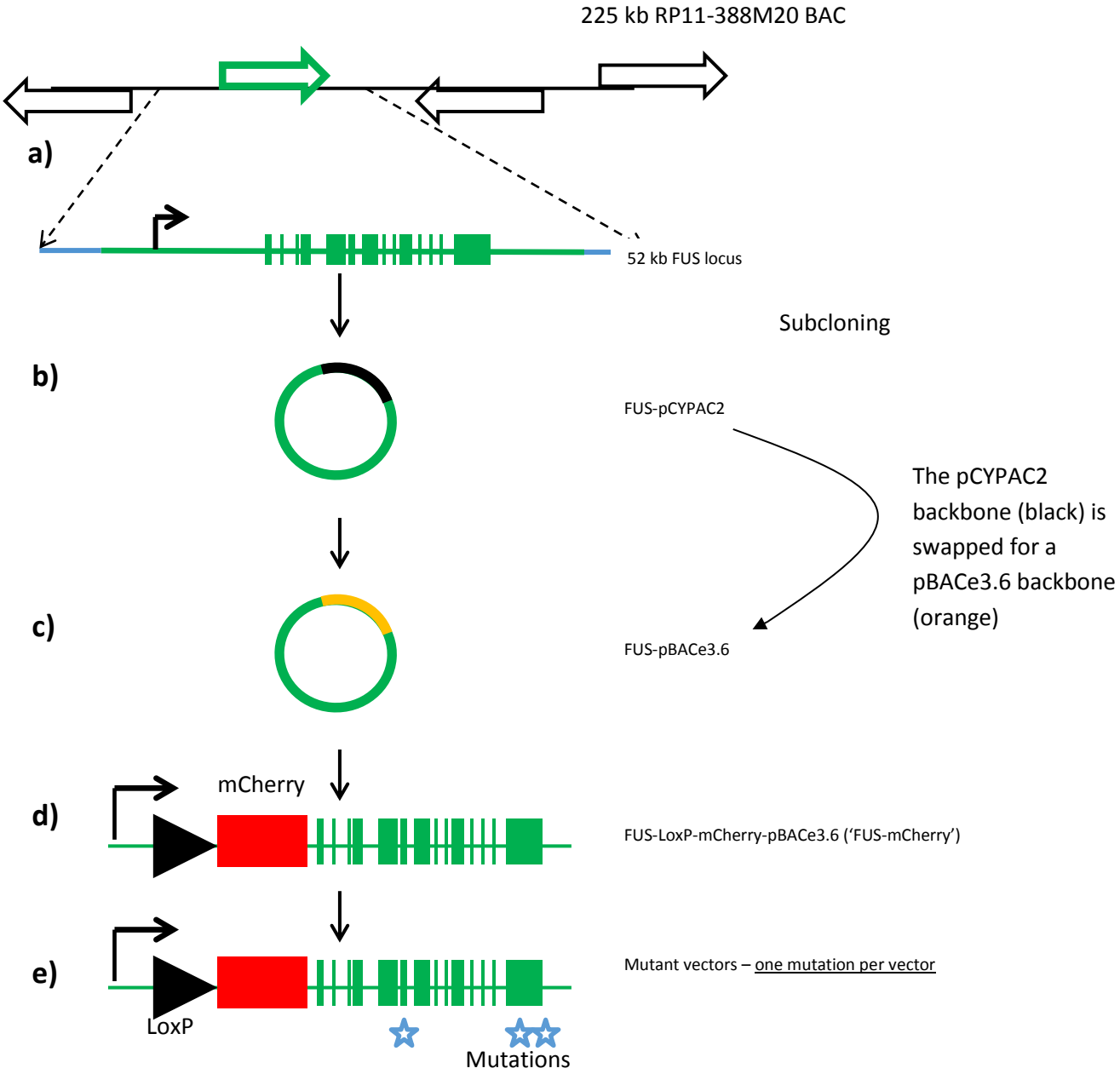

Figure 2 - Overview of cloning steps required to construct mCherry tagged WT and mutant FUS vectors

a) A locus containing *FUS* (green in diagram) within a large RP11 bacterial artificial chromosome (BAC) was selected and **b)** subcloned from the RP11 BAC into a pCYPAC2 vector (black sequence). **c)** The *FUS* locus is then transferred to a pBACe3.6 vector (orange sequence). **d)** mCherry and a LoxP511 site are inserted 5' of FUS exon 1. **e)** Three pathological mutations are inserted separately to create three mutant and one WT vector.

3.2. Results

3.2.1. Subcloning of *FUS* into a pCYPAC2 vector.

A bacterial artificial chromosome (BAC) vector, RP11-388M20, containing the human *FUS* genomic locus within a total vector size of 225 kb, was obtained from the BACPAC resource centre, Children's Hospital Oakland Research institute, CA. In order to isolate *FUS* from other genomic loci present within the original vector we 'subcloned' *FUS* into a new pCYPAC2 vector designed to accept large genomic DNA inserts (Figure 3a, b). The locus chosen for transfer between vectors contained the full *FUS* open reading frame (ORF) plus 31 kb of upstream sequence and 9.5 kb of downstream sequence to maximise the inclusion of regulatory regions. The limits of this cloning reflected the presence of other annotated genes or miRNAs within the RP11-388M20 insert, in this case *PYCARD* downstream and *PRSS36* upstream (Figure 3a, b).

Subcloning was achieved through 'recombineering' to allow seamless and accurate swapping of large genomic loci through homologous recombination (Box 1). The target pCYPAC2 vector backbone (containing essential vector features such as selective markers and an origin or replication) was amplified by PCR using primers containing arms homologous to the 5' and 3' limits of the *FUS* locus to be cloned. The PCR product was digested with Dpn1 to remove template DNA, purified, and electroporated into electrocompetent *E. coli* containing both RP11-388M20 and the recombination plasmid pSC101-BAD-gbaA (Figure 3b, c) (Box 1). Colonies grown on media containing kanamycin (the pCYPAC2 vector encodes kanamycin resistance whilst RP11-388M20 encodes chloramphenicol (Chl) resistance) were screened using colony PCR and confirmed by junction PCR, exon PCR and restriction digests (see Figure 3d, e and Figure 4 (d) for junction PCR schematic).

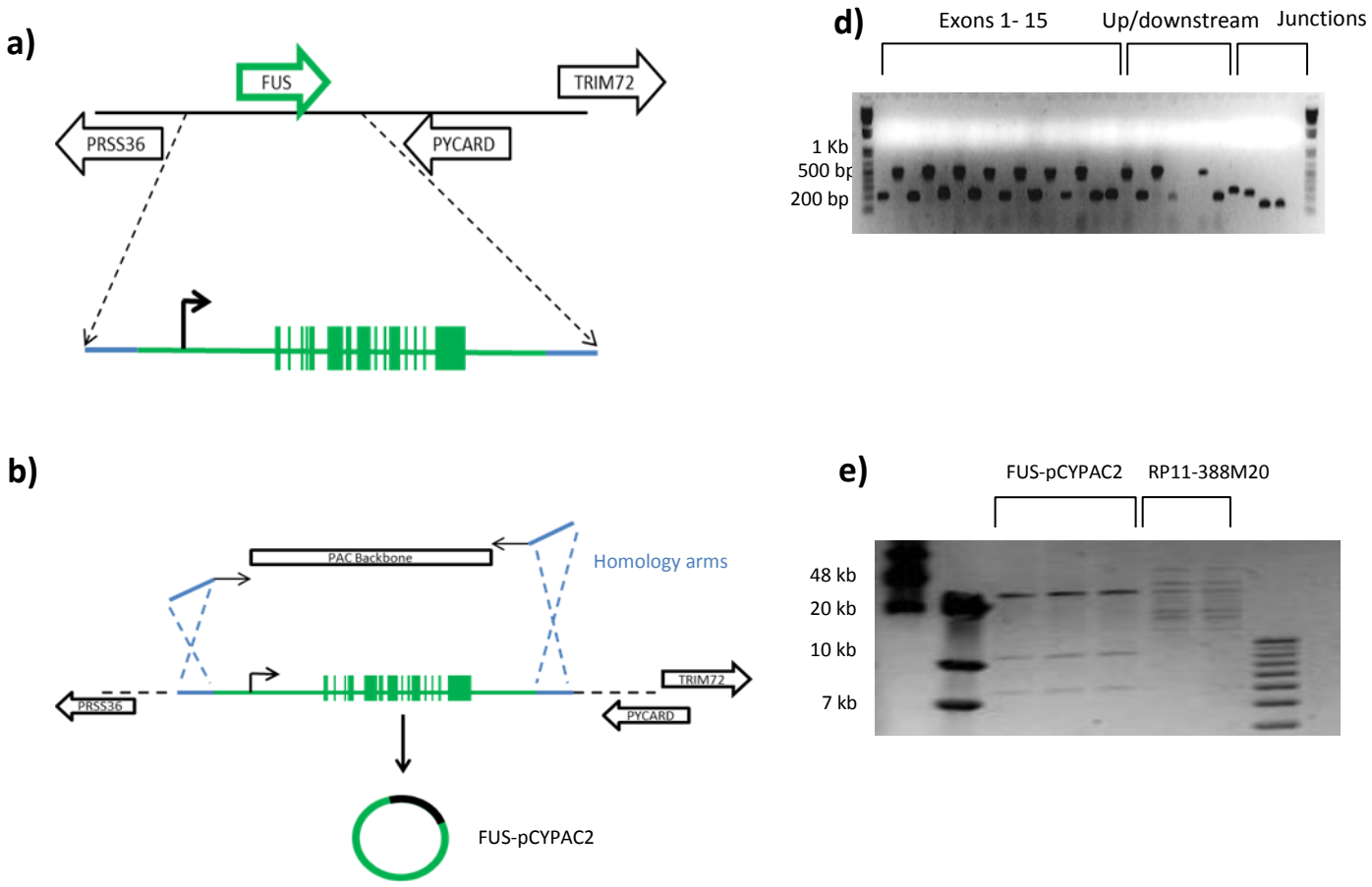

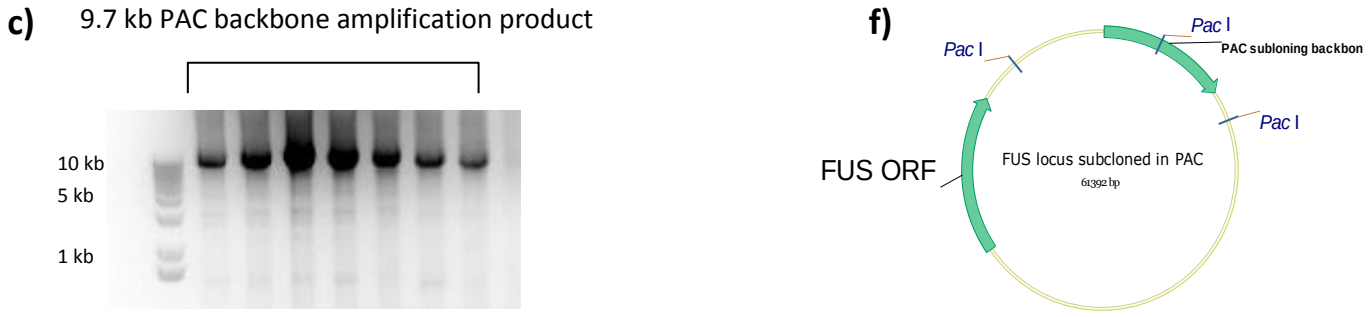

Figure 3: Subcloning *FUS* from RP11-388M20 to pCYPAC2.

a) A 52 kb locus containing *FUS* was chosen to be cloned from a large chromosome 16 locus. **b)** Subcloning of the *FUS* locus, replacing 172 kb of RP11-388M20 with a 9.7 kb portion of pCYPAC2 backbone, using recombineering. **c)** Successful amplification of the 9.7 kb pCYPAC2 backbone using long primers containing homology arms to the *FUS* locus boundaries. **d)** PCR showing the presence of all *FUS* exons, up and downstream regions at 5 kb intervals (with the band for 11kb downstream missing due to being cut off through recombination), and newly formed recombination junctions. **e)** Restriction digest with the PacI enzyme shows expected bands for FUS-pCYPAC2 (kb, 42.9, 11, 7.4). **f)** Vector map for FUS-pCYPAC2 showing PacI cut sites.

3.2.2. Cloning of the *FUS* locus from pCYPAC2 to pBACe3.6

After subcloning into the pCYPAC2 vector, the *FUS* locus was returned to a BAC-based vector to take advantage of a variant LoxP511 site present within the backbone of pBACe3.6 (Figure 4a and section 3.1.4). The variant LoxP511 will allow recombination, within the completed vector, between two LoxP sites and lead to separation of the *FUS* ORF from the *FUS* promoter, hence terminating expression (Figure 4b).

Switching of the locus from the pCYPAC2 vector to pBACe3.6 utilised the same methodology as the initial subcloning step. A core 6.8 kb section of the BAC backbone containing essential vector features (chloramphenicol resistance, origin of replication) was amplified using primers with homology arms to the edges of the selected FUS locus. Template DNA was removed and the PCR product concentrated, purified, and electroporated into *E. coli* cells containing both the FUS-pCYPAC2 and induced pSC101-BAD-gbaA vectors. Electroporated bacteria were grown on media containing chloramphenicol and screened for successful recombination by colony PCR and further confirmed by junction and exon PCR together with restriction digests (Figure 4c, d, e, f).

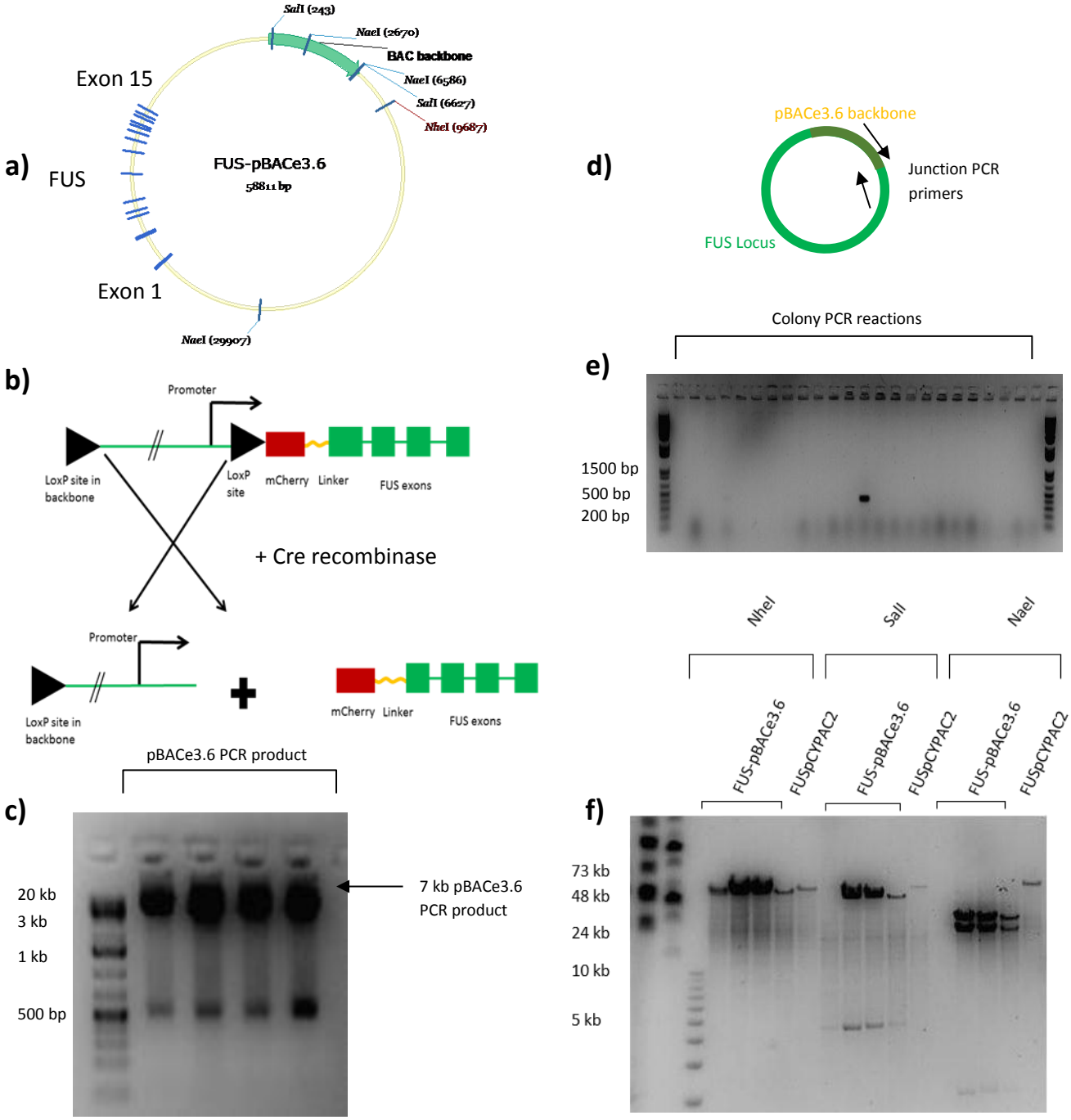

Figure 4: Cloning *FUS* from pCYPAC2 to pBACe3.6

a) Vector map for pBACe3.6-FUS showing *FUS* exons, BAC backbone and restriction sites. **b)** Schematic of how insertion of an additional LoxP511 (see 3.1.4), together with a second LoxP511 site within the pBACe3.6 backbone, will allow expression to be terminated on addition of Cre recombinase. **c)** Successful amplification of a 6.8 kb portion of the pBACe3.6 backbone with long primers containing homology arms to the boundaries of the FUS locus (see Figure 3, b). **d)** Location of PCR primers used to screen recombinants with colony PCR (and, together with a second primer pair at the other junction, junction PCR). **e)** Colony PCR showing a single positive recombinant. **f)** Restriction enzyme digest of FUS-pBACe3.6 and a control FUS-pCYPAC2 construct. Expected band sizes; NheI – FUS-pBACe3.6 = 58 kb, FUS-pCYPAC2 = 61 kb. SalI – FUS-pBACe3.6 = 52, 6 kb, FUS-pCYPAC2 = 61 kb. NaeI – FUS-pBACe3.6 = 32, 23, 4 kb. FUS-pCYPAC2 = 61 kb.

3.2.3. Addition of an mCherry tag and LoxP site 5' of FUS exon 1

Generation of a fluorescently-tagged fusion protein allows subcellular localisation, disrupted in FUS mutants, to be followed in real time. The red fluorescent protein mCherry was chosen to complement a YPET tagged TDP-43 vector already generated in the laboratory. Amongst the monomeric derivatives of DsRed, mCherry displays the greatest photostability, fastest maturation and tolerance of N terminal fusions making it ideal for a red fluorescent N terminal tag for FUS (Shaner et al., 2004).

Furthermore, to allow expression of *FUS* to be terminated, a variant LoxP511 site was inserted 5' of mCherry (Figure 4b). Together with the LoxP511 site within the pBACe3.6 backbone these sites will, on addition of Cre recombinase, specifically mediate recombination separating the *FUS* ORF from its promoter and hence terminate expression (Figure 4b). A 15 bp flexible linker encoding 5 small non-charged amino acids (Gly-Ala-Gly-Ala-Gly), previously shown to have excellent properties separating protein domains, was inserted between mCherry and exon 1 of *FUS* to minimise the impact of mCherry on nascent FUS polypeptide folding (Figure 5a) (Argos, 1990).

The mCherry and LoxP sequences were introduced together in a two stage process known as STEP (sequential insertion of target with overlapping primers) recombineering in which four overlapping primers are utilised to generate homology arms of up to 155 bp at each end of the PCR product to be inserted into the target vector (Alegre-Abarrategui et al., 2009). The greater the length of homology arms the greater the efficiency of homologous recombination, especially during negative selection steps (Figure 5). As most commercially available primers are limited to 100 bp (of which 20 bp are needed as the actual primer binding sequence) the use of two overlapping 100 bp primers at each end of the amplified donor sequence increases homology and recombination efficiency (Alegre-Abarrategui et al., 2009).

The following protocol was used to insert the mCherry tag and LoxP511 site:

1. A dual selection (encodes kanamycin resistance and streptomycin sensitivity) RpsL-neo cassette was inserted 5' of *FUS* exon 1 by recombineering (Figure 5). This cassette was amplified using 4 long primers, and electroporated into induced electrocompetent *E.coli* containing the FUS-pBACe3.6 vector. Recombination is then allowed to take place (see Figure 6 a, b and Methods). This PCR product is engineered such that the first section of the homology arms contain sequences required for the second, less efficient, recombination step (Figure 5).
2. The presence of RpsL-neo is selected for using kanamycin, and confirmed with PCR and restriction digests (Figure 6c, d).
3. mCherry is then amplified using four long primers and electroporated into induced elctrocompetent *E. coli* containing FUS-RpsL-pBACe3.6 to allow recombination (Figure 7a).
4. Replacement of RpsL-neo with mCherry is screened for by plating bacteria on streptomycin positive, kanamycin negative media and performing colony PCR followed by junction / exon PCR and restriction enzyme digests (Figure 7b, c)

This two stage process (insertion of RpsL-neo and replacement with mCherry) has two important functions:

1. Allows mCherry to be inserted seamlessly without a permanent selective marker being retained.
2. Allows extra homology required for the second, less efficient negative selection, stage to be inserted in the first, more efficient, stage. This improves the chances of successfully inserting a locus in the absence of positive selection.

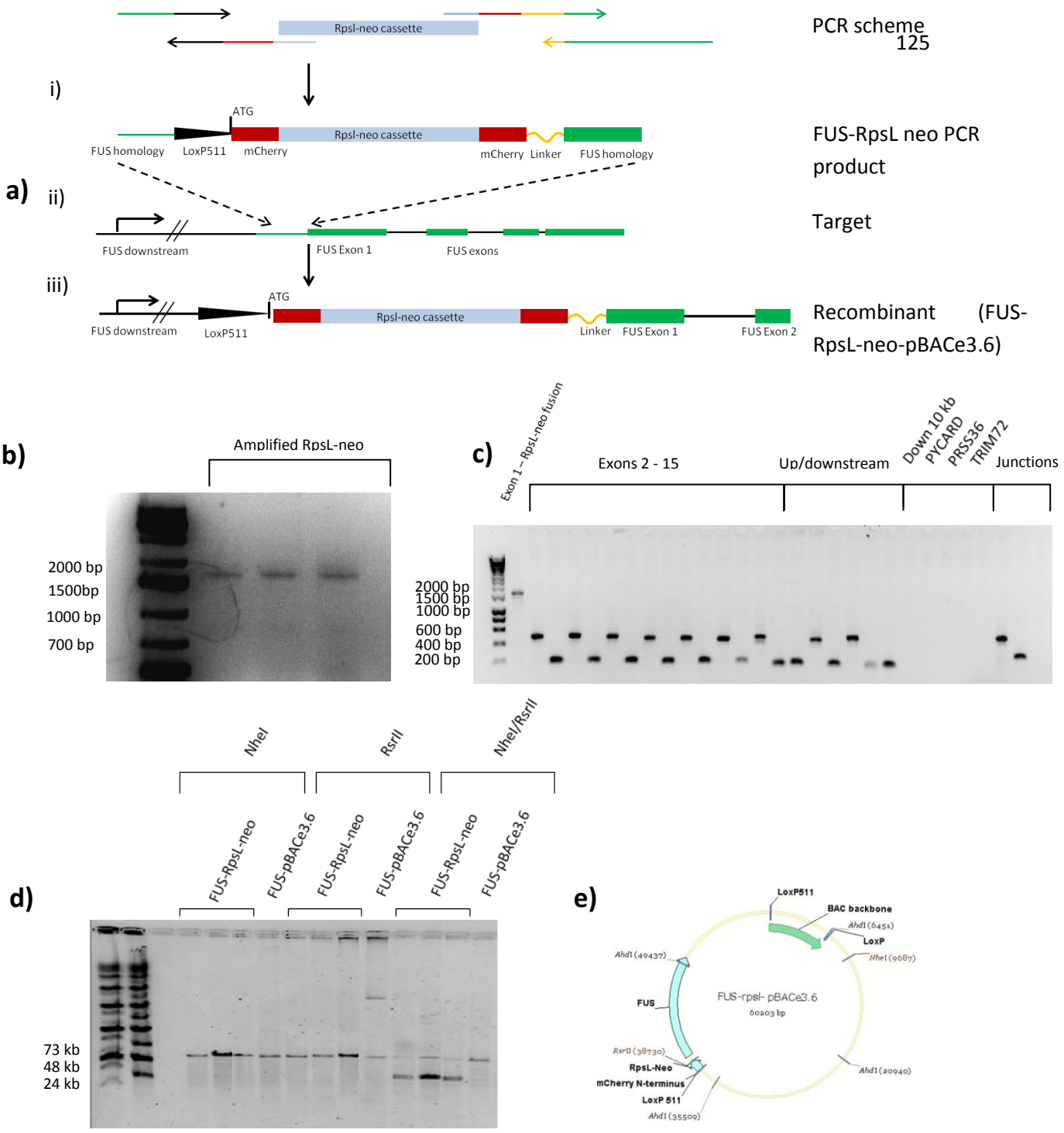

Figure 5: Tagging protocol – 1) Insertion of RpsL-neo cassette

a) i) RpsL-neo is amplified with four overlapping primers that encode both LoxP (43 bp) and mCherry C (35 bp) and N (16 bp) sequences together with homology arms to the FUS locus (58/87 bp). ii) This PCR product is inserted 5' of FUS exon 1 by recombination, iii) generating FUS-RpsL-neo-pBACe3.6. **b)** Column purified 1572 bp RpsL-neo PCR product (see Methods). **c)** Exon PCR showing all 15 *FUS* exons, all four recombination junctions, and a lack of cut off neighbouring genes and upstream 10.5 kb marker lost in the subcloning process. The 1727 bp band for exon 1 corresponds to the exon 1 - RpsL-neo fusion. **d)** Restriction enzyme digests of FUS-RpsL-pBACe.3.6 and a FUS-pBACe3.6 control. Expected bands (kb) – FUS-RpsL-pBACe.3.6 - NheI = 60.2, RsrII = 60.2, NheI/RsrII = 31.2, 29, FUS-pBACe3.6 -NheI = 58.9, RsrII = no cut, NheI/RsrII = 58.9. e) Vector map for FUS-RpsL-neo-pBACe3.6.

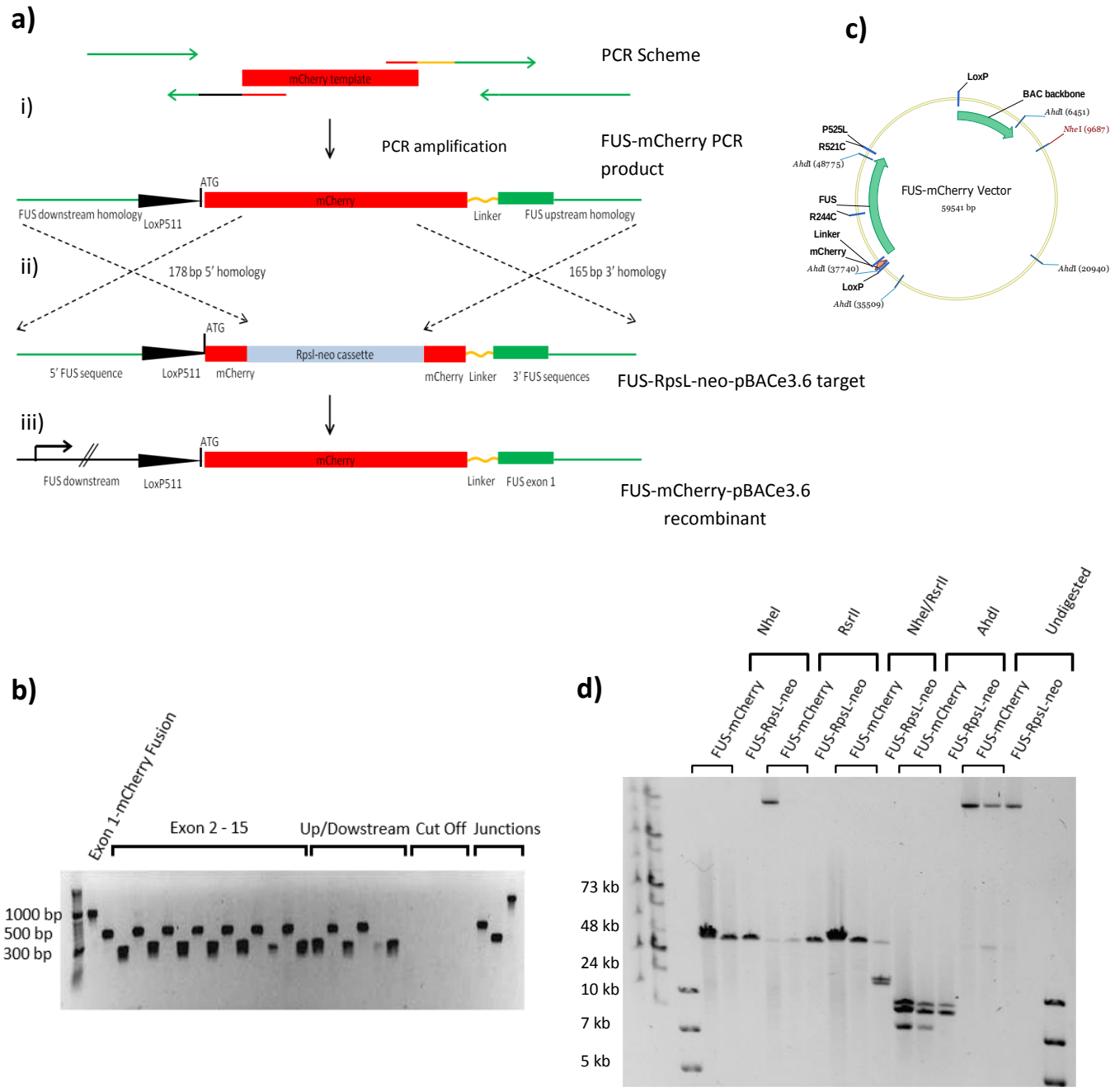

Figure 6: Tagging protocol – 2) Insertion of mCherry

a) i) mCherry is amplified using 4 long overlapping primers that encode homology to the insertion site in FUS-RpsL-neo. ii) These homology arms, together with the sequences inserted in stage one (Figure 5), generates a total of 178 and 165 bp of homology respectively, and mediate recombination to generate iii) the FUS-mCherry-pBACe3.6 vector (FUS-mCherry). **b)** PCR of successful recombinant showing the presence of all exons and new recombination junctions and absence of cut out genes/regions (downstream by 10.5 kb marker, PYCARD, PRSS35 and TRIM72). **c)** Vector map for FUS-mCherry showing restriction enzyme sites used in d). **d)** Restriction enzyme digest of FUS-mCherry and a FUS-RpsL-neo control showing correct band pattern. Expected band sizes (kb); mCherry-FUS-pBACe3.6 – NheI = 59.5, RsrII = no cut, NheI/RsrII = 59.5, AhdI = 17.2, 14.6, 14.5, 11. Control RpsL-FUS-pBACe3.6 – NheI = 60.2, RsrII = 60.2, NheI/RsrII = 31.2, 29, AhdI 17.2, 14.6, 14.5, 13.9

3.2.4. Insertion of pathogenic mutations

As *FUS* mutations are causative for ALS, we sought to model ALS pathogenesis by engineering one of three mutations, each described in ALS cases, independently into the vector. The three mutations selected were:

- R521C (exon 15) – the most frequently identified FUS mutation, shown to be causative for ALS in a number of independent families (Blair et al., 2010; Chio et al., 2011; Kabashi et al., 2011).
- P525L (exon 15) – a mutation shown to be associated with an early onset and severe form of ALS, hence likely to provide a strong cellular phenotype (Bäumer et al., 2010; Conte et al.; Huang et al., 2010).
- R244C (exon 6) – located away from the C terminal NLS (where R521C and P525L reside) and hence likely to have a different, and uncharacterised, method of pathogenesis (to R521C and P525L) (Kwiatkowski et al., 2009b).

Mutations were inserted in a four-stage process whereby;

1. Dual-selection RpsL-neo cassettes were inserted at the site of mutagenesis (one in exon 6, and one in exon 15) within the FUS-mCherry-pBACe3.6 vector in such a manner that the wild type bases to be modified were deleted (Figure 7).
2. Exons 6 and 15 were cloned out of the FUS-mCherry-pBACe3.6 vector by PCR and inserted into separate pGEMT vectors by TA cloning (Figure 8).
3. Mutations were inserted into cloned out exons 6 and 15 by site directed mutagenesis and confirmed by sequencing (Figure 8).
4. RpsL-neo cassettes were replaced by their respective mutated exons using homologous recombination. Successful insertion of mutated exons was followed by PCR, restriction digests and sequencing (Figure 9)

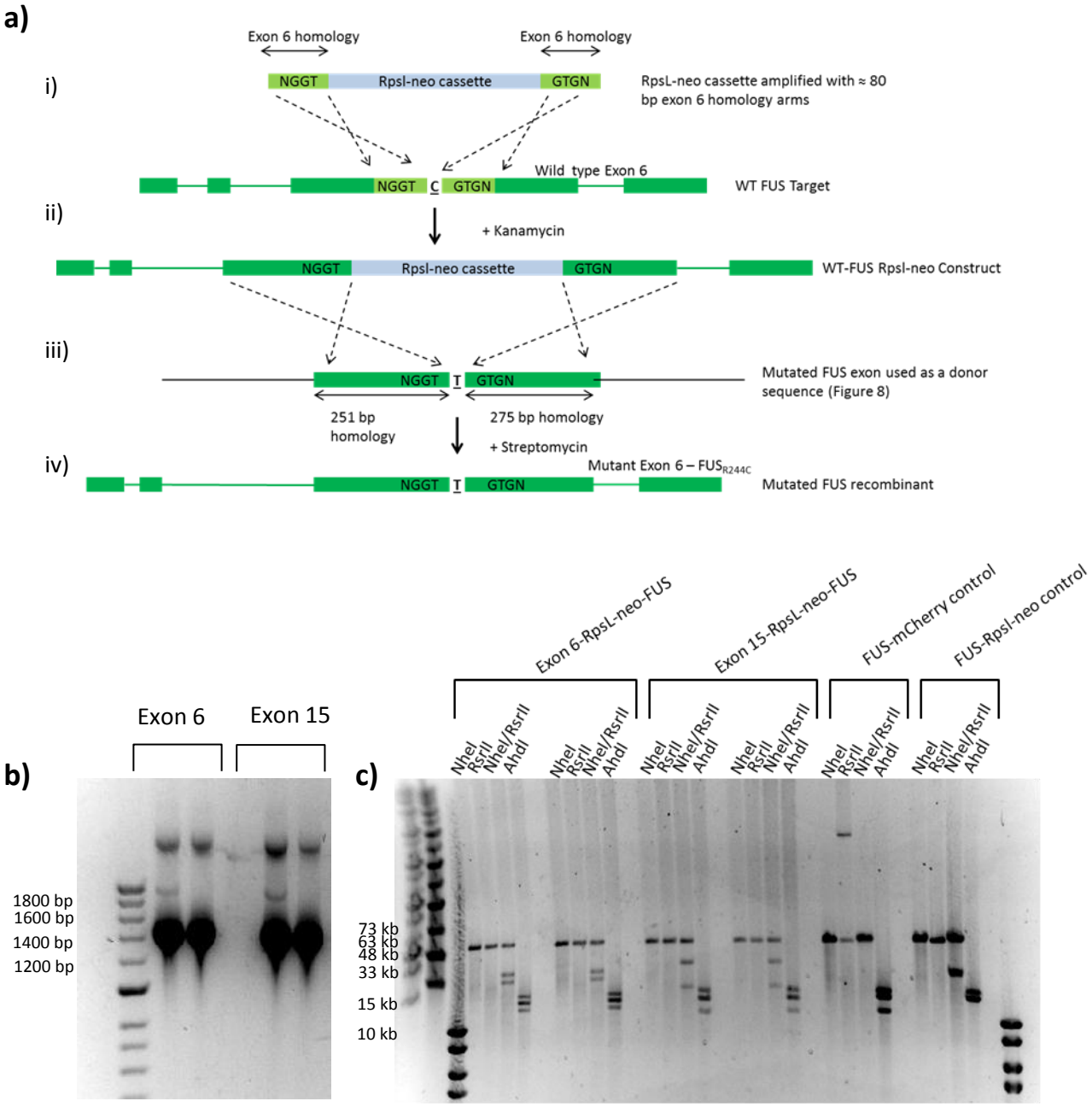

Figure 7: Mutagenesis – 1) Overall strategy and insertion of RpsL-neo

a) Insertion of mutations follows a four-step process, shown here for exon 6/R244C, whereby; i) RpsL-neo is amplified using long primers with homology arms to the target exon (homology arms finish either side of the base(s) to be mutated). ii) The RpsL-neo PCR products' homology arms mediate insertion into the required exon with loss of the base(s) to be mutated. A single RpsL-neo cassette is used to replace both exon 15 mutations, which are separated by only 12 bases. iii) Site directed mutagenesis is used to engineer a base change within a 526 bp region centreing around each putative mutation. iv) This mutated 526 bp section (E6/E15) is then used to replace the wild type sequence at exon 6 or 15, inserting the required mutation(s). **b)** Successful amplification of 1429 bp RpsL-neo product with exon 6 and exon 15 homology arms, respectively. **c)** Restriction enzyme digests for exon 6 and exon 15 RpsL-neo insertions and controls. Expected Band sizes (kb): Exon 6-RpsL – NheI = 60.8 kb, RsrII = 60.8 , NheI/RsrII = 34.6, 26.2, AhdI = 17.2, 14.5, 14.5, 12.2, 2.4. Exon 15-RpsL – NheI = 60.8, RsrII = 60.8, NheI/RsrII = 41, 20, AhdI = 18.5, 14.5, 14.4, 11.3, 2.1

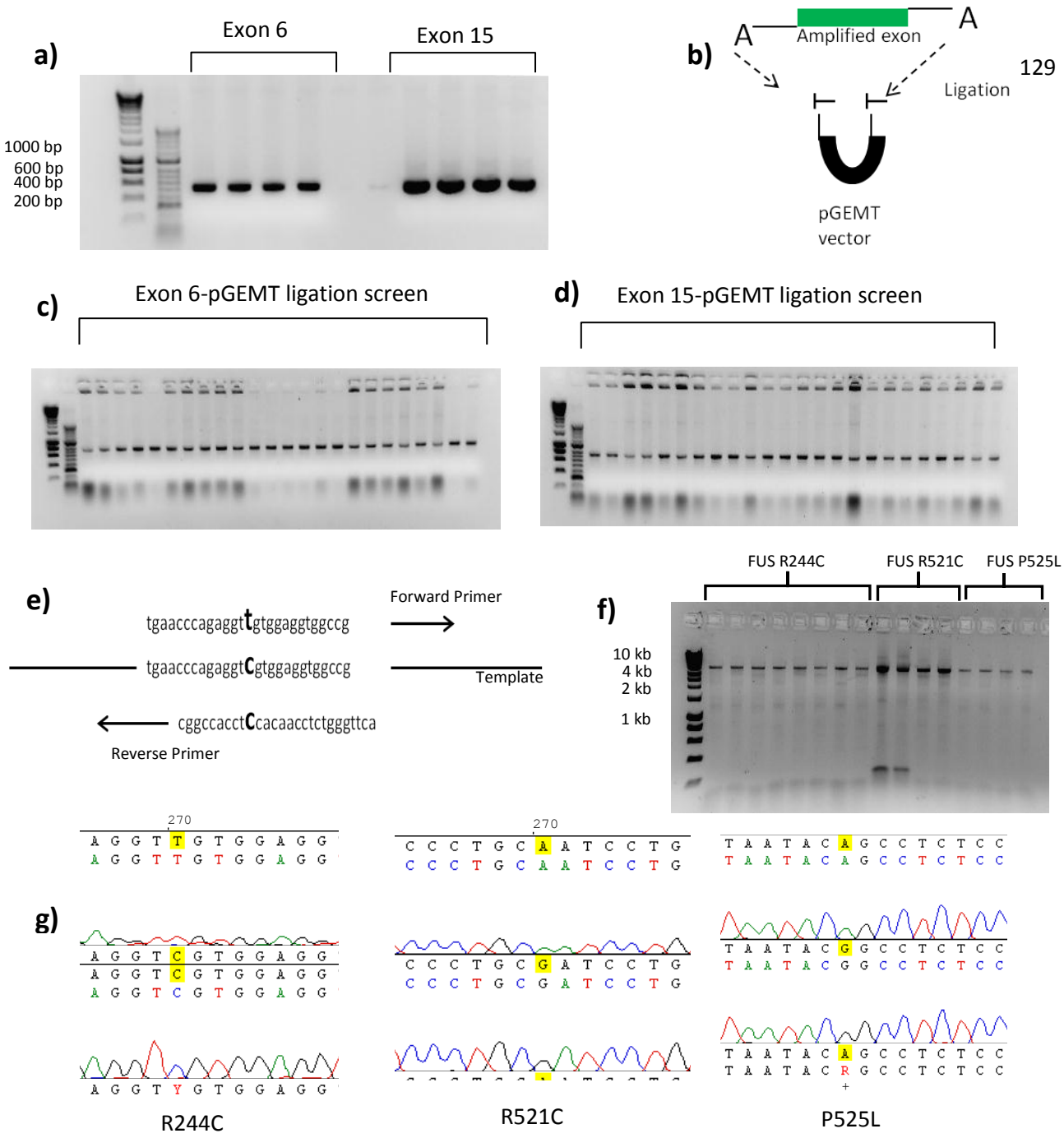

Figure 8: Mutagenesis – 2) Cloning out *FUS* exons and site directed mutagenesis

a) Successful amplification of 526 bp product containing exon 6 or 15 using a high fidelity PCR system (see Methods). **b)** TA cloning utilises overhanging T bases to mediate highly efficient ligation of PCR products into the pGEMT vector (Promega). **c, d)** Successful ligation of exons 6 and 15 into pGEMT, as demonstrated by colony PCR using primers to new vector junctions (junction PCR, see Methods). **e)** Site directed mutagenesis (SDM) primers used for insertion of the R244C mutation (for full list see Appendix). **f)** Successful site directed mutagenesis reactions shown by gel electrophoresis. **g)** Sequencing of each mutation construct confirmed successful mutagenesis, mutation sites are highlighted in yellow.

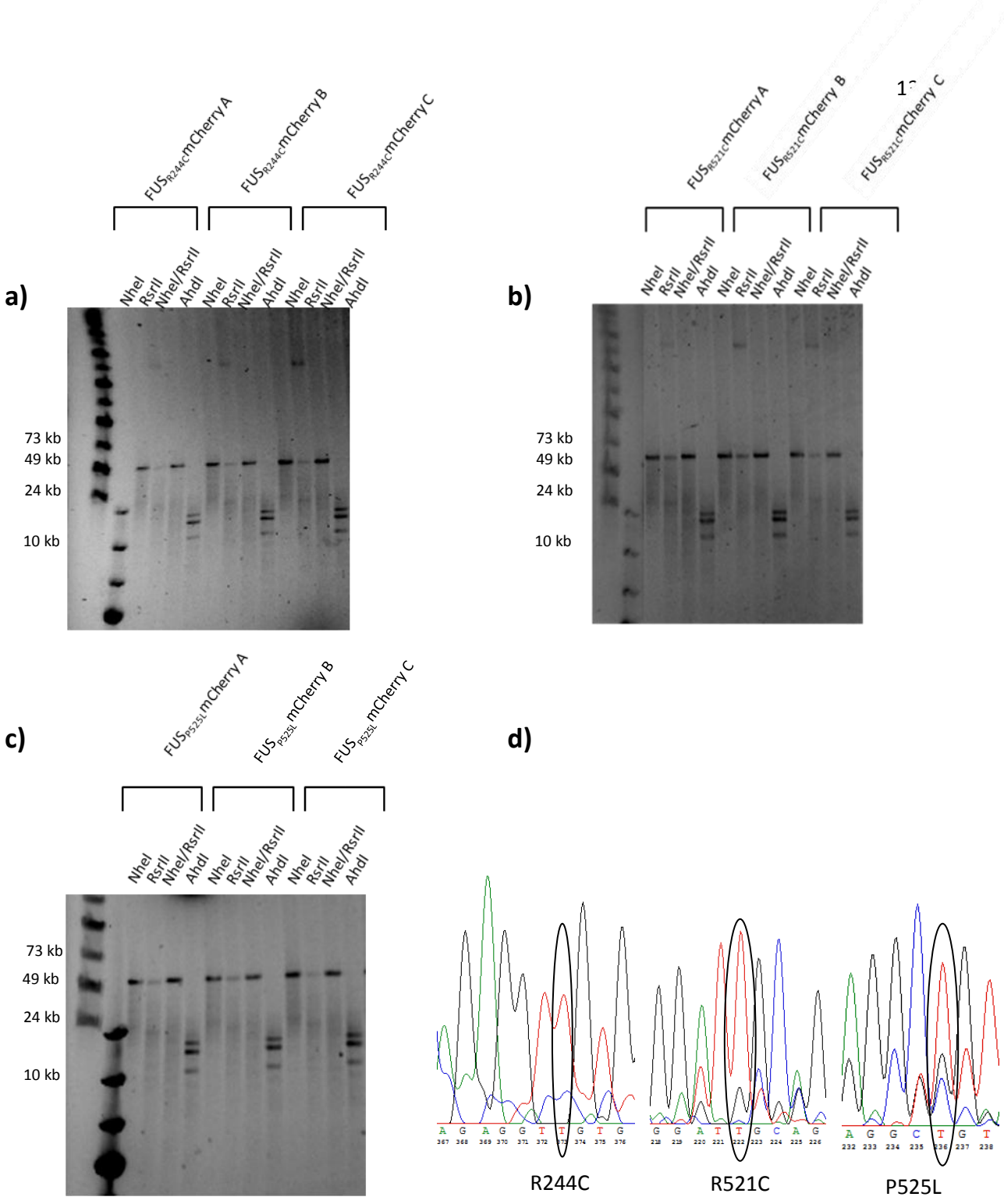

Figure 9: Mutagenesis – 3) Insertion of mutated exons 6 and 15

a) Restriction enzyme digests of three FUS_{R244C}mCherry recombinants (a, b and c). Expected band sizes (kb); NheI = 59.5 kb, RsrII = no cut, NheI/RsrII = 59.5 kb, AhdI = 17.2, 14.6, 14.5, 11. **b)** Restriction enzyme digests of FUS_{R521C}mCherry. Band sizes as in a). **c)** Restriction enzyme digests of FUS_{P525L}mCherry. Band sizes as in a). **d)** Sequence traces for mutated exons 6 and 15 showing the presence of the new base.

3.2.5. Caesium chloride-purification of supercoiled BAC DNA

Purified supercoiled BAC DNA for mouse transgenesis (by pronuclear injection) was generated by dual caesium chloride banding (See Methods). This procedure robustly purifies supercoiled BAC DNA through density gradient ultra-centrifugation using a caesium chloride solution. Purified supercoiled BAC DNA (FUS^{WT}mCherry and FUS^{P525L}mCherry) was used for pronuclear injections in order to generate mouse models of FUS dysfunction using our vectors (Transgenesis performed by Dr Ben Davies, Wellcome Trust Centre for Human Genetics, University of Oxford).

a)

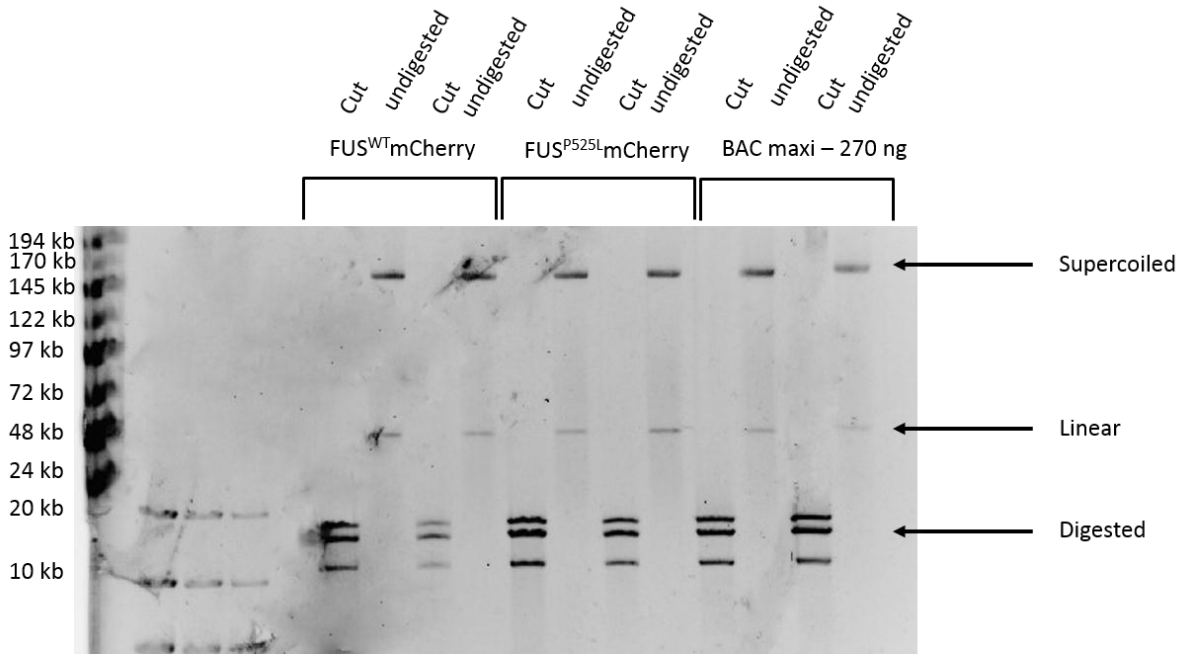

Figure 10 – Purification of supercoiled FUS-mCherry DNA

a) Purified supercoiled DNA extracted from FUS^{WT}mCherry and FUS^{P525L}mCherry constructs was separated by PFGE (see Methods). Clear supercoiled bands are seen for both WT and P525L constructs. Correct vector architecture was checked with by AhdI restriction digest (Expected band sizes (kb) = 17.2, 14.6, 14.5, 11).

3.3. Discussion

Here we describe the generation of BAC-based genomic DNA expression vectors containing the entire genomic locus of *FUS,* together with 31 kb and 9.5 kb of upstream and downstream regulatory sequence, respectively. The insertion of a whole genomic DNA locus, together with extensive up- and down-stream non-coding sequence, should maximise the inclusion of regulatory elements affecting *FUS* expression within the vector and accurately recapitulate the physiological expression pattern of *FUS*. Insertion of one of three separate pathogenic mutations – R244C, R521C and P525L - will allow the effect of these mutations on protein function and localisation within disease to be dissected within a highly physiological model system. To increase the power of these vectors to investigate *FUS* dysfunction, a fluorescent reporter was fused to the N terminal of the protein to allow live tracking of the protein and generate an epitope allowing the transgene to be differentiated from endogenous FUS. Furthermore, the addition of a variant LoxP site between the promoter and exon one of *FUS* will allow expression to be terminated on addition of Cre recombinase. Given the availability of inducible or tissue-specific Cre-expressing mice, this should allow powerful inferences to be made as to *FUS* dysfunction through time-course or tissue-specific termination of FUS expression. Genomic DNA expression systems controllable in this manner are highly novel, partially due to concerns about the distance between the LoxP sites affecting recombination efficiency, but should, if successful, allow a multitude of elegant and physiologically relevant experiments to be carried out *in vivo* and *in vitro*.

Utilising RedET recombination allowed accurate transfer of DNA sequences of up to 9.5 kb. Technical efficiencies were limited most by the generation of large PCR products, and by negative selection steps during the insertion of the mCherry tag (Figure 6).

Very low recombination efficiencies whilst swapping the RpsL-neo cassette for the mCherry tag (1 in ~ 2800 bacterial colonies screened positive) (Figure 6) were almost certainly due to a loss of streptomycin sensitivity in the RpsL-neo cassette after PCR amplification. It is possible that without

the use of STEP recombination, to increase the homology arm lengths in this step, that the recombination efficiency seen would have been even lower and further impeded progress. Future cloning projects utilising this dual-selection cassette should ensure both kanamycin resistance and streptomycin sensitivity are present, and that donor/target homology is maximised, before attempting to replace the cassette. Replacement of the RpsL-neo cassette during mutagenesis was much more efficient (approximately 5 to 10 % of screened recombinants were correct), by comparison to the same negative selection step during insertion of the mCherry, due to a likely combination of a smaller insert and target size, increased homology and functional streptomycin sensitivity. By contrast, the insertion of DNA sequences by positive selection was relatively efficient, even for very large inserts (up to 9.5 kb during subcloning), with efficiencies of between 1 in 50 and 1 in 200 bacteria screened (per correct recombinant) usually seen. For the insertion of smaller sequences such as the RpsL-neo cassette by positive selection, efficiencies approached 1 in 10. In general recombination efficiency appeared to depend upon:

- The size of the insert to be transferred: small insertions such as the mutant exons prepared by site directed mutagenesis were extremely efficient.
- The size of the homology arms flanking the sequence to be inserted, especially in the negative selection steps inserting mutated exons.
- The concentration and purity of the PCR product electroporated into *E. coli* cells for recombination.
- The concentration of the *E. coli* bacterial stock that the PCR product was electroporated into.
- The competency of the *E. coli* for electroporation (electrocompetencies of above 1 X 10^9 being ideal for the electroporation of large PCR products).

Generation of large PCR products proved challenging in some circumstances with annealing temperature, together with primer, template DNA, and magnesium chloride concentrations proving

critical and specific for each step. The use of *Taq* polymerases with proofreading activity appeared to successfully minimise the insertion of unwanted mutations during PCR amplifications of donor sequences (as assessed by whole insert sequencing).

The next chapters of this thesis explore the *in vitro* characterisation of these vectors, dissecting the impact of the inserted *FUS* mutations.

On completion of the *FUS* vectors, the FUS^{WT}mCherry and FUS^{P525L}mCherry vectors were also, in parallel with *in vitro* work, used to create transgenic mice strains through pronuclear injection of caesium chloride-purified supercoiled vector DNA (Figure 10, injections performed by Dr Ben Davies, Welcome Trust Centre for Human Genomics). Founders for both the mutant and wild type vectors have been generated and these mouse lines will be crossed onto a *FUS* knockout background to give an extremely physiological and controllable mouse model of *FUS* and its contribution to ALS and FTD. Initial data suggests that insertion of the FUS transgenes has not led to early, excessive toxicity and embryonic lethality was not seen (personal communication, Thomas Vizard, Nuffield Department of Clinical Neurosciences, University of Oxford)**.** Characterisation of these mice is outside the remit of this project but will be done within the University of Oxford in the group of Professor Kevin Talbot.

4. Chapter Four – Dissecting the Impact of *FUS* Mutations in a HEK293 Cell Model

4.1. HEK293 Cells as a model to study the effect of *FUS* mutations using FUS-mCherry genomic expression vectors

4.1.1. *In vivo* and *in vitro* transgene model systems

Expression of transgenes within immortalised cell lines is a long-established method for dissecting the fundamental impact of genetic mutations on protein localisation, function and toxicity. Whilst cell culture based models are often not seen as a disease model per se, they allow assays of disease-specific mutations to be quickly performed. Compared to *in vivo* experiments in transgenic animals, immortalised cell lines do not provide a physiological environment in which to model human neurological disease. The lack of interaction between different cell and tissue types, short expression time-courses, and a limitation to model events only at the cell and molecular level are all experimental issues present when modelling disease-associated mutations *in vitro*. There are, however, many benefits to *in vitro* models of mutation-associated phenotypes, especially when investigating dysfunction at the level of a single gene. *In vitro* models allow transgene-expressing cells to be studied on a timescale of days rather than the months, or even years, required to generate and breed transgenic animals. Rapid, and relatively cheap, production of transgene expressing cells also allows multiple investigative lines to be followed and high-throughput screening of compounds to modify any phenotypes seen. Furthermore, whilst whole animal models allow testing at levels above the cellular, the molecular function can be the most important level when investigating the basic impact of mutations on protein or RNA function. At this level cell culture systems are able to provide detailed molecular insights, with transgene localisation easily followed and multiple biochemical assays available for protein function and cytotoxicity. So far, in the case of

FUS, the majority of animal models have been highly descriptive – affirming the role of FUS in neurodegeneration but providing precious few clues as to the mechanism by which this might occur. It is here, in investigating the molecular mechanism of FUS dysfunction, that cell culture models have provided the recent insights. We therefore decided to model the effects of *FUS* mutations using the FUS-mCherry vectors within a tractable cell culture model.

4.1.2. Genomic DNA vectors and cell transformation

When using large genomic DNA vectors, insertion of the vector DNA into a cell line can be a major problem. Simple transfection of vectors above 50 kb in size can be problematic in many cell lines, with very low efficiencies seen. To avoid this problem two basic approaches can be used; selecting a cell line with very high transfection efficiency or using a more specialised delivery method suited to large vectors. Methods used to transduce 'inefficient' cells, such as neuronal cultures, include the use of infectious viruses such as *Herpes simplex* virus (HSV) amplicons whose genome has been modified such as to include the heterologous DNA to be expressed. Further systems used include taking advantage of site-specific recombination through the insertion of LoxP (or similar) sites within the donor (plasmid) and acceptor (the cell line to be transformed). Whilst this approach does allow efficient insertion of a vector into the host cells genome it does still require initial delivery of a plasmid to cells by transfection. Both these approaches do, however, require extensive further cloning after generating an expression vector, either to insert the vector into a viral genome or add recombination sites. The presence of variant LoxP sites between the promoter and exon 1 of the FUSpBACe3.6mCherry vectors meant that inserting further DNA sequences by simple Cre-mediated recombination was impossible and would have required additional recombineering steps. For rapid analysis we opted to use a tractable cell line offering very high transfection efficiencies, and to express our FUS-mCherry constructs in a transient manner by simple transfection.

4.1.3. HEK293 cells and expression of genomic vectors

HEK293 cells, a cell line derived from human embryonic kidney tissue in the early 1970s, have several features that allow expression of large genomic BAC vectors. HEK293 cells (from here on referred to as HEK cells) were originally generated by the transformation of embryonic kidney cells by insertion of adenovirus 5 DNA – a 4.5 kb viral insert is still found within chromosome 19 of the HEK cell genome (Graham et al., 1977). HEK cells have a highly complex karyotype and are described as being hypotriploid – possessing two or more copies of each chromosome and an average chromosome number of 64. Somewhat surprisingly, given their tissue origin, HEK cells appear to show neuronal features and express a number of neuronal proteins including the neurofilament subunits NF-M/NF-L and α-internexin (Shaw et al., 2002). This result has been reported for a number of independently derived human kidney cells suggesting a preferential transformation of neuronal lineage cells within mixed human kidney cell culture (Shaw et al., 2002). Notably, within the context of this thesis, HEK cells are considered one of the most easily transfected cells and previous work from our laboratory has shown they readily allow the expression of large genomic DNA vectors of up to 150 kb by transfection (Alegre-Abarrategui et al., 2009). HEK cells are also heavily used in the expression of transgenes due to their ability to correctly translate, modify and fold proteins (Thomas and Smart, 2005). The adherent nature of HEK cells also makes them ideal for fluorescent imaging, a useful feature when expressing fluorescently tagged proteins. As such, given large size of the FUS-mCherry vectors to be expressed, we selected HEK cells as a model system to dissect the functional impact of *FUS* mutations.

Examples of successful transgene modelling in within HEK293 cells include genomic cell culture models of genetic dysfunction in Friedrich's ataxia (FRDA) and Parkinson's disease (PD). A recent cell culture model expressing the whole genomic locus of the Frataxin gene (*FXN*) demonstrated reduced *FXN* expression on addition of a GAA repeat sequence within exon 1. GAA repeat expansions cause FRDA through a poorly characterised mechanism and this model elegantly demonstrates the advantages of a genomic cellular model in investigating a complex genetic contribution to disease (Lufino et al., 2013). Generation of a HEK293 cell line expressing this genomic *FXN* vector fused to a

luciferase reporter allowed the impact of repeat expansions on expression level to be modelled. Furthermore the utility of a basic cell line containing a whole genomic DNA locus (with all the DNA sequences regulating expression present) allowed screening of a library of small molecules to identify compounds that elevated mutant *FXN* expression. A lead compound showing a significant increase in mutant *FXN* expression was isolated and may have excellent therapeutic potential (Lufino et al., 2013). This model highlights the benefits of combining a highly regulated model of dysfunction at a genetic locus with a tractable and easily manipulated *in vitro* cell culture model.

A further example of a genomic DNA cellular reporter model that demonstrated the advantages of this system was seen in the expression of WT and mutant *LRRK2* at physiological levels within HEK293 cells (Alegre-Abarrategui et al., 2009). Expression of *LRRK2* from the native promoter allowed cellular localisation and action to be determined without the confounding issues of cDNA associated overexpression (in this model expression of *LRRK2* from a genomic vector led to 25-30 times less expression than from a cDNA based vector). Utilising a YPet (a YFP derivative) fluorescent tag LRRK2 was localised to components of the endosomal-autophagic pathway as well as to p62 and ubiquitin marked cytoplasmic puncta (Alegre-Abarrategui et al., 2009). Furthermore, expression of disease-associated mutations led to an impairment of autophagic balance within transfected cells. This model revealed a key role of LRRK2 in healthy cells (autophagy) and suggests a mechanism by which disease associated mutations could act upon this pathway (impaired autophagic flux) (Alegre-Abarrategui et al., 2009).

These two models highlight how genomic DNA cellular reporter models allow highly physiological expression of complete human genetic loci, whose encoded proteins can then be assessed for cellular localisation, function, and mutation-associated phenotypes within a highly modifiable and potentially high-throughput model system. These systems allow dysfunction at a single genetic locus to be dissected in fine detail. It is clear, therefore, that genomic DNA expression vectors can, and

should, be used in cell culture *in vitro*, rather than being the sole preserve of vertebrate transgenic models *in vivo*.

4.1.4. Results from recent FUS cellular models

Recently-published models of *FUS* dysfunction using basic cell lines have made several important discoveries over the last five years. Many of these results have been discussed in greater detail in Chapter One but are briefly highlighted here. Insertion of *FUS* NLS mutations in vectors transfected into HeLa cells was quickly shown to lead to a relocalisation of mutant FUS from the nucleus of the cell to the cytoplasm (Dormann et al., 2010). This report replicates findings in human disease and gave the first hints as to the mechanisms likely operating in the molecular pathogenesis of FUS. Interactions between mutant FUS and cytoplasmic stress granules have also be widely studied in cellular models, including HEK293 cells (Bosco et al., 2010b; Gal et al., 2011). Stress granules are cytoplasmic messenger ribonucleoprotein particles (mRNPs) that form under conditions where translation initiation is inhibited. mRNA molecules stalled during translation initiation accumulate in these particles, alongside translation initiation factors and RNA binding proteins such as TIA-1, TIA-R and poly(A)-binding protein (PABP) (Buchan and Parker, 2009). Assembly of stress granules is linked to various factors, including the pool of mRNAs stalled in translation initiation, protein modification status of translation initiation factors and microtubule network status. Protein-protein interactions between RNA binding proteins via Q/N rich prion-like domains, such as those suggested to be present in FUS and TDP-43, have also been suggested to modulate stress granule assembly (Udan and Baloh, 2011). Stress conditions such as excess heat, UV irradiation, viral infections and oxidative stress can all lead to stress granule induction through eIF2α kinases which monitor these cellular stresses and feedback onto translational initiation (Anderson and Kedersha, 2008). Cytoplasmically-localised FUS has frequently been show to localise to sodium arsenite-induced stress granules within

cell culture models but the relevance of this interaction to disease is yet to be defined (Andersson et al., 2008; Bosco et al., 2010a; Gal et al., 2011).

Perhaps the best characterised features of FUS biology discovered purely *in vitro* has been the mapping of wild type and mutant FUS binding sites in both DNA and mRNA (Blechingberg et al., 2012; Colombrita et al., 2012; Kino et al., 2011; Lagier-Tourenne et al., 2012). As discussed in more detail earlier, these studies (some of which were conducted in HEK293 cells) have begun to hint at the specific roles played by FUS, and what the impact of mutations on these roles might be. Recently published *in vitro* studies have also used arginine methylation inhibitors to reverse the mutation-associated cytoplasmic relocalisation of FUS. Whilst these studies show be of great importance in defining the mechanism of FUS toxicity (gain or loss of function) results have so far been mixed and no consensus has been found (see Chapter One).

4.1.5. Summary

We have chosen to investigate the impact of the inserted *FUS* mutations in a HEK293 cell model. HEK cells will allow the 60 kb FUS-mCherry vectors to be efficiently transfected and should provide a good model with which to dissect the impact of inserted *FUS* mutations. This *in vitro* model of FUS dysfunction will partner a more complex rodent model generated with the same vectors. This mouse model will act as a model of ALS and FTD whilst the *in vitro* model should allow more specific questions as to the molecular pathogenesis of FUS to be investigated.

4.2. Results

4.2.1. Transient transfection of FUS-mCherry vectors in HEK293 cells demonstrates expression of the generated fusion protein

FUS-mCherry vector DNA was transfected into human embryonic kidney cell line cells (HEK293 cells) using Lipofectamine (see Methods). Four days post-transfection, cells were analysed for expression of the predicted 102 kDa FUS-mCherry fusion protein by Western blot, RT-PCR and fluorescence microscopy (Figure 1a). Western blots against the mCherry tag demonstrated expression for all four constructs (WT, R244C, R521C and P525L) (Figure 1b). RT-PCR also demonstrated the presence of mRNA corresponding to the fusion protein in transfected cells (Figure 1c). RT-PCR further demonstrated that HEK293 cells express endogenous FUS at appreciable levels (Figure 1c). Clear fluorescence from the mCherry tag could be seen in live cells transfected with FUS-mCherry vectors, as visualised by fluorescence microscopy (Figure 1d). These data confirm that the FUS-mCherry vectors generated in Chapter 3 all express the encoded fusion protein in HEK293 cells at a level allowing clear detection using western blots, RT-PCR and live cell fluorescence imaging.

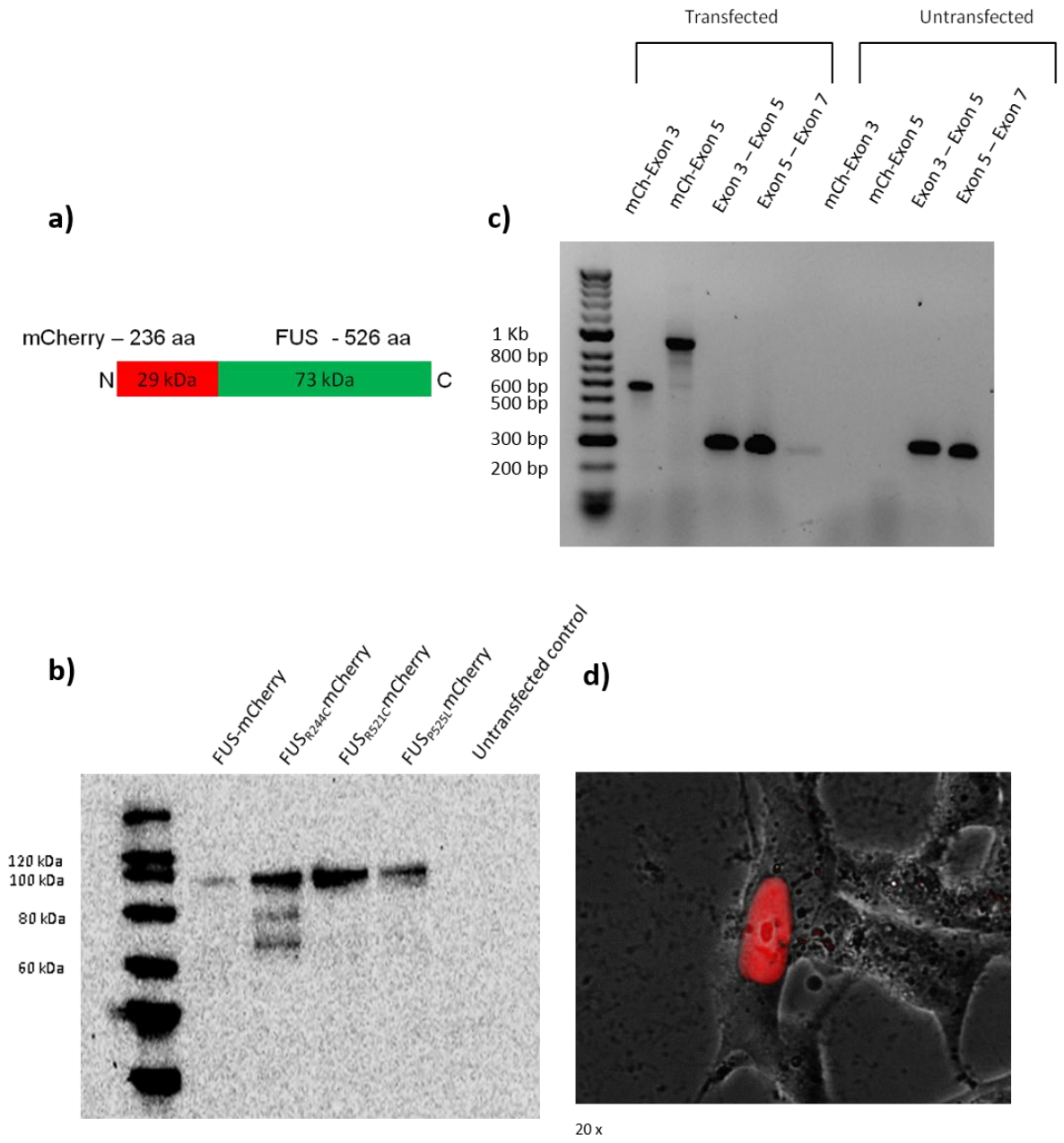

Figure 1 – *FUS*-pBACe3.6-mCherry vectors express mCherry tagged FUS in HEK293 cells

a) Schematic of the expected 102 kDa FUS-mCherry fusion protein expressed from the FUS-pBACe3.6-mCherry (FUS-mCherry) vectors. **b)** Demonstration of FUS expression in transiently transfected HEK293 cells by western blot using an anti-mCherry antibody (see Methods 2.2.3 and 2.2.3.2). Clear bands are seen at the expected 102 kDa range for the fusion protein for all constructs generated. **c)** RT-PCR using a primer anchored within the mCherry tag and paired with primers in either *FUS* exon 3 or 5 demonstrates expression in transfected cells only. Primers between *FUS* exons 3, 5 and 7 demonstrate the presence of endogenous FUS in HEK293 cells. **d)** Native/Live mCherry fluorescence in HEK293 cells transfected with the FUS^{WT}pBACe3.6-mCherry vector as visualised by fluorescence microscopy.

4.2.2. The R521C and P525L *FUS* mutations lead to a cytoplasmic relocalisation of FUS-mCherry, whilst the non-NLS R244C mutation does not

Wild type and mutant FUS-mCherry vectors were transfected into HEK293 cells and cytoplasmic localisation was determined using live fluorescence or by immunocytochemistry (ICC) to the mCherry tag in fixed cells. Live cell fluorescence imaging confirmed a nuclear localisation for FUS^{WT}mCherry whereas FUS^{P525L}mCherry was found throughout transfected cells, in both the cytoplasm and nucleus (Figure 2a). Closer inspection of localisation patterns using immunocytochemical staining for mCherry with a nuclear counterstain (DAPI) demonstrated a nuclear localisation for FUS^{WT}mCherry and FUS^{R244C}mCherry (Figure 2b). By contrast, the FUS NLS mutations R521C and P525L caused a clear cytoplasmic redistribution of FUS, with P525L leading to a greater accumulation of cytoplasmic FUS than R521C. Notably, the P525L mutation did not, however, lead to full clearance of FUS-mCherry from the nucleus (Figure 2b). Quantification of cytoplasmic FUS was achieved by counting cells showing appreciable cytoplasmic relocalisation. Cells that appeared dead or mitotic by DAPI staining were excluded due to their likely nuclear envelope breakdown. A significant cytoplasmic relocalisation was associated with the insertion of the R521C mutation with 31.8% (+/- 2.11) of cells showing appreciable cytoplasmic FUS (Figure 2c). Insertion of the P525L mutation was associated with a stronger relocalisation and was observed in 95.57% (+/- 4.62) of cells counted (Figure 2c). Notably, the degree of relocalisation induced by the inserted mutations corresponds with the age of onset of fALS cases associated with these mutations, suggesting the degree of cytoplasmic relocalisation may affect disease severity (Figure 2d).

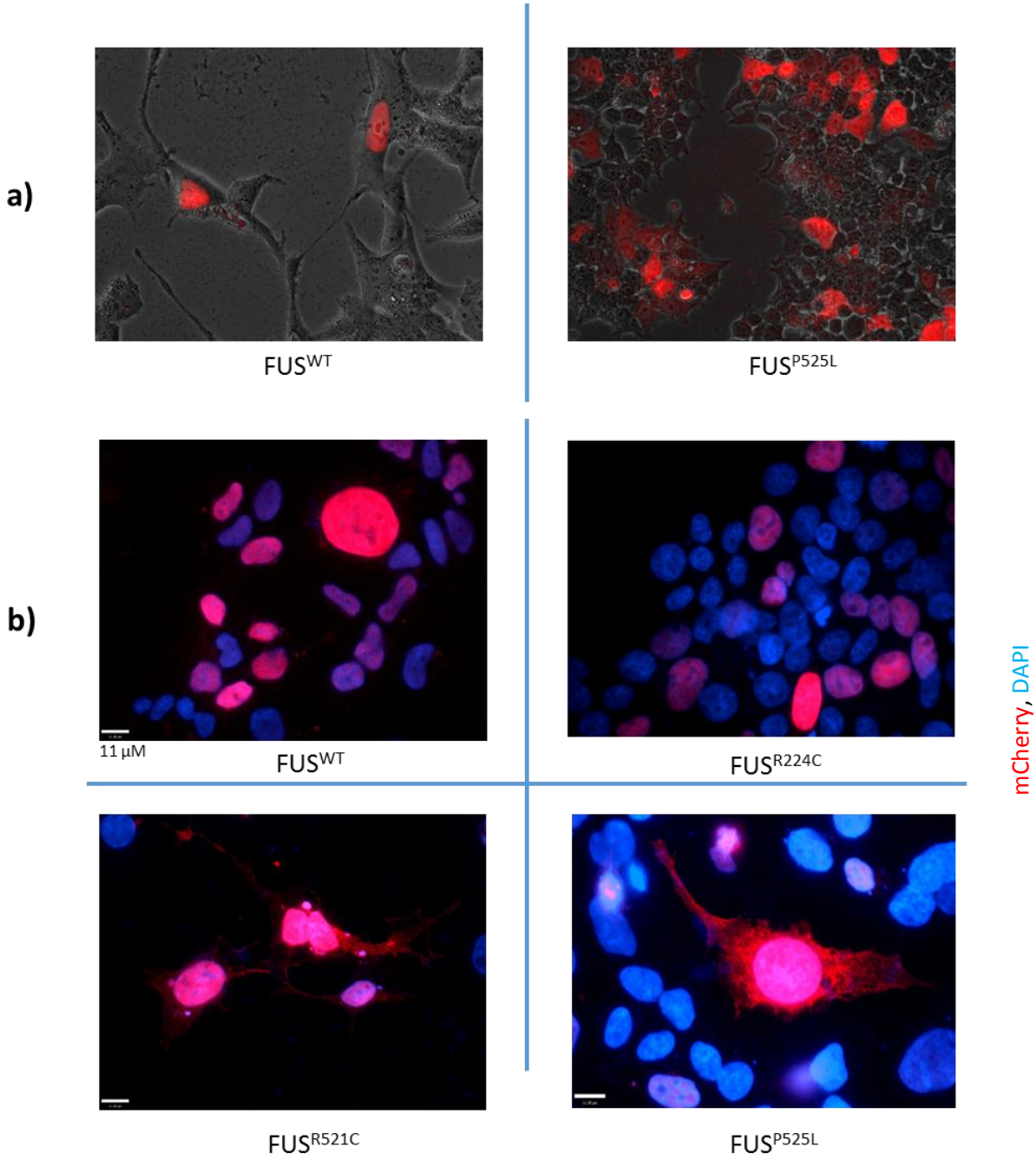

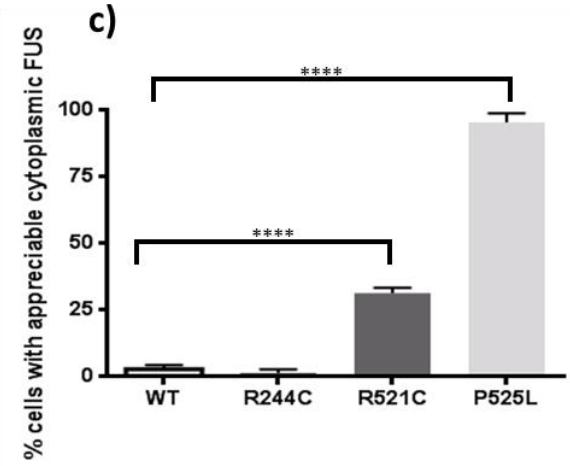

d)

Mutation	Affected individuals	Families described	Mean age at onset (years)
R244C	2	1	58
R521C	39	16	37.4
P525L	12	9	22

Figure 2 – The FUS Nuclear Localisation Sequence Mutations R521C and P525L lead to Cytoplasmic Relocalisation

a) Live fluorescence from transfected HEK cells expressing either WT or P525L FUS. WT FUS has a clear nuclear localisation and cannot be seen in the cytoplasm. By contrast, P525L FUS appears to be located throughout cells. **b)** Immunocytochemical staining for mCherry together with the nuclear marker DAPI in fixed HEK cells. **c)** Quantification of relocalisation phenotypes. Cells positive for mCherry were counted and scored positive for relocalisation if clear cytoplasmic FUS could be seen. Cells with necrotic or mitotic nuclei, as assessed by DAPI staining, were excluded. One-way ANOVA was performed using GraphPad Prism with corrections for multiple testing. Both R521C and P525L show highly significant relocalisation compared to W ($p > 0.0001$). No difference was observed between WT and R244C (Relocalisation, percentage transfected cells; WT – 2.9 (+/- 1.2), R244C – 2.08 (+/- 2.1), R521C – 31.49 (+/- 2.0), P525L – 95.59 (+/-1.9)). **d)** Table showing the number of patients described with the R244C, R521C or P525L mutation. The number of independent families in which each mutation has been described is listed, as are approximate mean ages at onset for each mutation (data from the AD and FTD mutation database, www.molgen.ua.ac.be)

4.2.3. P525L mutant FUS forms cytoplasmic aggregates in transfected cells

Expression of FUS^{P525L}mCherry in HEK293 cells led to the formation of strongly mCherry-immunoreactive puncta within the cytoplasm of a significant number of transfected cells (ranging between 5 and 20% depending on conditions) (Figure 3a). Puncta intensely-immunoreactive for mCherry showed irregular morphologies ranging from a rounded to filamentous shape, and were found only in cells expressing FUS^{P525L}mCherry. These puncta stained positively for both mCherry and FUS using dual immunocytochemical staining (Figure 3b). Whilst occasional puncta appeared weakly immunopositive for ubiquitin the vast majority were negative for ubiquitin staining (Figure 3b). Puncta were also negative for p62, HSP70 and tubulin (Figure 3b).

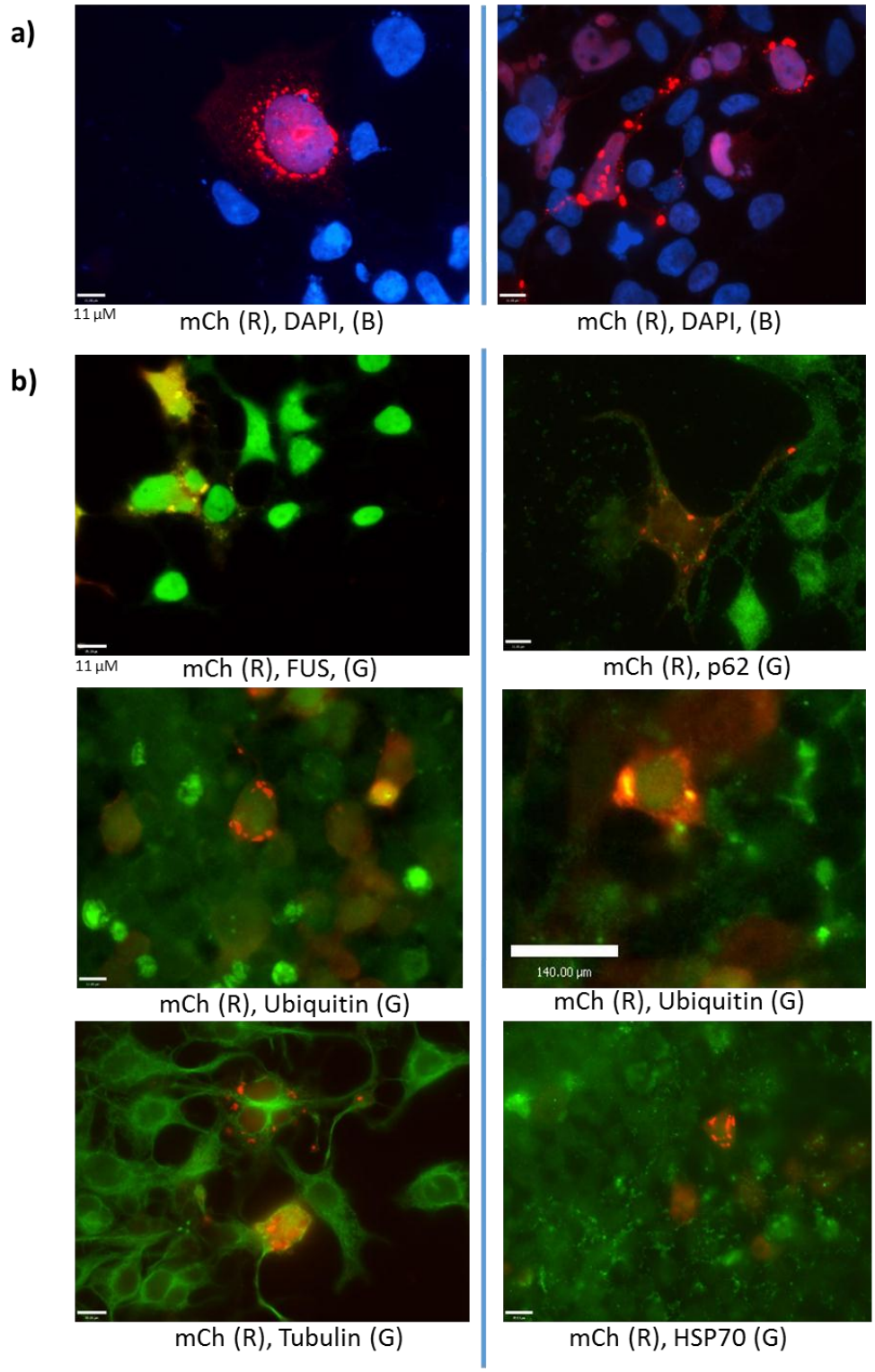

Figure 3 – P525L mutant FUS forms cytoplasmic aggregates in transfected cells

a) P525L, but not WT, R244C or R521C, FUS forms spontaneous cytoplasmic aggregates in transfected HEK293 cells as assessed by ICC against mCherry. **b)** Dual ICC for FUS, ubiquitin, p62, HSP70 and tubulin (green) alongside mCherry (red).

4.2.4. Relocalisation of mutant FUS does not impact on the localisation of WT FUS or TDP-43

Double-transfection of cells with FUS^{P525L}mCherry and a wild type FUS cDNA plasmid containing a HA tag (Addgene plasmid number 26374, Hoell et al., 2011) allowed dual immunocytochemical staining to determine the effect of mutant FUS upon the localisation pattern of wild type FUS (see Methods). Expression of FUS^{P525L}mCherry appeared not to impact upon the localisation of FUS^{WT}HA which remained nuclear in dual-transfected cells (Figure 4b). FUS^{WT}HA was not sequestered within FUS^{525L}mCherry aggregates in double-transfected cells with FUS^{P525L}mCherry aggregates (Figure 4c). Cells transfected with FUS^{P525L}mCherry were also assessed by ICC for TDP-43 localisation. Cytoplasmic accumulation of FUS^{P525L}mCherry had no impact on TDP-43 localisation which remained nuclear (Figure 4d).

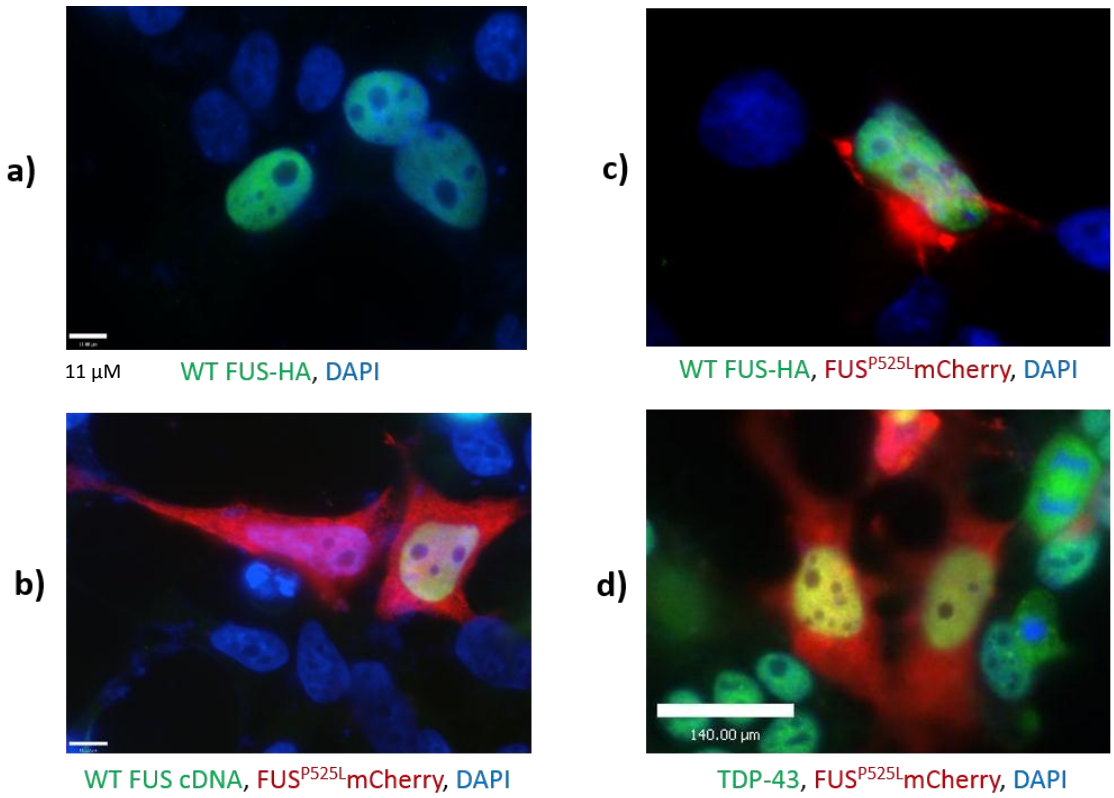

Figure 4 – Relocalisation of mutant FUS does not impact on the localisation of WT FUS or TDP-43

a) WT cDNA FUS-HA expressed from a pDEST-FUS-HA vector retains a nuclear localisation as assessed by ICC against HA and a nuclear DAPI stain. **b)** Dual transfection with FUS^{P525L}mCherry and FUS-HA and subsequent ICC against mCherry and HA showed no relocalisation of WT FUS-HA. **c)** In ICC stained double-transfected cells WT FUS-HA does not relocalise to mutant FUS^{P525L}mCherry aggregates. **d)** ICC against mCherry and TDP-43 in cells expressing FUS^{P525L}mCherry. TDP-43 localisation remains nuclear.

4.2.5. Cre recombinase mediates termination of FUS-mCherry expression

HEK293 cells were transfected with a Cre-expressing plasmid (Cre-EGFP) to test whether FUS expression could be terminated by Cre-mediated recombination between the two inserted LoxP511 sites (see Chapter 3). Transfection of FUS^{WT}mCherrry into HEK cells resulted in a large number of red fluorescent cells as assessed by live fluorescence microscopy (Figure 5a). Double-transfection with FUS^{WT}mCherrry and EGFP-Cre greatly reduced the number of red fluorescent cells observed, demonstrating that Cre recombinase terminates FUS expression (Figure 5b). No cells positive for both FUS^{WT}mCherrry and EGFP-Cre (dual red and green cells) were observed (Figure 5b). In order to assess whether FUS^{P525L}mCherrry remains within the cytoplasm after further expression is halted, HEK cells were transfected with FUS^{P525L}mCherrry and then 2 days subsequently transfected with EGFP-Cre. Four days after the initial FUS^{P525L}mCherrry transfection cells were fixed and assessed. The majority of EGFP-Cre positive cells showed no, or low levels, of FUS^{P525L}mCherrry. However some EGFP-Cre positive cells did show cytoplasmic FUS^{P525L}mCherrry and, extremely rarely, FUS^{P525L}mCherrry aggregates (Figure 5c). These data suggest that cytoplasmically-localised FUS^{P525L}mCherry protein remains in the cytoplasm up to two days after new expression is terminated.

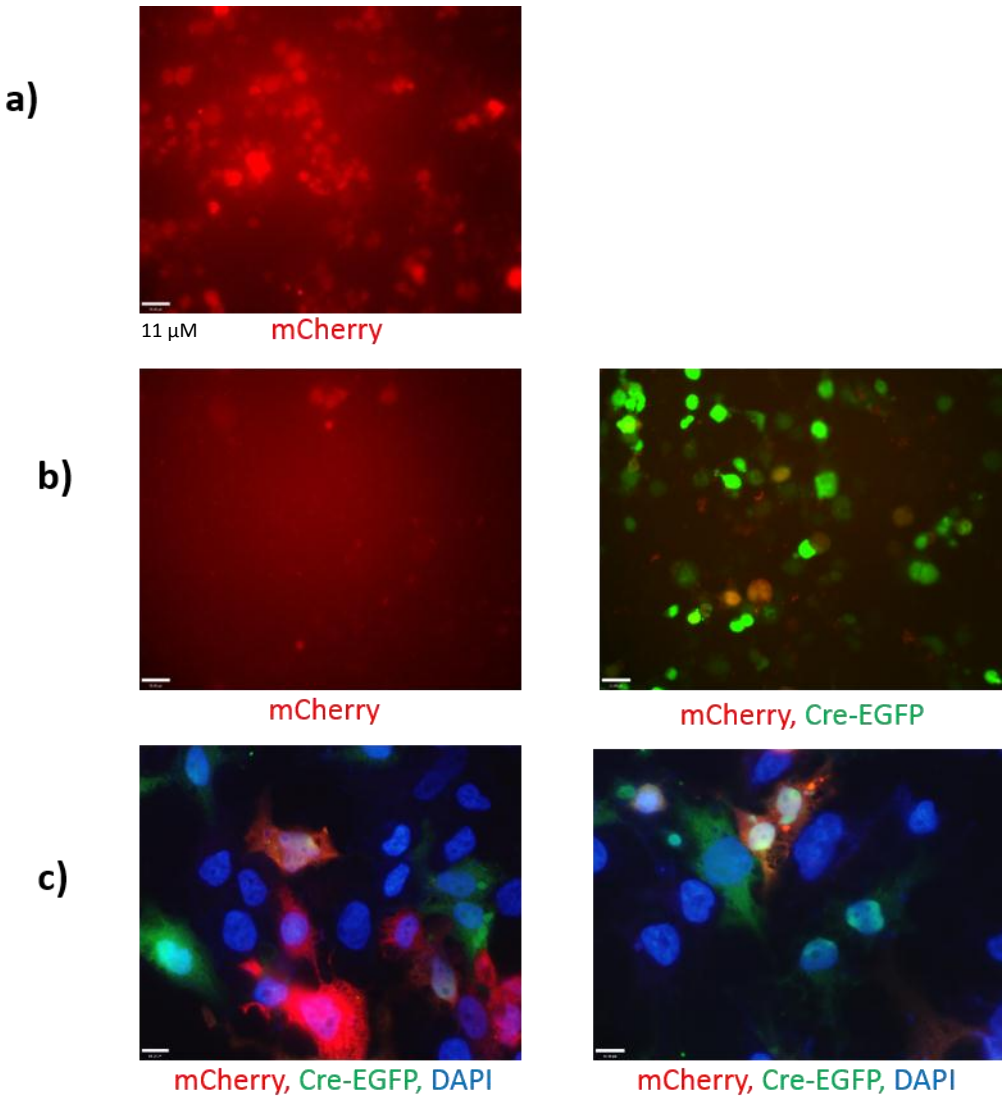

Figure 5 – Cre Recombinase Mediates Termination of FUS-mCherry Expression.

a) Representative fluorescence microscopy image of live HEK293 cells transfected with FUS-mCherry. **b)** Representative live fluorescence images of cells double-transfected with FUS^{WT}mCherry and Cre-EGFP. A greatly reduced number of red fluorescent cells (corresponding to cells expressing FUS^{WT}mCherry) is seen whilst a high number of EGFP-Cre expressing cells are present. Image acquisition settings remained consistent between the two conditions and cell density was approximately equal. Multiple transfections for each condition were checked with representative images shown. **c)** Mid time-course transfection of cells expressing FUS^{P525L}mCherry with EGFP-Cre demonstrates the persistence of cytoplasmic FUS^{P525L}mCherry and occasional aggregates in double-transfected cells.

4.2.6. Cytoplasmically localised FUS co-localises with stress granule markers in sodium arsenite treated cells

Transfected HEK293 cells were treated with 0.5 mM sodium arsenite to induce the formation of intracellular reactive oxygen species (ROS) (see Methods for details). Addition of sodium arsenite led to the formation of small intracytoplasmic puncta that stained with the well-characterised stress granule marker TIA-1 (Figure 6a). Addition of sodium arsenite to cells transfected with FUS-mCherry constructs was used, together with dual ICC for TIA-1 and mCherry, to assess whether FUS localised to these stress granules. A clear localisation of FUS to stress granules was seen for FUS^{P525L}mCherry and FUS^{R521C}mCherry, but not for FUS^{WT}mCherry and FUS^{R244C}mCherry (Figure 6b). Quantification by cell counting of the percentage of FUS expressing cells in which WT or mutant FUS colocalised with the stress granule marker TIA-1 was performed in fixed cells and demonstrated localisation of FUS to stress granules for the relocalising mutations R521C and P525L. Stress granule localisation of FUS was seen in approximately 80% of cells expressing FUS^{R521C}mCherry or FUS^{P525L}mCherry, with the remaining 20% of cells largely showing a lack of stress granule induction rather than a lack of colocalisation. This result additionally demonstrates that some degree of relocalisation is likely seen in all FUS^{R521C}mCherry expressing cells but that this relocalisation is not always detectable until cytoplasmic FUS is sequestered into dense, visible, puncta (see Figure 2). The non-relocalised WT and R244C FUS did not localise to stress granules except for in a very few cells where cytoplasmic relocalisation had likely occurred due to nuclear envelope breakdown (Figure 6c).

a)

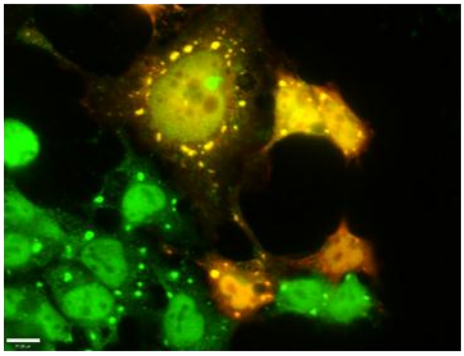

11 µM FUS^{P525L}mCherry, TIA-1

b)

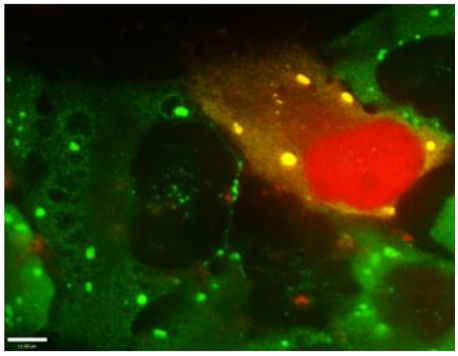

FUS^{P525L}mCherry, PABP

c)

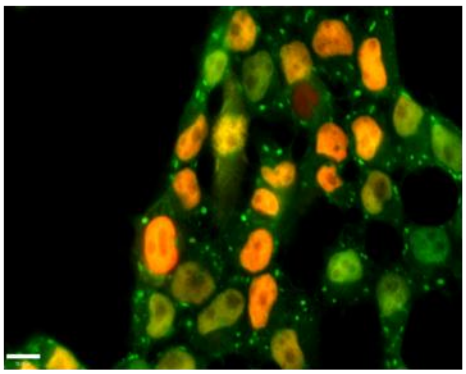

FUS^{WT}mCherry, TIA-1

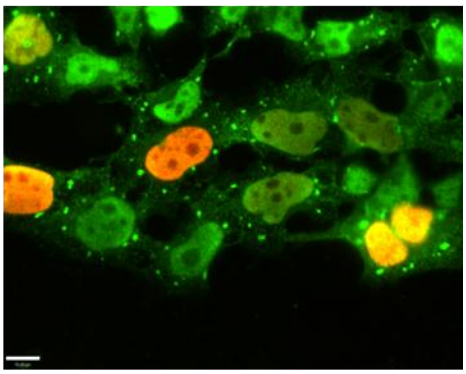

FUS^{R244C}mCherry, TIA-1

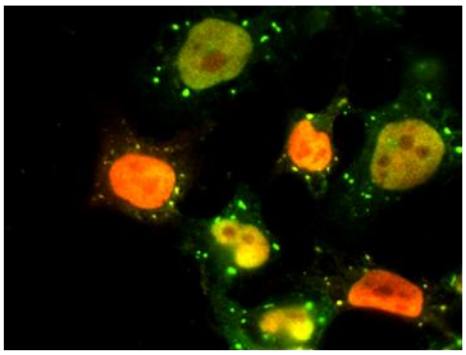

FUS^{R521C}mCherry, TIA-1

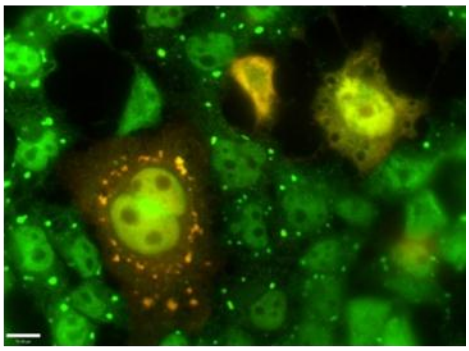

FUS^{P525L}mCherry, TIA-1

c)

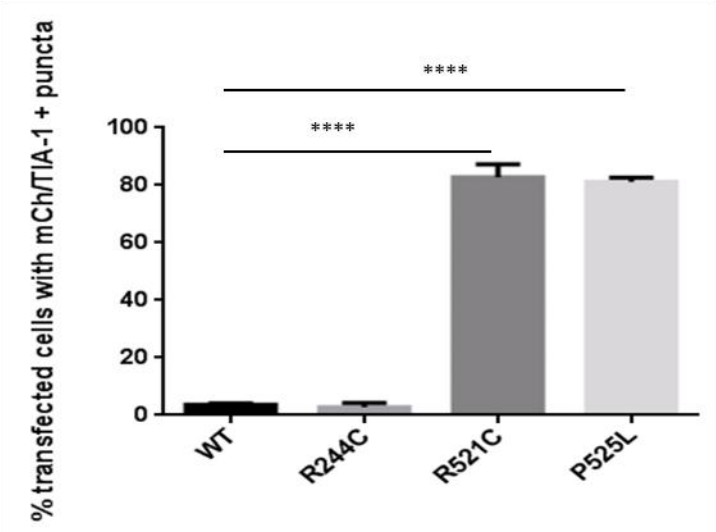

Figure 6 – Cytoplasmically localised FUS co-localises with stress granule markers in sodium arsenite treated cells

a) Sodium arsenite (0.5 mM) induces the formation of stress granules, as visualised by ICC against the core stress granule component TIA-1. Cytoplasmically localised FUS-mCherry localises to these discrete puncta. **b**) Dual ICC against mCherry and a further stress granule marker, PABP, after treatment with sodium arsenite **c)** Dual ICC for TIA-1 and mCherry in fixed, arseite treated, cells shows stress granule localisation of FUS^{R521C}mCherry and FUS^{P525L}mCherry. FUS^{R244C}mCherry shows no difference from WT FUS and does not localise to stress granules. **c)** Quantification of FUS-mCherry localisation to stress granules for WT and mutant constructs (N=2). Localisation of FUS to stress granules is seen in 82% (+/- 3.2) and 77% (+/- 2.8) of cells expressing either FUS^{R521C}mCherry or FUS^{P525L}mCherry respectively ($p \leq 0.0001$ vs WT). Very few cells expressing WT or R244C FUS-mCherry (3.7% (+/- 0.3) and 2.8% (+/- 0.6) of cells respectively) showed FUS/TIA-1 puncta.

4.2.7. Inhibition of the UPS leads to the formation of stress granules containing cytoplasmically localised FUS

Treatment of HEK293 cells with the UPS inhibitor MG132 lead to the formation of cytoplasmic puncta strongly immunoreactive to the stress granule marker TIA-1 (Figure 7a). By contrast addition of bafilomycin, previously shown to inhibit macroautophagy, did not induce stress granules (Figure 7b). Cytoplasmically localised FUS (FUS^{R521C}mCherry or FUS^{P525L}mCherry) co-localised with TIA-1 in MG132 induced stress granules (Figure 7a).

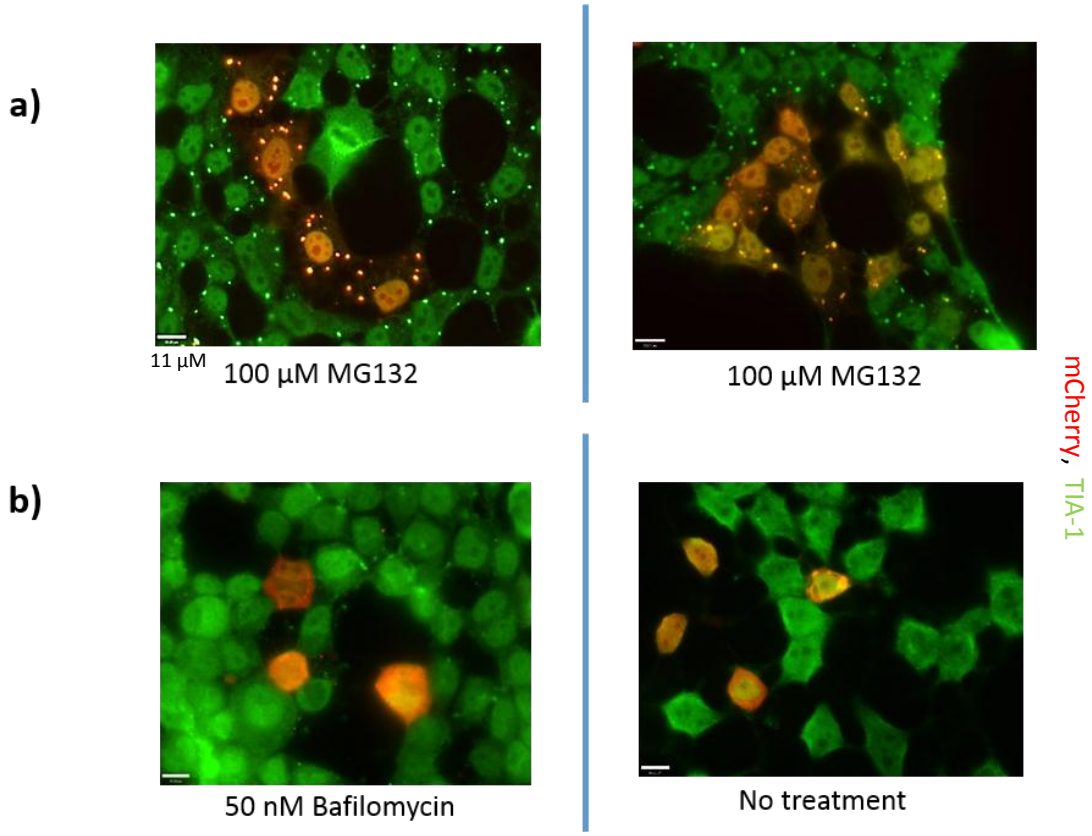

Figure 7 – Inhibition of the UPS leads to the formation of Stress Granules containing Cytoplasmically Localised FUS

a) Addition of 100 µM MG132 to FUS^{P525L}mCherry transfected cells for 2.5 hours followed by fixation and ICC for TIA-1 and mCherry demonstrated the formation of stress granules containing FUS^{P52L}mCherry. Treatment of cells with MG132 for longer time periods (12 hours) did not result in stress granule formation. **b)** Treatment of cells with 50 nM bafilomycin did not result in stress granule formation, showing no difference from untreated cells.

4.2.8. Stress Granules and their relationship to larger spontaneous FUS aggregates

Stress granules have frequently been suggested to be related to the larger FUS immunoreactive inclusions seen in FTD and ALS (see Introduction). In cells expressing FUS^{P525L}mCherry the morphology of FUS containing stress granules was often observed to be subtly different to non-FUS containing stress granules. FUS containing stress granules often had a less regular and rounded morphology, but were irregular and filamentous (Figure 8a). These FUS containing stress granules showed a morphology reminiscent of the spontaneous FUS aggregates seen in untreated cells (Figure 2a). In untreated cells spontaneous FUS^{P525L}mCherry aggregates were occasionally weakly immunopositive for the stress granule marker TIA-1, again suggesting a possible relationship between the two puncta types (Figure 8b and c).

To explore whether stress granules might seed longer-lasting aggregates, cells were treated with sodium arsenite for one hour and then were allowed to recover. After 12 hours the majority of stress granules disassembled and few TIA-1 puncta remained (Figure 8d). Some FUS positive, TIA-1 negative puncta with a morphology reminiscent of stress granules did however appear to remain (Figure 8e). To investigate whether inducing stress granule formation, and subsequently allowing cells to recover, affected FUS^{P525L}mCherry aggregation cells were stressed for 1 hour with sodium arsenite, allowed to recover for 12 hours, and then the percentage of transfected cells containing FUS positive (TIA-1 negative) inclusions was quantified. Neither a single treatment, nor three separate treatments with sodium arsenite (chronic treatment), affected the number of FUS positive inclusions seen after recovery (Figure 8f and g).

a)

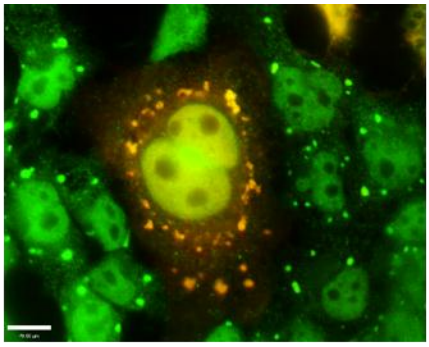

11 µM mCherry, TIA-1

b)

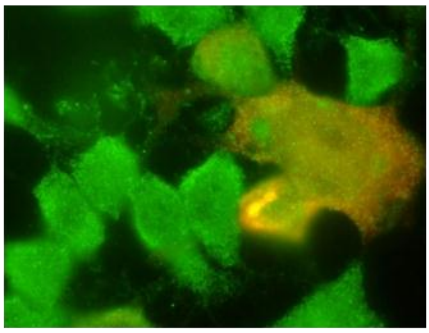

mCherry, TIA-1

c)

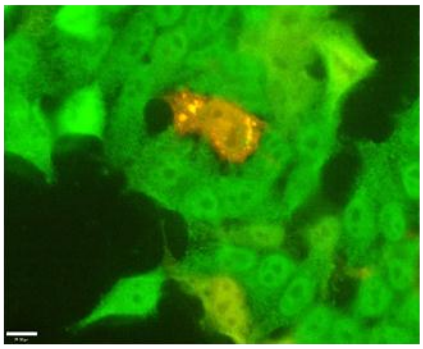

mCherry, TIA-1

d)

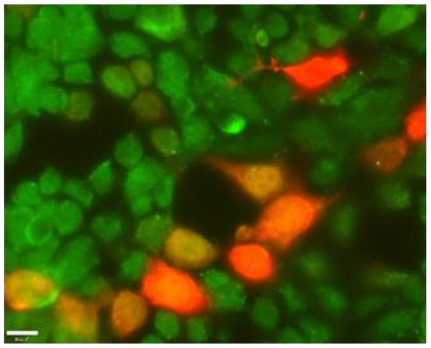

mCherry, TIA-1

e)

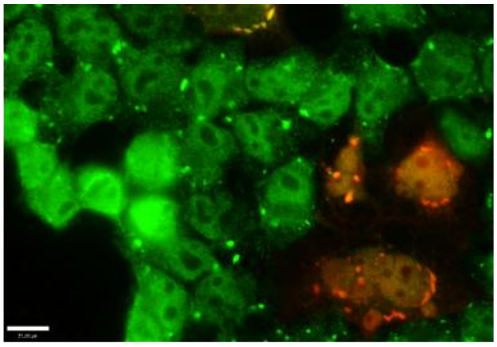

mCherry, TIA-1

f)

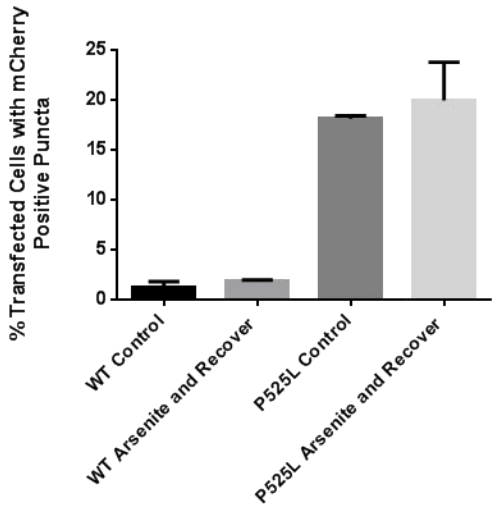

g)

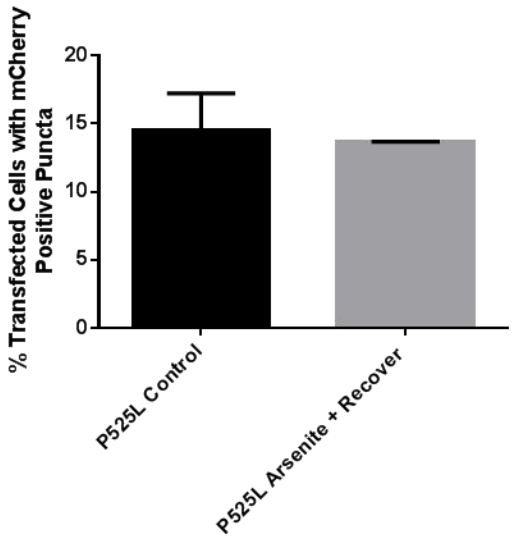

Figure 8 – Stress Granules and their Relationship to Larger FUS Aggregates

a) Dual ICC for mCherry and TIA-1 in sodium arsenite treated cells. TIA-1 positive puncta (stress granules) show a rounded punctate appearance. Subpopulations of FUS-containing SGs appear more filamentous and show less consistent morphology. **b and c)** Occasional mCherry positive aggregates in untreated cells are weakly labelled with TIA-1. **d)** Stress granules largely disassemble after removing sodium arsenite and allowing cells to recover for 12 hours. **e)** FUS, but not TIA-1 positive, puncta with a stress granule-like morphology are occasionally found in cells that have been allowed to recover after SG induction. **f)** Sodium arsenite treatment and subsequent recovery for 12 hours had no effect on the percentage of fixed, FUS^{P525L}mCherry transfected, cells with FUS positive aggregates (One-way ANOVA). **g)** Chronic sodium arsenite treatment (three treatments of one hour, 6 hours apart) and recovery lead to no increase in the percentage of FUS^{P525L}mCherry expressing cells with FUS aggregates (Unpaired T-test).

4.2.9. The P525L FUS mutation confers a gain of cytotoxicity

Cells transfected with wild type or mutant FUS-mCherry constructs were stained with a cleaved caspase-3 antibody to investigate apoptosis within these cells. Cleaved caspase-3 is produced by cleavage of a zymogen under conditions of cellular stress. This cleaved and activated form of caspase-3 then promotes apoptosis. Cleaved caspase-3 is therefore found only in cells undergoing, or about to undergo, apoptosis (Figure 9a and b). Cells expressing FUS^{WT}mCherry, FUS^{R244C}mCherry or FUS^{R521C}mCherry showed no increase in caspase-3 staining by comparison to untransfected cells. By contrast a significant increase in the number of FUS^{P525L}mCherry expressing cells positive for cleaved caspase-3 staining was seen by comparison to FUS^{WT}mCherry expressing cells (Figure 9c). No significant difference between cells expressing FUS^{WT}mCherry and untransfected cells was seen, suggesting that expression of FUS-mCherry from a genomic vector does not cause appreciable cytotoxicity.

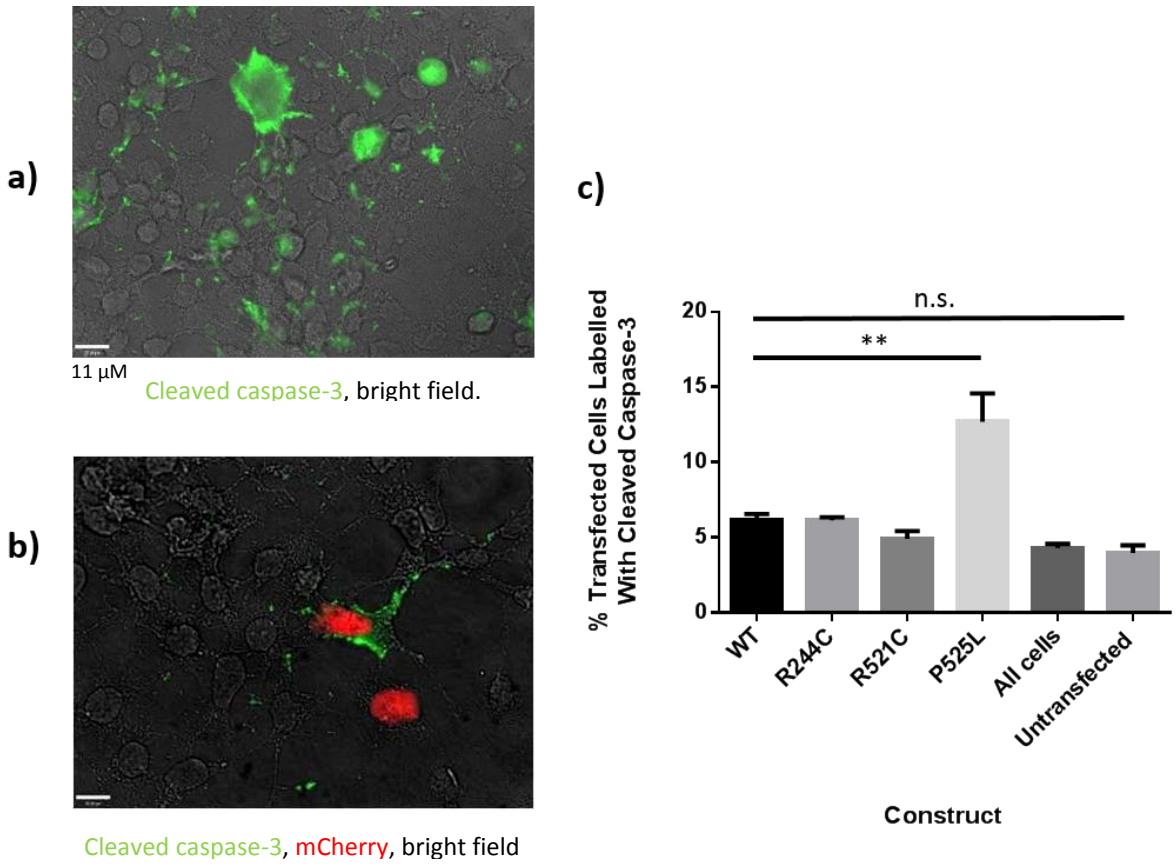

Figure 9 – The P525L FUS mutation confers a gain of cytotoxicity

a) HEK293 cells were fixed and stained for cleaved caspase-3 to assess apoptosis (see Methods). **b)** Dual ICC for mCherry and cleaved caspase-3 in FUS^{P525L}mCherry transfected cells. **c)** Quantification of dual caspase-3/mCherry ICC in cells transfected with WT or mutant FUS-mCherry. A significant increase in the number of FUS^{P525L}mCherry expressing cells that were additionally positive for cleaved caspase-3 was seen compared to other genotypes and untransfected cells (One-way ANOVA, $p \leq 0.01$). No difference in the percentage of cells positive for cleaved caspase-3 staining was seen between cells expressing FUS^{WT}mCherry and untransfected cells.

4.2.10. Addition of 200 µM hydrogen peroxide demonstrates toxicity for both 'relocalisation' mutations

In order to determine whether expression of non-P525L FUS-mCherry constructs leads to some cytotoxicity at an undetectable level, transfected cells were stressed with hydrogen peroxide (see Methods). Cells were transfected with FUS-mCherry constructs, hydrogen peroxide was added after 96 hours, and cells were fixed after 24 hours of exposure to hydrogen peroxide. Cytotoxicity was assessed by staining for the apoptotic marker cleaved caspase-3 and for abnormalities in nuclear morphology using DAPI staining (Figure 10a and b). Cells showing fragmented or highly condensed nuclei were considered to be either late apoptotic, necrotic or dead (Figure 10c). In cells treated with hydrogen peroxide, both FUS^{R521C}mCherry and FUS^{P525L}mCherry expression significantly increased the percentage of transfected cells positive for cleaved caspase-3 compared to FUS^{WT}mCherry (Figure 10a). FUS^{R244C}mCherry expression lead to no increase in cytotoxicity compared to wild type FUS-mCherry (Figure 10a). Analysis of hydrogen peroxide treated cells for abnormal nuclear morphology replicated the results seen for cleaved caspase-3, significantly more cells transfected with FUS^{R521C}mCherry and FUS^{P525L}mCherry had nuclear abnormalities by comparison to FUS^{R244C}mCherry and FUS^{WT}mCherry (Figure 10b).

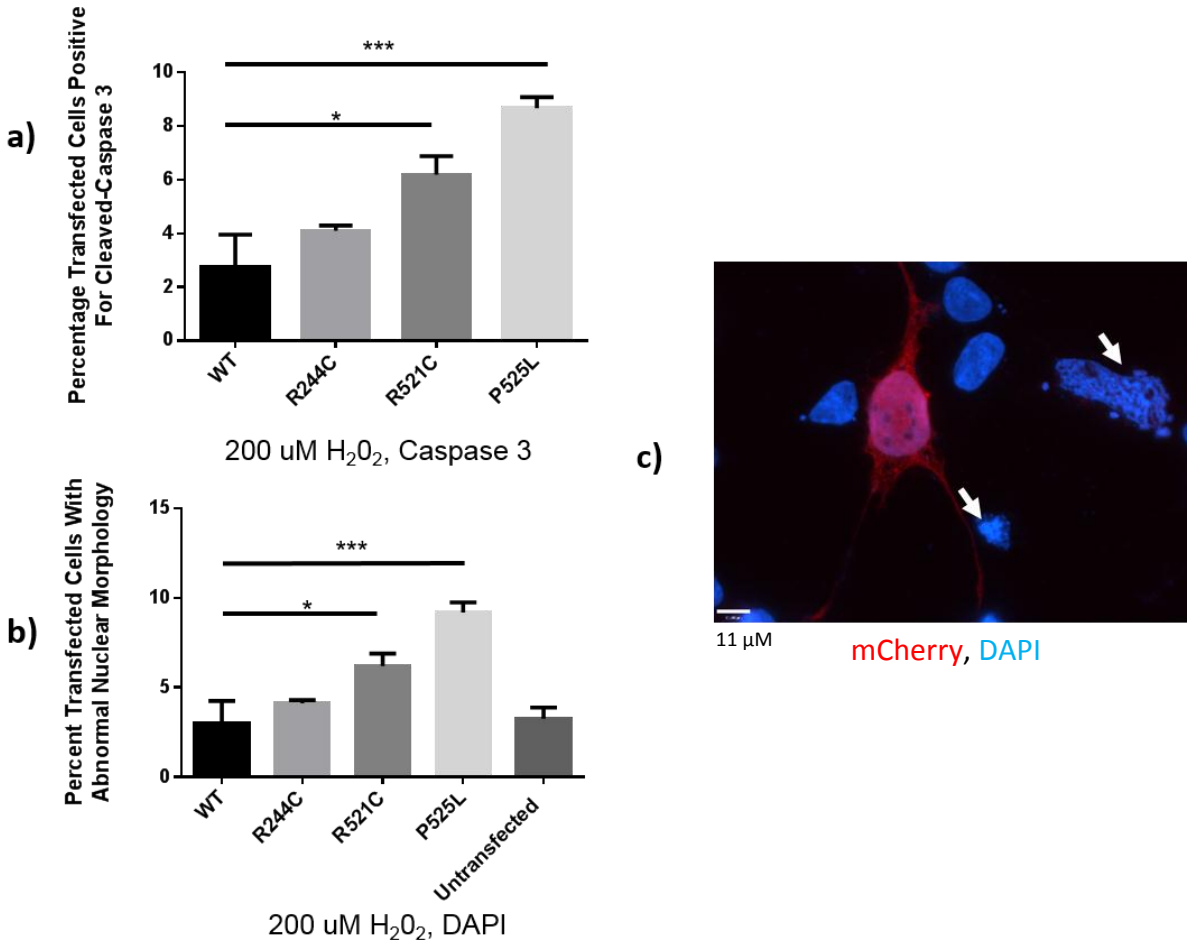

Figure 10 - Addition of 200 µM H_2O_2 demonstrates toxicity for both 'relocalisation' mutations

a) Cells were assessed for apoptosis by cleaved caspase-3 staining after incubation with 200 µM hydrogen peroxide for 24 hours. Significant toxicity were seen for the P525L ($p \leq 0.001$) and R521C mutations ($p \leq 0.05$) by comparison to WT. No gain of toxicity was seen for R244C (One-way ANOVA) (WT - 2.7% (+/- 1.2), R244C - 4.1% (+/- 0.2), R521C - 6.2% (+/- 1.69), P525L – 8.7% (+/- 0.4). **b)** After treatment with hydrogen peroxide cells were also assessed for late stage apoptosis or necrosis by nuclear fragmentation / condensation. DAPI nuclear stains were used to assess nuclear morphology. Significant increases in abnormal nuclear morphology were seen for the P525L ($p \leq 0.001$) and R521C ($p \leq 0.05$) mutations by comparison to WT or untransfected cells. No significant difference in nuclear morphology was seen for FUS^{WT}mCherry expressing cells compared to untransfected cells (WT – 3.0% (+/- 1.2), R244C – 4.1% (+/- 1.9%), R521C – 6.2% (+/- 0.69), P525L – 9.2% (+/- 0.57) (One-way ANOVA). **c)** Example DAPI stains for abnormal nuclear morphology, cells indicated by the arrowheads show fragmented or overly compacted nuclei respectively.

4.2.11. Treatment of FUS-mCherry expressing cells with the global arginine demthylase AdOx reverses mutation induced cytoplasmic relocalisation

AdOx, a global arginine methylation inhibitor, was added to cells transfected with FUS^{R521C}mCherry or FUS^{P525L}mCherry (see Methods). Cells were pretreated with 20 µM AdOx 4 hours before transfection, AdOx was added to the transfection media and the maintained for 72 hours after transfection until cells were fixed. AdOx appeared, at least in some cells, to maintain FUS^{P525L}mCherry in a nuclear-only localisation (Figure 11a and b). Quantification of relocalisation in AdOx treated cells demonstrated a significant reduction in the percentage of cells showing cytoplasmic accumulation of FUS^{R521C}mCherry or FUS^{P525L}mCherry (Figure 11c). The reversal of FUS^{P525L}mCherry cytoplasmic accumulation also significantly reduced the percentage of transfected cells containing mCherry immunoreactive inclusions (Figure 11d). Notably however, treatment of cells with AdOx gave highly inconsistent results. Further AdOx treatments showed little impact on the cellular localisation of FUS^{R521C}mCherry and FUS^{P525L}mCherry suggesting exact treatment times and maintenance of AdOx within the treatment media of cells may be critical. Furthermore, the global action of AdOx had dramatic off target effects – most easily seen in the inhibition of HEK293 cell growth/division. This inhibition may have partially caused the decrease in aggregate formation due to lowered cell density – a condition that appeared to affect aggregate formation.

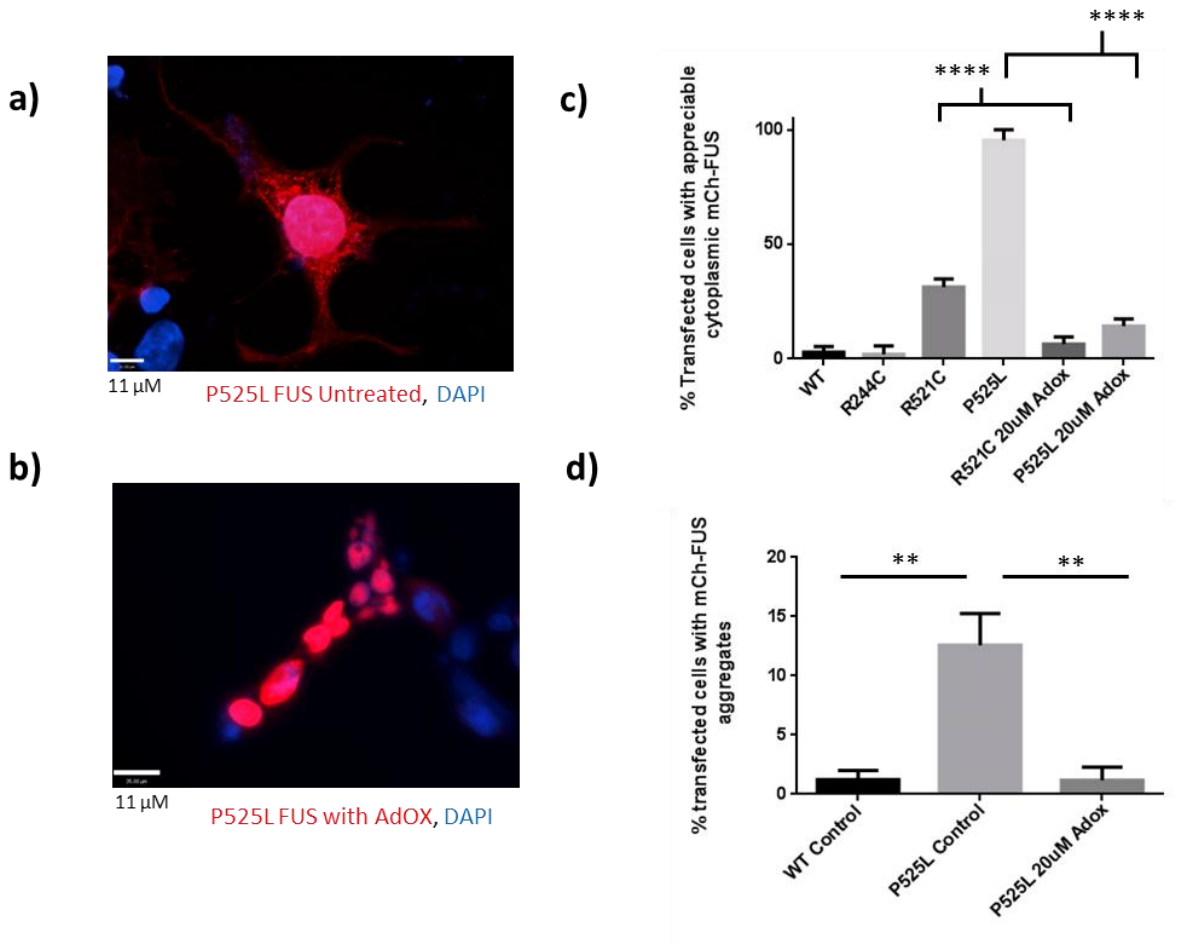

Figure 11 – AdOx causes a significant inhibition of mutation induced FUS relocalisation and aggregation

a) FUS^{P525L}mCherry shows a strong cytoplasmic relocalisation in untreated cells as assessed by ICC to mCherry and DAPI. **b**) Treatment of FUS^{P525L}mCherry expressing cells with AdOx results in purely nuclear localisation of FUS^{P525L}mCherry in a number of cells. **c**) Immunocytochemical analysis and quantification of cytoplasmic FUS-mCherry in AdOx treated cells as compared to previously analysed untreated cells (Figure 2) demonstrates a significant decrease in the percentage of transfected cells with cytoplasmic FUS after AdOx treatment (One-way ANOVA, P525L vs P525L + Adox, $p \leq 0.0001$, R521C vs R521C + Adox, $p \leq 0.0001$) (R521C AdOx – 6.5% (+/- 1.8), P525L AdOx – 14.3% (+/-1.8)). **d**) Quantification of cells with FUS^{P525L}mCherry inclusions by immunocytochemistry demonstrates a significant reduction in aggregate formation (Unpaired t-test, $p = 0.0024$) (P525L – 12.59% (+/- 1.5), P525L AdOx – 1.19 (+/- 0.6)).

4.2.12. AMI-1 treatment reduces the cytoplasmic relocalisation caused by the P525L mutations and leads to a concomitant reduction in cytotoxicity

Given the methodological issues using AdOx (non-specific effects) a second mechanism - AMI-1 treatment – was used. AMI-1, a small cell permeable sulphonated urea compound, specifically inhibits arginine methylation by the PRMT family. Cells were pre-treated with AMI-1 before being transfected with FUS-mCherry constructs, and AMI-1 was maintained continuously in the growth media (see Methods). ICC for mCherry in cells transfected with FUS^{P525L}mCherry demonstrated the presence of a large number of cells with purely nuclear FUS localisation after AMI-1 treatment (Figure 12a). A nuclear-only pattern of FUS^{P525L}mCherry localisation was not seen in control cells (Figure 12a). Quantification of the percentage of transfected cells showing cytoplasmic localisation demonstrated a significant reduction in the number of AMI-1 treated cells with cytoplasmic FUS^{P525L}mCherry compared to a control treatment (Figure 12b). Treatment with AMI-1 also significantly reduced the percentage of FUS^{P525L}mCherry expressing cells which stained positive for cleaved caspase-3, suggesting AMI-1 reduces the cytotoxicity associated with the P525L mutation (Figure 12c). This reduction of cytotoxicity was also confirmed using DAPI staining where treatment with AMI-1 lead to a significant reduction in the percentage of FUS^{P525L}mCherry expressing cells showing abnormal nuclear morphology (Figure 12c).

a)

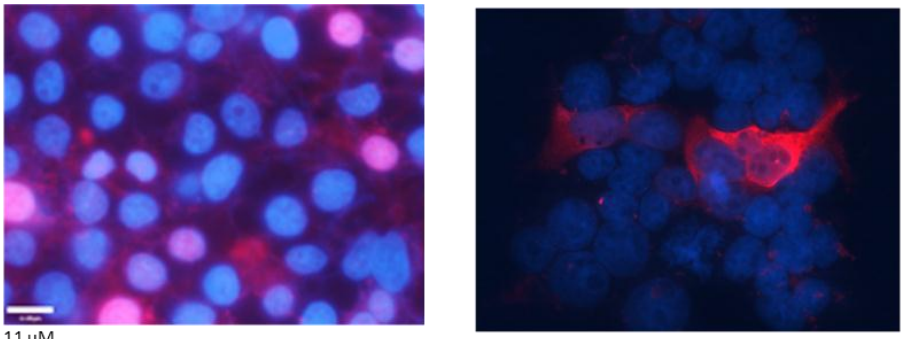

FUS^{P525L}mCherry, DAPI
with AMI-1 treatment

FUS^{P525L}mCherry, DAPI
no treatment

b)

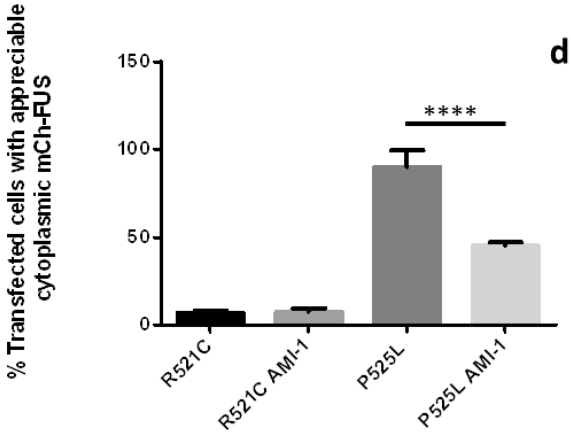

d)

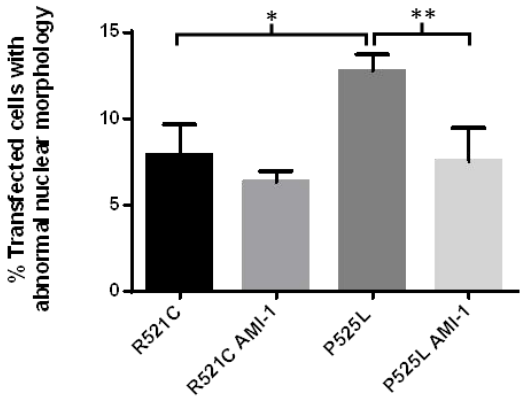

c)

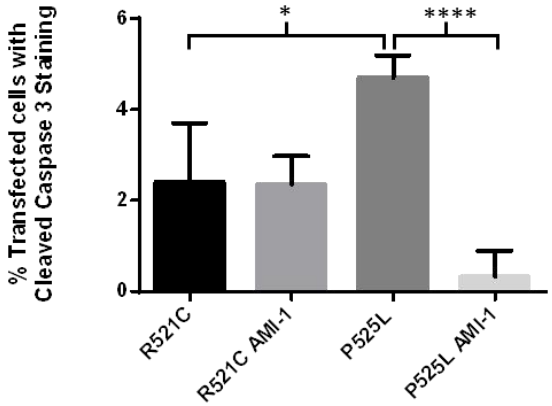

Figure 12 – AMI-1 treatment reduces the cytoplasmic relocalisation caused by the P525L mutations and leads to a concomitant reduction in cytotoxicity.

a) ICC against mCherry together with DAPI staining for AMI-1 treated and control cells expressing FUS^{P525L}mCherry. **b)** Quantification of the nuclear localisation of FUS-mCherry in AMI-1 treated and untreated (vehicle, see Methods) cells expressing FUS^{R521C}mCherry and FUS^{P525L}mCherry. Abnormally low levels of FUS^{R521C}mCherry were seen in both conditions whilst the addition of AMI-1 significantly reduced the number of cells showing cytoplasmic accumulation of FUS^{P525L}mCherry (One-way ANOVA, $p \leq 0.0001$) (91.46 % (+/- 4.83) vs. 49.38% (+/- 1.56)). **c)** Quantification of cytotoxicity for each genotype and treatment using ICC against cleaved caspase-3. No differences between treated and untreated cells expressing FUS^{R521C}mCherry were seen. A significant decrease in the percentage of cells expressing FUS^{P525L}mCherry that were additionally positive for cleaved caspase-3 was seen upon treatment with AMI-1 (One-way ANOVA, $p \leq 0.01$) (4.7% (+/- 0.29) vs. 0.6% (+/- 0.6). **d)** Assessment of cells for abnormal nuclear morphology using DAPI staining showed a significant reduction in nuclear abnormalities for AMI-1 treated cells expressing FUS^{P525L}mCherry compared to those treated with a vehicle only (One-way ANOVA, $p \leq 0.01$) (12.73% (+/- 0.56) vs. 7.558 (+/- 1.10). No difference was seen between treated and untreated cells expressing FUS^{R521C}mCherry.

4.3. Discussion

Transfection of FUSpBACe3.6mCherry vectors into HEK293 cells demonstrated successful expression of FUS-mCherry that could be detected by Western blot, RT-PCR and live mCherry fluorescence. Wild-type FUS localised, as expected, to the nucleus and did not appear to show any signs of cytotoxicity or aggregation that could be caused by overexpression or self-interaction of the protein tag. Furthermore, double-transfection with an EGFP-Cre plasmid demonstrated successful termination of FUS expression due to recombination between the inserted LoxP sites. Transfection efficiencies were very respectable for a large BAC construct (varying between approximately 10 and 20 % of cells), and provided sufficient transfected cells for cell counts and quantification. The vectors generated in Chapter 3 of this thesis have, therefore, been validated and appear suitable for use in both *in vitro* and *in vivo* models.

Expression of wild type and mutant *FUS* quickly revealed a cytoplasmic relocalisation phenotype for the two mutations, R521C and P525L, located within the NLS of FUS (Figure 2). Notably, the R244C mutation showed no cytoplasmic relocalisation suggesting an alternative mechanism of pathogenesis. The strength of relocalisation seen from each mutation corresponded well with the observed clinical features previously associated with each mutation (Figure 2). A clear inverse relationship between the degree of mutation-induced cytoplasmic relocalisation and associated age of disease onset is seen. This relationship strongly suggests that cytoplasmic relocalisation is either directly or indirectly responsible for FUS toxicity and disease in the majority of fALS cases. Notably, however, as the lack of relocalisation in the R244C demonstrates, a number of mutations are found away from the NLS of FUS (Introduction, 1.1.1, Figure 1) and may act in a separate manner. How the molecular pathogenesis of these mutations acts is currently unclear and is investigated in Chapter 5.

Notably, only cells expressing the most strongly relocalising mutation, P525L, exhibited any spontaneously-forming FUS inclusions (Figure 3). These inclusions did not stain positive, in the vast majority of cases, for ubiquitin or p62; two key markers of FUS inclusions in ALS/FTD-FUS. The aggregates did however stain very strongly for both mCherry and FUS and were reproducibly found only in cells expressing FUS^{P525L}mCherry. As such, it seems unlikely that these inclusions are simply an artefact of FUS overexpression or self-interaction mediated by the mCherry tag. Therefore, it appears that the formation of these aggregates is driven by cytoplasmic relocalisation of FUS. Furthermore, given that aggregates were not seen with expression of the intermediately relocalising R521C mutation, it appears that aggregate formation occurs once a threshold of cytoplasmically located FUS is reached. It would be of interest to test this hypothesis through the chronic overexpression of FUS containing the R521C mutation in the same cell line. Notably, these aggregates could occasionally be found persisting two days after FUS^{P525L}mCherry expression was terminated by Cre recombinase (Figure 5). As such, they may be a long lasting feature within the cytoplasm of affected cells.

Relocalisation of mutant FUS^{P525L}mCherry did not, contrary to recent reports, appear to affect the localisation of endogenous WT FUS which remained nuclear (Figure 4) (Vance et al., 2013). Endogenous FUS was not found in FUS^{P525L}mCherry inclusions suggesting WT FUS is not sequestered in these aggregates within our cellular model (see Chapter One for a discussion on possible WT FUS sequestration). Subcellular localisation of TDP-43 was also not affected by the cytoplasmic accumulation of FUS^{P525L}mCherry.

Localisation of FUS to cytoplasmic puncta positive for the stress granule marker TIA-1 was recorded for cytoplasmically relocalised FUS (Figure 6). These puncta were induced by the addition of sodium arsenite which produces reactive oxygen species in the cell – a condition well established to cause stress granule formation. Arsenite-induced stress granules showed a consistent small and rounded morphology, tending to form in a ring around the nucleus of cells (Figure 6). Notably, when the

ubiquitin proteasome system – of great importance in the degradation of proteins and linked to the ALS/FTD continuum – was inhibited using MG132, stress granules were induced at a level equal to that seen with sodium arsenite (Figure 7). This result suggests a novel further overlap between protein degradation pathways and ALS/FTD related RNA processing proteins such as FUS (see discussion in Chapter One).

Localisation to stress granules has frequently been suggested to be a possible mechanism within the pathogenesis pathway of FUS. However, how stress granule localisation of FUS might lead to toxicity remains unclear. Given the wide variety of RNA binding proteins found within stress granules the fact that cytoplasmically mislocalised FUS is found in these puncta is not, in itself, surprising. Indeed if FUS has aberrant functionality in the cytoplasm then sequestration in stress granules is likely to prevent any such activity and may be actively beneficial. The only plausible current suggestion for how stress granule localisation of mutant FUS could lead to toxicity is through the seeding of larger, disease associated aggregates. In this context, it is notable that stress granule markers such as TIA-1 have been described in the characteristic FUS positive inclusions found in *post-mortem* ALS and FTD tissue (Dormann et al., 2010; Liu-Yesucevitz et al., 2010). The spontaneous FUS-positive aggregates found in FUS^{P525L}mCherry expressing cells did, on occasion, stain weakly for TIA-1, but not to the extent necessary to form a causal link between these spontaneous and irregularly shaped aggregates and arsenite induced stress granules within our model (Figure 8). Some stress granules containing mutant FUS did show a morphology somewhat different to that normally seen for stress granules. These occasional stress granules had a more irregular and filamentous structure more reminiscent of the spontaneously forming FUS inclusions (Figure 8). It is possible that this observation reflects a change in stress granule morphology, toward that of a larger aggregate due to the sequestration of large amounts of FUS. However experiments to determine whether the induction of stress granules affected the number of FUS positive inclusions found after a recovery period suggested this was not the case (Figure 8). These experiments were, however, severely hampered by further factors that appeared to greatly affect the speed at which stress granules disassemble and the likelihood of

spontaneous aggregates being found. The tendency for stress granules to disassemble appeared to be highly dependent on cell density and greatly varied even within single dishes of cells. Similar observations were made for spontaneous aggregate presence. As such, data collected from cells on the maintenance or transition of stress granules was exceptionally noisy and highly dependent on the location within dishes that cells were sampled from. It is, therefore, hard to draw conclusions with any certainty that the induction of stress granules did not lead to the formation of overly stable stress granules or FUS positive/TIA-1 negative aggregates.

Assessing cleaved caspase-3 staining in cells transfected with FUS-mCherry constructs showed a reproducible gain of cytotoxicity associated with the P525L mutation (Figure 9). Addition of hydrogen peroxide, to further stress cells, again showed toxicity associated with the P525L mutation. Furthermore, within hydrogen peroxide-stressed cells, the R521C mutation also caused increased cytotoxicity compared to WT or R244C FUS, although not to such a degree as FUS^{P525L}mCherry (Figure 10). No such cytotoxicity was seen for FUS^{R224C}mCherry. It therefore appears that any gain of cytotoxicity is associated with cytoplasmic relocalisation of FUS. The requirement for additional cellular stress for cytotoxicity associated with the R521C mutation to be seen suggests that the gain of cytotoxicity is directly related to the cellular concentration of cytoplasmically localised FUS. The earlier onset and rapid disease progression of the P525L mutation, compared to the R521C mutation, further supports this hypothesis. Due to the presence of endogenous wild type FUS within this cell culture model, any toxicity seen is likely to reflect a gain of toxicity (see Figure 14). A loss of normal nuclear action, as often suggested for FUS mutations, should be compensated for by the presence of endogenous nuclear FUS (see Figure 14). In order to confirm this result we attempted to reverse FUS^{P525L}mCherry relocalisation and look for a concomitant loss of associated cytotoxicity. Inhibiting arginine methylation at the FUS RGG domain has previously been shown to reverse the impact of FUS NLS mutations (see Chapter 1, 1.1.2, Figure 2) (Scaramuzzino et al., 2013; Tradewell et al., 2012). Treating cells with the global arginine methylation inhibitor AdOx strongly reversed the

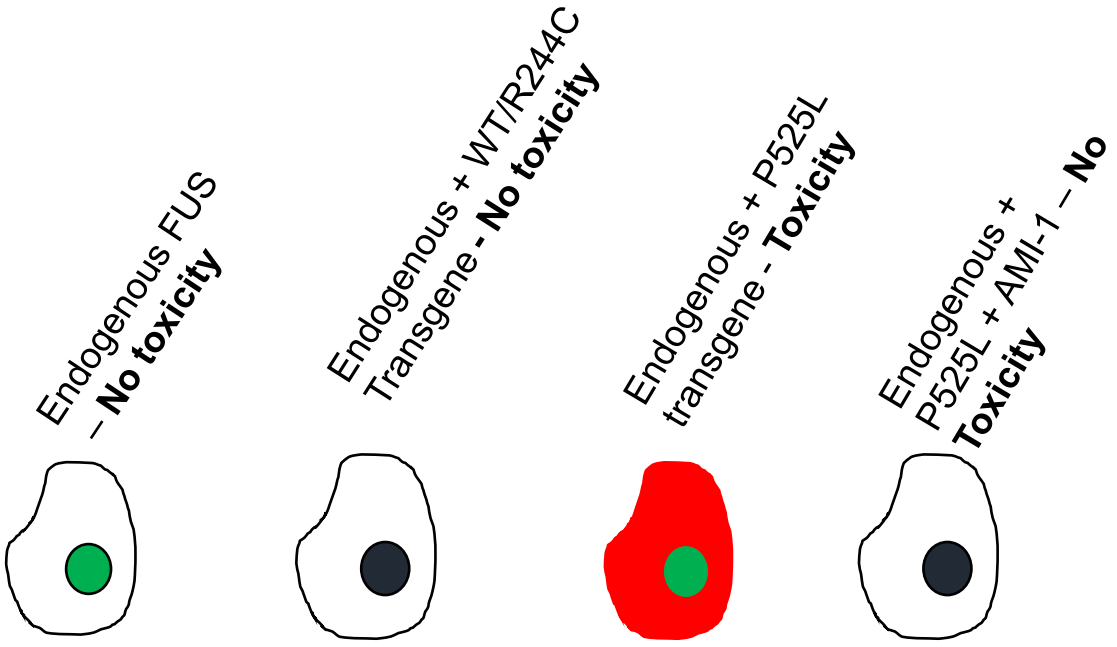

Figure 14 – Cytotoxicity of FUS relocalisation suggests a gain of toxic of function for *FUS* NLS mutations.

Under normal circumstances endogenous FUS (green) predominantly localises to the nucleus and carries out all normal cellular roles. Expression of WT or R244C FUS-mCherry (red) simply increases the amount of nuclear localised FUS and demonstrates no toxicity. Expression of NLS mutant *FUS* leads to a gain of cytoplasmic FUS whilst endogenous FUS remains nuclear (Figure 4). As such, cytotoxicity seen is unlikely to be caused by a loss of function, and hence a gain of cytoplasmic toxicity seems likely. Reversal of the nuclear relocalisation of FUS^{P525L}mCherry using AMI-1 significantly reduced toxicity back to WT levels further suggesting that a cytoplasmic gain of function mechanism is seen with *FUS* NLS mutations. This data suggests that within human disease a gain of cytoplasmic function is, at least partially, responsible for the associated toxicity of *FUS* NLS mutations. To establish whether a loss of function mechanism is also seen in disease it would be necessary to express mutant *FUS* on a knockout cellular background.

relocalisation associated with the P525L mutation and prevented the formation of aggregates (Figure 11). AdOx, however, had a clear impact on cell growth and/or division with cells failing to expand after initial seeding when treated with AdOx. It should also be noted that the decrease in cell density in AdOx treated cells may also have played a role in the reduction of FUS^{P525L}mCherry aggregates recorded. Given the likely effect of cell density on cytotoxicity we elected to try other methods of inhibiting FUS arginine methylation.

A further, and likely the most effective, manner in which FUS arginine methylation was inhibited utilised AMI-1. AMI-1 is thought to specifically inhibit the arginine methylation catalysed by the PRMT1 family. Therefore, none of the issues of possible genetic redundancy and low efficiency seen with the siRNA approach, and fewer of the non-specific effects likely with AdOx, should be found. Indeed AMI-1 treatment reversed much, though not all, of the P525L mutation induced relocalisation without showing any clear toxicity (Figure 12). Treatment with AMI-1 reversed the cytotoxicity associated with the P525L mutation, further suggesting that the cytotoxicity seen is due to a toxic gain of cytoplasmic function (Figure 12). Further testing this hypothesis could be done elegantly by crossing FUS^{P525L}mCherry transgenic animals with animals null for *PRMT1* and *PRMT8*.

In summary, here we demonstrate that the FUS-mCherry vectors generated in Chapter 3 express fluorescently tagged FUS when transiently transfected in HEK293 cells. Insertion of NLS mutations led to a cytoplasmic relocalisation phenotype with concomitant cytoplasmic aggregation and stress granule formation. This relocalisation was associated with clear, and likely concentration dependent, cytotoxicity. Inhibition of mutation-induced relocalisation removed this associated cytotoxicity and strongly suggests that *FUS* NLS mutations act, at least partially, through a cytoplasmic gain of function mechanism.

5. Chapter 5 – Insights into the *FUS* R244C Mutation

5.1. *FUS* Mutations are found outside the nuclear localisation sequence

Mutations in *FUS* are most frequently found within the C-terminal nuclear localisation sequence (NLS) (see Introduction) (Kwiatkowski et al., 2009b; Vance et al., 2009). This observation has led to a general paradigm in which *FUS* mutations have become synonymous with NLS changes and cytoplasmic relocalisation. However, a sizeable number of *FUS* mutations are found outside the NLS, largely within a glycine rich domain extending between amino acids 165 and 267. So far at least 11 single base pair substitutions outside the NLS of FUS have been described (AD & FTD Mutation Database, Lagier-Tourenne et al., 2010) (Figure 1). Segregation analysis for these mutations is generally lacking, only one mutation – R244C - has any available disease pedigree and has been assigned a putative autosomal dominant inheritance pattern in two affected patients from a single family. (Kwiatkowski et al., 2009a). Further reports of non-NLS mutations have highlighted miss-sense mutations concentrated within FUS exons 5 and 6 that were not present in controls, predicted to be deleterious, and found at conserved amino acid residues (Corrado et al., 2010; Ticozzi et al., 2009). Notably, miss-sense changes in fALS patients were found at the arginine 234 residue in two separate studies (and in controls in neither study) giving strong evidence for a disease association (Corrado et al., 2009; Ticozzi et al., 2009). Whilst none of these mutations meet the criteria to state that they are definitively causative for disease, their predicted pathogenic nature and concentration only within exons 5 and 6 (of the 15 exons screened) of *FUS*, which largely encode a glycine rich domain, argue for a functional impact.

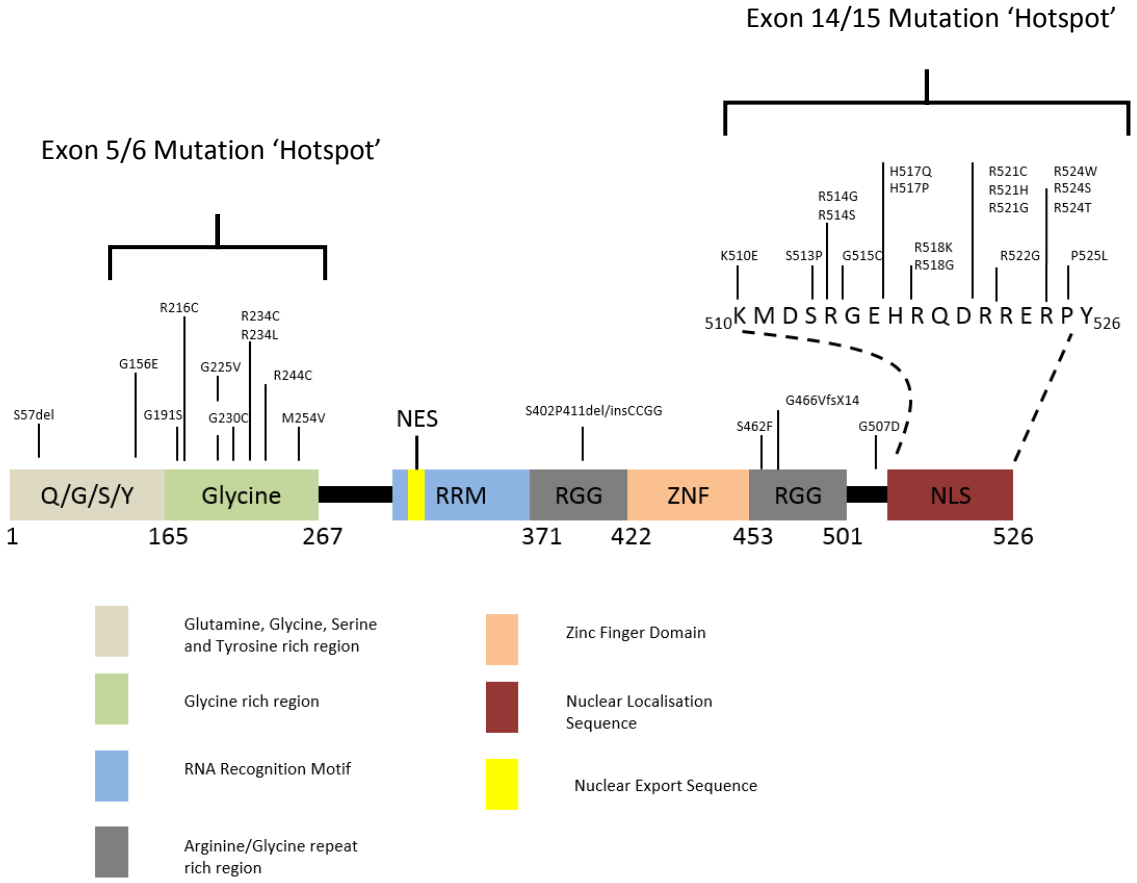

Figure 1 – Domain architecture and location of *FUS* mutations

Mutations in *FUS* cluster within a C terminal NLS but are also found elsewhere in the protein, predominantly in the glycine rich region. These two regions can be considered 'hotspots' for mutations suggesting their encoded protein domains are vital for protein function.

5.1.1. The molecular elephant in the room - the impact of non-NLS *FUS* mutations is poorly understood

The clustering of *FUS* mutations within the NLS, coupled with pathological findings demonstrating relocalisation of FUS in human disease, has led to a clear hypothesis as to the impact of *FUS* mutations which has been described and tested both *in vitro* and *in vivo*. This hypothesis, as described in more detail in the Introduction, states that *FUS* mutations lead to cytoplasmic relocalisation of FUS due to impaired interaction with the nuclear import factor transportin 1 (Dormann et al., 2010). This relocalisation then actively leads to a loss of nuclear and/or gain of cytoplasmic function (Bosco et al., 2010b; Dormann et al., 2010; Gal et al., 2011; Huang et al., 2011; Ito et al., 2011; Murakami et al., 2012; Tradewell et al., 2012; Verbeeck et al., 2012). Whilst this idea may well be correct for the majority of FUS mutations, loss of proper interaction with transportin 1 is unlikely to explain the molecular events underlying non-NLS mutations. These mutations, despite their possibility to explain other mechanisms of FUS pathogenesis have, until recently, been ignored in both *in vitro* and *in vivo* models of FUS dysfunction.

A recent report has, however, highlighted a new molecular mechanism for *FUS* mutations that links the two disease-associated mutational hot-spots in *FUS* (exons 5/6 and 14/15, see Figure 1) (Wang et al., 2013). Knock down of *FUS* within a cellular model was shown to inhibit the repair of double-strand DNA breaks (DSBR) by either homologous recombination or non-homologous end joining (NHEJ). This reduction in DSBR efficiency appears to be due to a loss of interaction between FUS and the histone deacytalase HDAC1, leading to failure to assemble the protein complexes required for DSBR. FUS is recruited early in the DSBR pathway to double-strand breaks, where it then recruits HDAC1. Notably, interaction with HDAC1 seems to be mediated by both the glycine rich region of FUS (exons 5/6) and the C terminal domain (exons 14/15) – the same two areas highlighted as deleterious mutation hotspots (Wang et al., 2013). Expression of FUS^{R244C}, FUS^{R514S}, FUS^{R521C} or

FUS^{H517Q} in a FUS knockdown cell line was used to investigate the role of *FUS* mutations on DNA repair pathways. Expression of FUS^{R244C} or FUS^{R514S} in this cell line lead to a significant deficiency in homologous and non-homologous recombination mediated double-strand break repair pathways. FUS^{R521C} and FUS^{H517Q} expression had a reduced, but still notable, impact on DSBR pathways (Wang et al., 2013). Insertion of the R244C, R514S and R521C mutations all lead to FUS failing to recruit HDAC1, and hence wider DSBR pathway components, to double-strand breaks (Wang et al., 2013). Disruption of the physical interaction between the C terminal and glycine rich regions of FUS with HDAC1 provides a further mechanism of action for the molecular pathogenesis of FUS that is not dependent on cytoplasmic relocalisation. The clear role of the R244C mutation in reducing DSBR efficiency gives weight to the pathogenic and functional nature of mutations within the glycine rich region, and demonstrates that cytoplasmic relocalisation may not be actively responsible for all aspects of FUS associated cytotoxicity.

Mutations in *TARDBP*, functionally related to FUS and linked to ALS/FTD (see Introduction) are predominantly found in a glycine rich region and do not cluster within an NLS (Lagier-Tourenne et al., 2010). The relocalisation associated with *TARDBP* mutations in post-mortem disease suggests possible a link between glycine rich region mutations and cytoplasmic accumulation, perhaps through increased aggregation tendency (Cairns et al., 2007; Lagier-Tourenne et al., 2010). As such, it is possible that non-NLS mutations within *FUS* may also indirectly impact upon subcellular localisation through a separate pathway to NLS mutations. In any case, the overlapping mutation hotspots of FUS and TDP-43 within a glycine rich region suggests that dysfunction in these domains may be of great importance within RNA processing proteins and warrants greater investigation.

In summary, two mechanism of action can be considered for non-NLS, exon 5/6, mutations; a direct impact on FUS functionality in the absence of relocalisation, or indirectly affecting nuclear import either through a novel mechanism, or, as discussed below, by affecting whole protein architecture.

5.1.2. Miss-sense mutations can affect whole protein architecture and function through post-transcriptional and post-translational modifications

One mechanism of action by which mutations located away from the NLS sequence of *FUS* could lead to cytoplasmic relocalisation is by affecting the splicing pattern of pre-mRNA or the folding and/or degradation of nascent FUS polypeptides. In this manner, a single base change located away from the domain responsible for cytotoxicity can still lead to disease. Splicing of pre-mRNA is used to remove intronic regions from transcribed RNA, leaving only the exons to be translated. Whilst many mRNA transcripts are spliced in the same manner every time, certain mRNAs, such as the FTD associated gene *MAPT*, have multiple alternative splicing possibilities that allow greater proteomic complexity to be achieved from a single genetic locus. In alternative splicing, whole exons can be skipped such as to vary the overall structure and function of the encoded protein. The architecture of the *MAPT* encoded tau protein provides an excellent example of this process; 6 isoforms of tau protein are produced with varying numbers of microtubule binding domains (3 or 4 'R') and N terminal inserts (0, 1 or 2 'N') and hence varying functions. This diversity is dependent on the inclusion or exclusion of exons 2, 3 and 10 within mature *MAPT* mRNA (Caffrey and Wade-Martins, 2007).

Splicing of exons is generally accomplished by the spliceosome complex which acts at specific splice acceptor and donor nucleotide sites, generally located at the start and end of exons. Further mRNA sequences may act as enhancers or repressors of splicing at these sites (Blencowe, 2000). Single base pair mutations at either splice acceptor/donor or enhancer/repressor sites may therefore lead to changes in the splicing pattern of nascent pre-mRNA and hence changes to protein sequence and function.

At the protein level single amino acid changes may lead to changes in post-translational modifications such as phosphorylation, acetylation, alkylation, lipidation, glycosylation. These examples and many other further modifications, relate to the addition of small chemical groups to specific amino acid side chains. Addition of these chemical groups can greatly affect the function of the modified protein. As many modifications are specific to certain amino acids, changes in protein sequences can affect protein modification status. Approximately 5 percent of all disease causing mutations affect post-translational modification sites, compared to 2 percent of presumed neutral mutations, suggesting that alterations in amino acids modifications play an important role in heritable disease (Li et al., 2010).

A further possibility for the action of a single mutation on the overall structure of a protein is to affect protein cleavage or degradation. Changes in amino acid sequence could affect consensus sites for proteases and hence lead to increased, decreased or novel cleavage events. For example, in the rare autosomal dominant movement disorder paroxysmal non-kinesigenic dyskinesia, disease-associated mutations impair normal protein cleavage events and lead to increased degradation of the mutant protein (Shen et al., 2011).

In summary, many single base pair changes can have large-scale impacts on protein structure and function that might not otherwise be predicted by from examining the basic effect of nucleotide changes on protein folding and function algorithms.

5.1.3. Investigating the molecular pathogenesis of the R244C mutation

Given the almost complete lack of investigation into non-NLS *FUS* mutations, we inserted the R244C mutation into our FUS-mCherry genomic DNA vectors (see Chapter 3) and expressed FUS^{R244C}mCherry within HEK cells. The R244C mutation was chosen for its unknown mechanism of pathogenesis and location away from the FUS NLS. Furthermore, the R244C mutation is, so far, the only non-NLS mutation described that has any degree of segregation demonstrated, with an autosomal dominant pattern suggested. The mutation was not present in 231 healthy controls

studied, giving weight to its likely pathogenesis (Kwiatkowski et al., 2009b). Expression of FUS^{R244C}mCherry in HEK cells demonstrated a nuclear localisation, unlike the NLS mutations R521C and P525L, confirming that the R244C likely acts through a separate mechanism of pathogenesis (Chapter 4 – Figure 2 - 4.2.2). Here we explore what other mechanisms of toxicity could be associated with the R244C mutation.

5.2. Results

5.2.1. Western blotting demonstrates additional FUS protein forms specifically associated with the R244C mutation

20 µM of total protein lysate from HEK293 cells transfected with either WT or mutant FUS-mCherry was separated by SDS-PAGE, transferred to a polyvinyl difluoride membrane, and subsequently immunoblotted using a clontech anti-mCherry antibody (1-1000 dilution, see Methods). Chemiluminescent imaging detected a band at approximately 100 kDa that corresponds to the FUS-mCherry fusion protein (predicted molecular weight of 102 kDa) from cell lysate corresponding to cells transfected with all WT and mutant FUS-mCherry constructs (Figure 1a and b). Notably the presence of two additional bands, at approximately 80 and 70 kDa respectively, were reproducibly seen in Western blots of FUS^{R244C}mCherry transfected cell lysate (Figure 1b). These additional bands were specific to cells transfected with FUS^{R244C}mCherry. We speculated that these additional bands may have a role in the currently unclear mechanism of pathogenesis for the R244C mutation.

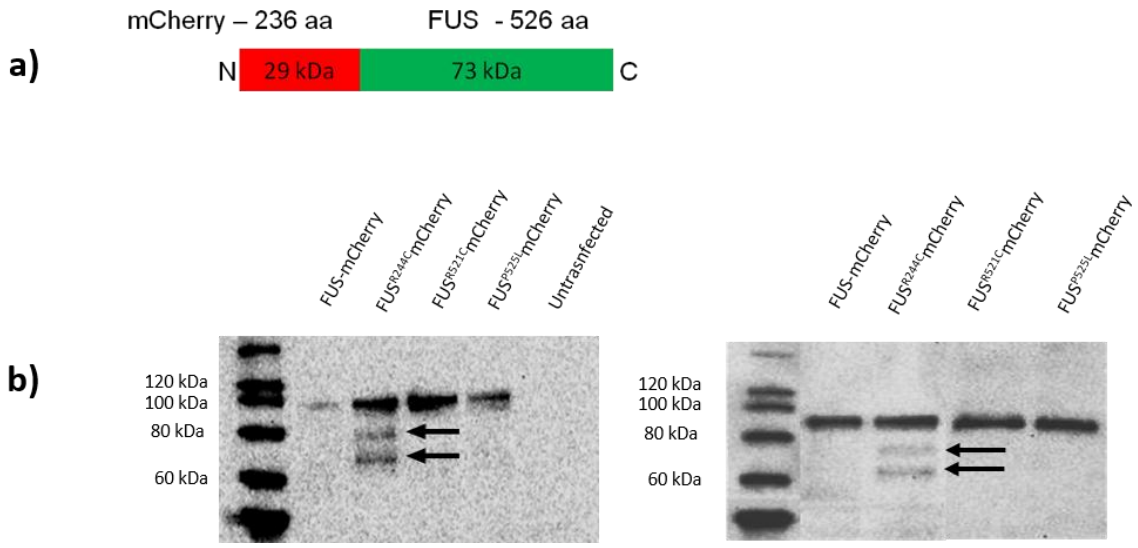

Figure 2 – Expression of FUS^{R244C} mCherry is associated with additional protein forms

a) Schematic of the FUS-mCherry fusion protein with a predicted molecular weight of 102 kDa. **b**) Western blots of FUS-mCherry transfected cells using an anti-mCherry antibody. Full length FUS-mCherry is seen at approximately 100 kDa for cells transfected with wild type or mutant FUS-mCherry. Two extra bands, at approximately 80 kDa and 70 kDa, are seen only in cells transfected with FUS^{R244C} mCherry.

5.2.2. Long range RT-PCR analysis demonstrates that R244C mutation induced changes to FUS structure are post-translational

In order to assess whether the additional forms of FUS^{R244C}mCherry seen by Western blot might correspond to changes in FUS pre-mRNA splicing, we amplified full length FUS^{R244C}mCherry mRNA using RT-PCR. In order to restrict amplification to transgenic, rather than endogenous, *FUS* a forward primer was anchored within the mCherry tag and used in conjunction with reverse primers within FUS exons 13 and 15 (Figure 2a). Amplifying across this region should detect any splicing changes, which would be likely to occur in the vicinity of exon 6. RT-PCR demonstrated amplification of expected product sizes, corresponding to full length predicted FUS mRNA. No differences were observed between FUS^{WT}mCherry and FUS^{R244C}mCherry (Figure 2b). As such, insertion of the R224C mutation appears not affect the production of *FUS* mRNA.

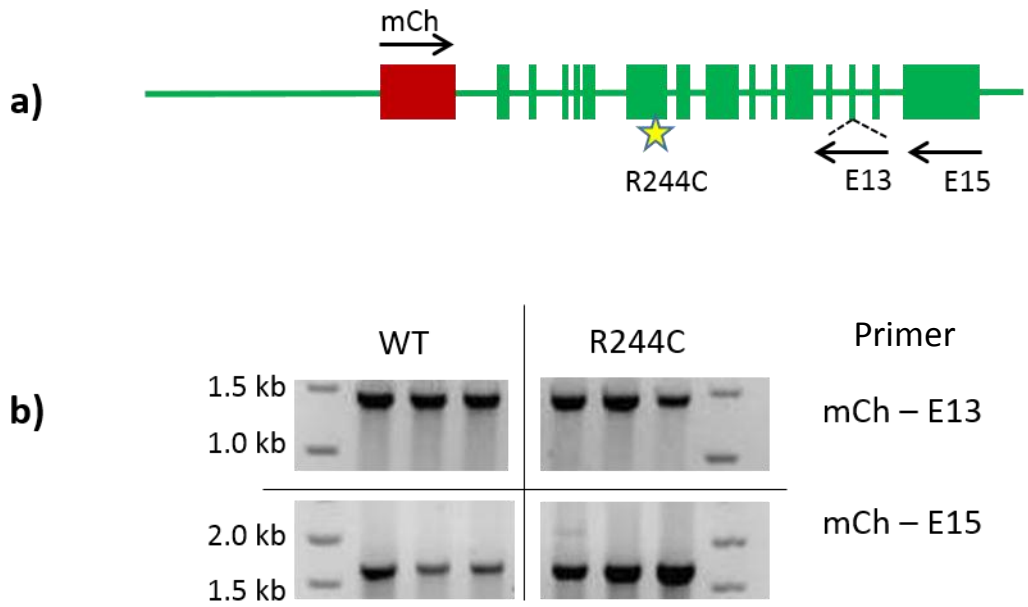

Figure 2 – Additional protein forms associated with FUS^{R244C}mCherry are not caused by altered splicing events

a) Schematic for long range RT-PCR to assess whether the R244C mutation affected mRNA formation. One primer (mCh) was anchored within the mCherry tag to ensure only transgenic FUS mRNA was amplified. Antisense primers were placed within Exon 13 and Exon 15 to capture any possible changes in mRNA length. **b**) RT-PCR amplifying two regions, mCherry – Exon 13 (1456 bp) and mCherry – Exon 15 (1680 bp) from mRNA isolated from cells expressing FUS^{WT}mCherry and FUS^{R244C}mCherry.

5.2.3. Generation of vectors expressing a cDNA FUS^{R244C} transgene tagged with HA

To establish whether expression of FUS^{R244C} from a separate vector also led to the production of aberrant forms of FUS, we generated cDNA FUS vectors expressing the R244C mutation. A further benefit of using a cDNA vector was to further rule out post-transcriptional changes in the production of aberrant FUS forms (due to a lack of introns, and hence alternative splicing, in the cDNA vectors). In order to express mutant and WT cDNA FUS we obtained a pDest-FUS-HA plasmid expressing a cDNA copy of FUS under the heterologous and constitutive CMV promoter (Addgene plasmid 26374, (Hoell et al., 2011). A HA tag was fused in frame at the N terminus of FUS (as with FUS-mCherry) to allow the fusion protein to be differentiated from endogenous FUS by way of an antibody epitope. Site-directed mutagenesis was then performed using primers containing a single central mismatch allowing insertion of the R244C mutation (Figure 3a and b) (See Methods). Insertion of the R244C mutation was confirmed by sequencing which also demonstrated a lack of further base changes throughout the FUS cDNA sequence (Figure 3c). Restriction enzyme digests confirmed vector integrity was maintained after mutagenesis (Figure 3d).

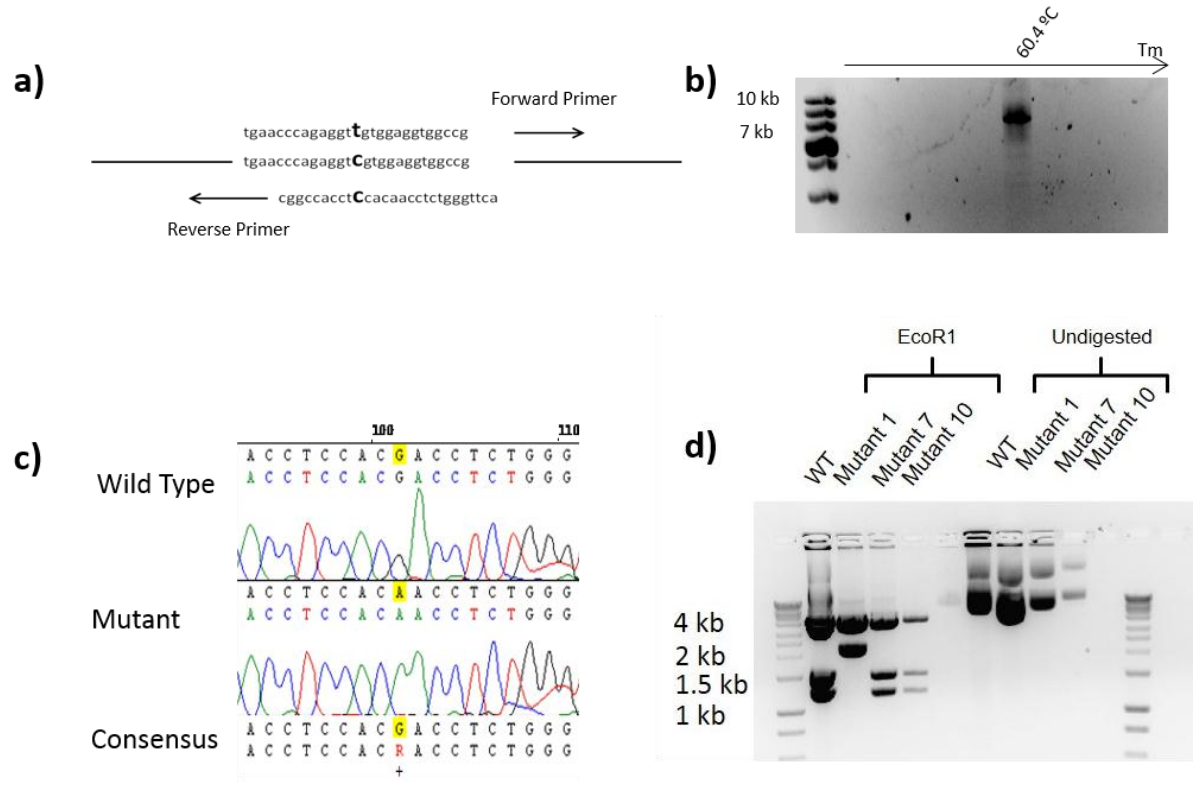

Figure 3 – Generation of a FUS^{R244C}HA cDNA Vector

a) Primers used for site directed mutagenesis to insert the R244C mutation. **b**) Successful amplification of FUS-pDest-HA using R244C SDM primers. **c**) Successful insertion of the R244C mutation as demonstrated by sequencing. **d**) Restriction enzyme digest demonstrates a correct digest pattern for 2 of the 3 isolated mutant vectors (clones 7 and 10). EcoR1 digest expected band sizes; 4171, 1498 and 1211 base pairs.

5.2.4. Expression of FUS^{R244C}pDest-HA is associated with additional FUS forms.

Western blotting using lysate from HEK cells transfected with either FUS^{WT}pDest-HA or FUS^{R244C}pDest-HA demonstrated the presence of additional bands specific to the FUS^{R244C}pDest-HA vector (Figure 4a). These bands were reproducibly seen using independently-derived vectors expressing the R244C mutation and were not seen for FUS^{WT}pDest-HA transfected cells (Figure 4b). Additional bands were present at approximately 55 and 45 kDa respectively, by comparison to the approximately 75 kDa FUS^{WT}pDest-HA band (Figure 4a and b). This reflects a drop in detected protein molecular weight of 20 and 30 kDa respectively, giving approximately the same result as with the FUS^{R244C}mCherry vector (Figure 1). Western blotting for FUS detected both the FUSpDest-HA transgene and endogenous FUS (Figure 4c). However faint bands corresponding to the additional protein forms associated with the R244C mutation could also been seen with an anti-FUS antibody (Figure 4c). These results confirm the initial finding with the FUS-mCherry vectors and demonstrate the additional FUS forms detected by western blot are post-translational and mutation, not vector, specific.

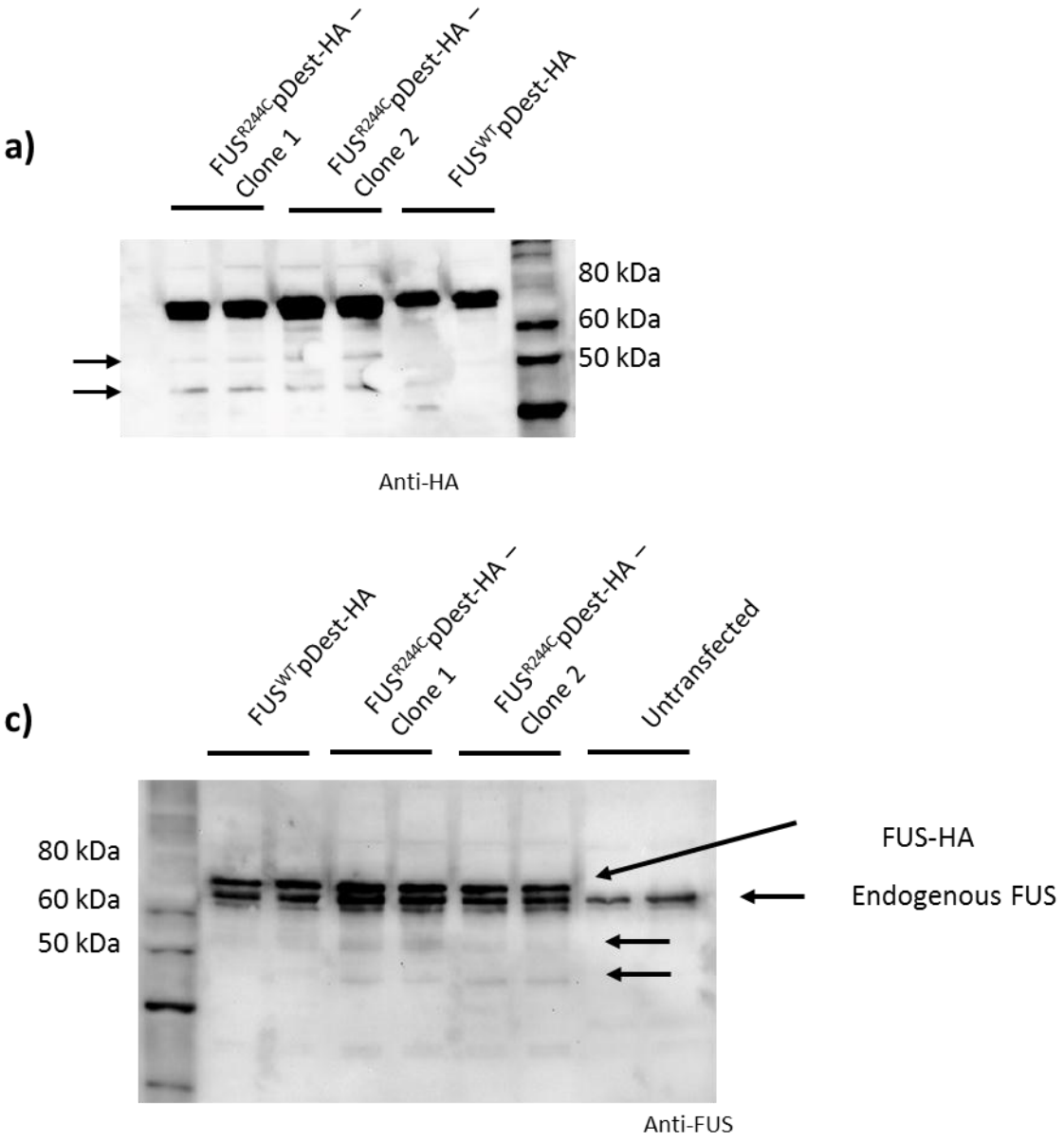

Figure 4 – FUS^{R244C} pDest-HA vectors recapitulate findings from the genomic FUS^{R244C} mCherry system

a) Western blot using an anti-HA antibody and lysate from cells transfected with either two separately derived FUS^{R244C} pDest-HA vectors (clones 7 and 10, Figure 3, a) or with FUS^{WT} pDest-HA as a control. **c**) Western blot of cells transfected with FUS^{R244C} pDest-HA and FUS^{WT} pDest-HA vectors using an anti-FUS antibody.

5.2.5. Immunoprecipitation and mass spectronomy suggest the R244C mutation causes N terminal amino acid loss

In order to investigate the cause of the lower molecular weight bands associated with the R244C mutation we immunoprecipitated FUS^{WT}mCherry and FUS^{R244C}mCherry from transfected cell lysates (Figure 5a) (see Methods). Faint lower molecular weight bands specific to immunoprecipitated FUS^{R244C}mCherry could be seen by gel electrophoresis and protein staining (see Methods) (Figure 5a). The full length and lower molecular weight bands were isolated and sent for mass spectronomy analysis. Identified fragments were aligned to the amino acid sequence of FUS (Mass spectronomy performed and analysed by Dr Benedikt Kessler, Ubiquitin Proteolysis Group, Nuffield Department of Clinical Medicine, University of Oxford). A lack of tryptic digest sites within the N terminal region of FUS meant coverage was not available between amino acids 1 and 179 (of 526). Coverage reported for the full length and the intermediate smaller band was essentially identical, suggesting that the loss of amino acids seen in the intermediate band might be located within amino acid residues 1 – 179 (Figure 5b and c). Coverage reported for the smallest band began at amino acid 307, suggesting a second loss of amino acids between 179 and 307 (Figure 5b and c). Given that the mCherry tag, located at the N terminus of the protein, must have been present for the immunoprecipitation to occur this result suggests sequential internal loss of amino acids within the N terminal half of FUS (Figure 5c). However, it should be noted that protein coverage was far from ideal, and that these results may not reflect a genuine loss of amino acids but rather, a lack of coverage in two of the samples. It will be vital to reproduce, and improve, the mass spectronomy results before any conclusions as to the identification of the lower molecular weight FUS forms can be reached.

a)

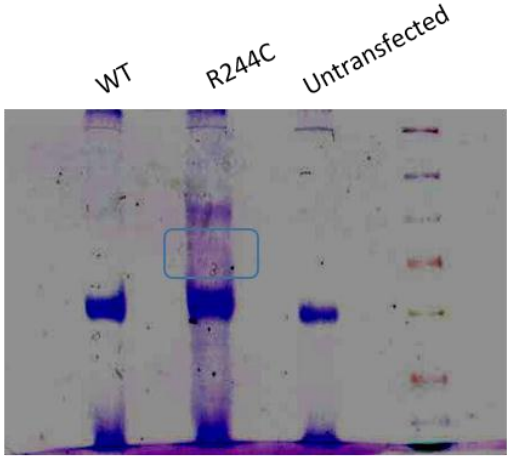

b)

Coverage; Amino Acids (1 -526)

Full

Protein sequence coverage: 37%

Matched peptides shown in ***bold red***.

```
  1 MASNDYTQQA TQSYGAYPTQ PGQGYSQQSS QPYGQQSYSG YSQSTDTSGY
 51 GQSSYSSYGQ SQNTGYGTQS TPQGYGSTGG YGSSQSSQSS YGQQSSYPGY
101 GQQPAPSSTS GSYGSSSQSS SYGQPQSGSY SQQPSYGGQQ QSYGQQQSYN
151 PPQGYGQQNQ YNSSSGGGGG GGGGGNYGQD QSSMSSGGGS GGGYGNQDQS
201 GGGGSGGYGQ QDRGGRGRGG SGGGGGGGGG GYNRSSGGYE PRGRGGGRGG
251 RGGMGGSDRG GFNKFGGPRD QGSRMDSEQD NSDNNTIFVQ GLGENVTIES
301 VADYFKQIGI IKTNKKTGQP MINLYTDRET GKLKGEATVS FDDPPSAKAA
351 IDWFDGKEFS GNPIKVSFAT RRADFNRGGG NGRGGRGRGG PMGRGGYGGG
401 GSGGGGRGGF PSGGGGGGGQ QRAGDWKCPN PTCENMNFSW RNECNQCKAP
451 KPDGPGGGPG GSHMGGNYGD DRRGGRGGYD RGGYRGRGGD RGGFRGGRGG
501 GDRGGFGPGK MDSRGEHRQD RRERPY
```

179 - 472

Middle Band

Protein sequence coverage: 31%

Matched peptides shown in ***bold red***.

```
  1 MASNDYTQQA TQSYGAYPTQ PGQGYSQQSS QPYGQQSYSG YSQSTDTSGY
 51 GQSSYSSYGQ SQNTGYGTQS TPQGYGSTGG YGSSQSSQSS YGQQSSYPGY
101 GQQPAPSSTS GSYGSSSQSS SYGQPQSGSY SQQPSYGGQQ QSYGQQQSYN
151 PPQGYGQQNQ YNSSSGGGGG GGGGGNYGQD QSSMSSGGGS GGGYGNQDQS
201 GGGGSGGYGQ QDRGGRGRGG SGGGGGGGGG GYNRSSGGYE PRGRGGGRGG
251 RGGMGGSDRG GFNKFGGPRD QGSRHDSEQD NSDNNTIFVQ GLGENVTIES
301 VADYFKQIGI IKTNKKTGQP MINLYTDRET GKLKGEATVS FDDPPSAKAA
351 IDWFDGKEFS GNPIKVSFAT RRADFNRGGG NGRGGRGRGG PMGRGGYGGG
401 GSGGGGRGGF PSGGGGGGGQ QRAGDWKCPN PTCENMNFSW RNECNQCKAP
451 KPDGPGGGPG GSHMGGNYGD DRRGGRGGYD RGGYRGRGGD RGGFRGGRGG
501 GDRGGFGPGK MDSRGEHRQD RRERPY
```

179 - 513

Lower Band

Protein sequence coverage: 19%

Matched peptides shown in ***bold red***.

```
  1 MASNDYTQQA TQSYGAYPTQ PGQGYSQQSS QPYGQQSYSG YSQSTDTSGY
 51 GQSSYSSYGQ SQNTGYGTQS TPQGYGSTGG YGSSQSSQSS YGQQSSYPGY
101 GQQPAPSSTS GSYGSSSQSS SYGQPQSGSY SQQPSYGGQQ QSYGQQQSYN
151 PPQGYGQQNQ YNSSSGGGGG GGGGGNYGQD QSSMSSGGGS GGGYGNQDQS
201 GGGGSGGYGQ QDRGGRGRGG SGGGGGGGGG GYNRSSGGYE PRGRGGGRGG
251 RGGMGGSDRG GFNKFGGPRD QGSRHDSEQD NSDNNTIFVQ GLGENVTIES
301 VADYFKQIGI IKTNKKTGQP MINLYTDRET GKLKGEATVS FDDPPSAKAA
351 IDWFDGKEFS GNPIKVSFAT RRADFNRGGG NGRGGRGRGG PMGRGGYGGG
401 GSGGGGRGGF PSGGGGGGGQ QRAGDWKCPN PTCENMNFSW RNECNQCKAP
451 KPDGPGGGPG GSHMGGNYGD DRRGGRGGYD RGGYRGRGGD RGGFRGGRGG
501 GDRGGFGPGK MDSRGEHRQD RRERPY
```

307 - 472

c)

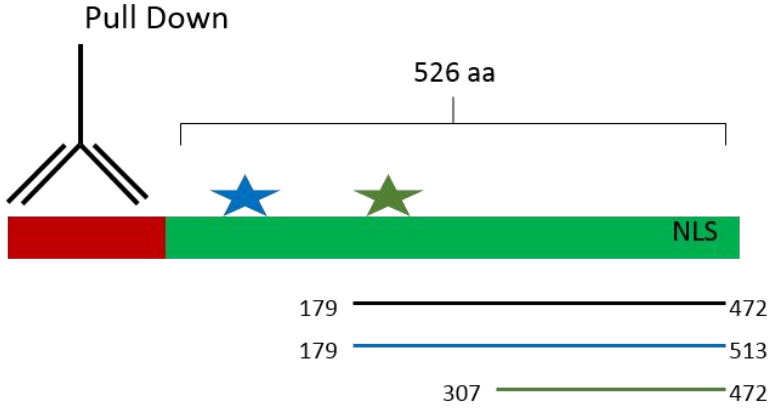

Figure 5 – FUS^{R244C} mCherry immunoprecipitation and mass spectronomy suggests N terminal loss of amino acids

a) WT and R244C FUS-mCherry were immunoprecipitated using dual anti-mCherry antibodies (see Methods) and separated by gel electrophoresis. Brilliant Blue staining allowed band visualisation. **b**) Mass spectronomy results for FUS^{WT} mCherry and FUS^{R244C} mCherry protein cut from the gel in **a**. Coverage is demonstrated by amino acids highlighted in red (Coverage (amino acids, of 1 – 526); full length band - 179 to 472, middle R244C band – 179 to 513, lower R244C band – 307 to 472. **c**) Experimental schematic showing positions of immunoprecipitation, mass spectronomy coverage and the R244C mutation. Likely regions responsible for the loss of amino acids are highlighted with stars.

5.2.6. Overexpression of FUS containing the R244C mutation is not associated with cytotoxicity

Expression of FUS from genomic vectors lead to cytotoxicity associated with the R521C and P525L mutations, but not the R244C mutation (Chapter 4). We decided to investigate whether overexpression of FUS^{R244C} from a cDNA vector would lead to detectable cytotoxicity. Cells were transfected with FUS^{R244C}pDest-HA or FUS^{WT}pDest-HA vectors and cleaved caspase-3 staining was used as an apoptotic marker (Figure 6a). Quantification of dual ICC staining for cleaved caspase-3 and the HA tag demonstrated no change in the percentage of transfected cells positive for cleaved caspase-3 between WT and R244C expressing cells (Figure 6b). DAPI staining was then used to assess nuclear morphology as a further measure of cytotoxicity (Figure 6c). Quantification of the percentage of FUS^{WT}pDest-HA and FUS^{R244C}pDest-HA expressing cells with abnormal nuclear morphology demonstrated no difference in the associated cytotoxicity of the two vectors. It appears, therefore, that the R244C mutation leads to no detectable cytotoxicity, even when overexpressed.

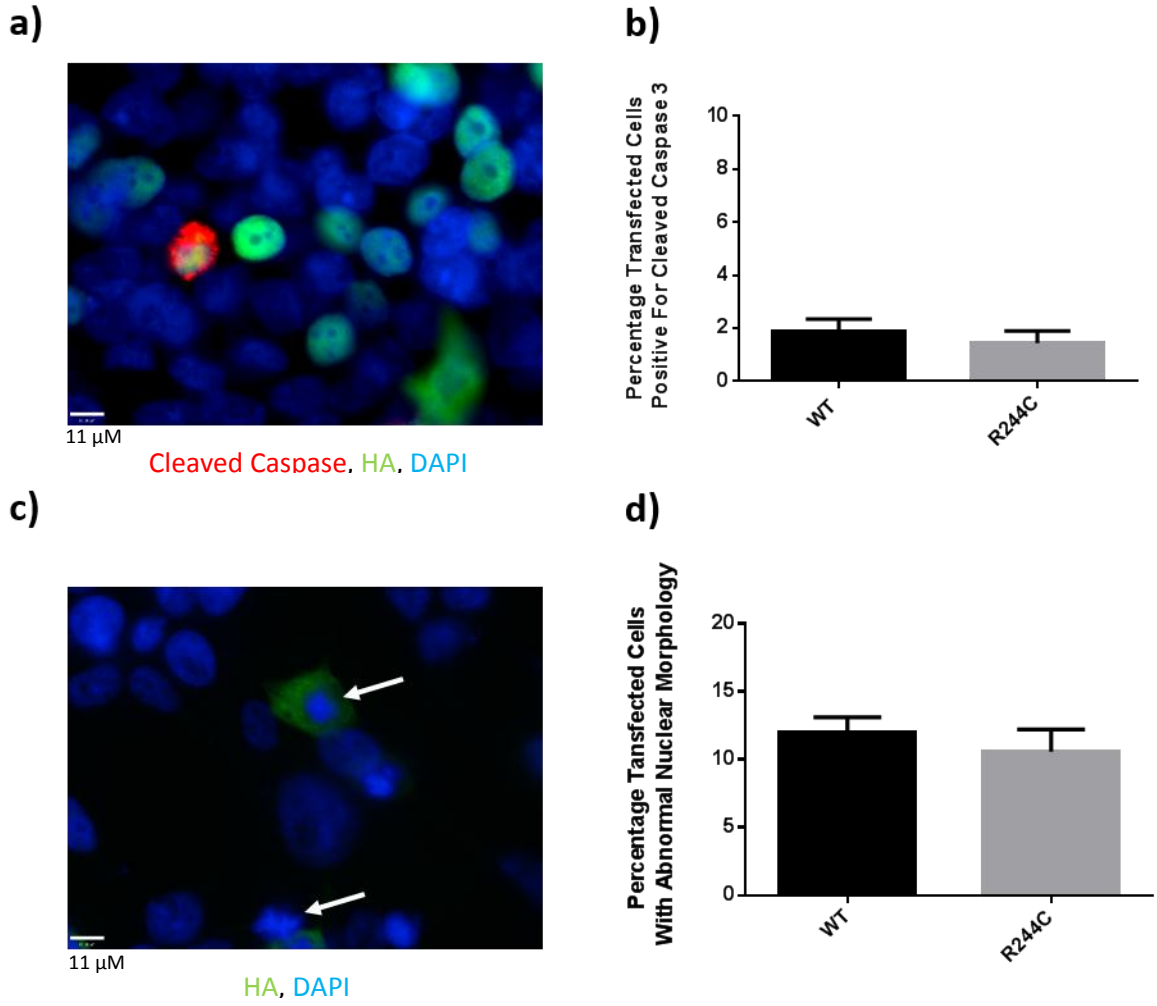

Figure 6 – Overexpression of FUS^{R244C}HA From a cDNA construct does not cause cytotoxicity in HEK293 cells

a) Cleaved caspase-3 staining specifically highlights apoptotic cells also expressing FUS^{R244C}HA. **b**) Quantification of dual ICC staining for HA and cleaved caspase-3. No change in the percentage of transfected cells positive for cleaved caspase-3 was seen with insertion of the R244C mutation (Student's t-test). **c**) DAPI staining highlights transfected cells with abnormal nuclear morphology (see arrows for examples). **d**) Quantification of nuclear abnormalities in transfected cells. No differences were seen between cells expressing FUS^{WT}HA and FUS^{R244C}HA (Student's t-test).

5.3. Discussion

In this chapter I describe the expression of both genomic and cDNA FUS vectors expressing the exon 6 R244C mutation. In Chapter 4 we demonstrated that the so far under investigated R244C mutation does not lead to a cytoplasmic relocalisation of FUS. Given that all models of genetic dysfunction of FUS have so far been based around expressing mutant FUS that demonstrates cytoplasmic relocalisation, this is a notable result. A recent publication expressing the R244C mutation demonstrated a novel role of the mutation in reducing the efficiency of FUS mediated DNA repair, highlighting the functionality and importance of non-NLS mutations in FUS. It appears, therefore, that at least some aspects of the molecular pathogenesis of FUS may not require cytoplasmic relocalisation.

Expression of FUS^{R244C}mCherry in our genomic cellular expression system reproducibly led to the formation of additional FUS protein forms of approximately 70 and 80 kDa respectively. These bands could reflect proteins lacking 20 and 30 kDa of amino acid sequence respectively (Figure 1). RT-PCR analysis demonstrated that this was not due to changes in the incorporation of exons within mature mRNA through alternative splicing (Figure 2). Furthermore, generation and expression of cDNA vectors expressing FUS^{R244C}HA replicated the additional FUS protein forms (Figure 3 and 4). Therefore, these additional forms cannot be due to post-transcriptional changes in splicing. Consequently, it seems likely that aberrant post-translational events induced by the R244C mutation impact on the structure of FUS.

Expression of the FUS^{R244C} from both genomic and cDNA vectors revealed novel FUS forms of approximately 20 and 30 kDa less than the normal mature 73 kDa FUS protein. We therefore hypothesised that these changes may have been due to aberrant protein cleavage. Bioinformatics, using protease site prediction, did not however show any differences between the wild type and mutant amino acid sequences in the predicted cleavage of cellular proteases (results not shown). Immunoprecipitation of FUS containing the R244C mutation pulled down small amounts of the 70

and 80 kDa FUS forms which were analysed by mass spectronomy (MS). This analysis did not give an ideal level of coverage, and was somewhat hampered by a lack of N terminal tryptic digests sites within FUS, meaning that the small peptides required for MS identification could not be generated. The lack of N terminal coverage, combined with poor levels of general coverage, makes it impossible to state where amino acids appear to have been lost. Ideally, a greater, and reproducible, coverage of FUS by MS would be utilised to define these sites in more detail. The cDNA vectors generated were designed with this aim in mind, as much higher levels of mutant FUS would be available to pull down, however time limitations and poor IP performance from anti-HA antibodies meant this aim was not achieved. Alternative proteomic methods, such as purifying FUS through liquid ion chromatography and sequencing the ends of each fragment by Edman degradation may prove more accurate in defining the exact make-up of each fragment. Alternatively, greater pull down and purification of the sample combined with improved mass spectrometry techniques such as MALDI-TOF may allow characterisation of the fragments to a much improved degree.

Using a genomic expression system, cytotoxicity was only seen for the NLS mutations R521C and P525L. We attempted to investigate whether cytotoxicity might be seen for the R244C mutation when overexpressed. Expression of FUS^{R244C} from a cDNA vector did not, however, lead to any detectable toxicity. This result may be explained by the late onset nature of R244C mutations (54 +/- 8.5 years) compared to the other expressed mutations (R521C, onsets of around 30 - 40 years frequently reported, P525L, onset at under 25 years generally seen) (Bäumer et al., 2010; Belzil et al., 2009; Blair et al., 2010; Chio et al., 2009; Kwiatkowski et al., 2009b; Mackenzie et al., 2011a; Ticozzi et al., 2009; Vance et al., 2009). A further, and perhaps more elegant explanation, is that the R244C mutation leads to disease through a loss of function mechanism. Due to the presence of endogenous FUS in our cellular model, a loss of function mutation would not lead to toxicity unless it acted in a dominant negative fashion. This concept fits with a model in which the NLS mutations R521C and P525L cause a gain of toxic function through cytoplasmic relocalisation, whilst the R244C mutation, which does not lead to relocalisation, leads to a general loss of FUS function. The

suggested inheritance pattern for the R244C mutation is, however, autosomal dominant, a pattern generally associated with gain of function mutations (Kwiatkowski et al., 2009b). Notably however, cellular levels of FUS are thought to be tightly controlled (see Introduction), making a dominantly inherited haploinsufficiency mechanism a distinct possibility. The recent demonstration that the R244C mutation affects HDAC1 binding and DNA damage repair, could fit with a loss of function mechanism in which changes in protein structure, centred around the exon 5/6 glycine rich region required for HDAC1 binding, lead to a lack of DSBR pathway components being recruited to DNA damage sites.

In summary, here we show evidence that the non-NLS R244C does not affect the nuclear localisation of FUS but leads to the formation of protein forms lacking N terminal amino acids. This finding hints at alternative mechanisms of pathogenesis that centre on a loss of function in FUS. Therefore, these data suggest a general model whereby FUS dysfunction can be caused by both loss and gain of function mutations. Gain of function mutations such as R521C and P525L appear to mediate their impact through a cytoplasmic relocalisation, whilst loss of function mutations may not affect cellular localisation, but rather affect the basic functionality of FUS.

6. Chapter 6 – Discussion

In this chapter I will discuss the overall outcome of my thesis. Individual results and their importance to the wider scientific literature are discussed at the end of each relevant results chapter, and only a brief overview is given here, so as to avoid repetition. In this context, I will now address the success of the project in answering the currently unresolved questions posed in the introduction:

- Can a more physiological and regulated model of *FUS* dysfunction, and hence ALS/FTD-FUS be generated?

    - This project has generated a BAC-based vector expressing the whole genomic *FUS* locus together with large up- and down-stream regulatory regions. Furthermore, expression of the transgene has been shown to be terminated on the addition of Cre recombinase. Using these vectors, both an *in vitro* cell model and a mouse model of *FUS* dysfunction have been generated. Whilst expression patterns of the FUS-mCherry transgene have not been investigated, if they replicate the accuracy normally seen with BAC-based genomic vectors, this project has generated a highly physiological and regulatable model. Whether *in vivo* models develop features of ALS and FTD, and hence act as full disease models, remains to be seen.

- Do mutations in *FUS* lead to toxicity through a gain of toxicity, a loss of function, or a combination of the two?

    - The results described in Chapter 4 strongly suggest that cytoplasmic accumulation of FUS, due to NLS mutations, leads to disease through a gain of function mechanism (discussed in detail in Chapter 4). By contrast, expression of the non-NLS mutation R244C appears to be associated with a loss of function mechanism (Chapter 5). As such, we present results that suggest both gain and loss of function events can be associated with specific *FUS* mutations. The limits of our *in vitro* model meant that loss of function events could not be directly assessed (see Chapters 4 and 5). Therefore, it is possible

that both loss and gain of function of events are associated with NLS mutations (rather than gain of function alone), and that both contribute to disease.

- Is the toxicity of mutant *FUS* directly due to cytoplasmic relocalisation?

  - The results described in Chapter 4 for the NLS mutations R521C and P525L strongly support the idea that the gain of toxicity seen is associated with cytoplasmic relocalisation. Inhibition of relocalisation elegantly reduced cytotoxicity back to a baseline level, providing powerful evidence for a causal link between relocalisation and toxicity. The lack of relocalisation for the disease-associated R244C mutation demonstrates that protein dysfunction can be found in the absence of visible relocalisation, but that this toxicity may be specific to loss of function events.

- Can relocalisation of FUS be inhibited by arginine demethylases?

  - As discussed in Chapter 4, relocalisation of NLS mutant FUS was inhibited by preventing arginine methylation through AMI-1, and more variably, by AdOx treatment and *PRMT1* siRNA knockdown.

- Does inhibition of relocalisation reverse any toxicity seen?

  - Inhibition of relocalisation successfully reversed the gain of function cytotoxicity associated with the P525L mutation (as discussed in Chapter 5). Whether any toxicity relating to a possible loss of function mechanism is reversed could not be answered due to limitation in our model (a *FUS* knockout background would be required).

- What is the role of stress granules in the formation of cytoplasmic FUS aggregations?

  - Whilst certain pieces of anecdotal evidence suggested a possible relationship between FUS containing stress granules and larger, spontaneously forming, aggregates (discussed in detail in Chapter 5), quantitative counts demonstrated no increase in FUS-positive

aggregates after stress granule induction. However, cell counts for stress granules and aggregates gave highly variable data (see discussion in Chapter 5). To this end, further work looking at the relationship between these inclusions will need to thoroughly minimise all possible variables. Our work, therefore, has not fully answered this question but does, at least, suggest that any transition of stress granules to disease-associated aggregates (as proposed multiple times as a "two-hit" model) may be relatively subtle and occur only over long time periods or specific conditions. A more detailed longitudinal study, perhaps using neuronal cultures, may be required to fully determine the importance of stress granules in ALS and FTD. Attempts to use a different approach to investigate the importance of stress granule localisation to aggregate formation – inhibition of stress granule formation – failed, but may hold promise for further studies.

This thesis has, therefore, addressed, at least partially, all the questions and aims that were originally set out. Further experiments that would increase the power of these answers have been suggested in the individual chapter discussions, the most pertinent of which are listed below;

i. Further, and more sensitive, measures of cytotoxicity in FUS-mCherry transfected cells to rule out gain of function events for the R244C mutation. Attempts to achieve this aim using fluorescence activated cell sorting (FACS) were not successfully achieved, but given further investigation should be possible.
ii. Generation of a *FUS* knock-out cell line to actively assess loss of function derived cytotoxicity. This model would allow greater inferences to be made as to the mechanism of action of the R521C, P525L and, especially, the R244C mutation.
iii. Generation of a cellular model expressing FUs-mCherry on a *PRMT1/PRMT8* knockout background to more elegantly establish the role of FUS methylation on both wild type and mutant FUS function and toxicity. A rodent model null for PRMT family protein would also allow the effect of arginine methylation on sporadic FUSopathies to be investigated.

iv. More accurate mass spectronomy (MS) coverage of the R244C mutation induced FUS protein forms. Greater immunoprecipitation efficiencies and different protein fragmentation technologies would allow the smaller FUS fragments to be more accurately defined, allowing these molecular events to be matched to suggested mutational impacts.

v. *In vivo* modelling of FUS dysfunction using the FUS-mCherry vectors. This aim, which greatly influenced the design of the FUS vectors, and should allow the most physiological model of the impact of FUS mutations on ALS/FTD onset, is not part of this thesis. However, transgenic mice model using the vectors generated in this thesis have been generated, and are beginning to be described (see Chapter 3 discussion). The experiments described here should, therefore, directly help generate an exceptionally physiological and controllable model of *FUS* dysfunction.

In summary, here we demonstrate the generation of a BAC-based genomic DNA vector for the ALS and FTD associated gene *FUS*. This vector will allow physiological expression of *FUS*, and combines this feature with a novel insertion of variant LoxP sites to allow time-course or tissue-specific termination of FUS-mCherry expression. We utilised these vectors to assess the effect of *FUS* mutations in HEK293 cells, making the following key observations;

1. The NLS mutations R521C and P525L cause a cytoplasmic accumulation of FUS, whilst the R244C mutation does not affect localisation.
2. Relocalised FUS^{P525L}mCherry forms cytoplasmic aggregations, whilst FUS^{R521C}mCherry does not.
3. Cytoplasmically localised FUS is incorporated into stress granules. Induction of stress granules does not appear to induce long-lasting aggregates. Notably, inhibition of the ubiquitin proteasome system led to the formation of FUS-containing stress granules providing a novel link between these two ALS/FTD related pathways.

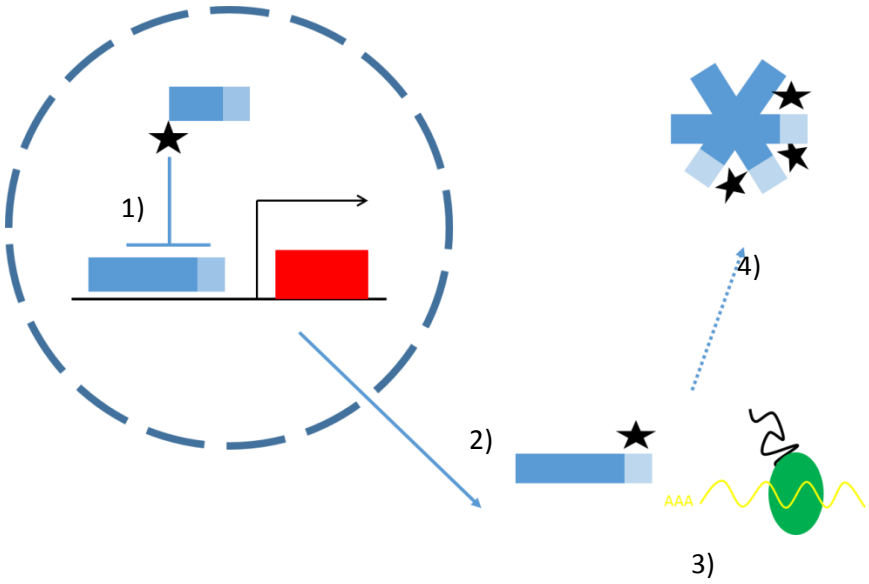

Figure 1 – Expression of FUS-mCherry vectors suggests a model for FUS pathogenesis

1. Non-NLS mutations lead to a loss of function within the nucleus. The R244C mutation leads to aberrant forms of FUS that may be defective in DNA repair pathways.
2. NLS mutations lead to cytoplasmic accumulation of FUS.
3. A gain of function cytotoxicty is associated with cytoplasmic accumulation, through either aberrant functionality, 4. aggregation within the cytoplasm, or a combination of the two.

4. The R521C and P525L mutations led to a gain of cytotoxicity which can be reversed by inhibiting cytoplasmic accumulation. This suggests a cytoplasmic gain of function for *FUS* NLS mutations. Notably, the greater impact of the P525L mutation, compared to the R521C mutation, on both cytoplasmic relocalisation and cytotoxicity suggests that gain of cytoplasmic function may occur in a concentration dependent manner.
5. The R244C mutation induces the formation of aberrant FUS protein forms that appear to result from undetermined N terminal cleavage events.
6. A lack of cytotoxicity, even when chronically overexpressed, with expression of the R244C mutation supports a loss of nuclear function mechanism.

This thesis, therefore, makes novel contributions toward understanding the molecular pathogenesis associated with FUS mutations. Recently published data supports a number of the conclusions reached in this thesis. In the experiments of Daigle *et al*., mutating four phenylalanine residues (305, 341, 359, 368) blocked the RNA binding ability of FUS (Daigle et al., 2013). Within both a yeast and *Drosophila* model inhibition of RNA binding ability rescued FUS mutation-dependent toxicity and neurodegeneration. This result argues for an RNA-dependent gain of function event after an initial NLS mutation induced mislocalisation of FUS. Daigle *et al*., then demonstrate that the same RNA-binding impaired FUS neither localises to stress granules nor relocalises to the cytoplasm, even on the insertion of severe NLS mutations (Daigle et al., 2013). Further studies have also demonstrated a requirement for functional RNA binding in order for FUS to localise to stress granules, and that expression of mutant FUS affects stress granule dynamics, however this result does not prove that stress granule association is needed for FUS toxicity (Bentmann et al., 2012) (Baron et al., 2013). Aberrant mRNA binding could give the same result, with impaired stress granule binding simply being an additional, non-toxic, consequence of impaired RNA binding. It will be necessary to separate these two possibilities, perhaps through inhibition of stress granule formation, in order to tease out the exact mechanism of FUS gain of function. Notably, the finding that cytoplasmic

relocalisation in NLS-mutant FUS required functional RNA binding is interesting but was not found in a further comprehensive study expressing sequential FUS deletions (Bentmann et al., 2012).

A further recent study has elucidated a novel phenotype for a non-NLS FUS mutation. In this report, expression of the G156E mutation led to relocalisation independent toxicity by way of increasing the tendency of FUS to form intranuclear inclusions (Nomura et al., 2013). Whilst this mechanism is quite different to that suggested for the R244C mutation it does further highlight the importance, and functional significance, of non-NLS FUS mutations within FUSopathies.

These data suggest possibilities, and directions to be focussed on, in order to reverse the effects of FUS dysfunction in ALS and FTD. In the vast majority of familial disease cases the mutation found is within the NLS, and hence likely to lead to a cytoplasmic gain of function. Therefore, treatments capable of reversing this relocalisation, such as arginine demethylases, could hold great promise. The challenge here will be to develop specific demethylases whose action does not affect the biological function of the whole FET protein family. The frequently observed relocalisation of FUS in sporadic FTD-FUS means that treatments developed to combat relocalisation in familial disease could also work within sporadic disease. Affecting the methylation status of the FET family proteins could hold great promise within this area. If the toxicity associated with FUS relocalisation is predominantly a gain of function then reversing cytoplasmic accumulation could effectively remove any toxicity in up to 99% of all ALS/FTD-FUS cases.

Combatting a loss of function, such as that suggested for the R244C mutation, may be more problematic. However, the finding that most FUS mutations, including R244C, have an autosomal dominant pattern suggests that expression levels may be important. For a loss of function to be inherited in a dominant pattern suggests a possible haploinsufficiency, something which could perhaps be countered through raising *FUS* expression levels pharmacologically.

In conclusion, it can be seen that determining the molecular mechanisms of FUS-linked neuronal death may help develop much needed treatments to reverse, or modify, the clinical features of both ALS and FTD. Within this thesis we demonstrate the development of genomic DNA vectors for *FUS* that allow this aim to be explored both *in vitro* and *in vivo*. These vectors allowed novel findings as to the effect of *FUS* mutations to be generated within a cellular model, and may help to begin to unravel the molecular mechanism of FUS-associated pathogenesis.

7. Bibliography

Alegre-Abarrategui, J., Christian, H., Lufino, M.M., Mutihac, R., Venda, L.L., Ansorge, O., and Wade-Martins, R. (2009). LRRK2 regulates autophagic activity and localizes to specific membrane microdomains in a novel human genomic reporter cellular model. Hum Mol Genet *18*, 4022-4034.
Andersen, P.M., and Al-Chalabi, A. (2011). Clinical genetics of amyotrophic lateral sclerosis: what do we really know? Nature reviews Neurology *7*, 603-615.
Anderson, P., and Kedersha, N. (2008). Stress granules: the Tao of RNA triage. Trends Biochem Sci *33*, 141 - 150.
Andersson, M.K., Stahlberg, A., Arvidsson, Y., Olofsson, A., Semb, H., Stenman, G., Nilsson, O., and Aman, P. (2008). The multifunctional FUS, EWS and TAF15 proto-oncoproteins show cell type-specific expression patterns and involvement in cell spreading and stress response. BMC cell biology *9*, 37.
Arai, T., Hasegawa, M., Akiyama, H., Ikeda, K., Nonaka, T., Mori, H., Mann, D., Tsuchiya, K., Yoshida, M., Hashizume, Y.*, et al.* (2006). TDP-43 is a component of ubiquitin-positive tau-negative inclusions in frontotemporal lobar degeneration and amyotrophic lateral sclerosis. Biochem Biophys Res Commun *351*, 602-611.
Araya, N., Hiraga, H., Kako, K., Arao, Y., Kato, S., and Fukamizu, A. (2005). Transcriptional down-regulation through nuclear exclusion of EWS methylated by PRMT1. Biochem Biophys Res Commun *329*, 653-660.
Argos, P. (1990). An investigation of oligopeptides linking domains in protein tertiary structures and possible candidates for general gene fusion. Journal of Molecular Biology *211*, 943-958.
Baker, M., Mackenzie, I.R., Pickering-Brown, S.M., Gass, J., Rademakers, R., Lindholm, C., Snowden, J., Adamson, J., Sadovnick, A.D., Rollinson, S.*, et al.* (2006). Mutations in progranulin cause tau-negative frontotemporal dementia linked to chromosome 17. Nature *442*, 916-919.
Barbeito, L.H., Pehar, M., Cassina, P., Vargas, M.R., Peluffo, H., Viera, L., Estevez, A.G., and Beckman, J.S. (2004). A role for astrocytes in motor neuron loss in amyotrophic lateral sclerosis. Brain research Brain research reviews *47*, 263-274.
Bartolome, F., Wu, H.C., Burchell, V.S., Preza, E., Wray, S., Mahoney, C.J., Fox, N.C., Calvo, A., Canosa, A., Moglia, C.*, et al.* (2013). Pathogenic VCP mutations induce mitochondrial uncoupling and reduced ATP levels. Neuron *78*, 57-64.
Battistini, S., Giannini, F., Greco, G., Bibbò, G., Ferrera, L., Marini, V., Causarano, R., Casula, M., Lando, G., Patrosso, M.C.*, et al.* (2005). SOD1 mutations in amyotrophic lateral sclerosis. J Neurol *252*, 782-788.
Bäumer, D., Hilton, D., Paine, S.M.L., Turner, M.R., Lowe, J., Talbot, K., and Ansorge, O. (2010). Juvenile ALS with basophilic inclusions is a FUS proteinopathy with FUS mutations. Neurology *75*, 611-618.
Beck, J., Rohrer, J.D., Campbell, T., Isaacs, A., Morrison, K.E., Goodall, E.F., Warrington, E.K., Stevens, J., Revesz, T., Holton, J.*, et al.* (2008). A distinct clinical, neuropsychological and radiological phenotype is associated with progranulin gene mutations in a large UK series. Brain *131*, 706-720.
Belzil, V.V., Valdmanis, P.N., Dion, P.A., Daoud, H., Kabashi, E., Noreau, A., Gauthier, J., Hince, P., Desjarlais, A., Bouchard, J.P.*, et al.* (2009). Mutations in FUS cause FALS and SALS in French and French Canadian populations. Neurology *73*, 1176-1179.
Benajiba, L., Le Ber, I., Camuzat, A., Lacoste, M., Thomas-Anterion, C., Couratier, P., Legallic, S., Salachas, F., Hannequin, D., Decousus, M.*, et al.* (2009). TARDBP mutations in motoneuron disease with frontotemporal lobar degeneration. Ann Neurol *65*, 470-473.
Bence, N.F., Sampat, R.M., and Kopito, R.R. (2001). Impairment of the Ubiquitin-Proteasome System by Protein Aggregation. Science *292*, 1552-1555.

Bentmann, E., Neumann, M., Tahirovic, S., Rodde, R., Dormann, D., and Haass, C. (2012). Requirements for stress granule recruitment of fused in sarcoma (FUS) and TAR DNA-binding protein of 43 kDa (TDP-43). J Biol Chem *287*, 23079-23094.
Bertolotti, A., Bell, B., and Tora, L. (1999). The N-terminal domain of human TAFII68 displays transactivation and oncogenic properties. Oncogene *18*, 8000-8010.
Bjørkøy, G., Lamark, T., Brech, A., Outzen, H., Perander, M., Øvervatn, A., Stenmark, H., and Johansen, T. (2005). p62/SQSTM1 forms protein aggregates degraded by autophagy and has a protective effect on huntingtin-induced cell death. The Journal of Cell Biology *171*, 603-614.
Bjørkøy, G., Lamark, T., and Johansen, T. (2006a). p62/SQSTM1 - A missing link between protein aggregates and the autophagy machinery. Autophagy *2*, 138-139.
Bjørkøy, G., Lamark, T., and Johansen, T. (2006b). p62/SQSTM1: a missing link between protein aggregates and the autophagy machinery. Autophagy *2*, 138-139.
Blair, I.P., Williams, K.L., Warraich, S.T., Durnall, J.C., Thoeng, A.D., Manavis, J., Blumbergs, P.C., Vucic, S., Kiernan, M.C., and Nicholson, G.A. (2010). FUS mutations in amyotrophic lateral sclerosis: clinical, pathological, neurophysiological and genetic analysis. Journal of Neurology, Neurosurgery & Psychiatry *81*, 639-645.
Blechingberg, J., Luo, Y., Bolund, L., Damgaard, C.K., and Nielsen, A.L. (2012). Gene Expression Responses to FUS, EWS, and TAF15 Reduction and Stress Granule Sequestration Analyses Identifies FET-Protein Non-Redundant Functions. PLoS One *7*, e46251.
Blencowe, B.J. (2000). Exonic splicing enhancers: mechanism of action, diversity and role in human genetic diseases. Trends Biochem Sci *25*, 106-110.
Borroni, B., Archetti, S., Del Bo, R., Papetti, A., Buratti, E., Bonvicini, C., Agosti, C., Cosseddu, M., Turla, M., Di Lorenzo, D*., et al.* (2010). TARDBP mutations in frontotemporal lobar degeneration: frequency, clinical features, and disease course. Rejuvenation research *13*, 509-517.
Borroni, B., Bonvicini, C., Alberici, A., Buratti, E., Agosti, C., Archetti, S., Papetti, A., Stuani, C., Di Luca, M., Gennarelli, M*., et al.* (2009). Mutation within TARDBP leads to Frontotemporal Dementia without motor neuron disease. Human Mutation *30*, E974-E983.
Bosco, D.A., Lemay, N., Ko, H.K., Zhou, H., Burke, C., Kwiatkowski, T.J., Jr., Sapp, P., McKenna-Yasek, D., Brown, R.H., Jr., and Hayward, L.J. (2010a). Mutant FUS proteins that cause amyotrophic lateral sclerosis incorporate into stress granules. Hum Mol Genet *19*, 4160-4175.
Bosco, D.A., Lemay, N., Ko, H.K., Zhou, H.R., Burke, C., Kwiatkowski, T.J., Sapp, P., McKenna-Yasek, D., Brown, R.H., and Hayward, L.J. (2010b). Mutant FUS proteins that cause amyotrophic lateral sclerosis incorporate into stress granules. Hum Mol Genet *19*, 4160-4175.
Bose, J.K., Huang, C.C., and Shen, C.K. (2011). Regulation of autophagy by neuropathological protein TDP-43. J Biol Chem *286*, 44441-44448.
Boxer, A.L., and Boeve, B.F. (2007). Frontotemporal Dementia Treatment: Current Symptomatic Therapies and Implications of Recent Genetic, Biochemical, and Neuroimaging Studies. Alzheimer Dis Assoc Dis *21*, S79-S87 10.1097/WAD.1090b1013e31815c31345e.
Brady, O.A., Meng, P., Zheng, Y., Mao, Y., and Hu, F. (2011). Regulation of TDP-43 aggregation by phosphorylation and p62/SQSTM1. J Neurochem *116*, 248-259.
Brettschneider, J., Van Deerlin, V.M., Robinson, J.L., Kwong, L., Lee, E.B., Ali, Y.O., Safren, N., Monteiro, M.J., Toledo, J.B., Elman, L*., et al.* (2012). Pattern of ubiquilin pathology in ALS and FTLD indicates presence of C9ORF72 hexanucleotide expansion. Acta Neuropathol.
Brooks, B.R. (1994). El Escorial World Federation of Neurology criteria for the diagnosis of amyotrophic lateral sclerosis. Subcommittee on Motor Neuron Diseases/Amyotrophic Lateral Sclerosis of the World Federation of Neurology Research Group on Neuromuscular Diseases and the El Escorial "Clinical limits of amyotrophic lateral sclerosis" workshop contributors. J Neurol Sci *124 Suppl*, 96-107.
Buchan, J.R., and Parker, R. (2009). Eukaryotic Stress Granules: The Ins and Outs of Translation. Mol Cell *36*, 932-941.

Buratti, E., Brindisi, A., Giombi, M., Tisminetzky, S., Ayala, Y.M., and Baralle, F.E. (2005). TDP-43 binds heterogeneous nuclear ribonucleoprotein A/B through its C-terminal tail - An important region for the inhibition of cystic fibrosis transmembrane conductance regulator exon 9 splicing. J Biol Chem *280*, 37572-37584.
Caffrey, T.M., Joachim, C., Paracchini, S., Esiri, M.M., and Wade-Martins, R. (2006). Haplotype-specific expression of exon 10 at the human MAPT locus. Hum Mol Genet *15*, 3529-3537.
Caffrey, T.M., and Wade-Martins, R. (2007). Functional MAPT haplotypes: bridging the gap between genotype and neuropathology. Neurobiol Dis *27*, 1-10.
Cairns, N.J., Neumann, M., Bigio, E.H., Holm, I.E., Troost, D., Hatanpaa, K.J., Foong, C., White, C.L., 3rd, Schneider, J.A., Kretzschmar, H.A.*, et al.* (2007). TDP-43 in familial and sporadic frontotemporal lobar degeneration with ubiquitin inclusions. Am J Pathol *171*, 227-240.
Calvio, C., Neubauer, G., Mann, M., and Lamond, A.I. (1995). Identification of hnRNP P2 as TLS/FUS using electrospray mass spectrometry. RNA *1*, 724-733.
Carrasquillo, M.M., Nicholson, A.M., Finch, N., Gibbs, J.R., Baker, M., Rutherford, N.J., Hunter, T.A., DeJesus-Hernandez, M., Bisceglio, G.D., Mackenzie, I.R.*, et al.* (2010). Genome-wide screen identifies rs646776 near sortilin as a regulator of progranulin levels in human plasma. American journal of human genetics *87*, 890-897.
Chen-Plotkin, A.S., Martinez-Lage, M., Sleiman, P.M.A., Hu, W., Greene, R., Wood, E.M., Bing, S., Grossman, M., Schellenberg, G.D., Hatanpaa, K.J.*, et al.* (2011). Genetic and Clinical Features of Progranulin-Associated Frontotemporal Lobar Degeneration. Arch Neurol *68*, 488-497.
Chesselet, M.-F., and Richter, F. (2011). Modelling of Parkinson's disease in mice. The Lancet Neurology *10*, 1108-1118.
Chio, A., Calvo, A., Moglia, C., Ossola, I., Brunetti, M., Sbaiz, L., Lai, S.L., Abramzon, Y., Traynor, B.J., and Restagno, G. (2011). A de novo missense mutation of the FUS gene in a "true" sporadic ALS case. Neurobiol Aging *32*.
Chio, A., Restagno, G., Brunetti, M., Ossola, I., Calvo, A., Mora, G., Sabatelli, M., Monsurro, M.R., Battistini, S., Mandrioli, J.*, et al.* (2009). Two Italian kindreds with familial amyotrophic lateral sclerosis due to FUS mutation. Neurobiol Aging *30*, 1272-1275.
Cho, S.W., Kim, S., Kim, Y., Kweon, J., Kim, H.S., Bae, S., and Kim, J.S. (2014). Analysis of off-target effects of CRISPR/Cas-derived RNA-guided endonucleases and nickases. Genome research *24*, 132-141.
Christian, M., Cermak, T., Doyle, E.L., Schmidt, C., Zhang, F., Hummel, A., Bogdanove, A.J., and Voytas, D.F. (2010). Targeting DNA double-strand breaks with TAL effector nucleases. Genetics *186*, 757-761.
Ciechanover, A., and Brundin, P. (2003). The Ubiquitin Proteasome System in Neurodegenerative Diseases: Sometimes the Chicken, Sometimes the Egg. Neuron *40*, 427-446.
Cleveland, D.W., and Rothstein, J.D. (2001). From Charcot to Lou Gehrig: Deciphering selective motor neuron death in ALS. Nat Rev Neurosci *2*, 806-819.
Colombrita, C., Onesto, E., Megiorni, F., Pizzuti, A., Baralle, F.E., Buratti, E., Silani, V., and Ratti, A. (2012). TDP-43 and FUS RNA-binding Proteins Bind Distinct Sets of Cytoplasmic Messenger RNAs and Differently Regulate Their Post-transcriptional Fate in Motoneuron-like Cells. J Biol Chem *287*, 15635-15647.
Colombrita, C., Zennaro, E., Fallini, C., Weber, M., Sommacal, A., Buratti, E., Silani, V., and Ratti, A. (2009). TDP-43 is recruited to stress granules in conditions of oxidative insult. J Neurochem *111*, 1051-1061.
Cong, L., Ran, F.A., Cox, D., Lin, S., Barretto, R., Habib, N., Hsu, P.D., Wu, X., Jiang, W., Marraffini, L.A.*, et al.* (2013). Multiplex genome engineering using CRISPR/Cas systems. Science *339*, 819-823.
Conte, A., Lattante, S., Zollino, M., Marangi, G., Luigetti, M., Del Grande, A., Servidei, S., Trombetta, F., and Sabatelli, M. P525L FUS mutation is consistently associated with a severe form of juvenile Amyotrophic Lateral Sclerosis. Neuromuscular Disorders.

Cook, C., Gendron, T.F., Scheffel, K., Carlomagno, Y., Dunmore, J., DeTure, M., and Petrucelli, L. (2012a). Loss of HDAC6, a novel CHIP substrate, alleviates abnormal tau accumulation. Hum Mol Genet.
Cook, C., Gendron, T.F., Scheffel, K., Carlomagno, Y., Dunmore, J., DeTure, M., and Petrucelli, L. (2012b). Loss of HDAC6, a novel CHIP substrate, alleviates abnormal tau accumulation. Hum Mol Genet *21*, 2936-2945.
Copeland, N.G., Jenkins, N.A., and Court, D.L. (2001). Recombineering: a powerful new tool for mouse functional genomics. Nature reviews Genetics *2*, 769-779.
Corrado, L., Del Bo, R., Castellotti, B., Ratti, A., Cereda, C., Penco, S., Soraru, G., Carlomagno, Y., Ghezzi, S., Pensato, V.*, et al.* (2010). Mutations of FUS gene in sporadic amyotrophic lateral sclerosis. J Med Genet *47*, 190-194.
Corrado, L., Ratti, A., Gellera, C., Buratti, E., Castellotti, B., Carlomagno, Y., Ticozzi, N., Mazzini, L., Testa, L., Taroni, F.*, et al.* (2009). High frequency of TARDBP gene mutations in Italian patients with amyotrophic lateral sclerosis. Human Mutation *30*, 688-694.
Crozat, A., Aman, P., Mandahl, N., and Ron, D. (1993). FUSION OF CHOP TO A NOVEL RNA-BINDING PROTEIN IN HUMAN MYXOID LIPOSARCOMA. Nature *363*, 640-644.
Cruts, M., Gijselinck, I., van der Zee, J., Engelborghs, S., Wils, H., Pirici, D., Rademakers, R., Vandenberghe, R., Dermaut, B., Martin, J.J.*, et al.* (2006). Null mutations in progranulin cause ubiquitin-positive frontotemporal dementia linked to chromosome 17q21. Nature *442*, 920-924.
Dai, R.M., and Li, C.C. (2001). Valosin-containing protein is a multi-ubiquitin chain-targeting factor required in ubiquitin-proteasome degradation. Nat Cell Biol *3*, 740-744.
Daigle, J.G., Lanson, N.A., Jr., Smith, R.B., Casci, I., Maltare, A., Monaghan, J., Nichols, C.D., Kryndushkin, D., Shewmaker, F., and Pandey, U.B. (2013). RNA-binding ability of FUS regulates neurodegeneration, cytoplasmic mislocalization and incorporation into stress granules associated with FUS carrying ALS-linked mutations. Hum Mol Genet *22*, 1193-1205.
Dalal, S., Rosser, M.F.N., Cyr, D.M., and Hanson, P.I. (2004). Distinct Roles for the AAA ATPases NSF and p97 in the Secretory Pathway. Molecular Biology of the Cell *15*, 637-648.
DeJesus-Hernandez, M., Mackenzie Ian, R., Boeve Bradley, F., Boxer Adam, L., Baker, M., Rutherford Nicola, J., Nicholson Alexandra, M., Finch NiCole, A., Flynn, H., and Adamson, J. (2011a). Expanded GGGGCC Hexanucleotide Repeat in Noncoding Region of C9ORF72 Causes Chromosome 9p-Linked FTD and ALS. Neuron *72*, 245 - 256.
Dejesus-Hernandez, M., Mackenzie, I.R., Boeve, B.F., Boxer, A.L., Baker, M., Rutherford, N.J., Nicholson, A.M., Finch, N.A., Flynn, H., Adamson, J.*, et al.* (2011b). Expanded GGGGCC Hexanucleotide Repeat in Noncoding Region of C9ORF72 Causes Chromosome 9p-Linked FTD and ALS. Neuron *72*, 245-256.
Del Bo, R., Tiloca, C., Pensato, V., Corrado, L., Ratti, A., Ticozzi, N., Corti, S., Castellotti, B., Mazzini, L., Sorarù, G.*, et al.* (2011). Novel optineurin mutations in patients with familial and sporadic amyotrophic lateral sclerosis. Journal of Neurology, Neurosurgery & Psychiatry.
Deng, H.X., Bigio, E.H., Zhai, H., Fecto, F., Ajroud, K., Shi, Y., Yan, J.H., Mishra, M., Ajroud-Driss, S., Heller, S.*, et al.* (2011a). Differential Involvement of Optineurin in Amyotrophic Lateral Sclerosis With or Without SOD1 Mutations. Arch Neurol *68*, 1057-1061.
Deng, H.X., Chen, W.J., Hong, S.T., Boycott, K.M., Gorrie, G.H., Siddique, N., Yang, Y., Fecto, F., Shi, Y., Zhai, H.*, et al.* (2011b). Mutations in UBQLN2 cause dominant X-linked juvenile and adult-onset ALS and ALS/dementia. Nature *477*, 211-U113.
Deng, H.X., Zhai, H., Bigio, E.H., Yan, J., Fecto, F., Ajroud, K., Mishra, M., Ajroud-Driss, S., Heller, S., Sufit, R.*, et al.* (2010). FUS-immunoreactive inclusions are a common feature in sporadic and non-SOD1 familial amyotrophic lateral sclerosis. Ann Neurol *67*, 739-748.
Dennissen, F.J.A., Kholod, N., and van Leeuwen, F.W. (2012). The ubiquitin proteasome system in neurodegenerative diseases: Culprit, accomplice or victim? Progress in Neurobiology *96*, 190-207.
Dickson, D., Kouri, N., Murray, M., and Josephs, K. (2011). Neuropathology of Frontotemporal Lobar Degeneration-Tau (FTLD-Tau). Journal of Molecular Neuroscience *45*, 384-389.

Dopper, E.G., Seelaar, H., Chiu, W.Z., de Koning, I., van Minkelen, R., Baker, M.C., Rozemuller, A.J., Rademakers, R., and van Swieten, J.C. (2011). Symmetrical corticobasal syndrome caused by a novel C.314dup progranulin mutation. J Mol Neurosci *45*, 354-358.
Dormann, D., Madl, T., Valori, C.F., Bentmann, E., Tahirovic, S., Abou-Ajram, C., Kremmer, E., Ansorge, O., Mackenzie, I.R., Neumann, M.*, et al.* (2012). Arginine methylation next to the PY-NLS modulates Transportin binding and nuclear import of FUS. EMBO J *31*, 4258-4275.
Dormann, D., Rodde, R., Edbauer, D., Bentmann, E., Fischer, I., Hruscha, A., Than, M.E., Mackenzie, I.R., Capell, A., Schmid, B.*, et al.* (2010). ALS-associated fused in sarcoma (FUS) mutations disrupt Transportin-mediated nuclear import. EMBO J *29*, 2841-2857.
Elden, A.C., Kim, H.-J., Hart, M.P., Chen-Plotkin, A.S., Johnson, B.S., Fang, X., Armakola, M., Geser, F., Greene, R., Lu, M.M.*, et al.* (2010). Ataxin-2 intermediate-length polyglutamine expansions are associated with increased risk for ALS. Nature *466*, 1069-1075.
Fecto, F., Yan, J., Vemula, S.P., Liu, E., Yang, Y., Chen, W., Zheng, J.G., Shi, Y., Siddique, N., Arrat, H.*, et al.* (2011). SQSTM1 Mutations in Familial and Sporadic Amyotrophic Lateral Sclerosis. Arch Neurol *68*, 1440-1446.
Fidani, L., Kalinderi, K., Bostantjopoulou, S., Clarimon, J., Goulas, A., Katsarou, Z., Hardy, J., and Kotsis, A. (2006). Association of the Tau haplotype with Parkinson's disease in the Greek population. Movement disorders : official journal of the Movement Disorder Society *21*, 1036-1039.
Fiesel, F.C., and Kahle, P.J. (2011). TDP-43 and FUS/TLS: cellular functions and implications for neurodegeneration. The FEBS journal *278*, 3550-3568.
Fiesel, F.C., Voigt, A., Weber, S.S., Van den Haute, C., Waldenmaier, A., Gorner, K., Walter, M., Anderson, M.L., Kern, J.V., Rasse, T.M.*, et al.* (2010). Knockdown of transactive response DNA-binding protein (TDP-43) downregulates histone deacetylase 6. EMBO J *29*, 209-221.
Forman, M.S., Farmer, J., Johnson, J.K., Clark, C.M., Arnold, S.E., Coslett, H.B., Chatterjee, A., Hurtig, H.I., Karlawish, J.H., Rosen, H.J.*, et al.* (2006). Frontotemporal dementia: Clinicopathological correlations. Annals of Neurology *59*, 952-962.
Fujii, R., Okabe, S., Urushido, T., Inoue, K., Yoshimura, A., Tachibana, T., Nishikawa, T., Hicks, G.G., and Takumi, T. (2005). The RNA binding protein TLS is translocated to dendritic spines by mGluR5 activation and regulates spine morphology. Current Biology *15*, 587-593.
Fujii, R., and Takumi, T. (2005). TLS facilitates transport of mRNA encoding an actin-stabilizing protein to dendritic spines. J Cell Sci *118*, 5755-5765.
Furukawa, Y., Kaneko, K., Watanabe, S., Yamanaka, K., and Nukina, N. (2011). A Seeding Reaction Recapitulates Intracellular Formation of Sarkosyl-insoluble Transactivation Response Element (TAR) DNA-binding Protein-43 Inclusions. J Biol Chem *286*, 18664-18672.
Gal, J., Zhang, J., Kwinter, D., Zhai, J., Jia, H., Jia, J., and Zhu, H. (2011). Nuclear localization sequence of FUS and induction of stress granules by ALS mutants. Neurobiol Aging *32*, 2323.e2327 - 2323.e2340.
Gass, J., Cannon, A., Mackenzie, I.R., Boeve, B., Baker, M., Adamson, J., Crook, R., Melquist, S., Kuntz, K., Petersen, R.*, et al.* (2006). Mutations in progranulin are a major cause of ubiquitin-positive frontotemporal lobar degeneration. Hum Mol Genet *15*, 2988-3001.
Gass, J., Lee, W.C., Cook, C., Finch, N., Stetler, C., Jansen-West, K., Lewis, J., Link, C.D., Rademakers, R., Nykjaer, A.*, et al.* (2012). Progranulin regulates neuronal outgrowth independent of Sortilin. Molecular neurodegeneration *7*, 33.
Gellera, C., Tiloca, C., Del Bo, R., Corrado, L., Pensato, V., Agostini, J., Cereda, C., Ratti, A., Castellotti, B., Corti, S.*, et al.* (2013). Ubiquilin 2 mutations in Italian patients with amyotrophic lateral sclerosis and frontotemporal dementia. J Neurol Neurosurg Psychiatry *84*, 183-187.
Gendron, T.F., Belzil, V.V., Zhang, Y.J., and Petrucelli, L. (2014). Mechanisms of toxicity in C9FTLD/ALS. Acta Neuropathol.
Ghoshal, N., Dearborn, J.T., Wozniak, D.F., and Cairns, N.J. (2012). Core features of frontotemporal dementia recapitulated in progranulin knockout mice. Neurobiol Dis *45*, 395-408.

Gijselinck, I., Van Langenhove, T., van der Zee, J., Sleegers, K., Philtjens, S., Kleinberger, G., Janssens, J., Bettens, K., Van Cauwenberghe, C., Pereson, S*., et al.* (2012). A C9orf72 promoter repeat expansion in a Flanders-Belgian cohort with disorders of the frontotemporal lobar degeneration-amyotrophic lateral sclerosis spectrum: a gene identification study. The Lancet Neurology *11*, 54-65.
Gitcho, M.A., Bigio, E.H., Mishra, M., Johnson, N., Weintraub, S., Mesulam, M., Rademakers, R., Chakraverty, S., Cruchaga, C., Morris, J.C*., et al.* (2009a). TARDBP 3'-UTR variant in autopsy-confirmed frontotemporal lobar degeneration with TDP-43 proteinopathy. Acta Neuropathol *118*, 633-645.
Gitcho, M.A., Strider, J., Carter, D., Taylor-Reinwald, L., Forman, M.S., Goate, A.M., and Cairns, N.J. (2009b). VCP Mutations Causing Frontotemporal Lobar Degeneration Disrupt Localization of TDP-43 and Induce Cell Death. J Biol Chem *284*, 12384-12398.
Gong, S., Zheng, C., Doughty, M.L., Losos, K., Didkovsky, N., Schambra, U.B., Nowak, N.J., Joyner, A., Leblanc, G., Hatten, M.E*., et al.* (2003). A gene expression atlas of the central nervous system based on bacterial artificial chromosomes. Nature *425*, 917-925.
Gordon, P., Corcia, P., and Meininger, V. (2013). New therapy options for amyotrophic lateral sclerosis. Expert Opin Pharmacother.
Graham, F.L., Smiley, J., Russell, W.C., and Nairn, R. (1977). Characteristics of a Human Cell Line Transformed by DNA from Human Adenovirus Type 5. Journal of General Virology *36*, 59-72.
Gregory, R.I., Yan, K.P., Amuthan, G., Chendrimada, T., Doratotaj, B., Cooch, N., and Shiekhattar, R. (2004). The Microprocessor complex mediates the genesis of microRNAs. Nature *432*, 235-240.
Gunnarsson, L.G., Dahlbom, K., and Strandman, E. (1991). Motor neuron disease and dementia reported among 13 members of a single family. Acta Neurologica Scandinavica *84*, 429-433.
Gurney, M.E., Pu, H., Chiu, A.Y., Dal Canto, M.C., Polchow, C.Y., Alexander, D.D., Caliendo, J., Hentati, A., Kwon, Y.W., Deng, H.X*., et al.* (1994). Motor neuron degeneration in mice that express a human Cu,Zn superoxide dismutase mutation. Science *264*, 1772-1775.
Guyant-Marechal, L., Laquerriere, A., Duyckaerts, C., Dumanchin, C., Bou, J., Dugny, F., Le Ber, I., Frebourg, T., Hannequin, D., and Campion, D. (2006). Valosin-containing protein gene mutations: clinical and neuropathologic features. Neurology *67*, 644-651.
He, C.Z., and Hays, A.P. (2004). Expression of peripherin in ubiquinated inclusions of amyotrophic lateral sclerosis. J Neurol Sci *217*, 47-54.
Heintz, N. (2001). BAC to the future: the use of bac transgenic mice for neuroscience research. Nature reviews Neuroscience *2*, 861-870.
Hicks, G.G., Singh, N., Nashabi, A., Mai, S., Bozek, G., Klewes, L., Arapovic, D., White, E.K., Koury, M.J., Oltz, E.M*., et al.* (2000). Fus deficiency in mice results in defective B-lymphocyte development and activation, high levels of chromosomal instability and perinatal death. Nat Genet *24*, 175-179.
Hirano, M., Quinzii, C.M., Mitsumoto, H., Hays, A.P., Roberts, J.K., Richard, P., and Rowland, L.P. (2011). Senataxin mutations and amyotrophic lateral sclerosis. Amyotroph Lateral Scler *12*, 223-227.
Hodges, J.R., Davies, R.R., Xuereb, J.H., Casey, B., Broe, M., Bak, T.H., Kril, J.J., and Halliday, G.M. (2004). Clinicopathological correlates in frontotemporal dementia. Ann Neurol *56*, 399-406.
Hoell, J.I., Larsson, E., Runge, S., Nusbaum, J.D., Duggimpudi, S., Farazi, T.A., Hafner, M., Borkhardt, A., Sander, C., and Tuschl, T. (2011). RNA targets of wild-type and mutant FET family proteins. Nat Struct Mol Biol *18*, 1428-1431.
Hortobágyi, T., Troakes, C., Nishimura, A., Vance, C., van Swieten, J., Seelaar, H., King, A., Al-Sarraj, S., Rogelj, B., and Shaw, C. (2011). Optineurin inclusions occur in a minority of TDP-43 positive ALS and FTLD-TDP cases and are rarely observed in other neurodegenerative disorders. Acta Neuropathologica *121*, 519-527.
Hsiung, G.-Y.R., DeJesus-Hernandez, M., Feldman, H.H., Sengdy, P., Bouchard-Kerr, P., Dwosh, E., Butler, R., Leung, B., Fok, A., Rutherford, N.J*., et al.* (2012). Clinical and pathological features of familial frontotemporal dementia caused by C9ORF72 mutation on chromosome 9p. Brain *135*, 709-722.

Hu, W.T., Trojanowski, J.Q., and Shaw, L.M. Biomarkers in frontotemporal lobar degenerations--Progress and challenges. Progress in Neurobiology *In Press, Uncorrected Proof*.
Hua, Y., and Zhou, J. (2004). Survival motor neuron protein facilitates assembly of stress granules. FEBS Lett *572*, 69-74.
Huang, C., Zhou, H., Tong, J., Chen, H., Liu, Y.J., Wang, D., Wei, X., and Xia, X.G. (2011). FUS transgenic rats develop the phenotypes of amyotrophic lateral sclerosis and frontotemporal lobar degeneration. PLoS Genet *7*, e1002011.
Huang, E.J., Zhang, J., Geser, F., Trojanowski, J.Q., Strober, J.B., Dickson, D.W., Brown, R.H., Shapiro, B.E., and Lomen-Hoerth, C. (2010). Extensive FUS-Immunoreactive Pathology in Juvenile Amyotrophic Lateral Sclerosis with Basophilic Inclusions. Brain Pathol *20*, 1069-1076.
Hudson, A.J. (1981). Amyotrophic lateral sclerosis and its association with dementia, parkinsonism and other neurological disorders: a review. Brain : a journal of neurology *104*, 217-247.
Iko, Y., Kodama, T.S., Kasai, N., Oyama, T., Morita, E.H., Muto, T., Okumura, M., Fujii, R., Takumi, T., Tate, S.-i*., et al.* (2004). Domain Architectures and Characterization of an RNA-binding Protein, TLS. J Biol Chem *279*, 44834-44840.
Ince, P.G., Highley, J.R., Kirby, J., Wharton, S.B., Takahashi, H., Strong, M.J., and Shaw, P.J. (2011). Molecular pathology and genetic advances in amyotrophic lateral sclerosis: an emerging molecular pathway and the significance of glial pathology. Acta Neuropathol *122*, 657-671.
Isaacs, A.M., Johannsen, P., Holm, I., and Nielsen, J.E. (2011). Frontotemporal dementia caused by CHMP2B mutations. Curr Alzheimer Res *8*, 246-251.
Ito, D., Seki, M., Tsunoda, Y., Uchiyama, H., and Suzuki, N. (2011). Nuclear transport impairment of amyotrophic lateral sclerosis-linked mutations in FUS/TLS. Ann Neurol *69*, 152 - 162.
Janezic, S., Threlfell, S., Dodson, P.D., Dowie, M.J., Taylor, T.N., Potgieter, D., Parkkinen, L., Senior, S.L., Anwar, S., Ryan, B*., et al.* (2013). Deficits in dopaminergic transmission precede neuron loss and dysfunction in a new Parkinson model. Proc Natl Acad Sci U S A *110*, E4016-4025.
Jiang, H., Mankodi, A., Swanson, M.S., Moxley, R.T., and Thornton, C.A. (2004). Myotonic dystrophy type 1 is associated with nuclear foci of mutant RNA, sequestration of muscleblind proteins and deregulated alternative splicing in neurons. Hum Mol Genet *13*, 3079-3088.
Johnson, B.S., Snead, D., Lee, J.J., McCaffery, J.M., Shorter, J., and Gitler, A.D. (2009). TDP-43 Is Intrinsically Aggregation-prone, and Amyotrophic Lateral Sclerosis-linked Mutations Accelerate Aggregation and Increase Toxicity. J Biol Chem *284*, 20329-20339.
Johnson, J.O., Mandrioli, J., Benatar, M., Abramzon, Y., Van Deerlin, V.M., Trojanowski, J.Q., Gibbs, J.R., Brunetti, M., Gronka, S., Wuu, J*., et al.* (2010). Exome Sequencing Reveals VCP Mutations as a Cause of Familial ALS. Neuron *68*, 857-864.
Josephs, K., Hodges, J., Snowden, J., Mackenzie, I., Neumann, M., Mann, D., and Dickson, D. (2011). Neuropathological background of phenotypical variability in frontotemporal dementia. Acta Neuropathologica *122*, 137-153.
Ju, J.-S., Fuentealba, R.A., Miller, S.E., Jackson, E., Piwnica-Worms, D., Baloh, R.H., and Weihl, C.C. (2009). Valosin-containing protein (VCP) is required for autophagy and is disrupted in VCP disease. The Journal of Cell Biology *187*, 875-888.
Ju, S., Tardiff, D.F., Han, H., Divya, K., Zhong, Q., Maquat, L.E., Bosco, D.A., Hayward, L.J., Brown, R.H., Jr., Lindquist, S*., et al.* (2011). A Yeast Model of FUS/TLS-Dependent Cytotoxicity. PLoS Biol *9*, e1001052.
Kabashi, E., Bercier, V., Lissouba, A., Liao, M., Brustein, E., Rouleau, G.A., and Drapeau, P. (2011). *FUS* and *TARDBP* but Not *SOD1* Interact in Genetic Models of Amyotrophic Lateral Sclerosis. PLoS Genet *7*, e1002214.
Kabashi, E., Valdmanis, P.N., Dion, P., Spiegelman, D., McConkey, B.J., Velde, C.V., Bouchard, J.P., Lacomblez, L., Pochigaeva, K., Salachas, F*., et al.* (2008). TARDBP mutations in individuals with sporadic and familial amyotrophic lateral sclerosis. Nature Genet *40*, 572-574.

Kawashima, T., Kikuchi, H., Takita, M., Doh-ura, K., Ogomori, K., Oda, M., and Iwaki, T. (1998). Skein-like inclusions in the neostriatum from a case of amyotrophic lateral sclerosis with dementia. Acta Neuropathol *96*, 541-545.
Kertesz, A., Blair, M., McMonagle, P., and Munoz, D.G. (2007). The diagnosis and course of frontotemporal dementia. Alzheimer Dis Assoc Dis *21*, 155-163.
Kiernan, M.C., Vucic, S., Cheah, B.C., Turner, M.R., Eisen, A., Hardiman, O., Burrell, J.R., and Zoing, M.C. (2011). Amyotrophic lateral sclerosis. Lancet *377*, 942-955.
Kim, C., Choi, H., Jung, E.S., Lee, W., Oh, S., Jeon, N.L., and Mook-Jung, I. (2012). HDAC6 Inhibitor Blocks Amyloid Beta-Induced Impairment of Mitochondrial Transport in Hippocampal Neurons. PLoS ONE *7*, e42983.
King, A., Maekawa, S., Bodi, I., Troakes, C., and Al-Sarraj, S. (2011). Ubiquitinated, p62 immunopositive cerebellar cortical neuronal inclusions are evident across the spectrum of TDP-43 proteinopathies but are only rarely additionally immunopositive for phosphorylation-dependent TDP-43. Neuropathology *31*, 239-249.
Kino, Y., Washizu, C., Aquilanti, E., Okuno, M., Kurosawa, M., Yamada, M., Doi, H., and Nukina, N. (2011). Intracellular localization and splicing regulation of FUS/TLS are variably affected by amyotrophic lateral sclerosis-linked mutations. Nucleic Acids Res *39*, 2781-2798.
Ko, H.S., Uehara, T., Tsuruma, K., and Nomura, Y. (2004). Ubiquilin interacts with ubiquitylated proteins and proteasome through its ubiquitin-associated and ubiquitin-like domains. FEBS Lett *566*, 110-114.
Komatsu, M., Waguri, S., Chiba, T., Murata, S., Iwata, J., Tanida, I., Ueno, T., Koike, M., Uchiyama, Y., Kominami, E*., et al.* (2006). Loss of autophagy in the central nervous system causes neurodegeneration in mice. Nature *441*, 880-884.
Komatsu, M., Waguri, S., Koike, M., Sou, Y.S., Ueno, T., Hara, T., Mizushima, N., Iwata, J., Ezaki, J., Murata, S*., et al.* (2007). Homeostatic levels of p62 control cytoplasmic inclusion body formation in autophagy-deficient mice. Cell *131*, 1149-1163.
Korolchuk, V.I., Menzies, F.M., and Rubinsztein, D.C. (2010). Mechanisms of cross-talk between the ubiquitin-proteasome and autophagy-lysosome systems. FEBS Lett *584*, 1393-1398.
Kovacs, G.G., Murrell, J.R., Horvath, S., Haraszti, L., Majtenyi, K., Molnar, M.J., Budka, H., Ghetti, B., and Spina, S. (2009). TARDBP Variation Associated with Frontotemporal Dementia, Supranuclear Gaze Palsy, and Chorea. Mov Disord *24*, 1843-1847.
Kuroda, M., Sok, J., Webb, L., Baechtold, H., Urano, F., Yin, Y., Chung, P., de Rooij, D.G., Akhmedov, A., Ashley, T*., et al.* (2000). Male sterility and enhanced radiation sensitivity in TLS(-/-) mice. EMBO J *19*, 453-462.
Kwiatkowski, T., Bosco, D., LeClerc, A., Tamrazian, E., Vanderburg, C., Russ, C., Davis, A., Gilchrist, J., Kasarskis, E., and Munsat, T. (2009a). Mutations in the FUS/TLS Gene on Chromosome 16 Cause Familial Amyotrophic Lateral Sclerosis. Science *323*, 1205 - 1208.
Kwiatkowski, T.J., Bosco, D.A., LeClerc, A.L., Tamrazian, E., Vanderburg, C.R., Russ, C., Davis, A., Gilchrist, J., Kasarskis, E.J., Munsat, T*., et al.* (2009b). Mutations in the FUS/TLS Gene on Chromosome 16 Cause Familial Amyotrophic Lateral Sclerosis. Science *323*, 1205-1208.
Lagier-Tourenne, C., Polymenidou, M., and Cleveland, D.W. (2010). TDP-43 and FUS/TLS: emerging roles in RNA processing and neurodegeneration. Hum Mol Genet *19*, R46-R64.
Lagier-Tourenne, C., Polymenidou, M., Hutt, K.R., Vu, A.Q., Baughn, M., Huelga, S.C., Clutario, K.M., Ling, S.C., Liang, T.Y., Mazur, C*., et al.* (2012). Divergent roles of ALS-linked proteins FUS/TLS and TDP-43 intersect in processing long pre-mRNAs. Nat Neurosci *15*, 1488-1497.
Lai, S.L., Abramzon, Y., Schymick, J.C., Stephan, D.A., Dunckley, T., Dillman, A., Cookson, M., Calvo, A., Battistini, S., Giannini, F*., et al.* (2011). FUS mutations in sporadic amyotrophic lateral sclerosis. Neurobiol Aging *32*.
Lander, E.S., Linton, L.M., Birren, B., Nusbaum, C., Zody, M.C., Baldwin, J., Devon, K., Dewar, K., Doyle, M., FitzHugh, W*., et al.* (2001). Initial sequencing and analysis of the human genome. Nature *409*, 860-921.

Lanson, N., and Pandey, U. (2012). FUS-related proteinopathies: Lessons from animal models. Brain Res *1462*, 44 - 60.
Lattante, S., Le Ber, I., Camuzat, A., Pariente, J., Brice, A., Kabashi, E., French Research Network on, F.T.D., and Ftd, A.L.S. (2013). Screening UBQLN-2 in French frontotemporal lobar degeneration and frontotemporal lobar degeneration-amyotrophic lateral sclerosis patients. Neurobiol Aging *34*, 2078 e2075-2076.
Lee, B.J., Cansizoglu, A.E., Suel, K.E., Louis, T.H., Zhang, Z., and Chook, Y.M. (2006). Rules for nuclear localization sequence recognition by karyopherin beta 2. Cell *126*, 543-558.
Lee, J.-Y., Koga, H., Kawaguchi, Y., Tang, W., Wong, E., Gao, Y.-S., Pandey, U.B., Kaushik, S., Tresse, E., Lu, J.*, et al.* (2010). HDAC6 controls autophagosome maturation essential for ubiquitin-selective quality-control autophagy. EMBO J *29*, 969-980.
Lee, Y.B., Chen, H.J., Peres, J.N., Gomez-Deza, J., Attig, J., Stalekar, M., Troakes, C., Nishimura, A.L., Scotter, E.L., Vance, C.*, et al.* (2013). Hexanucleotide repeats in ALS/FTD form length-dependent RNA foci, sequester RNA binding proteins, and are neurotoxic. Cell reports *5*, 1178-1186.
Lefebvre, S., Burglen, L., Reboullet, S., Clermont, O., Burlet, P., Viollet, L., Benichou, B., Cruaud, C., Millasseau, P., Zeviani, M.*, et al.* (1995). IDENTIFICATION AND CHARACTERIZATION OF A SPINAL MUSCULAR ATROPHY-DETERMINING GENE. Cell *80*, 155-165.
Lerga, A., Hallier, M., Delva, L., Orvain, C., Gallais, I., Marie, J., and Moreau-Gachelin, F. (2001). Identification of an RNA binding specificity for the potential splicing factor TLS. J Biol Chem *276*, 6807-6816.
Levine, T.P., Daniels, R.D., Gatta, A.T., Wong, L.H., and Hayes, M.J. (2013). The product of C9orf72, a gene strongly implicated in neurodegeneration, is structurally related to DENN Rab-GEFs. Bioinformatics *29*, 499-503.
Li, S., Iakoucheva, L.M., Mooney, S.D., and Radivojac, P. (2010). Loss of post-translational modification sites in disease. Pacific Symposium on Biocomputing Pacific Symposium on Biocomputing, 337-347.
Li, T., Huang, S., Jiang, W.Z., Wright, D., Spalding, M.H., Weeks, D.P., and Yang, B. (2011). TAL nucleases (TALNs): hybrid proteins composed of TAL effectors and FokI DNA-cleavage domain. Nucleic Acids Res *39*, 359-372.
Li, Y., Liu, W., Oo, T.F., Wang, L., Tang, Y., Jackson-Lewis, V., Zhou, C., Geghman, K., Bogdanov, M., Przedborski, S.*, et al.* (2009). Mutant LRRK2(R1441G) BAC transgenic mice recapitulate cardinal features of Parkinson's disease. Nat Neurosci *12*, 826-828.
Liu-Yesucevitz, L., Bilgutay, A., Zhang, Y.-J., Vanderwyde, T., Citro, A., Mehta, T., Zaarur, N., McKee, A., Bowser, R., Sherman, M.*, et al.* (2010). Tar DNA Binding Protein-43 (TDP-43) Associates with Stress Granules: Analysis of Cultured Cells and Pathological Brain Tissue. PLoS ONE *5*, e13250.
Livet, J., Weissman, T.A., Kang, H., Draft, R.W., Lu, J., Bennis, R.A., Sanes, J.R., and Lichtman, J.W. (2007). Transgenic strategies for combinatorial expression of fluorescent proteins in the nervous system. Nature *450*, 56-62.
Lomen-Hoerth, C., Anderson, T., and Miller, B. (2002). The overlap of amyotrophic lateral sclerosis and frontotemporal dementia. Neurology *59*, 1077-1079.
Lufino, M.M.P., Silva, A.M., Németh, A.H., Alegre-Abarrategui, J., Russell, A.J., and Wade-Martins, R. (2013). A GAA repeat expansion reporter model of Friedreich's ataxia recapitulates the genomic context and allows rapid screening of therapeutic compounds. Hum Mol Genet.
Mackenzie, I., Ansorge, O., Strong, M., Bilbao, J., Zinman, L., Ang, L.-C., Baker, M., Stewart, H., Eisen, A., Rademakers, R.*, et al.* (2011a). Pathological heterogeneity in amyotrophic lateral sclerosis with FUS mutations: two distinct patterns correlating with disease severity and mutation. Acta Neuropathologica *122*, 87-98.
Mackenzie, I., Munoz, D., Kusaka, H., Yokota, O., Ishihara, K., Roeber, S., Kretzschmar, H., Cairns, N., and Neumann, M. (2011b). Distinct pathological subtypes of FTLD-FUS. Acta Neuropathol *121*, 207 - 218.

Mackenzie, I., Neumann, M., Bigio, E., Cairns, N., Alafuzoff, I., Kril, J., Kovacs, G., Ghetti, B., Halliday, G., Holm, I.*, et al.* (2009). Nomenclature for neuropathologic subtypes of frontotemporal lobar degeneration: consensus recommendations. Acta Neuropathologica *117*, 15-18.
Mackenzie, I.R., Rademakers, R., and Neumann, M. (2010). TDP-43 and FUS in amyotrophic lateral sclerosis and frontotemporal dementia. Lancet Neurol *9*, 995-1007.
Mackenzie, I.R.A., Foti, D., Woulfe, J., and Hurwitz, T.A. (2008). Atypical frontotemporal lobar degeneration with ubiquitin-positive, TDP-43-negative neuronal inclusions. Brain *131*, 1282-1293.
Mackenzie, I.R.A., and Rademakers, R. (2008). The role of transactive response DNA-binding protein-43 in amyotrophic lateral sclerosis and frontotemporal dementia. Curr Opin Neurol *21*, 693-700.
Mah, A.L., Perry, G., Smith, M.A., and Monteiro, M.J. (2000). Identification of ubiquilin, a novel presenilin interactor that increases presenilin protein accumulation. J Cell Biol *151*, 847-862.
Majounie, E., Renton, A.E., Mok, K., Dopper, E.G.P., Waite, A., Rollinson, S., Chiò, A., Restagno, G., Nicolaou, N., Simon-Sanchez, J.*, et al.* (2012). Frequency of the C9orf72 hexanucleotide repeat expansion in patients with amyotrophic lateral sclerosis and frontotemporal dementia: a cross-sectional study. The Lancet Neurology *11*, 323-330.
Mann, D.M., Rollinson, S., Robinson, A., Bennion Callister, J., Thompson, J.C., Snowden, J.S., Gendron, T., Petrucelli, L., Masuda-Suzukake, M., Hasegawa, M.*, et al.* (2013). Dipeptide repeat proteins are present in the p62 positive inclusions in patients with frontotemporal lobar degeneration and motor neurone disease associated with expansions in C9ORF72. Acta neuropathologica communications *1*, 68.
Maruyama, H., Morino, H., Ito, H., Izumi, Y., Kato, H., Watanabe, Y., Kinoshita, Y., Kamada, M., Nodera, H., Suzuki, H.*, et al.* (2010). Mutations of optineurin in amyotrophic lateral sclerosis. Nature *465*, 223-226.
Matsumoto, S., Goto, S., Kusaka, H., Imai, T., Murakami, N., Hashizume, Y., Okazaki, H., and Hirano, A. (1993). Ubiquitin-positive inclusion in anterior horn cells in subgroups of motor neuron diseases: a comparative study of adult-onset amyotrophic lateral sclerosis, juvenile amyotrophic lateral sclerosis and Werdnig-Hoffmann disease. J Neurol Sci *115*, 208-213.
McKhann, G.M., Albert, M.S., Grossman, M., Miller, B., Dickson, D., and Trojanowski, J.Q. (2001). Clinical and pathological diagnosis of Frontotemporal Dementia - Report of the work group on Frontotemporal Dementia and Pick's disease. Arch Neurol *58*, 1803-1809.
McKhann Gm, A.M.S.G.M.M.B.D.D.T.J.Q. (2001). Clinical and pathological diagnosis of frontotemporal dementia: Report of the work group on frontotemporal dementia and pick's disease. Arch Neurol *58*, 1803-1809.
McLaughlin, R.L., Kenna, K.P., Vajda, A., Byrne, S., Bradley, D.G., and Hardiman, O. (2014). UBQLN2 mutations are not a frequent cause of amyotrophic lateral sclerosis in Ireland. Neurobiol Aging *35*, 267 e269-211.
Melià, M.J., Kubota, A., Ortolano, S., Vílchez, J.J., Gámez, J., Tanji, K., Bonilla, E., Palenzuela, L., Fernández-Cadenas, I., Přistoupilová, A.*, et al.* (2013). Limb-girdle muscular dystrophy 1F is caused by a microdeletion in the transportin 3 gene. Brain *136*, 1508-1517.
Meyer, H., Bug, M., and Bremer, S. (2012). Emerging functions of the VCP/p97 AAA-ATPase in the ubiquitin system. Nat Cell Biol *14*, 117-123.
Michel, G. (1993). Tau protein and the neurofibrillary pathology of Alzheimer's disease. Trends in Neurosciences *16*, 460-465.
Miller, J.W., Urbinati, C.R., Teng-umnuay, P., Stenberg, M.G., Byrne, B.J., Thornton, C.A., and Swanson, M.S. (2000). Recruitment of human muscleblind proteins to (CUG)(n) expansions associated with myotonic dystrophy. Embo J *19*, 4439-4448.
Mitchell, J.C., McGoldrick, P., Vance, C., Hortobagyi, T., Sreedharan, J., Rogelj, B., Tudor, E.L., Smith, B.N., Klasen, C., Miller, C.C.*, et al.* (2013). Overexpression of human wild-type FUS causes progressive motor neuron degeneration in an age- and dose-dependent fashion. Acta Neuropathol *125*, 273-288.
Mitchell, J.D., and Borasio, G.D. (2007). Amyotrophic lateral sclerosis. Lancet *369*, 2031-2041.

Mizuno, Y., Amari, M., Takatama, M., Aizawa, H., Mihara, B., and Okamoto, K. (2006). Immunoreactivities of p62, an ubiqutin-binding protein, in the spinal anterior horn cells of patients with amyotrophic lateral sclerosis. Journal of the Neurological Sciences *249*, 13-18.
Moisse, K., Volkening, K., Leystra-Lantz, C., Welch, I., Hill, T., and Strong, M.J. (2009). Divergent patterns of cytosolic TDP-43 and neuronal progranulin expression following axotomy: Implications for TDP-43 in the physiological response to neuronal injury. Brain Research *1249*, 202-211.
Morlando, M., Dini Modigliani, S., Torrelli, G., Rosa, A., Di Carlo, V., Caffarelli, E., and Bozzoni, I. (2012). FUS stimulates microRNA biogenesis by facilitating co-transcriptional Drosha recruitment. EMBO J *31*, 4502-4510.
Morohoshi, F., Ootsuka, Y., Arai, K., Ichikawa, H., Mitani, S., Munakata, N., and Ohki, M. (1998). Genomic structure of the human RBP56/hTAFII68 and FUS/TLS genes. Gene *221*, 191-198.
Moscat, J., and Diaz-Meco, M.T. (2009). p62 at the Crossroads of Autophagy, Apoptosis, and Cancer. Cell *137*, 1001-1004.
Murakami, T., Yang, S., Xie, L., Kawano, T., Fu, D., Mukai, A., Bohm, C., Chen, F., Robertson, J., and Suzuki, H. (2012). ALS mutations in FUS cause neuronal dysfunction and death in Caenorhabditis elegans by a dominant gain-of-function mechanism. Hum Mol Genet *21*, 1 - 9.
Muyrers, J.P.P., Zhang, Y., Testa, G., and Stewart, A.F. (1999). Rapid modification of bacterial artificial chromosomes by ET-recombination. Nucleic Acids Research *27*, 1555-1557.
Nagy, A. (2000). Cre recombinase: The universal reagent for genome tailoring. genesis *26*, 99-109.
Nakashima-Yasuda, H., Uryu, K., Robinson, J., Xie, S.X., Hurtig, H., Duda, J.E., Arnold, S.E., Siderowf, A., Grossman, M., Leverenz, J.B.*, et al.* (2007). Co-morbidity of TDP-43 proteinopathy in Lewy body related diseases. Acta Neuropathol *114*, 221-229.
Nalbandian, A., Llewellyn, K.J., Badadani, M., Yin, H.Z., Nguyen, C., Katheria, V., Watts, G., Mukherjee, J., Vesa, J., Caiozzo, V.*, et al.* (2013). A progressive translational mouse model of human valosin-containing protein disease: the VCP(R155H/+) mouse. Muscle & nerve *47*, 260-270.
Neary, D., Snowden, J., and Mann, D. (2005). Frontotemporal dementia. The Lancet Neurology *4*, 771-780.
Neumann, M., Bentmann, E., Dormann, D., Jawaid, A., DeJesus-Hernandez, M., Ansorge, O., Roeber, S., Kretzschmar, H.A., Munoz, D.G., Kusaka, H.*, et al.* (2011). FET proteins TAF15 and EWS are selective markers that distinguish FTLD with FUS pathology from amyotrophic lateral sclerosis with FUS mutations. Brain *134*, 2595-2609.
Neumann, M., Mackenzie, I.R., Cairns, N.J., Boyer, P.J., Markesbery, W.R., Smith, C.D., Taylor, J.P., Kretzschmar, H.A., Kimonis, V.E., and Forman, M.S. (2007). TDP-43 in the ubiquitin pathology of frontotemporal dementia with VCP gene mutations. J Neuropathol Exp Neurol *66*, 152-157.
Neumann, M., Rademakers, R., Roeber, S., Baker, M., Kretzschmar, H.A., and Mackenzie, I.R.A. (2009). A new subtype of frontotemporal lobar degeneration with FUS pathology. Brain *132*, 2922-2931.
Neumann, M., Sampathu, D.M., Kwong, L.K., Truax, A.C., Micsenyi, M.C., Chou, T.T., Bruce, J., Schuck, T., Grossman, M., Clark, C.M.*, et al.* (2006). Ubiquitinated TDP-43 in frontotemporal lobar degeneration and amyotrophic lateral sclerosis. Science *314*, 130-133.
Neumann, M., Valori, C.F., Ansorge, O., Kretzschmar, H.A., Munoz, D.G., Kusaka, H., Yokota, O., Ishihara, K., Ang, L.C., Bilbao, J.M.*, et al.* (2012). Transportin 1 accumulates specifically with FET proteins but no other transportin cargos in FTLD-FUS and is absent in FUS inclusions in ALS with FUS mutations. Acta Neuropathol *124*, 705-716.
Pandey, U.B., Nie, Z., Batlevi, Y., McCray, B.A., Ritson, G.P., Nedelsky, N.B., Schwartz, S.L., DiProspero, N.A., Knight, M.A., Schuldiner, O.*, et al.* (2007). HDAC6 rescues neurodegeneration and provides an essential link between autophagy and the UPS. Nature *447*, 859-863.
Parker, S.J., Meyerowitz, J., James, J.L., Liddell, J.R., Crouch, P.J., Kanninen, K.M., and White, A.R. (2012). Endogenous TDP-43 localized to stress granules can subsequently form protein aggregates. Neurochemistry International *60*, 415-424.

Pasinelli, P., and Brown, R.H. (2006). Molecular biology of amyotrophic lateral sclerosis: insights from genetics. Nat Rev Neurosci *7*, 710-723.
Pickering-Brown, S.M., Baker, M., Gass, J., Boeve, B.F., Loy, C.T., Brooks, W.S., Mackenzie, I.R., Martins, R.N., Kwok, J.B., Halliday, G.M.*, et al.* (2006). Mutations in progranulin explain atypical phenotypes with variants in MAPT. Brain *129*, 3124-3126.
Polymenidou, M., Lagier-Tourenne, C., Hutt, K.R., Huelga, S.C., Moran, J., Liang, T.Y., Ling, S.-C., Sun, E., Wancewicz, E., Mazur, C.*, et al.* (2011). Long pre-mRNA depletion and RNA missplicing contribute to neuronal vulnerability from loss of TDP-43. Nat Neurosci *14*, 459-468.
Prasad, D.D., Ouchida, M., Lee, L., Rao, V.N., and Reddy, E.S. (1994). TLS/FUS fusion domain of TLS/FUS-erg chimeric protein resulting from the t(16;21) chromosomal translocation in human myeloid leukemia functions as a transcriptional activation domain. Oncogene *9*, 3717-3729.
Rabbitts, T.H., Forster, A., Larson, R., and Nathan, P. (1993). Fusion of the dominant negative transcription regulator CHOP with a novel gene FUS by translocation t(12;16) in malignant liposarcoma. Nat Genet *4*, 175-180.
Ratovitski, T., Chighladze, E., Arbez, N., Boronina, T., Herbrich, S., Cole, R.N., and Ross, C.A. (2012). Huntingtin protein interactions altered by polyglutamine expansion as determined by quantitative proteomic analysis. Cell Cycle *11*, 2006-2021.
Renton, A.E., Chio, A., and Traynor, B.J. (2014). State of play in amyotrophic lateral sclerosis genetics. Nat Neurosci *17*, 17-23.
Renton, A.E., Majounie, E., Waite, A., Simon-Sanchez, J., Rollinson, S., Gibbs, J.R., Schymick, J.C., Laaksovirta, H., van Swieten, J.C., Myllykangas, L.*, et al.* (2011). A Hexanucleotide Repeat Expansion in C9ORF72 Is the Cause of Chromosome 9p21-Linked ALS-FTD. Neuron *72*, 257-268.
Renton Alan, E., Majounie, E., Waite, A., Simon-Sanchez, J., Rollinson, S., Gibbs, J., Schymick Jennifer, C., Laaksovirta, H., van Swieten John, C., and Myllykangas, L. (2011). A Hexanucleotide Repeat Expansion in C9ORF72 Is the Cause of Chromosome 9p21-Linked ALS-FTD. Neuron *72*, 257 - 268.
Ringholz, G.M., Appel, S.H., Bradshaw, M., Cooke, N.A., Mosnik, D.M., and Schulz, P.E. (2005). Prevalence and patterns of cognitive impairment in sporadic ALS. Neurology *65*, 586-590.
Ritson, G.P., Custer, S.K., Freibaum, B.D., Guinto, J.B., Geffel, D., Moore, J., Tang, W., Winton, M.J., Neumann, M., Trojanowski, J.Q.*, et al.* (2010). TDP-43 Mediates Degeneration in a Novel Drosophila Model of Disease Caused by Mutations in VCP/p97. The Journal of Neuroscience *30*, 7729-7739.
Roberson, E.D. (2012). Mouse models of frontotemporal dementia. Ann Neurol *72*, 837-849.
Rohrer, J.D., and Warren, J.D. (2011). Phenotypic signatures of genetic frontotemporal dementia. Curr Opin Neurol *24*, 542-549.
Rosen, D.R., Siddique, T., Patterson, D., Figlewicz, D.A., Sapp, P., Hentati, A., Donaldson, D., Goto, J., Oregan, J.P., Deng, H.X.*, et al.* (1993). MUTATIONS IN CU/ZN SUPEROXIDE-DISMUTASE GENE ARE ASSOCIATED WITH FAMILIAL AMYOTROPHIC-LATERAL-SCLEROSIS. Nature *362*, 59-62.
Rosso, S.M., Kaat, L.D., Baks, T., Joosse, M., de Koning, I., Pijnenburg, Y., de Jong, D., Dooijes, D., Kamphorst, W., Ravid, R.*, et al.* (2003). Frontotemporal dementia in The Netherlands: patient characteristics and prevalence estimates from a population-based study. Brain *126*, 2016-2022.
Rothenberg, C., Srinivasan, D., Mah, L., Kaushik, S., Peterhoff, C.M., Ugolino, J., Fang, S., Cuervo, A.M., Nixon, R.A., and Monteiro, M.J. (2010). Ubiquilin functions in autophagy and is degraded by chaperone-mediated autophagy. Hum Mol Genet *19*, 3219-3232.
Rubino, E., Rainero, I., Chiò, A., Rogaeva, E., Galimberti, D., Fenoglio, P., Grinberg, Y., Isaia, G., Calvo, A., Gentile, S.*, et al.* (2012). SQSTM1 mutations in frontotemporal lobar degeneration and amyotrophic lateral sclerosis. Neurology.
Rubinsztein, D.C. (2006). The roles of intracellular protein-degradation pathways in neurodegeneration. Nature *443*, 780-786.
Sasaki, S., and Maruyama, S. (1994). Immunocytochemical and ultrastructural studies of the motor cortex in amyotrophic lateral sclerosis. Acta Neuropathol *87*, 578-585.
Sauer, B., and Henderson, N. (1988). Site-specific DNA recombination in mammalian cells by the Cre recombinase of bacteriophage P1. Proc Natl Acad Sci U S A *85*, 5166-5170.

Scaramuzzino, C., Monaghan, J., Milioto, C., Lanson, N.A., Jr., Maltare, A., Aggarwal, T., Casci, I., Fackelmayer, F.O., Pennuto, M., and Pandey, U.B. (2013). Protein Arginine Methyltransferase 1 and 8 Interact with FUS to Modify Its Sub-Cellular Distribution and Toxicity <italic>In Vitro</italic> and <italic>In Vivo</italic>. PLoS ONE *8*, e61576.
Schymick, J.C., Yang, Y., Andersen, P.M., Vonsattel, J.P., Greenway, M., Momeni, P., Elder, J., Chiò, A., Restagno, G., Robberecht, W*., et al.* (2007). Progranulin mutations and amyotrophic lateral sclerosis or amyotrophic lateral sclerosis–frontotemporal dementia phenotypes. Journal of Neurology, Neurosurgery & Psychiatry *78*, 754-756.
Seelaar, H., Klijnsma, K., de Koning, I., van der Lugt, A., Chiu, W., Azmani, A., Rozemuller, A., and van Swieten, J. (2010). Frequency of ubiquitin and FUS-positive, TDP-43-negative frontotemporal lobar degeneration. J Neurol *257*, 747-753.
Seelaar, H., Rohrer, J.D., Pijnenburg, Y.A.L., Fox, N.C., and van Swieten, J.C. (2011). Clinical, genetic and pathological heterogeneity of frontotemporal dementia: a review. J Neurol Neurosurg Psychiatry *82*, 476-486.
Seltman, R., and Matthews, B. (2012). Frontotemporal Lobar Degeneration. CNS Drugs *26*, 841-870.
Sephton, C.F., Cenik, C., Kucukural, A., Dammer, E.B., Cenik, B., Han, Y., Dewey, C.M., Roth, F.P., Herz, J., Peng, J*., et al.* (2011). Identification of neuronal RNA targets of TDP-43-containing ribonucleoprotein complexes. J Biol Chem *286*, 1204-1215.
Shaner, N.C., Campbell, R.E., Steinbach, P.A., Giepmans, B.N.G., Palmer, A.E., and Tsien, R.Y. (2004). Improved monomeric red, orange and yellow fluorescent proteins derived from Discosoma sp. red fluorescent protein. Nat Biotech *22*, 1567-1572.
Shaw, G., Morse, S., Ararat, M., and Graham, F.L. (2002). Preferential transformation of human neuronal cells by human adenoviruses and the origin of HEK 293 cells. FASEB journal : official publication of the Federation of American Societies for Experimental Biology *16*, 869-871.
Shelkovnikova, T.A., Peters, O.M., Deykin, A.V., Connor-Robson, N., Robinson, H., Ustyugov, A.A., Bachurin, S.O., Ermolkevich, T.G., Goldman, I.L., Sadchikova, E.R*., et al.* (2013). Fused in Sarcoma (FUS) Protein Lacking Nuclear Localization Signal (NLS) and Major RNA Binding Motifs Triggers Proteinopathy and Severe Motor Phenotype in Transgenic Mice. J Biol Chem *288*, 25266-25274.
Shen, Y., Lee, H.-Y., Rawson, J., Ojha, S., Babbitt, P., Fu, Y.-H., and Ptáček, L.J. (2011). Mutations in PNKD causing paroxysmal dyskinesia alters protein cleavage and stability. Hum Mol Genet *20*, 2322-2332.
Shizuya, H., Birren, B., Kim, U.J., Mancino, V., Slepak, T., Tachiiri, Y., and Simon, M. (1992). Cloning and stable maintenance of 300-kilobase-pair fragments of human DNA in Escherichia coli using an F-factor-based vector. Proc Natl Acad Sci U S A *89*, 8794-8797.
Sieben, A., Van Langenhove, T., Engelborghs, S., Martin, J.J., Boon, P., Cras, P., De Deyn, P.P., Santens, P., Van Broeckhoven, C., and Cruts, M. (2012). The genetics and neuropathology of frontotemporal lobar degeneration. Acta Neuropathol *124*, 353-372.
Simón-Sánchez, J., Dopper, E.G.P., Cohn-Hokke, P.E., Hukema, R.K., Nicolaou, N., Seelaar, H., de Graaf, J.R.A., de Koning, I., van Schoor, N.M., Deeg, D.J.H*., et al.* (2012). The clinical and pathological phenotype of C9orf72 hexanucleotide repeat expansions. Brain.
Snowden, J., Hu, Q., Rollinson, S., Halliwell, N., Robinson, A., Davidson, Y., Momeni, P., Baborie, A., Griffiths, T., Jaros, E*., et al.* (2011). The most common type of FTLD-FUS (aFTLD-U) is associated with a distinct clinical form of frontotemporal dementia but is not related to mutations in the FUS gene. Acta Neuropathologica *122*, 99-110.
Snowden, J., Neary, D., and Mann, D. (2007). Frontotemporal lobar degeneration: clinical and pathological relationships. Acta Neuropathologica *114*, 31-38.
Snowden, J.S., Pickering-Brown, S.M., Mackenzie, I.R., Richardson, A.M., Varma, A., Neary, D., and Mann, D.M. (2006). Progranulin gene mutations associated with frontotemporal dementia and progressive non-fluent aphasia. Brain *129*, 3091-3102.

Snowden, J.S., Rollinson, S., Thompson, J.C., Harris, J.M., Stopford, C.L., Richardson, A.M., Jones, M., Gerhard, A., Davidson, Y.S., Robinson, A.*, et al.* (2012). Distinct clinical and pathological characteristics of frontotemporal dementia associated with C9ORF72 mutations. Brain *135*, 693-708.
Stanford, P.M., Brooks, W.S., Teber, E.T., Hallupp, M., McLean, C., Halliday, G.M., Martins, R.N., Kwok, J.B.J., and Schofield, P.R. (2004). Frequency of tau mutations in familial and sporadic frontotemporal dementia and other tauopathies. J Neurol *251*, 1098-1104.
Subramaniam, J.R., Lyons, W.E., Liu, J., Bartnikas, T.B., Rothstein, J., Price, D.L., Cleveland, D.W., Gitlin, J.D., and Wong, P.C. (2002). Mutant SOD1 causes motor neuron disease independent of copper chaperone-mediated copper loading. Nat Neurosci *5*, 301-307.
Sun, Z., Diaz, Z., Fang, X., Hart, M.P., Chesi, A., Shorter, J., and Gitler, A.D. (2011). Molecular Determinants and Genetic Modifiers of Aggregation and Toxicity for the ALS Disease Protein FUS/TLS. PLoS Biol *9*, e1000614.
Swarup, V., Phaneuf, D., Bareil, C., Robertson, J., Rouleau, G.A., Kriz, J., and Julien, J.-P. (2011). Pathological hallmarks of amyotrophic lateral sclerosis/frontotemporal lobar degeneration in transgenic mice produced with TDP-43 genomic fragments. Brain *134*, 2610-2626.
Synofzik, M., Born, C., Rominger, A., Lummel, N., Schols, L., Biskup, S., Schule, C., Grasshoff, U., Klopstock, T., and Adamczyk, C. (2013). Targeted high-throughput sequencing identifies a TARDBP mutation as a cause of early-onset FTD without motor neuron disease. Neurobiol Aging.
Synofzik, M., Maetzler, W., Grehl, T., Prudlo, J., Vom Hagen, J.M., Haack, T., Rebassoo, P., Munz, M., Schols, L., and Biskup, S. (2012). Screening in ALS and FTD patients reveals 3 novel UBQLN2 mutations outside the PXX domain and a pure FTD phenotype. Neurobiol Aging *33*, 2949 e2913-2947.
Takeuchi, R., Toyoshima, Y., Tada, M., Shiga, A., Tanaka, H., Shimohata, M., Kimura, K., Morita, T., Kakita, A., Nishizawa, M.*, et al.* (2013). Transportin 1 accumulates in FUS inclusions in adult-onset ALS without FUS mutation. Neuropathol Appl Neurobiol *39*, 580-584.
Tan, A.Y., and Manley, J.L. (2009). The TET Family of Proteins: Functions and Roles in Disease. Journal of Molecular Cell Biology *1*, 82-92.
Thomas, M., Alegre-Abarrategui, J., and Wade-Martins, R. (2013). RNA dysfunction and aggrephagy at the centre of an amyotrophic lateral sclerosis/frontotemporal dementia disease continuum. Brain.
Thomas, P., and Smart, T.G. (2005). HEK293 cell line: a vehicle for the expression of recombinant proteins. Journal of pharmacological and toxicological methods *51*, 187-200.
Ticozzi, N., Silani, V., LeClerc, A.L., Keagle, P., Gellera, C., Ratti, A., Taroni, F., Kwiatkowski, T.J., Jr., McKenna-Yasek, D.M., Sapp, P.C.*, et al.* (2009). Analysis of FUS gene mutation in familial amyotrophic lateral sclerosis within an Italian cohort. Neurology *73*, 1180-1185.
Tollervey, J.R., Curk, T., Rogelj, B., Briese, M., Cereda, M., Kayikci, M., Konig, J., Hortobagyi, T., Nishimura, A.L., Zupunski, V.*, et al.* (2011). Characterizing the RNA targets and position-dependent splicing regulation by TDP-43. Nat Neurosci *14*, 452-458.
Tradewell, M.L., Yu, Z., Tibshirani, M., Boulanger, M.-C., Durham, H.D., and Richard, S. (2012). Arginine methylation by PRMT1 regulates nuclear-cytoplasmic localization and toxicity of FUS/TLS harbouring ALS-linked mutations. Hum Mol Genet *21*, 136-149.
Tresse, E., Salomons, F.A., Vesa, J., Bott, L.C., Kimonis, V., Yao, T.P., Dantuma, N.P., and Taylor, J.P. (2010). VCP/p97 is essential for maturation of ubiquitin-containing autophagosomes and this function is impaired by mutations that cause IBMPFD. Autophagy *6*, 217-227.
Troakes, C., Maekawa, S., Wijesekera, L., Rogelj, B., Siklós, L., Bell, C., Smith, B., Newhouse, S., Vance, C., Johnson, L.*, et al.* (2012). An MND/ALS phenotype associated with C9orf72 repeat expansion: Abundant p62-positive, TDP-43-negative inclusions in cerebral cortex, hippocampus and cerebellum but without associated cognitive decline. Neuropathology, no-no.
Tümer, Z., Bertelsen, B., Gredal, O., Magyari, M., Nielsen, K.C., LuCamp, Grønskov, K., and Brøndum-Nielsen, K. (2012). A novel heterozygous nonsense mutation of the OPTN gene segregating in a Danish family with ALS. Neurobiol Aging *33*, 208.e201-208.e205.

Udan, M., and Baloh, R.H. (2011). Implications of the prion-related Q/N domains in TDP-43 and FUS. Prion *5*, 1-5.
Uranishi, H., Tetsuka, T., Yamashita, M., Asamitsu, K., Shimizu, M., Itoh, M., and Okamoto, T. (2001). Involvement of the pro-oncoprotein TLS (translocated in liposarcoma) in nuclear factor-kappa B p65-mediated transcription as a coactivator. J Biol Chem *276*, 13395-13401.
Urwin, H., Josephs, K., Rohrer, J., Mackenzie, I., Neumann, M., Authier, A., Seelaar, H., Van Swieten, J., Brown, J., Johannsen, P.*, et al.* (2010). FUS pathology defines the majority of tau- and TDP-43-negative frontotemporal lobar degeneration. Acta Neuropathologica *120*, 33-41.
van Blitterswijk, M., Wang, E.T., Friedman, B.A., Keagle, P.J., Lowe, P., Leclerc, A.L., van den Berg, L.H., Housman, D.E., Veldink, J.H., and Landers, J.E. (2013). Characterization of FUS Mutations in Amyotrophic Lateral Sclerosis Using RNA-Seq. PLoS ONE *8*, e60788.
Van Den Bosch, L. (2011). Genetic Rodent Models of Amyotrophic Lateral Sclerosis. Journal of Biomedicine and Biotechnology *2011*.
van der Zee, J., Gijselinck, I., Dillen, L., Van Langenhove, T., Theuns, J., Engelborghs, S., Philtjens, S., Vandenbulcke, M., Sleegers, K., Sieben, A.*, et al.* (2013). A pan-European study of the C9orf72 repeat associated with FTLD: geographic prevalence, genomic instability, and intermediate repeats. Hum Mutat *34*, 363-373.
van Eersel, J., Ke, Y.D., Gladbach, A., Bi, M., Götz, J., Kril, J.J., and Ittner, L.M. (2011). Cytoplasmic Accumulation and Aggregation of TDP-43 upon Proteasome Inhibition in Cultured Neurons. PLoS ONE *6*, e22850.
Van Langenhove, T., van der Zee, J., Engelborghs, S., Vandenberghe, R., Santens, P., Van den Broeck, M., Mattheijssens, M., Peeters, K., Nuytten, D., Cras, P.*, et al.* Ataxin-2 polyQ expansions in FTLD-ALS spectrum disorders in Flanders-Belgian cohorts. Neurobiol Aging.
Van Langenhove, T., van der Zee, J., Sleegers, K., Engelborghs, S., Vandenberghe, R., Gijselinck, I., Van den Broeck, M., Mattheijssens, M., Peeters, K., De Deyn, P.P.*, et al.* (2010). Genetic contribution of FUS to frontotemporal lobar degeneration. Neurology *74*, 366-371.
Vance, C., Rogelj, B., Hortobagyi, T., De Vos, K.J., Nishimura, A.L., Sreedharan, J., Hu, X., Smith, B., Ruddy, D., Wright, P.*, et al.* (2009). Mutations in FUS, an RNA Processing Protein, Cause Familial Amyotrophic Lateral Sclerosis Type 6. Science *323*, 1208-1211.
Vance, C., Scotter, E.L., Nishimura, A.L., Troakes, C., Mitchell, J.C., Kathe, C., Urwin, H., Manser, C., Miller, C.C., Hortobagyi, T.*, et al.* (2013). ALS mutant FUS disrupts nuclear localization and sequesters wild-type FUS within cytoplasmic stress granules. Hum Mol Genet *22*, 2676-2688.
Velayati, A., Yu, W., and Sidransky, E. (2010). The Role of Glucocerebrosidase Mutations in Parkinson Disease and Lewy Body Disorders. Current Neurology and Neuroscience Reports *10*, 190-198.
Venter, J.C., Adams, M.D., Myers, E.W., Li, P.W., Mural, R.J., Sutton, G.G., Smith, H.O., Yandell, M., Evans, C.A., Holt, R.A.*, et al.* (2001). The sequence of the human genome. Science *291*, 1304-1351.
Verbeeck, C., Deng, Q., DeJesus-Hernandez, M., Taylor, G., Ceballos-Diaz, C., Kocerha, J., Golde, T., Das, P., Rademakers, R., Dickson, D.*, et al.* (2012). Expression of Fused in sarcoma mutations in mice recapitulates the neuropathology of FUS proteinopathies and provides insight into disease pathogenesis. Molecular neurodegeneration *7*, 53.
Wade-Martins, R. (2012). Genetics: The MAPT locus-a genetic paradigm in disease susceptibility. Nat Rev Neurol *8*, 477-478.
Wagner, S., Carpentier, I., Rogov, V., Kreike, M., Ikeda, F., Lohr, F., Wu, C.J., Ashwell, J.D., Dotsch, V., Dikic, I.*, et al.* (2008). Ubiquitin binding mediates the NF-[kappa]B inhibitory potential of ABIN proteins. Oncogene *27*, 3739-3745.
Wan, J., Yourshaw, M., Mamsa, H., Rudnik-Schoneborn, S., Menezes, M.P., Hong, J.E., Leong, D.W., Senderek, J., Salman, M.S., Chitayat, D.*, et al.* (2012). Mutations in the RNA exosome component gene EXOSC3 cause pontocerebellar hypoplasia and spinal motor neuron degeneration. Nat Genet.
Wang, W.Y., Pan, L., Su, S.C., Quinn, E.J., Sasaki, M., Jimenez, J.C., Mackenzie, I.R., Huang, E.J., and Tsai, L.H. (2013). Interaction of FUS and HDAC1 regulates DNA damage response and repair in neurons. Nat Neurosci *16*, 1383-1391.

Wang, X.T., Arai, S., Song, X.Y., Reichart, D., Du, K., Pascual, G., Tempst, P., Rosenfeld, M.G., Glass, C.K., and Kurokawa, R. (2008). Induced ncRNAs allosterically modify RNA-binding proteins in cis to inhibit transcription. Nature *454*, 126-U111.
Weihl, C.C., Pestronk, A., and Kimonis, V.E. (2009). Valosin-containing protein disease: inclusion body myopathy with Paget's disease of the bone and fronto-temporal dementia. Neuromuscul Disord *19*, 308-315.
Wider, C., Vilariño-Güell, C., Jasinska-Myga, B., Heckman, M.G., Soto-Ortolaza, A.I., Cobb, S.A., Aasly, J.O., Gibson, J.M., Lynch, T., Uitti, R.J.*, et al.* (2010). Association of the MAPT locus with Parkinson's disease. European Journal of Neurology *17*, 483-486.
Wild, P., Farhan, H., McEwan, D.G., Wagner, S., Rogov, V.V., Brady, N.R., Richter, B., Korac, J., Waidmann, O., Choudhary, C.*, et al.* (2011). Phosphorylation of the Autophagy Receptor Optineurin Restricts Salmonella Growth. Science *333*, 228-233.
Williams, K.L., Warraich, S.T., Yang, S., Solski, J.A., Fernando, R., Rouleau, G.A., Nicholson, G.A., and Blair, I.P. (2012a). UBQLN2/ubiquilin 2 mutation and pathology in familial amyotrophic lateral sclerosis. Neurobiol Aging *33*, 2527 e2523-2510.
Williams, K.L., Warraich, S.T., Yang, S., Solski, J.A., Fernando, R., Rouleau, G.A., Nicholson, G.A., and Blair, I.P. (2012b). UBQLN2/ubiquilin 2 mutation and pathology in familial amyotrophic lateral sclerosis. Neurobiol Aging *33*, 2527.e2523-2527.e2510.
Wszolek, Z.K., Tsuboi, Y., Ghetti, B., Pickering-Brown, S., Baba, Y., and Cheshire, W.P. (2006). Frontotemporal dementia and parkinsonism linked to chromosome 17 (FTDP-17). Orphanet J Rare Dis *1*, 30.
Wu, C.-H., Fallini, C., Ticozzi, N., Keagle, P.J., Sapp, P.C., Piotrowska, K., Lowe, P., Koppers, M., McKenna-Yasek, D., Baron, D.M.*, et al.* (2012). Mutations in the profilin 1 gene cause familial amyotrophic lateral sclerosis. Nature.
Wu, D., Yu, W., Kishikawa, H., Folkerth, R.D., Iafrate, A.J., Shen, Y., Xin, W., Sims, K., and Hu, G.F. (2007). Angiogenin loss-of-function mutations in amyotrophic lateral sclerosis. Ann Neurol *62*, 609-617.
Xi, Z., Zinman, L., Grinberg, Y., Moreno, D., Sato, C., Bilbao, J.M., Ghani, M., Hernandez, I., Ruiz, A., Boada, M.*, et al.* (2012). Investigation of C9orf72 in 4 Neurodegenerative Disorders. Arch Neurol, 1-8.
Xu, Y.F., Gendron, T.F., Zhang, Y.J., Lin, W.L., D'Alton, S., Sheng, H., Casey, M.C., Tong, J., Knight, J., Yu, X.*, et al.* (2010). Wild-type human TDP-43 expression causes TDP-43 phosphorylation, mitochondrial aggregation, motor deficits, and early mortality in transgenic mice. J Neurosci *30*, 10851-10859.
Xu, Y.F., Zhang, Y.J., Lin, W.L., Cao, X., Stetler, C., Dickson, D.W., Lewis, J., and Petrucelli, L. (2011). Expression of mutant TDP-43 induces neuronal dysfunction in transgenic mice. Molecular neurodegeneration *6*, 73.
Yamamoto, A., and Simonsen, A. (2011). The elimination of accumulated and aggregated proteins: A role for aggrephagy in neurodegeneration. Neurobiology of Disease *43*, 17-28.
Yamashita, T., Hideyama, T., Hachiga, K., Teramoto, S., Takano, J., Iwata, N., Saido, T.C., and Kwak, S. (2012). A role for calpain-dependent cleavage of TDP-43 in amyotrophic lateral sclerosis pathology. Nature communications *3*, 1307.
Yang, H., Wang, H., Shivalila, Chikdu S., Cheng, Albert W., Shi, L., and Jaenisch, R. (2013). One-Step Generation of Mice Carrying Reporter and Conditional Alleles by CRISPR/Cas-Mediated Genome Engineering. Cell *154*, 1370-1379.
Yang, L., Embree, L.J., and Hickstein, D.D. (2000). TLS-ERG leukemia fusion protein inhibits RNA splicing mediated by serine-arginine proteins. Molecular and Cellular Biology *20*, 3345-3354.
Yin, F., Dumont, M., Banerjee, R., Ma, Y., Li, H., Lin, M.T., Beal, M.F., Nathan, C., Thomas, B., and Ding, A. (2010). Behavioral deficits and progressive neuropathology in progranulin-deficient mice: a mouse model of frontotemporal dementia. FASEB journal : official publication of the Federation of American Societies for Experimental Biology *24*, 4639-4647.

Yoshida, S., Mulder, D.W., Kurland, L.T., Chu, C.P., and Okazaki, H. (1986). Follow-up study on amyotrophic lateral sclerosis in Rochester, Minn., 1925 through 1984. Neuroepidemiology *5*, 61-70.
Zamiri, B., Reddy, K., Macgregor, R.B., Jr., and Pearson, C.E. (2013). TMPyP4 Distorts RNA G-Quadruplex Structures of the Disease-Associated r(GGGGCC)n Repeat of the C9orf72 Gene and Blocks Interaction of RNA-Binding Proteins. J Biol Chem.
Zhang, Y.B., Howitt, J., McCorkle, S., Lawrence, P., Springer, K., and Freimuth, P. (2004). Protein aggregation during overexpression limited by peptide extensions with large net negative charge. Protein expression and purification *36*, 207-216.
Zhang, Y.J., Xu, Y.F., Cook, C., Gendron, T.F., Roettges, P., Link, C.D., Lin, W.L., Tong, J., Castanedes-Casey, M., Ash, P.*, et al.* (2009). Aberrant cleavage of TDP-43 enhances aggregation and cellular toxicity. Proc Natl Acad Sci U S A *106*, 7607-7612.
Zhang, Y.J., Xu, Y.F., Dickey, C.A., Buratti, E., Baralle, F., Bailey, R., Pickering-Brown, S., Dickson, D., and Petrucelli, L. (2007). Progranulin mediates caspase-dependent cleavage of TAR DNA binding protein-43. J Neurosci *27*, 10530-10534.
Zhou, H., Huang, C., Chen, H., Wang, D., Landel, C.P., Xia, P.Y., Bowser, R., Liu, Y.J., and Xia, X.G. (2010). Transgenic rat model of neurodegeneration caused by mutation in the TDP gene. PLoS Genet *6*, e1000887.
Zinszner, H., Sok, J., Immanuel, D., Yin, Y., and Ron, D. (1997). TLS (FUS) binds RNA in vivo and engages in nucleo-cytoplasmic shuttling. J Cell Sci *110 (Pt 15)*, 1741-1750.